MODELING AND EXPERIMENTAL STUDY OF PLATE TYPE INDIRECT EVAPORATIVE COOLER (IEC) FOR ENERGY RECOVERY IN HOT AND HUMID REGIONS

CHEN YI

Ph.D

The Hong Kong Polytechnic University

2016

The Hong Kong Polytechnic University

Department of Building Services Engineering

Modeling and experimental study of plate type indirect evaporative cooler (IEC) for energy recovery in hot and humid regions

CHEN Yi

A thesis submitted in partial fulfillment of the requirements for the Degree of Doctor of Philosophy

June 2016

Certificate of Originality

I hereby declare that this thesis is my own work and that, to the best of my knowledge and belief, it reproduces no material previously published or written, nor material that has been accepted for the award of any other degree or diploma, except where due acknowledgement has been made in the text.

____ __ (Signed)

_____Chen Yi_____(Name of student)

Department of Building Services Engineering

The Hong Kong Polytechnic University

Hong Kong SAR, China

June, 2016

Abstract

Indirect evaporative cooler (IEC) which uses water evaporation to produce cooling air without adding extra moisture has become increasingly attractive as a natural cooling technology. It has a number of advantages over the traditional mechanical vapor compression refrigeration (MVCR) system such as energy efficiency, environmental friendly, low energy consumption and easy maintenance.

The IEC is widely used in hot and dry regions because larger cooling capacity can be achieved with low air humidity. In hot and humid regions, the IEC application is restricted to the high humidity in the past. In recent decant, however, the hybrid IEC and mechanical cooling system (also called IEC energy recovery system) has been proposed to break the regional limitation of IEC application and attracts great research interest for its high energy saving potential. In this hybrid system, IEC is used as an energy recovery device installed before an AHU or cooling coil in an air-conditioning system. The exhausted air from air-conditioned space is used as secondary air.

Although IEC is being extensively used and related experimental and simulation research work has been carried out, current efforts focus on evaluating the performance in dry and moderate regions, where it was initially used. Little previous studies involving the modeling of IEC in hot and humid regions can be identified. Furthermore,

no experimental study on evaluating IEC performance in humid regions can be found in open literatures. In dry or moderate regions, there would be no condensation from primary air, so it is understandable that only sensible cooling performance is discussed in previous studies. However, owing to the high humidity of fresh air in humid areas, condensation would occur on the primary air side. The heat and mass transfer process is much more complicated in this case compared with that of dry region cases. The condensation would greatly affect the overall performance of IEC, not only in sensible cooling but also newly brought latent cooling. The lack of modeling and experimental research of IEC with condensation provides obstacle for applying IEC energy recovery system in humid regions.

Therefore, a programmed research work on modeling and experimental investigation of IEC, with an emphasis on IEC performances with condensation from high humidity primary air, has been carried out in this thesis.

This thesis begins with establishing a short-cut analytical model for IEC considering condensation. The models for IEC under non-condensation, total condensation and partial condensation states were established and a method for judging the three states was proposed. The availability of the simplified IEC model would help facilitate annual performance prediction of IEC energy recovery system.

Secondly, the thesis presents a novel method for annual simulation of IEC energy recovery system based on the above IEC model. The simulation is achieved by incorporating IEC model into TRNSYS software, so that the annual performance can be precisely predicted by considering possible condensation of IEC, chiller operating state and dynamic cooling load. A detailed case study of a wet market in Hong Kong was presented and the simulation results were validated by a field measurement. The results shows that condensation in IEC takes up a large proportion (47.7%) of operation hours in hot and humid regions, especially in summer. Besides, the IEC shows a great potential in energy saving and peak load reduction.

Thirdly, the development of a novel numerical IEC model considering condensation and wettability ratio is presented. A comprehensive parameter analysis under three operating states (non-condensation, partial condensation and total condensation) was firstly presented. The results show that the condensation lowers the wet-bulb efficiency, but improves the total heat transfer rate. Besides, the increase of secondary air velocity, decrease of channel gap and improvement of wettability under condensation state improves IEC cooling performance more effectively than in non-condensation state.

Fourthly, the parameter sensitivity analysis of IEC by orthogonal test is presented based on the above numerical model. The influence rank of seven parameters was obtained

under IEC condensation state. The optimization was conducted to the most influential parameters: channel gap and cooler height. The optimal channel gap is 2–3 mm and 3–4 mm under condensation and non-condensation state, respectively, while the optimal NTU_p is 4–7 and 3–5, respectively.

Finally, experimental study is conducted to evaluate the plate type air cooler performance under four operating modes. Under dry operating mode, the air cooler serves as a traditional air cooler, while under wet operating mode, it works as an IEC. Comparisons can be made between traditional air cooler and IEC under both non-condensation and condensation conditions. The cooler dynamic performance during different operating mode transition and steady performance under different parameter influence were investigated. The results shows condensation weakens sensible heat transfer but improves total heat transfer. The wet operating benefits both the sensible and latent heat transfer rates. The COP varies in a wide range under different operating mode and the highest COP achieved by IEC is 9.0.

Publications during PhD study

Journal papers

[1] Chen, Y., Luo, Y., & Yang, H. (2015). A simplified analytical model for indirect evaporative cooling considering condensation from fresh air: Development and application. Energy and Buildings, 108, 387-400.

[2] Chen, Y., Yang, H., & Luo, Y. (2016). Indirect evaporative cooler considering condensation from primary air: Model development and parameter analysis. Building and Environment, 95, 330-345.

[3] Chen, Y., Yang, H., & Luo, Y. Parameter sensitivity analysis and configuration optimization of indirect evaporative cooler (IEC) considering condensation. Applied Energy. (In press, doi:10.1016/j.apenergy.2016.06.121)

[4] Chen, Y., Yang, H., & Luo, Y. (2016). Experimental study of plate type air cooler performances under four operating modes. Building and Environment, 104, 296-310.

[5] Chen, Y., Zhang, T., Yang, H., & Peng, J. (2016). Study on energy and economic benefits of converting a combined heating and power system to a tri-generation system for sewage treatment plants in subtropical area. Applied Thermal Engineering, 94, 24-

39.

[6] Chen, Y., Luo, Y., & Yang, H. (2016) An optimization method for design and operation of combined cooling, heating, and power systems toward a smart grid, Science and Technology for the Built Environment, 22:6, 766-782, DOI: 10.1080/23744731.2016.1198188.

[7] Luo, Y., Chen, Y., Yang, H., & Wang, Y. (2016). Study on an internally-cooled liquid desiccant dehumidifier with CFD model. Applied Energy. (In press, http://dx.doi.org/10.1016/j.apenergy.2016.05.133)

Conference papers

[1] Chen, Y., Luo, Y., & Yang, H. (2014). Fresh Air Pre-cooling and Energy Recovery by Using Indirect Evaporative Cooling in Hot and Humid Region–A Case Study in Hong Kong. Energy Procedia, 61, 126-130. (ICAE2014, Taiwan)

[2] Chen, Y., & Yang, H. (2015). Thermal Performances Comparison between Dry-Coil and Wet-Coil Indirect Evaporative Cooler under the Same Configuration. Energy Procedia, 75, 3162-3167. (ICAE2015, Abu Dhabi)

[3] Chen, Y., Yang, H., & Luo, Y. (2016). Parameter Sensitivity Analysis of Indirect

Evaporative Cooler (IEC) with Condensation from Primary Air. Energy Procedia, 88, 498-504. (CUE2015, Fuzhou, China)

[4] Chen, Y., Luo, Y., & Yang, H. Energy saving potential of hybrid liquid desiccant and evaporative cooling air-conditioning system in Hong Kong, ICAE 2016, Beijing, China. (Accepted)

Project reports

[1] Chen, Y., & Yang, H. Indirect Evaporative Cooling (IEC) for Energy Recovery in Tung Chung 56 Wet Market, prepared for Housing Authority of Hong Kong, SAR of China. Project No. K-ZJK1.

[2] Yang, H., Lu, L., Chen, Y., Zhang, T., Peng, J., & Luo, Y. Tri-generation of Power, Chilled Water and Hot Water at Shatin Sewage Treatment Works: Feasibility study report. Prepared for Shatin Sewage Treatment Works. Project No. ST1/2/ST2013/13.

[3] Yang, H., Lu, L., Chen, Y., Zhang, T., Peng, J. Tri-generation of Power, Chilled Water and Hot Water at Shatin Sewage Treatment Works: Preliminary design report. Prepared for Shatin Sewage Treatment Works. Project No. ST1/2/ST2013/13.

Acknowledgements

I must express my sincere grateful thanks to my Chief Supervisor, Professor Yang Hongxing, from Department of Building Services Engineering (BSE), The Hong Kong Polytechnic University, for his readily available supervision, invaluable suggestions, patient guidance and continuous helps throughout the course of my study. Without him, it is impossible for me to complete the thesis. What's more, his optimism and friendly personality also set an example for my life-long learning.

My special appreciation is also devoted to Dr. Lu Lin for her insightful view and valuable suggestions on my research work.

I also wish to express sincerest gratitude to Professor Xiaofei Wang and Professor Anthony M. Jacobi of University of Illinois at Urbana-Champaign (UIUC), USA, for accepting me as a visiting scholar to their laboratory and providing all the supervision, equipment and guidance needed to conduct experiment during my three months visit.

Furthermore, I would like to express my thanks to all the members in the Renewable Energy Research Group (RERG) for their help during my PhD study. In particular, I'm deeply indebted to Mr. Shen Zhicheng for his great help with the installation of the test rig. I would also like to thank the technicians in HVAC Laboratory of BSE Department

for their assistances in the experimental work.

My special thanks go to the Research Grant Council (RGC) of Hong Kong and the Hong Kong Polytechnic University for financially supporting this research work.

Last but not least I wish to express my gratitude and love to my family for their supports, patience and encouragement.

Table of Contents

List of Figures

Chapter 4

Chapter 5

List of Tables

Chapter 7

Chapter 8

Nomenclature

Variable	Description	unit
A	heat transfer area	m^2
B	atmospheric pressure	pa
c_{pa}	specific heat of air	J/kg ºC
c_{paw}	modified specific heat capacity on wet surface	J/kg ºC
c_{pw}	specific heat of water	J/kg ºC
Cr	heat capacity ratio	DL
d_e	hydraulic diameter of channel	m
e	slope of the saturated moist air	DL
g	acceleration of gravity	m/s^2
H	cooler height	m
h	heat transfer coefficient	W/m^2 ºC
h_{fg}	latent heat of vaporization of water	J/kg
h_m	mass transfer coefficient	kg/m^2 s
h_w	modified heat transfer coefficient on wet surface	W/m^2 ºC
i	enthalpy of air	J/kg ºC
K	total heat transfer coefficient	W/m^2 ºC
L	cooler length	m
m	mass flow rate	kg/s
n	number of channels	DL
P	pressure	pa

P_{bq}	saturated water vapor partial pressure	pa
Pr	Prandtl number	DL
Q	heat transfer rate	W
q	heat transfer rate per unit mass	W/kg
R	condensation ratio	DL
R	heat resistance	m^2 ºC/W
Re	Reynold number	DL
s	channel gap	m
t	Celsius temperature	℃
T	thermodynamic temperature	K
u	air velocity	m/s
x	coordinate axis	m
η	efficiency	DL
α	thermal diffusivity	m^2/s
δ	thickness	m
ε	enlargement coefficient	DL
λ	thermal conductivity	W/m ºC
μ	dynamic viscosity	Pa s
σ	wettability	DL
υ	kinematic viscosity	m^2/s
ω	moisture content of air	kg/kg
Γ	water drenching density	kg/m s

Note: DL: Dimensionless

Subscripts

b	saturated
c	condensation
cw	condensate water
dew	dew-point
e	evaporation
ew	evaporation water
in	inlet
inter	interface of water and air
lat	latent heat
nc	non-condensation
new	new value after iteration
out	outlet
p	primary/fresh air
s	secondary/exhaust air
sen	sensible heat
surf	surface
tot	total heat
turn	turn point of condensation region
w	wall/wet surface
wb	wet-bulb

List of Abbreviations

A/C	Air-conditioning
AHU	Air handling unit
CFC	Chlorofluorocarbon
COP	Coefficient of performance
DEC	Direct evaporative cooler
DEC/IEC	Hybrid DEC and IEC system
Desiccant/IEC	Hybrid desiccant and IEC system
EC	Evaporative cooler
EER	Energy efficiency ratio
FDM	Finite difference method
HVAC	Heating, ventilation and air-conditioning
IEC	Indirect evaporative cooler
MVCR	Mechanical vapor compression refrigeration system
NTU	Number of transfer unit
REC	Regenerative evaporative cooler
RH	Relative humidity
RIEC	Regenerative indirect evaporative cooler
SIEC	Semi indirect evaporative cooler
VAV	Variable air volume

Chapter 1

Introduction

With the improvement of living standards, the demand for thermally comfortable indoor environment is increasing. Consequently, energy use for A/C has significantly increased over the last few decades [Perez-Lombard et al. 2008]. Nowadays, A/C market is dominated by MVCR system, which is based on reverse Carnot cycle. The refrigerant, usually CFCs, circulates in the loop to complete the thermodynamic cycle. The main shortcoming of this kind of system is the high dependency on the energy-intensive electricity-driven compressor. The electricity, which mainly produced from fossil fuel, gives rise to huge CO_2 emission and global warming. Besides, the CFCs are now regarded as the culprit in causing the ozone hole. It is reported that 1506 Mtoe energy was consumed and 4762 million tons of carbon was discharged by HVAC system in China in 2013 [Global Energy Statistical Yearbook 2015]. With the growing population and increasing demand for building comfort, the energy demand for A/C will continue increasing.

The increasingly serious circumstance of energy shortage and environmental pollution worldwide put pressure on building sector to seek new ways to reduce fossil consumption and make the best use of natural and renewable energy resources for A/C.

Evaporative cooler, which uses water evaporation to produce cooling air, stands out as a promising natural cooling technology for its high efficient, low energy consumption, pollution-free and easy maintenance features. The evaporative cooler includes direct evaporative cooler (DEC) and indirect evaporative cooler (IEC). Compared with DEC, IEC adds no extra moist to the produced air, so it provides higher thermal comfort and wider applications. The IEC consists of a heat exchanger, a water circulation and distribution system. The heat exchanger is composed of alternative wet and dry channels which are separated by thin plates. In the wet channels, the spraying water drops form a thin water film on the plate surface and consistently evaporates into the main stream of the secondary air. The primary air in the adjacent dry channels is cooled by the low temperature wall.

The IEC is widely used for cooling in hot and dry regions because larger cooling capacity can be achieved with low humidity fresh air [Krüger 2010, Jaber & Ajib 2011, Bajwa et al. 1993]. The cooled primary air is supplied to the interior directly in these regions. In hot and humid regions, the supplied primary air temperature is limited to the high wet-bulb temperature of fresh air. Thus, it is used as an energy recovery device installed before an AHU or cooling coil in an A/C system [Chen et al. 1993]. The exhausted air with lower wet-bulb temperature from air-conditioned space is used as secondary air to pre-cool the primary air. This hybrid cooling system consisted of IEC

and mechanical cooling receives great attention in recent years for its attractive energy saving potential [Delfani et al. 2010, Jain et al. 2013, Cianfrini et al. 2014].

Although the cooling performances of various kinds of IEC and IEC systems have been extensively studied, theoretical model of IEC operating under humid condition is very limited in the open literature, especially when condensation from primary air occurs. Under the condensation operating mode in humid regions, the primary air is not only sensibly cooled but also dehumidified. The simultaneous sensible and latent heat transfer process on the primary air side would make the cooling performance different from that of traditional dry cases. The IEC operating characteristics with condensation are important references for the annual performance prediction, parameter study, sensitivity analysis and configuration optimization in hot and humid regions.

Besides, no intensive experimental work can be identified in the open literature on evaluating both the sensible and latent performances of IEC under condensation operating mode. Currently, all the experimental work focus on evaluating only the IEC sensible cooling performance, water consumption, water dissipate and energy consumption. The potential of IEC energy recovery technology in achieving energy saving in humid regions has not yet been fully explored.

Therefore, a modeling and experimental study of an IEC, with an emphasis on its cooling performance under condensation operating mode, have been carried out and presented in this thesis. To begin with, a comprehensive literature review on a number of important issues related to the modeling and experimental work of IEC is presented in Chapter 2. Firstly, history and current status of EC was briefly introduced. The structure and working principle of DEC and various kinds of IEC were then described. This is followed by a review on the previous studies on the operating performances of IEC system, including IEC multi-stage system for independent cooling and IEC energy recovery system for pre-cooling. Next, the comprehensive review was conducted about previous theoretical studies on modeling of IEC, thermal comfort evaluation, regional feasibility study, economic and environmental analysis. Furthermore, the previous experimental work related to IEC material study, laboratory test and field measurement were reviewed. Finally, several important issues, where further in-depth research relating the IEC application in humid regions is required, have been identified and are summarized as the research gap.

In Chapter 3, following the required further research work identified in the comprehensive literature review presented in Chapter 2, a proposal for the research work is presented, including project title, objectives and methodologies.

Chapter 4 established a short-cut analytical model for IEC considering condensation from high humidity primary air. The models for IEC under non-condensation, total condensation and partial condensation states were established and a method for judging the three states was proposed as well. The models were then validated by the published data from literatures.

In Chapter 5, a novel method was proposed for simulating the annual dynamic performance of IEC energy recovery system based on the model developed in Chapter 4. The model was incorporated with TRNSYS software, so the system performance can be precisely predicted by taking consideration of IEC non-condensation and condensation states, dynamic cooling load and chiller operating states. A detailed case study of a wet market in Hong Kong was presented and the annual simulation results were validated by a field measurement.

Chapter 6 established a new numerical model of IEC taking the condensation into consideration. The temperature and humidity distribution inside the IEC under two typical condensation conditions were illustrated. Besides, a comprehensive parameter analysis under three operation states (non-condensation, partial condensation and total condensation) was presented using four proposed evaluation indexes (condensation ratio, wet-bulb efficiency, enlargement coefficient and total heat transfer rate).

In Chapter 7, the parameter sensitivity analysis by orthogonal test was presented based on the numerical model developed in Chapter 6. The sensitivity of seven parameters (t_p, RH_p, t_s, RH_s, u_p/u_s, S, H) on three evaluation indexes (η_{wb}, ε, $\eta_{wb}\cdot\varepsilon$) were analyzed in order to rank their influence under IEC condensation state. At last, configuration optimization was conducted to the most influential parameters: channel gap and cooler height.

The experimental study was introduced in Chapter 8. An experimental test rig was built up and experimental study was conducted to evaluate the plate type air cooler performance under four operating modes. Under dry operating mode, the air cooler serves as a traditional air cooler; while under wet operating mode, it works as an IEC. So comparisons can be made between traditional air cooler and IEC under both non-condensation and condensation conditions. The cooler dynamic performance during different operating mode transition and steady performance (sensible and latent efficiencies) under different parameter influence were investigated. The cooler capacity and COP were also compared among four operating modes.

Finally, the conclusions of the thesis and the proposed future work are presented in Chapter 9.

Chapter 2

Literature review

2.1 History and current status

In fact, evaporative cooling is an oldest approach for cooling and firstly came into being as early as 2500 B.C in Egypt. Later, the technology was introduced to Middle East and spread across the hot and arid regions. With being increasingly adopted, the technology was proved to be simple as well as effective. Numerous similar built-ups such as porous water pots, water ponds and thin water chutes appeared and were combined into the building constructions in order to create the cooling effects for buildings [Watt & Brown 1997].

The modern EC were originated from USA. At first, EC was mainly invented for cleaning and cooling the air in textile mills and factories. As early as 1900s, the first air washer was invented at New England and Southern Coastline for providing proper air temperature and humidity in textile mills. During that period, DEC and IEC were also manufactured in Arizona and California, USA [Duan et al. 2012]. The massive production of EC began in early 1950s and received wide application in U.S, Canada and Australia. The EC was firstly introduced to China in 1980s and was well known by

Chinese A/C professionals in late 1990s [Chen 1988a, Chen 1988b, Chen et al. 1993].

As the latest decades witness the increasingly serious circumstance of energy shortage and environmental pollution worldwide, the EC has gained growing attention for its energy efficient and environmental friendly features. The IEC, in particular, which adds no moisture to the produced air and guarantees thermal comfort compared with DEC, its global commercial market continues expanding over the decades. A survey reported that nearly 20 million residential EC were under operation in 1999, of which India accounts for 8-10 million. The rest installations were in America, Australia, South Africa, Pakistan and Saudi Arabia [Bom et al. 1999].

Nowadays, the wide application of EC is mainly found in hot and dry regions in many countries. The biggest share of EC application is in Australia, where EC have occupied 20% of the A/C market up to 2105 [NAEEEC 2006]. The installation and operation are mainly in southern Australia, where the climate is hot and arid. The EC accounts for 5% of the commercial A/C market in U.S and the ratio is growing annually [Saudi Arabian Standards Organization 1997]. The installation amount increases rapidly in China (mainly in Western regions) from thousands in 1998 to 500,000 in 2009 [Song et al. 2010].

The main research areas of EC at the beginning lie in heat and mass transfer modelling, configuration optimization and potential energy-saving analysis. As the rapid development of the technology, the research not only limit to these areas, but also in novel heat exchangers development, water distributor optimization, novel system development to break regional limitations, hydrophilic coating application and automatic control. The research from a single field discipline to multidisciplinary research areas (including thermodynamics, materials science and chemical engineering) are witnessed.

The research hot points and trend for future technical and commercial development of EC can be classified into nine aspects: 1) develop and research on inexpensive and efficient packing material; 2) optimize the structure of equipment; 3) improve water distribution; 4) develop and research on inexpensive and efficient heat exchanger; 5) design fan special for evaporative cooling; 6) strengthen research on evaporative air filtration device; 7) depth study in hybrid systems; 8) development and research on automatic control system; 9) evaporative cooling technology standards. The 7^{th} point is what the thesis is working on.

2.2 Structure and working principle of DEC

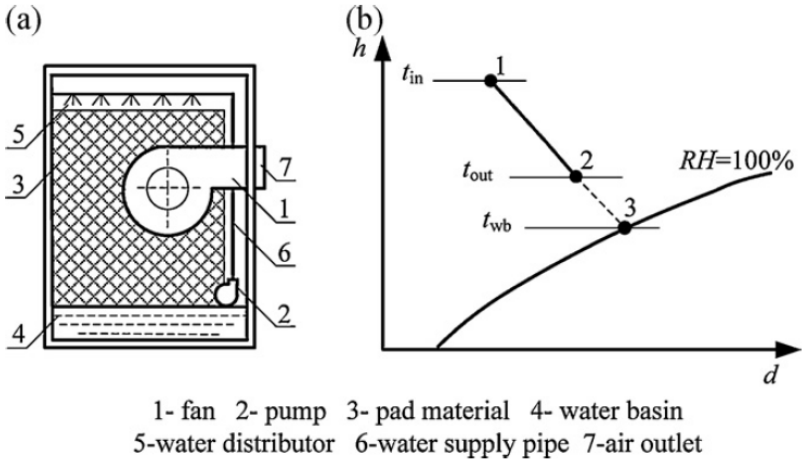

Fig. 2.1 Schematics and psychrometric process of DEC

DEC is an oldest and simplest EC in which the air is cooled by directly contacts the water [Yu & Chan 2005, Hao et al. 2013]. The water is pumped to the distribution system above and sprayed to wet the pads by spraying nozzles. The air inhaled by the fan is cooled and humidified inside the pads following an approximately constant enthalpy and leaves the cooler as 'washed air'. In theory, the leaving air can approach its wet-bulb temperature and reach a saturated state. However, it is impossible in practice as the contact area and time between the air and water are limited. The schematics and psychrometric process of DEC are shown in Fig. 2.1 [Xuan et al. 2012]. Most of the commercial DEC in the market can reach a saturation efficiency of 70% ~ 95%, depending on the unit configuration and operation conditions. DEC is favorable for its

simple configuration, low energy consumption and high efficient. The main shortcoming of this device, however, is the increasing of produced air humidity. Consequently, it can be only used in the places without humidity requirement or need simultaneous humidification and cooling.

2.3 Structure and working principle of various types of IEC

The IEC was developed by Dr. Willi Elfert in 1903. Compared with DEC, IEC cools the air without humidification, so it appears more attractive for commercial and residential use. The traditional and most commonly used IEC include tubular type, plate type and heat pipe type. The cooling capacity of traditional IEC is limited by ambient air wet-bulb temperature, thus some novel IECs were invented in recent years by reforming the interior structure and altering air flows pattern based on traditional plate-type IEC, to achieve outlet air temperature lower than the wet-bulb temperature. This kind of IEC is called dew-point IEC, mainly includes regenerative IEC (RIEC) and M-cycle IEC. For each kind of IEC, the structure, working principle and air handling process were reviewed as follows.

2.3.1 Plate, tubular and heat pipe IEC

The schematic diagram of plate type, tubular type and heat pipe IEC is shown in Fig. 2.2

[Xuan et al. 2012]. Typically, a plate type IEC is consisted of a series of thin parallel plates assembled to form a multi-layer sandwich of alternating dry and wet channels [Liu et al. 2013], which are also called primary/product air channel and secondary/working air channel, respectively. The water drop sprayed into the wet channels and cools the plate surface with aid of water film evaporation on the wet surface. The primary air in the dry channel is sensibly cooled by the low temperature plate, while the secondary air is humidified and exhausted. The primary air and secondary air usually form the cross-flow in the air-to-air heat exchanger.

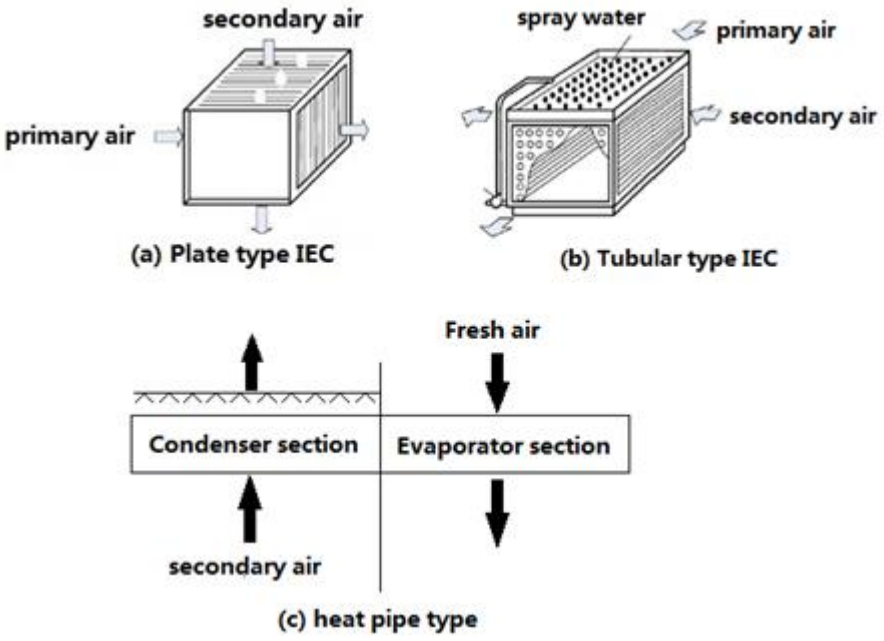

Fig. 2.2 Schematic diagram of plate type, tubular and heat pipe IEC

The cooling principle of tubular type IEC is the same with that of plate type. The inner

tubes work as dry channels and the space outside tubes are wet channels. The water film covers the exterior tubes and continues evaporating into the secondary air. Compared with the plate type IEC, the tubular type is less compact but easier to be cleaned.

The heat pipe IEC consists of condenser section and evaporator section. The cooling medium in the heat pipe absorb the heat from primary air and evaporates to the condenser, in which it will condense when the secondary air (cooled by the evaporative cooling) passes by the section. In the end, the cooling medium inside condenser will back to the evaporator and repeat this cycle. The heat pipe works as a transportation device, which transfer the sensible heat from primary air to the secondary air.

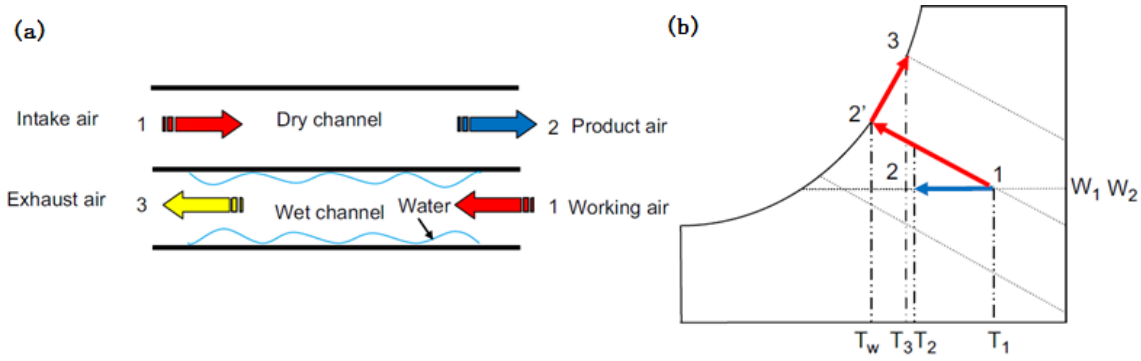

Fig. 2.3 (a) schematics and (b) psychrometric process of traditional IEC

The working principle and air handling process of traditional IEC are shown in Fig. 2.3. As the primary air has no direct contact with water, the humidity remains unchanged while the temperature decreases from point 1 to point 2. The air temperature in the

secondary air channel firstly decreases as it enters, and then increases along the saturation line from point 1 to point 2' to point 3. It is because the water evaporation absorbs the sensible heat from secondary air and becomes latent heat at the beginning. As it further gains moisture, the latent heat transfer becomes less significate. To rate the IEC, the wet-bulb efficiency is commonly used, expressed as:

$$\eta_{wb} = \frac{t_{p,in} - t_{p,out}}{t_{p,in} - t_{wb,s,in}} \tag{2.1}$$

Existing commercial IEC in the market can achieve the wet-bulb efficiency from 50% to 70%, depending on the structure and operating conditions [Watt & Brown 1997].

At the very beginning, the material for manufacturing IEC is plastic [Pescod 1968]. Because of the low thermal conductivity, it was then taken place by metal, fiber, zeolite, ceramic or carbon which has their own advantages in thermal conductivity, porosity, shaping ability, compatibility with coating contamination prevention and cost. It was found out by comparison study that wick (sintered, meshes, grooves or whiskers) attained metals (cooper or aluminum) are the most adequate material over the others, of which wick-attained aluminum sheet is the most suitable for application owing to cheaper cost [Zhao et al. 2008].

2.3.2 Dew-point IEC

The lowest possible outlet primary air temperature of traditional IEC is the wet-bulb temperature of secondary air. In order to further lower the produced air temperature and improve IEC efficiency, dew-point IEC was invented. It is able to cool the primary air to a temperature below the wet-bulb temperature of secondary air and close to dew point temperature. There are two kinds of dew point IEC: RIEC and M-cycle IEC.

2.3.2.1 Regenerative IEC (RIEC)

Regenerative IEC is designed to improve the cooling efficiency of traditional IEC by regenerating a part of produced primary air. As early as 1979, Pescod [1979] indicated the target wet-bulb temperature of the working air would be lowered by splitting a portion of produced air to the wet passage. This kind of IEC was then nominated as ‘RIEC’ by Maclaine-cross and Banks [1981].

The cooling unit takes the similar form of traditional plate type IEC which consists of dry channels and wet channels arranged compact with each other. The wet channel extracts a part of primary air from outlet of the dry channel to form a secondary air flow in the wet channel. It can lower the limitation of wet-bulb temperature of the secondary air, but the total cooling capacity will be reduced because a proportion of the produced

air used as working air. The schematics and psychrometric of RIEC is shown in Fig. 2.4. It was reported that the cooling capacity is the maximum when the extraction ratio from the dry channel to the wet channel is 0.3 [Lee & Lee 2013]. The wet-bulb efficiency can reach as high as 150% when NTU=6 [Hasan 2012]. Apart from wet-bulb efficiency, dew-point efficiency is proposed for rating the dew-point IEC, expressed as:

$$\eta_{dew} = \frac{t_{p,in} - t_{p,out}}{t_{p,in} - t_{dew,s,in}} \tag{2.2}$$

In general, the dew-point efficiency of dew-point IEC ranges from 55% to 85%, depending on its geometrical dimensions and operating conditions.

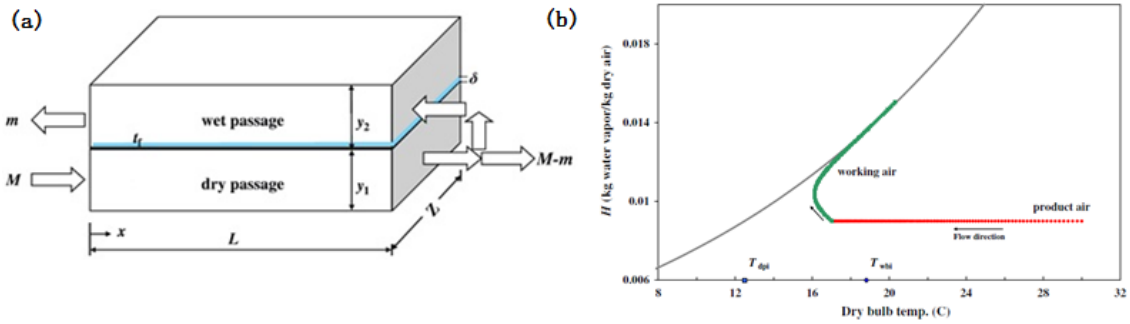

Fig. 2.4 (a) Schematics and (b) psychrometric process of RIEC

2.3.2.2 M-cycle IEC

The cross-flow dew-point IEC or M-Cycle IEC was firstly proposed by Maisotsenko et al. [2003]. It consists of one dry channel for primary air, and two channels for working

air, with numerous holes distributed regularly on the adjacent plate. When the working air flows along the dry side of the working air channel, it is cooled and partially diverted to the wet side through the hole. As the working air constantly transfers from the dry channel to the wet channel though the holes, the status of working air in the wet channel is changing, resulting in a changeable limiting value of the working air in wet channel. In the end, the limiting value of the working air approaches the dew point temperature of the entering primary air. The schematics and psychrometric of M-cycle IEC is shown in Fig. 2.5. Compared with traditional IEC, M-cycle IEC can achieve 10% ~30% higher wet-bulb efficiency. The wet-bulb efficiency can reach as high as 81%~91% and dew point efficiency ranges from 50%~60% according to a laboratory test by Coolerado [Elberling 2006].

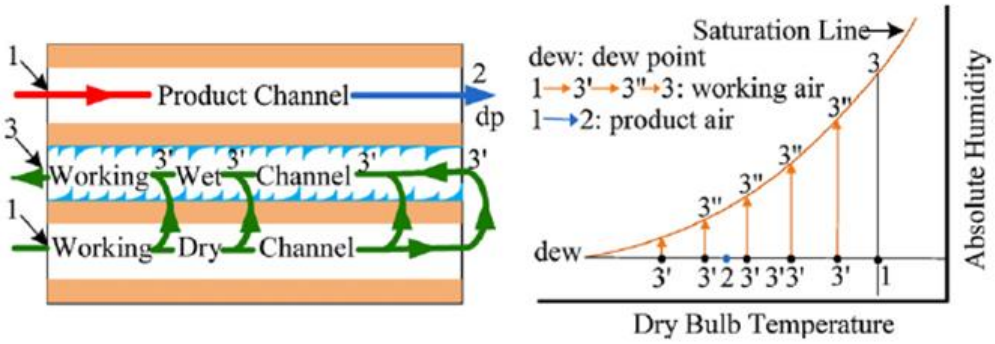

Fig. 2.5 Schematics and air handling process of M-cycle IEC

Counter-flow dew-point IEC was firstly proposed by Zhao et al. [2008] aimed at further improving the cooling efficiency of M-cycle IEC. The structure is shown as Fig. 2.6.

Unlike the M-cycle IEC that has the perforated holes widely spreading across the flow paths, the new exchanger positions those holes to the end of the flow channels to ensure the air fully cooled before diverted to the wet channel. During operation, both the primary air and secondary air are directed into the dry channels and have sensible heat exchange with the adjacent wet channels. At the end of the channel, the primary air is supposed to approach the dew point temperature of the inlet secondary air. Compared to the cross-flow M-cycle IEC, the counter-flow heat exchanger offers 15% ~ 23% higher dew-point and wet-bulb efficiency under the same configuration and operating conditions [Zhan et al. 2011].

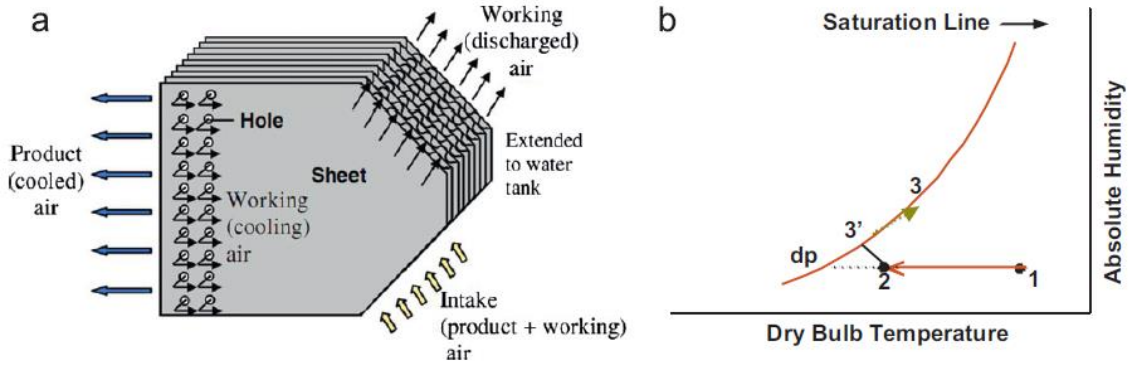

Fig. 2.6 Schematics and air handling process of Counter-flow dew-point IEC

2.3.3 Semi IEC

Semi IEC (SIEC) uses non-organic porous ceramic as the heat exchanger material rather than the metal [Gómez et al. 2005]. The size of the pores were specifically designed and

manufactured so that only water molecules can pass through. Because of these holes, both heat as well as mass can be transferred between primary air and secondary air, providing great potential for application in total energy recovery in an A/C system. The mass transfer rate between the two air flows is decided on the partial pressure of water vapor in the air. When the primary air humidity is low, the evaporated water outside the tube will transfer to the primary air side through the pores. If the primary air humidity is high, dehumidification would occur when the tube surface temperature was lower than the dew point temperature of primary air.

2.4 Indirect evaporative cooling system

The most notable feature of IEC cooling performance is the high dependency on the ambient air conditions. Thus, the IEC performance varies greatly in different climate regions and application fields. The feasibility of IEC application zones in China were determined based on the wet-bulb temperature of outdoor air. Single-stage IEC can be worked for independent cooling in warm/hot and dry regions, however, it is inapplicable to work alone in humid regions ($t_{wb,s} \geq 28$ ℃) [Di 2008, Di 2010]. So various hybrid IEC cooling systems were proposed to break the regional limitation or improve cooling capacity for different demands. The hybrid IEC cooling system can be generally classified into: 1. hybrid system for independent cooling without MVCR; 2. energy recovery system for pre-cooling with MVCR, which are reviewed as follows.

2.4.1 Single-stage IEC for independent cooling without MVCR

The single-stage IEC cooling system is usually applied in hot/warm and arid region [Chen 1994]. Krüger et al. [2010] conducted a long-term temperature monitoring in a building uses an IEC for passive cooling in Sde Boqer, Israel, and compared with a high-mass building. Results showed that IEC alone will drop the nighttime temperatures to values lower than the lower adaptive comfort limit. In China, majority of the IEC projects are in northwest, especially in Xinjiang, where has a hot and arid climate in summer. A series of tests have been conducted and results shows that single-stage IEC can satisfy the indoor environment for either spinning workshop and textile mills [Huang et al. 2002, Zhou & Huang 2005]. However, the efficiency of single-stage IEC is limited (η_{wb} < 80%) and it has strict requirement for the climate conditions, these difficulties limit its wide application in project with large cooling load and in other climate regions, the hybrid system is therefore proposed.

2.4.2 Hybrid system for independent cooling without MVCR

2.4.2.1 Hybrid DEC and IEC system (DEC/IEC)

Hybrid DEC and IEC system (DEC/IEC) is a multi-stage EC system which uses additional DEC or IEC to improve the cooling efficiency of a stand-alone DEC. The

DEC/IEC includes two-stage IEC+DEC system and three-stage IEC+IEC+DEC system. The psychrometric process of hybrid DEC and IEC system is shown in Fig. 2.7. The primary is sensibly cooled from point 1 to point 2 in first-stage IEC, and then further cooled to point 3 by DEC. The supply air temperature of three-stage IEC+IEC+DEC system would be lower than that of two-stage IEC+DEC system and much lower than single-stage DEC system under the same operating conditions.

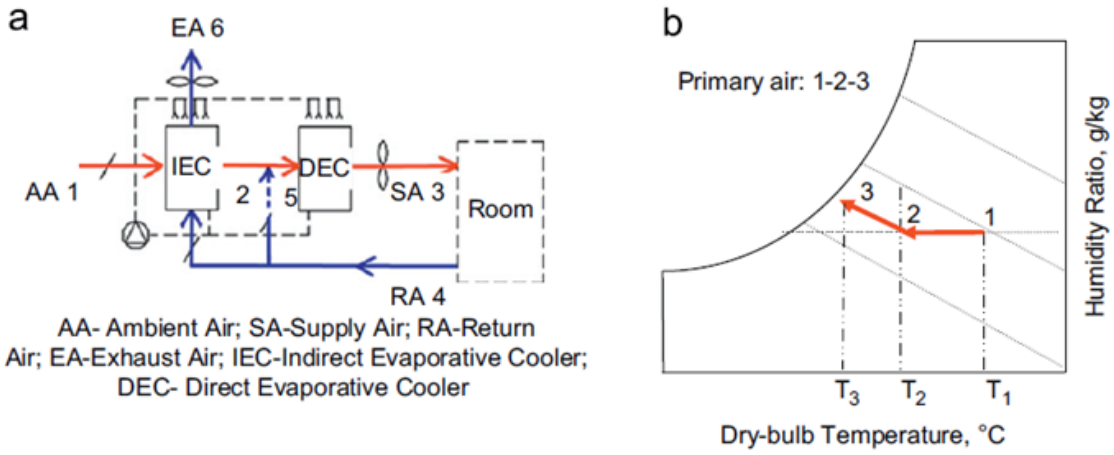

Fig. 2.7 Hybrid DEC and IEC system (a) System diagram and (b) psychrometric process

The performances of DEC/IEC have been extensively studied by experimental test, field measurement and theoretical modeling in recent decent. Representative research work is summarized as Table 2.1.

Table 2.1 Summary of research work on DEC/IEC

System	Method	Results	Conditions	Reference
IEC/DEC	Field test	η_{wb}: 90-120% Nu: 150–450	Kuwait 45℃ in summer	[El-Dessouky et al. 2004]
IEC/DEC	Theoretical	Suitability of cooling method in different regions	multi-climate regions in Iran	[Heidarinejad et al. 2008]
IEC/DEC	Experiment	η_{wb}: 108-111% 60% power saving 55% more water used	multi-climate regions in Iran	[Heidarinejad et al. 2009]
IEC/DEC	Experiment	$\eta_{DEC:}$ 71.9-98.3% η_{wb} 74.3-119.5% Q_{DEC}: 3240-45427 kJ/h Q_{system}: 4679-43771 kJ/h	t_p: 39-43℃; RH_p: 37-46%; m_p: 0.078-1.011 kg/s	[Kulkarni & Rajput 2010]
IEC/DEC	Numerical model	$\eta_{wb:}$ 76-81%; water evaporation rate was discussed	multi-climate regions in Iran	[Moshari et al. 2016]
IEC/DEC	Numerical model	provide thermal comfort for cities in Iran where DEC is inappropriate	multi-climate regions in Iran	[Heidarinejad & Bozorgmehr 2008]
IEC+IEC +DEC	Field test	$t_{p,out}$: 14.3-16℃; $t_{wb,p,out}$: 13.5-14.5℃ indoor: 22.7-23.8℃	t_p: 35.2-37℃; $t_{wb,p}$: 18.5-20℃	[Huang et al. 2004]
IEC+IEC +DEC	Field test	$t_{p,out}$ can reach 14.5℃ consumption: 26.1 kW	Xinjiang, China V_p = 40,000 m^3/h	[Huang et al. 2005]

In sum, the research show that DEC/IEC can great improve the cooling efficiency of the whole system (η_{wb}: 75-120%), the supply air temperature can even lower than the wet-bulb temperature of secondary air. In dry regions, the hybrid system can provide the cooled air lower than 14℃. So it can totally substitute MVAC system with much lower operating cost. Based on a field measurement, the power consumption was only 7.4 W/m^2, much lower than 40 W/m^2 in MVAC system [Zhu 2004]. However, its huge dimensions limit its application in practical projects.

2.4.2.2 Hybrid desiccant and IEC system (Desiccant/IEC)

To overcome the restricted application of EC in humid regions, the hybrid desiccant and IEC system (Desiccant/IEC) was proposed. The air firstly enters the desiccant dehumidifier to have the excess moisture removed before further cooled down by EC. The regeneration heat source can be waste energy, electrical energy or solar energy. The Desiccant/IEC provides a path for independent control of humidity and temperature in A/C system. Besides, the possible application of low grade energy makes it a green and sustainable cooling technology. When powered by solar energy or waste heat, it can significantly reduce the operating costs and increase the accessibility of A/C for the populations in remote areas.

The Desiccant/IEC is one of the research hotspots in recent decade. The research includes feasibility study, performance analysis and optimization both theoretically and experimentally. In term of feasibility study, Jain et al. [1995] evaluated the potential cycles for 16 typical Indian cities to achieve standard comfort conditions in the room. It is found that Dunkle cycle is better for a wide range of outdoor conditions. Feasibility studies of solar driven desiccant cooling in diverse European cities (different climatic zones) were studied by Mavroudaki et al. [2002] and Halliday et al. [2002]. It was reported that primary energy savings can be achieved in all climate zones but a decline in energy savings was noticed in high humid zones. Kim et al. [2013] studied the energy saving potential of hybrid liquid desiccant and IEC/DEC cooling system by detailed energy simulation (TRNSYS and a commercial equation solver program). Solar water heating system is used for regenerating the desiccant solution. It showed an energy saving ratio of 51% over the conventional VAV A/C system. The energy saving potential of a similar hybrid system was also investigated in Hong Kong [Luo et al. 2013].

The real performance of Desiccant/IEC was investigated by both field measurement and lab test. Finocchiaro et al. [2012] proposed a solar assisted desiccant and DEC system. A real project located in the Solar Laboratory of the University of Palermo was described and data collected was analyzed. La et al. [2012] proposed a novel desiccant

cooling system which consists of two-stage dehumidification and REC, aimed at producing chilled water and dried air. The experimental study were conducted in three outdoor conditions (temperate, humid, high humid) and results showed the supply chilled water is around 15~20 ℃, which can be the cooling source for radiation refrigerator.

Some experimental and theoretical work has been done to optimize the operating conditions of the Desiccant/IEC. Goldsworthy and White [2011] analyzed the performance of a combined solid desiccant and IEC system by solving the heat and mass transfer equations for both components simultaneously. Results showed that 70 ℃ regeneration temperature, a supply/regeneration flow ratio of 0.67 and secondary/primary flow ratio of 0.3 gives the best performance with COP > 20. Enteria et al. [2013] evaluated the Desiccant/IEC by exergetic method. The results showed that air-heating coil, air fans and desiccant wheel contributed to large percentage of exergy destruction. El Hourani et al. [2014] examined the design and operation of a hybrid solid desiccant system with two-stage EC. The hybrid system has been optimized with respect to energy and water consumption while maintaining occupant thermal comfort.

2.4.3 Energy recovery system for pre-cooling

The hybrid cooling system, consisting of IEC and MVCR, was introduced for IEC

application in high humidity areas. The IEC, installed before an AHU or cooling coil or evaporative coil, is used to pre-cool the incoming fresh air for energy conservation of A/C system [Chen et al. 1993]. In this system, the cool and dry exhausted air from A/C space is used as secondary air. The system diagram and psychrometric process are shown in Fig. 2.8. The primary air is cooled by IEC before entering into the cooling coil for further cooling (served with either chilled water or refrigerant), results in a measurable operational saving in compressor, chilled water and cooling water pumps.

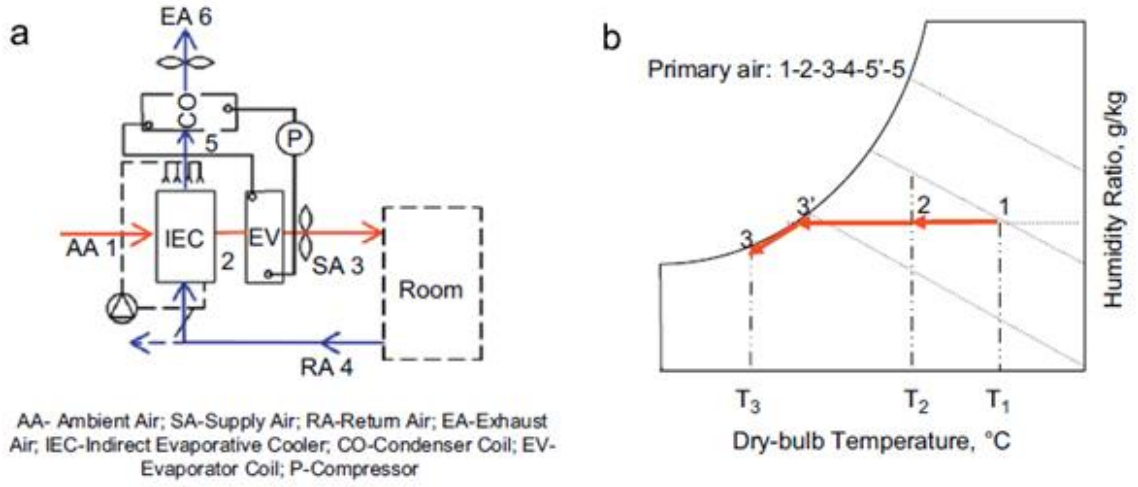

Fig. 2.8 IEC energy recovery system (a) system diagram and (b) psychrometric process

The mechanical cooling combined with one IEC is the most commonly used because it can meet the demands of majority applications. It was reported that [Higgins & Reichmuth 2007] the primary air can fell below 15℃ after being cooled by IEC and further cooled by cooling coil. The secondary air with inlet condition of 18 ~ 20 ℃

would achieve an outlet state of 21 ~ 24℃ and 80 ~ 90% RH. An IEC heat recovery system was installed in Kowloon Park Swimming Pool in Hong Kong. A 4-month operation data were collected to study the system energy saving potential by data regression [Chu 2002]. However, no rigorous theoretical model was presented. Delfani et al. [2010] conducted an experiment study to look into the energy saving potential of IEC as a pre-cooling unit combined with PUA (packaged unit conditional) in Iran, where has a climate variety. The results proved that the electrical power saving is 25% in worse conditions and 68% in best conditions compared with that of MVCR. Cianfrini et al. [2014] numerically analyzed the performances of IEC combined with a cooling/reheating unit. It showed that the proposed system may imply reductions of energy consumption by 40 ~ 60%. A dimensionless empirical equation that correlates the cooling effectiveness has also been developed for engineering calculation. Cui et al. [Cui et al. 2014 & 2015] developed a model to theoretically study the heat and mass transfer process in IEC with condensation from the primary air by utilizing the exhausted air as the secondary air. It estimated that IEC can remove about 35 ~ 47% of the cooling load in humid regions. Porumb et al. [2016] presented a complex evaluation of IEC potential to reduce the energy consumption in A/C system, of an office building in Cluj-Napoca, Romania. It was concluded that the evaporative system allowed almost 80% reduction of energy consumption.

When extra low temperature air is needed on special occasions such as freezing rooms, the combination of two-stage EC and mechanical cooling system is adopted. The two-stage IEC is worked as a pre-cooling device [Khalajzadeh et al. 2012]. The system diagram and psychrometric process of this hybrid system is shown in Fig. 2.9. The multi-step system has higher effectiveness than conventional two-stage evaporative coolers and an energy saving is 75 ~ 79% compared to MVCR, but much more complexity involves [Farmahini-Farahani & Heidarinejad 2012].

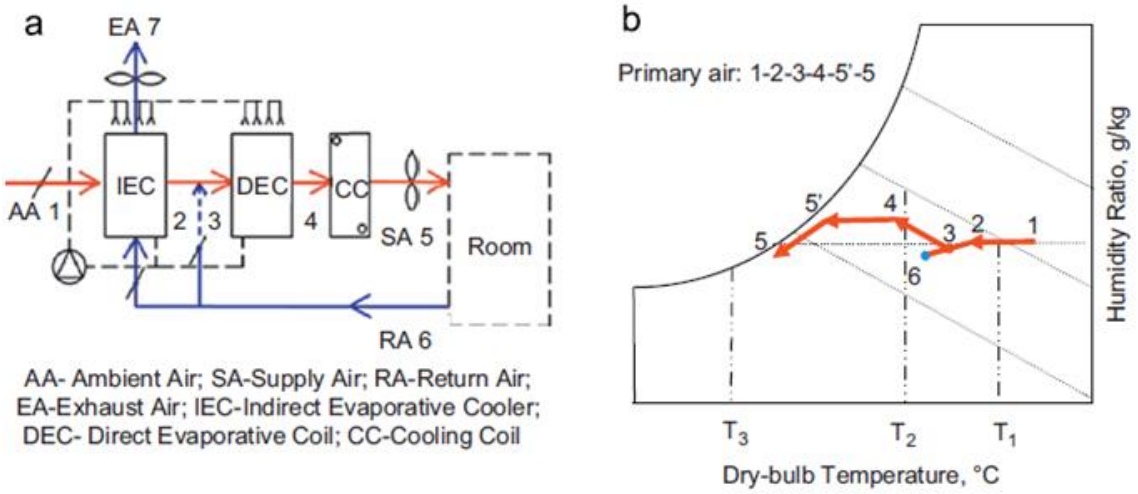

Fig. 2.9 IEC/DEC energy recovery system (a) system diagram and (b) psychrometric process

Apart from hybrid IEC and mechanical cooling system, the hybrid DEC and mechanical cooling system have also been investigated. Jiang and Zhang [2006] studied the energy saving potentials of using DEC for pre-cooling in an A/C system in 15 typical cities in China. The enhancement of system COP can be achieved but varies from 47% in

Urumqi (hot and dry) and 13.7% in Hong Kong (hot and humid). You et al. [1999] conducted a similar research to investigate the EER improvement by IEC pre-cooling in Tianjin. Varun Jain et al. [2013] conducted a financial feasibility study of a hybrid-mode operation of a DEC with an A/C unit to reduce electricity usage. The hybrid mode operation is found financially attractive for cinema and waiting hall for all the climatic conditions.

These studies prove that the energy saving and economic benefit are optimistic and attractive for the hybrid cooling system. But condensation of IEC was usually not taken into consideration in the hybrid system evaluation. Besides, the hourly dynamic operating conditions (weather data, hourly cooling load, air velocity, on/off state of chiller) were not considered in the above studies.

2.5 Theoretical research of IEC

The modeling is a core aspect in theoretical research of IEC. The established models were mainly used for performance prediction, parameter study and optimization. In general, the modeling can be classified into numerical modeling and analytical modeling. Before reviewing the two modeling methods, the Lewis relationship, assumptions and simplifications applied in IEC modeling were summarized. The thermal comfort

evaluation, regional feasibility, economic and environmental benefits were reviewed.

2.5.1 Lewis relationship

Lewis relationship is an important theory in modeling IEC. Lewis relationship refers to the law that the ratio of the convective heat transfer coefficient h and mass transfer coefficient h_m is constant in a certain two-phase flows (water-air flow in IEC), given by:

$$\frac{h}{h_m} = \frac{c_{pa}}{Le^{-\frac{2}{3}}} \tag{2.3}$$

For water-air system, Lewis factor is usually in the range of $0.9<Le<1.15$, but in many models its value is assumed to be 1 because this assumption makes useful simplifications possible later [Halasz 1998]. Thus, we can conclude that in the water-air system, h and h_{m} have certain quantitative relations in a small range of air temperature and humidity. Lewis relationship is a very important law which provides an approach for determining h_{m} between the wet surface and air by knowing h. The h is usually obtained by experiment-based empirical formula. Table 2.2 lists the commonly used empirical heat transfer coefficient in IEC modeling.

Table 2.2 Empirical heat transfer coefficient

Reference	Equation	Type	Condition
[Pescod 1974]	$h = 54u^{0.7}$	parallel air channel	fully developed laminar flow
[Yang 1992]	$h = \frac{0.023\left(\frac{u}{\upsilon}\right)^{0.8} \cdot Pr^{0.3} \cdot \lambda}{d_e^{0.2}}$	parallel air channel	fully developed laminar flow
[Cengel 2006]	$Nu = 8.235$	parallel air channel	fully developed laminar flow
[Stoitchkov 1989]	$h_s = 36.31(\rho u)^{0.68}(L/d_e)^{-0.08}$	parallel air channel	NA
[Wilke 1962]	$Nu = \frac{h\delta_e}{\lambda_e} = 1.88$	water film	water to vertical wall

The assumption of *Le*=1 was widely used in IEC modeling and the simulation results were validated by various experimental test. In some improved analytical and numerical models, the non-unity Lewis number was taken into consideration for more accurate theoretical analysis [Ren & Yang 2006], but how to determine the Lewis factor under different conditions were not presented. A study points out the assumption of *Le*=1 would lead to discrepancy, especially when the inlet air to wet side was cold and dry [Liu et al. 2013]. A recent publication [Anisimov & Pandelidis 2015] presents a theoretical study of the basic cycles for IEC by 2D and 3D numerical analysis. The paper reveals the violation of the Lewis relation unity (0.91-1.09 in the studied cases) under a certain inlet and operation conditions.

2.5.2 Assumptions and simplifications in modeling

Because of the complicated heat and mass transfer process in IEC, some assumptions and simplification should be made in modeling. In general, less assumptions result in higher accuracy, but leads to complex governing equations and time-consuming calculation. More assumptions bring simplification of governing equations and less or even no iteration in calculation process, but lead to lower accuracy. So there is a trade-off between complexity and accuracy. In general, the simplified models are usually used in annual performance prediction and feasibility study. The improved models are more often used in design optimization and parameter analysis. The commonly used assumptions in modeling IEC by three methods are summarized in Table 2.3. '√' represents the assumption is essential and '○' represents it is non-essential. The three typical modeling methods were elaborated later. Different literature features the model by unnecessarily adopting one or more non-essential assumptions.

Table 2.3 Assumptions in simplified model, ε-NTU model and FDM

Assumptions	Simplified	ε-NTU	FDM
The unit is adiabatic and no heat transfer to the surroundings	√	√	√
Air flows in both channels are fully developed, thermo-physical properties of air and water are constant	√	√	√
The wet surface of the wall is entirely saturated with	√	√	√

water			
Air is treated as incompressible gas	√	√	√
The specific enthalpy of moist air is a linear function of temperature and humidity	√	√	√
The moisture content of the air in equilibrium with the water surface is a linear function of the water surface temperature t_w	√	√	○
Heat is transferred vertically across the separating plate, no heat flow occurs along the air flow direction	√	√	○
The wet channel surface is fully covered by the water film (wettability equals to 1)	√	√	○
The water film is continuously replenished with water at the same temperature	√	√	○
The water film is in steady state, no convection occurs in the water film	√	○	○
No condensation from primary air	√	○	○
The amount of water evaporation is neglected	√	√	○
Lewis factor equals to 1	√	√	○
Secondary air never becomes super-saturation	√	√	○

2.5.3 Numerical modeling

The two typical numerical methods in IEC modeling are Finite Difference Method (FDM) and Finite Volume Method (FVM). The latter one is usually used with the assistant of Computational Fluid Dynamics (CFD) software.

2.5.3.1 Finite difference method (FDM)

The FDM is the most widely adopted method in IEC modeling. The main idea is to discretize differential equations into algebraic form. In this method, all the derivate terms in the governing equations and boundary conditions are replaced in terms of their discrete equivalents. The conversion of differential equations into a difference form can be achieved by Taylor series expansion at grid node. In the end, a set of algebraic equations is solved by simultaneously equation solver algorithm.

One-dimensional numerical resolution is usually adopted for counter flow IEC and two-dimensional resolution is for cross flow IEC. The numerical modeling of IEC is usually based on two typical models, Merkel model and Poppe model. Merkel model is a simplified model while Poppe model is an improved model by considering more factors.

Merkel model was firstly proposed by Merkel for cooling tower performance analysis [Merkel 1925]. Many improved models are based on it for analyzing various industrial devices involving water-air interaction, including IEC. The control volume and entire boundary of IEC are shown in Fig. 2.10. In Merkel theory, several critical assumptions are made includes: 1) $Le = 1$; 2) secondary air is saturated and its enthalpy being a linear function of only the wet-bulb temperature; 3) water evaporation rate is neglected; 4) heat transfer resistance of water film is neglected. These assumptions allow the differential equations to be reduced to single separable differential equations [Rubio-

Castro et al. 2011].

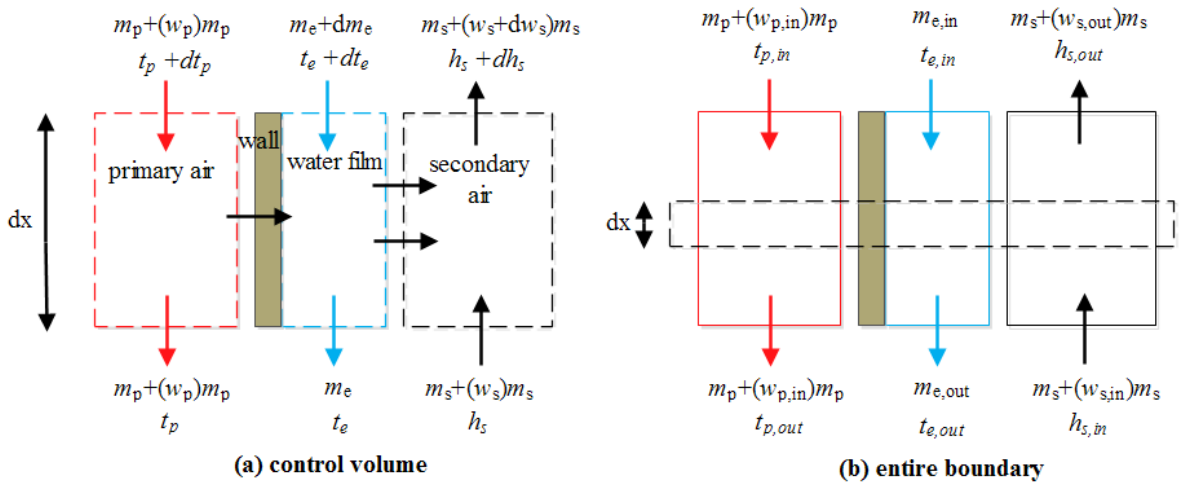

Fig. 2.10 (a) Control volume and (b) entire boundary of IEC

The Merkel model can be fully described by the following equations, which include: 1) sensible heat balance in primary air channel; 2) total heat balance in secondary air channel; 3) heat balance of water film.

$$m_p c_{pa} dt_p = -h_p (t_w - t_p) dA \tag{2.4}$$

$$m_s di_s = h_{ms} (i_{s,(t_w)} - i_s) dA \tag{2.5}$$

$$m_e c_{pw} dt_e = -m_s di_s - m_p c_{pa} dt_p \tag{2.6}$$

The boundary conditions for counter flow IEC device are:

$$t_p\big|_{x=H} = t_{p,in},\ i_s\big|_{x=0} = i_{s,in},\ t_e\big|_{x=0} = t_{e,in} \tag{2.7}$$

Because the Merkel model does not consider the water mass loss by evaporation, only the outlet temperature of secondary air can be obtained. In order to calculate the secondary air humidity, Merkel assumed that the leaving air is saturated. The model can avoid iteration process and can dramatically save compute time, but they lead to the reduced accuracy, so it has been widely applied only in evaluation of smaller sized system and development of the initial design scheme [Kloppers & Kröger 2005].

Poppe model was firstly proposed by Poppe and Rögener for analysis the performance of cooling tower [Poppe et al. 1991]. It takes fully consideration of super-saturation of moisture air, non-unity Lewis factor, water temperature variation and water evaporation. Both unsaturated and supersaturated secondary air conditions are deliberated in Poppe model. In case of under-saturated air condition, the IEC was fully modelled by Eq. (2.8) to (2.12). The Lewis factor can be described as Eq. (2.14) proposed by Bosnjakovic [1965].

$$d\omega_s = -dm_e / m_s \tag{2.8}$$

$$m_e c_{pw} dt_e + m_s di_s + c_{pw} t_e dm_e + m_p c_{pa} dt_p = 0 \tag{2.9}$$

$$dm_e = -h_{ms}(\omega_{s,t_w} - \omega_s)dA \tag{2.10}$$

$$m_s di_s = h_{ms}\{(i_{s,t_w} - i_s) + (Le-1)[(i_{s,t_w} - i_s) - (\omega_{s,t_w} - \omega_s)h_{fg}]\}dA \tag{2.11}$$

$$m_p c_{pa} dt_p = -K(t_p - t_w)dA \tag{2.12}$$

$$K = (\frac{1}{h_p} + \frac{\delta_w}{\lambda_w} + \frac{1}{h_s})^{-1} \tag{2.13}$$

$$Le = 0.865^{2/3}(\frac{\omega_{s,t_w} + 0.622}{\omega_s + 0.622} - 1) / \mathrm{In}(\frac{\omega_{s,t_w} + 0.622}{\omega_s + 0.622}) \tag{2.14}$$

In case of saturated and supersaturated air, Eq.(2.10) and Eq.(2.11) should be re-written as Eq.(2.15) and Eq.(2.16).

$$dm_e = -h_{ms}(\omega_{s,t_w} - \omega_{s,sat})dA \tag{2.15}$$

$$\begin{aligned} m_s di_s = h_{ms}\{&(i_{s,t_w} - i_s) + (Le-1)[(i_{s,t_w} - i_s) - (\omega_{s,t_w} - \omega_{s,sat})h_{fg}] \\ &+ Le \cdot c_{pw} t_w(\omega_s - \omega_{s,sat})\}dA \end{aligned} \tag{2.16}$$

The Poppe model is appropriate for accurate prediction of water temperature, water evaporation amount, moisture air temperature and humidity. However, it involves complicated iterative process, so it is suitable for optimizing the design and system operation.

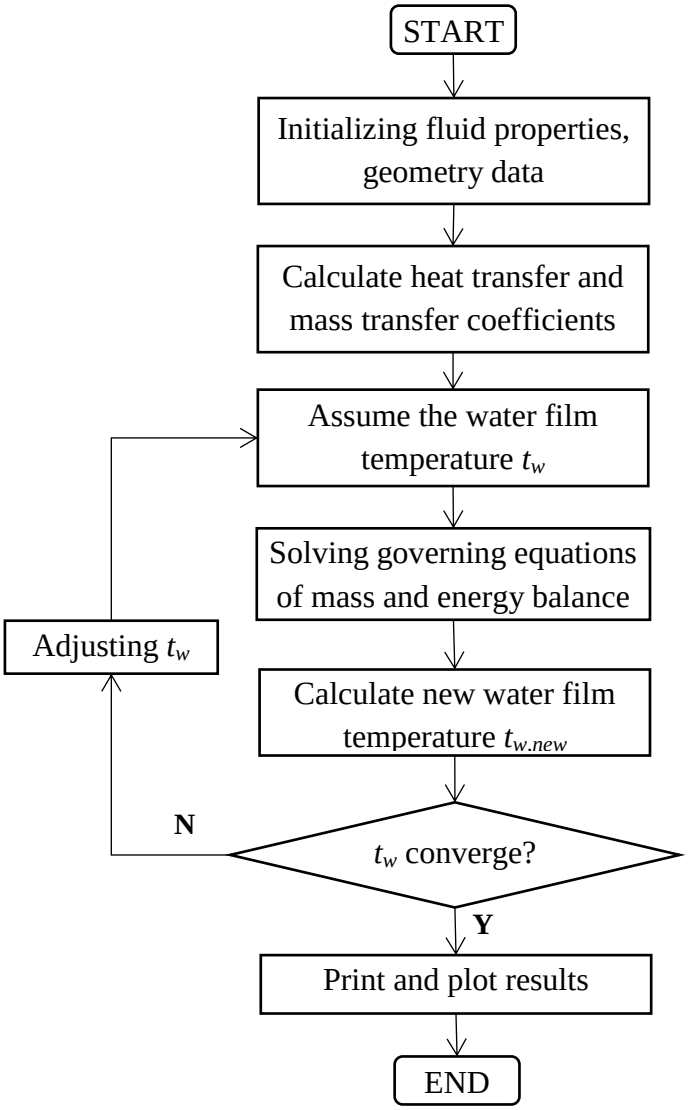

Fig. 2.11 Calculation procedure of solving IEC model by FDM

In general, the procedure for solving the ordinary differential equations of IEC by FDM is shown as Fig .2.11. The water film temperature is iterated until all the energy balance equations can be satisfied. All the later IEC models were developed based on either Merkel model or Poppe model by introducing some novel flow patterns (RIEC and M-cycle) and heat exchanger structure (corrugated plate, fin-type), or taking account some

other factors (wettability, longitudinal heat conduction of wall, two-dimensional heat exchange, variation of water temperature et al.) or improving the solution procedure. Some representative numerical models by FDM are summarized in Table 2.4.

Table 2.4 Representative numerical models by FDM

Model	IEC type	Accuracy	Features
Guo and Zhao [1998]	cross-flow plate type IEC	N/A	2D, detailed parameters study
Kettleborough and Hsieh [1983]	cross-flow plate type IEC	14% in cooling efficiency	1D, consider incomplete wetting and variation water temperature
Lee et al. [2013]	RIEC(flat plate, corrugated plate & finned channel type)	Validated by other exp results	three different RIEC configurations were compared for the most compact one
Zhan et al. [2010]	Counter flow and cross flow IEC	0.01~1.09 ℃ in supply air	length-to-width ratio of counter flow with rectangle channels was optimized
Riangvilaikul & Kumar [2010]	RIEC	Efficiency $<\pm 10\%$	influence of major operating parameters under various inlet conditions
Hettiarachchi et al. [2007]	cross flow IEC	Validated by other simulation results	investigate the effect of longitudinal heat conduction in heat exchanger wall
Hasan [2010]	Two-stage IEC	7.4% in outlet temperature	Sub-bulb temperature can be achieved; η_{wb} of different IEC were calculated
Heidarinejad &	counter flow	−2% ~1% in	Considering wall

Moshari [2015]	RIEC	outlet temperature	longitudinal heat conduction.
Zhan et al. [2011]	M-cycle IEC	3.4% in outlet temperature; 7.3%e9.4% in efficiency	model was developed using the EES; parameter study; recommendation for channel height and length
Anisimov et al. [2014]	M-cycle IEC	7% in cooling capacity; 6% in efficiency	various ambient and operational conditions;
Fakhrabadi & Kowsary [2016]	RIEC	Validated by other exp results	channel length and channel height optimized to be 0.4-0.6m and 4-6 mm using room cooling capacity as optimized criterion
Anisimov & Pandelidis [2015]	parallel, counter, cross and regenerative IEC	Validated by other exp results	2D and 3D models; A theoretical method for estimating *Le* was proposed.
Pandelidis & Anisimov [2015]	plate-fin heat exchanger with M-Cycle	Validated by exp results	2D modified ε-NTU model; cooling performance of 8 types of IEC were compared to obtain highest efficiency.

2.5.3.2 Computational fluid dynamics (CFD) simulations

Although FDM can achieve satisfactory simulation results with reasonable computing time, it is difficult to handle 3D problems together with more complex hydraulic and thermal performance. CFD, as a sophisticated fluid analysis technology, is able to analyze the complex heat and mass transfer processes by solving the continuity,

momentum, energy and species equations with the help of rapid development of computer technology. The velocity, pressure, temperature and concentration profiles in the IEC can be obtained.

Limited to the computer hardware and software, the CFD for IEC analysis had not been applied until recent decade. The 3D heat and mass transfer process in a plate-type IEC has been simulated by CFD for analyzing the distributions of pressure, temperature, concentration field and mean Nusselt and Sherwood numbers [Ren & Zhang 2005, Ding & Ren 2006a, Ding & Ren 2007]. Cui et al. [2014] analyzed a novel dew point evaporative cooler by ANSYS FLUENT 14.0. The wet surface was not regarded as a thin water film but treated as evenly dispersed droplets.

In summary, CFD method can deal with more consideration in modeling, such as 3D heat exchanger, scattered water drops, various embossments on the plates, but consumed much more compute resources and time. However, it has great potential for design and optimization of novel IEC with higher efficiency and more complex structure.

2.5.4 Analytical modeling

2.5.4.1 Simplified models

The simplified model treats IEC as a single element and the outlet parameters can be obtained directly by analytically integrated the differential equations into a simple-to-use model. The simplified model can provide the advantages as: 1) short computational time; 2) reasonable accuracy; 3) easy to be incorporated into dynamic building simulation packages. Simplified models usually based on many assumptions as listed in Table 2.3 in Section 2.5.2.

A linear approximate model was proposed for analyzing IEC by Maclaine-cross and Banks [1981]. Two most crucial assumptions are made: 1) the specific enthalpy of the moist air is a linear function of air temperature and air moisture content, i.e., $i_s = i_{so} + c_{pa} t_s + h_{fg} \omega_s$; 2) the moisture content of the air in equilibrium with the water surface is a linear function of water surface temperature,, i.e., $\omega_{t_w} = d + e t_w$. By substituting the above assumptions into the governing equations derived from Merkel equations, the solution of the wet bulb depression model yields:

$$t_{p,out} = t_{wb,p,out} + (t_{p,in} - t_{wb,p,in}) \cdot \exp(-\frac{h_p A}{m_p c_{pa}}) \quad (2.17)$$

Another simplified model was developed by Erens and Dreyer [1993] by making a comparison among Poppe model and Merkel model. The assumed recirculating water temperature is constant enable the differential equations of fresh air temperature and secondary air enthalpy can be integrated independently. It was found that the simplified model can provide enough accuracy for design purpose. The extra effect and computer time required in Poppe model for simulation is not justified by the small improvement in accuracy. Besides, the optimum fraction of cooled primary air of a RIEC, plate spacing and secondary to primary air side area ratio were proposed.

Later, San Jose Alonso et al. [1998] developed a more user-friendly simplified model for analyzing the thermal performance of plate type IEC. An equivalent water temperature was introduced and applied into the calculation. The simulation results were validated with data from Pescod model [1974] and Erens and Dreyer model [1993] with discrepancy ranging from 2.2℃ to 2.4℃ and -0.1℃ to -0.6 ℃, respectively.

Stoitchkov and Dimitrov [1998] proposed a short-cut method based on the Maclaine-cross and Banks model [1981] for calculating the effectiveness of cross flow IEC. The model considered the flowing down water film under the real condition. The

improvement of the model lies in the estimation method for mean water surface temperature and the introduced equation for calculating the ratio of total to sensible heat considering the barometric pressure.

2.5.4.3 Improved models

The above simplified methods usually assume the constant spray water temperature, unity Lewis factor and full wetting surface, which sacrifice accuracy for simplicity of solutions. However, it was reported that the incomplete wetting can be often observed in real operation [Facao & Oliveira 2000, Yang et al. 2003]. Besides, the assumption of a unity Lewis factor might be invalid for some operating conditions [Liu et al. 2013]. In order to improve the accuracy of performance prediction, improved analytical model was proposed, of which the model developed by Ren & Yang [2006] was regarded as the most comprehensive analytical model for IEC analysis. The model takes account the spray water evaporation, spraying water temperature variation and spray water enthalpy change along the heat exchanger surface. Besides, the Lewis factor and wettability were not regarded as one. Four different flow arrangements with parallel/countercurrent flow configurations were analyzed.

2.5.4.2 Modified ε-NTU model

The Effectiveness-Number of Transfer Unit method, short for ε-NTU method, is a traditional method for verification and design of the cooling tower and heat exchanger [Jaber & Webb 1989, Stabat & Marchio 2004]. In this method, the efficiency of the heat exchanger is expressed as a function of three independent factors: heat capacity ratio C_r, flow pattern and NTU. As the wet surface of IEC involves simultaneous heat and mass transfer process, which differs from dry surface heat exchanger. Modified ε-NTU method was proposed with proper adjustments made by redefining some parameters and assuming a linear saturation temperature-enthalpy relation of air. Two representative modified ε–NTU methods are listed in Table 2.5, in comparison with traditional ε–NTU method from all aspects.

- **Modified ε-NTU method 1:**

This modified method usually adopted when referring to a kind of psychrometric chart, in which the x-axis is the air temperature and y-axis is the air enthalpy. The parameter $\overline{k}$ is adopted to modify other parameters, which can be interpreted as assuming a linear slope for the saturation temperature-enthalpy relation of air.

- **Modified ε-NTU method 2:**

Similar with method 1, the slope $\overline{k}$ is also adopted. But the modification of the heat

capacity and the heat transfer coefficient are different. For solving $\bar{k}$, the relationship between correlating saturation air temperatures and associated enthalpies can be calculated by a three-order polynomial [ASHRAE 2009].

Table 2.5 Comparison between traditional ε-NTU method and modified ε-NTU method

Traditional ε-NTU	Modified method 1 [Hasan 2012]	Modified method 2 [Liu et al. 2013]
c_{pa}	c_{pa}	$c_{paw} = \bar{k}$
$C_p = m_p c_{pa}, C_s = m_s c_{pa}$	$C_p^* = m_p c_{pa} / \bar{k}, C_s^* = m_s$	$C_p = m_p c_{pa}, C_s^* = m_s c_{paw}$
$C_r = \frac{(mc)_{\min}}{(mc)_{\max}} (C_r \le 1)$	$C_r^* = \frac{\min(C_p^*, C_s^*)}{\max(C_p^*, C_s^*)} (C_r \le 1)$	$C_r^* = \frac{(mc)_{\min}}{(mc)_{\max}} = \frac{m_p c_{pa}}{m_s c_{paw}}$
h_s	h_s	$h_{sw} = \frac{\bar{k} \cdot h_s}{c_{pa}}$
NA	$\bar{k} = \frac{h_{s,sat,out} - h_{s,sat,in}}{t_{wb,s,out} - t_{wb,s,in}}$	$\bar{k} = \frac{h_{s,sat,out} - h_{s,sat,in}}{t_{wb,s,out} - t_{wb,s,in}}$
$NTU = \frac{KA}{(mc)_{\min}}$	$NTU^* = \frac{K^* A}{\min(C_1^*, C_2^*)}$	$NTU^* = \frac{K^* A}{(mc)_{\min}}$
$K = (\frac{1}{h_p} + \frac{\delta_w}{\lambda_w} + \frac{1}{h_s})^{-1}$	$K^* = [\bar{k}(\frac{1}{h_p} + \frac{\delta_e}{\lambda_e} + \frac{\delta_w}{\lambda_w}) + \frac{1}{h_{pm}}]^{-1}$	$K^* = (\frac{1}{h_p} + \frac{\delta_w}{\lambda_w} + \frac{\delta_e}{\lambda_e} + \frac{1}{h_{sw}})^{-1}$
$q = c_{pa} m_p (t_{p,in} - t_{p,out})$ $= c_{pa} m_s (t_{s,out} - t_{s,in})$	$q = \varepsilon \cdot \min(C_p^*, C_s^*) \cdot [h_s(t_{p,in}) - h_{s,in}]$	$q = c_{pa} m_p (t_{p,in} - t_{p,out})$ $= m_s \bar{k} (t_{wb,s,out} - t_{wb,s,in})$
$\varepsilon = \frac{(t_{in} - t_{out})_{\max}}{t_{p,in} - t_{s,in}}$	$\varepsilon = \frac{C_s^* (h_{s,out} - h_{s,in})}{\min(C_p^*, C_s^*) \cdot [h_s(t_{p,in}) - h_{s,in}]}$	$\varepsilon = \frac{t_{p,out} - t_{p,in}}{t_{p,in} - t_{wb,s,in}}$

2.5.5 Thermal comfort and regional applicability

The thermal comfort and regional applicability of IEC have been investigated in

different countries and cities with various climate conditions. Di et al. [2008 & 2010] classified 177 Chinese cities into four typical zones (ventilation, highly applicable, fully applicable and inapplicable) according to the wet-bulb temperature of fresh air. It was concluded that $t_{wb} > 28℃$ was not applicable for IEC. Jiang and Xie [2010] present theoretical analysis of an innovative IEC for producing high temperature chilled water. It showed that indirect evaporative chiller has potentially wide application in dry regions, especially for large scale commercial buildings. Cruz and Krüger [2015] assessed the applicability of IEC in prototypical dwelling modeled across the Brazilian territory. Results suggested that the system is capable of ensuring thermal comfort for most of the cities (411 Brazilian cities in all). Pomianowski et al. [2015] conducted annual regional feasibility analysis of various EC system based on hourly weather data for 15 cities located in Denmark and 123 European cities. Baca et al. [2011] investigated the comfort potential improvement by EC in Spanish different geographic location. Jaber [2016] conducted thermal and economic performance analysis of IEC system in Berlin, Amman and Aqaba. Steeman et al. [2009] examined the interaction between the moisture balance and the thermal comfort for a typical IEC application in Belgian climate. It showed that indoor comfort and operation time increase with high ventilation rates and the thermal comfort decreases with increasing indoor moisture production. Duan [2011] analyzed the geographic feasibility of M-cycle IEC in Europe and China by considering energy saving, economic measures and environment impacts. In sum, IEC is recognized

as a passive technique that can provide thermal comfort in different climatic situations, not only in dry regions as it was initially applied but also in temperate and maritime ones owing to the rapid development of hybrid IEC technology.

2.5.6 Economic and environmental analysis

Due to the low energy consumption and high cooling efficiency compared with MVCR, IEC has a great potential in bill reduction and CO_2 reduction. Navon and Arkin [1994] developed a thermo-economic model for the desert cooler (DEC/IEC) to estimate the value of such a system as an alternative to the air-conditioner in Israel. The life cycle cost was calculated by using the annual equivalent cost and initial cost. Jaber and Ajib [2011] reported about 1084 GWh/annual energy could be saved and 637,873 Ton CO_2 emission could be reduced if IEC was used instead of MVCR in 500,000 Mediterranean residential buildings. The payback period is less than two years. Jaber [2016] also conducted economic analysis of IEC using Life Cycle Cost (LCC) and Payback Period criterion in Amman, Aqaba and Berlin..

2.6 Experimental research of IEC

The experimental research aims at: 1) testing the operational characteristics of IEC exchangers/systems under controlled laboratory and real building conditions; 2)

verifying the established IEC model. The experimental studies mainly focus on following aspects: (1) cooling performance (cooling capacity, cooling effectiveness, COP, EER) evaluation; (2) influence of operating parameters (inlet air temperature, humidity and velocity, spray water temperature and flow rate); (3) energy consumption by fans and pump; (4) optimization of operating conditions and configuration (air velocity, primary air to secondary air ratio, water flow rate, spray nozzle arrangement); (5) optimization of heat exchanger material; (6) indoor thermal evaluation.

2.6.1 Laboratory test

The laboratory test is usually conducted under controllable air parameters. The inlet air can be processed to a desired state by heater, humidifier and controller in the ducts or chambers. So the laboratory test is suitable for investigating the influence of parameter and suggesting favorable operating conditions.

Velasco Gómez et al. [2012] investigated a polycarbonate-made IEC under two operational modes: with spray water and without spray water. Results proved that the spraying water, higher fresh air temperature and air flow rate can enhance the cooling performance. Zhang et al. [2006] experimentally figured out the optimum spray water rate for aluminum foil plate type IEC is 15-20 kg/m/h with water film thickness of 0.5-0.55 mm. De Antonellis et al. [2016] carried out 112 experiments to test a cross flow

IEC. The effects of water flow rate, nozzles setup, secondary air temperature, humidity and flow rate have been widely investigated. Results showed that performance is slightly dependent on nozzles number and size but it is strongly influenced by the water flow rate. In addition, nozzles in counter flow arrangement perform better than in parallel flow configuration.

The uniform of water distribution is a most crucial factor affects IEC performance. Thus, many experimental studies have been done to improve the wettability of plate wall. Huang et al. [2006] made an experimental study focused on improving the structure of water distributors and selecting water absorbing materials. A secondary water distribution which was made of several layers of metal nets was proposed to improve unevenly water distribution by breaking the spraying water drop into smaller ones. Besides, experiments on fabric absorbent and water retention properties were conducted in order to select suitable fibre material coated on the surface of tube IEC. Fan et al. [2007] made a preliminary study to improve the hydrophilic and antibacterial performance of the EC A/C unit. Three methods, including hydrophilic heat exchanger materials, nanometer photochemical catalysis technology and coating hydrophilic fibers outside heat exchanger tube, were put forward to improve its hydrophilic performance and solve the problem of bacterium multiplies in A/C system. Fan [2009] also investigated the heat and mass transfer enhancement methods of tubular IEC, include

that aluminum foil tube was coated by water absorbent fiber fabric, aluminum foil surface coated by hydrophilic membrane. And the best volume ratio of secondary air and primary air, water-spraying density were studied by experiment.

Besides the traditional tube type and plate type IEC, some novel IECs and IEC systems, such as RIEC, M-cycle IEC, DEC/IEC, desiccant/IEC, IEC air-water system had also been tested. Riangvilaikul and Kumar [2010] experimentally studied the outlet air conditions and sensible cooling effectiveness of RIEC system at different inlet air conditions (dry, temperate and humid). The results showed that η_{wb} ranged between 92 ~ 114% and η_{dew} between 58 ~ 84%. Cross flow and counter flow M-cycle IEC have been experimentally tested for parameter study, optimization of geometry and operating conditions [Elberling 2006, Riangvilaikul & Kumar 2010, Zhan 2011, Duan 2011]. Jain [2007] developed a two-stage evaporative cooler to enhance the effectiveness of IEC under high humidity condition. The cooling effectiveness can reach 1.1 to 1.2 under the test condition. Kulkarni and Rajput [2011] tested the performance of a two stage IEC and optimized the system by using different shapes and cooling media in direct stage. Similar two-stage system had been tested by Heidarinejad G, et al. [2009]. Finocchiaro et al. [2012] designed a desiccant/IEC to achieve better energy performance. It showed that 21 ~ 22 ℃ supply temperature can be achieved without using an auxiliary cooling coil. The performances of IEC for providing cooling water were experimentally studied

by Jiang & Xie [2010] and Costelloe and Finn [2003 & 2007]. The test indicated that the outlet water temperature could be reduced to 14 ~ 20 ℃. The cooling tower air flow rate and secondary water flow rate have a strong impact to the cooling effectiveness of the evaporative air-water cooling system.

2.6.2 Field measurement

The short term and long term field measurement of IEC system are usually incorporated with a real building or room in certain climatic zones. The dynamic operating characteristic, energy consumptions and indoor thermal comfort can be monitored and analyzed under constantly changing operating conditions. Besides, problems associated with IEC real operation can be found, providing meaningful optimization guidance for future design and operation.

Pescod [1979] firstly proposed the plate type IEC can be used for heat recovery in a ventilated A/C system and reported the measured IEC efficiency. Bajwa et al. [1993] evaluated the comfort conditions in a two-storey house provided by EC in the gulf region of the Kingdom of Saudi Arabia. The results showed that EC reduced the operation time of A/C significantly during the overhead period of the maritime-desert climate. An IEC with plastic tube heat exchanger was fabricated and tested during summer months in Indore by Tulsidasani et al. [1997]. It was found that the maximum

COP can reach 22 with 10.4℃ drop of primary air. The optimized u_p and u_s are 3.5 m/s and 3 m/s, respectively. El-Dessouky et al. [2004] constructed an experimental rig of IEC/DEC and tested it in Kuwait, where t_p can be higher than 45 ℃. Results show that the efficiency varies in 90 ~ 120% and heat transfer coefficient is 0.1–0.4 kW/m^2 K. The similar IEC/DEC has also been tested in Xinjing by Huang et al. [2004 & 2005]. Qiu [2007] examined the practical performances of an IEC module product. The study indicates that real efficiency of an IEC is much lower than the values given by the product specifications. The reason lies in the poor water distribution for only 1/2-2/3 of surfaces were wetted.

2.7 Summary of previous research and research gap

2.7.1 Summary of previous research

Since the IEC was massively produced in U.S about 30 years ago, IEC technology has been widely studied. Most existing research and development efforts related to IEC and IEC systems focused on four main areas: (1) analytical and numerical modeling; (2) operating performances evaluation and energy saving estimation; (3) optimal configuration in terms of higher system efficiency and better indoor thermal comfort; (4) developing novel heat exchanger and hybrid system to achieve higher efficiency. A large number of previous studies on IEC and IEC systems can be identified in the open

literature. These studies are either simulation or experimental based.

The modeling methods include analytical modeling and numerical modeling, of which numerical modeling was more widely adopted. The easy-to-use simplified analytical model usually adopts most assumptions and can provide reasonable accuracy results with short computational time. Closed form analytical solutions are very useful for obtaining an immediate idea of outlet air parameters. So it can be useful for annual energy performance prediction by being incorporated into dynamic building simulation packages. However, the availability of analytical model is mostly restricted to simple geometries and linear governing equations. For more general geometries and complex process, recourse needs to be taken towards numerical solutions of the governing differential equations. Both FDM and CFD method can take a variety of factors into consideration (water evaporation loss, water temperature variation, non-unity Lewis number, et al.) and output results at the discrete node with numerical calculation method, of which CFD method can deal with more complex geometries and flow pattern. Numerical modeling is mostly found for parameter study, sensitivity analysis and configuration optimization for IEC in open literature. Current modeling work including numerical and analytical models considers only the sensible heat transfer on primary air side. This may appear understandable since most current research efforts focus on the IEC application in hot and dry/moderate regions, where condensation would not happen

on primary air side.

The experimental studies include laboratory test and field measurement, mainly focusing on (1) cooling performance evaluation; (2) influence of parameters; (3) energy consumption by fans and pump; (4) optimization of operating conditions and configuration; (5) optimization of heat exchanger material; (6) indoor thermal comfort evaluation. The cooling performance of single stage IEC was tested mainly in dry regions. In recent decant, more research interests are put into IEC hybrid systems (including DEC/IEC, desiccant/IEC, hybrid IEC and mechanical cooling system and evaporative air-water system) and novel dew-point IEC (including traditional IEC, RIEC and M-cycle IEC). Higher cooling efficiency and COP can be achieved by the novel IECs and IEC systems, providing more flexibility and adaptability in various climatic regions and application fields. The theoretical and experimental research on the novel IECs and hybrid IEC systems is still at fast developing stage.

2.7.2 Research gap

Although IEC is being extensively used and related experimental and simulation research work has been carried out, current efforts have focused on evaluating the performance under dry and moderate conditions. Little previous studies involving the heat and mass transfer modeling of IEC in hot and humid conditions can be identified.

Furthermore, no experimental studies on evaluating IEC energy recovery performance in humid regions can be found in open literatures. In dry or moderate regions, there will be no condensation from primary air, thus, only sensible cooling performances were discussed in previous studies. However, owing to the high dew point temperature of fresh (primary) air in humid areas, condensation would occur on primary air side, which results in not only sensible cooling but also dehumidification. The heat and mass transfer process is much more complicated in this case compared with that of dry region cases. The condensation would greatly affect the overall performance of IEC, not only in sensible cooling but also in newly brought latent cooling. The lack of modeling and experimental research of IEC with condensation provide obstacles for applying hybrid IEC and mechanical cooling system in humid regions, in terms of intensive parameter study, configuration optimization and system performance prediction.

The literature review presented in this chapter has demonstrated that although there have been significant research interests and efforts to study IEC, there are still a number of areas where further in-depth research works are required focus on the IEC application in hot and humid regions, which summarized as follows.

1) The thermal model of IEC considering condensation from high humidity primary air has received little scholarly attention and experimental-based validation.

2) The estimation of annual energy saving of IEC in majority existing studies was based on typical design weather conditions; no study has been conducted for year-round dynamic simulation of IEC heat recovery system considering both non-condensation and condensation conditions.

3) The parameters study and sensitivity analysis of IEC with condensation is lacking. Not only the sensible but also the latent performance of IEC should be investigated.

4) The optimized geometric dimensions of IEC under condensation condition were not presented in previous literatures. It can be deduced that the optimized IEC configuration under condensation state may differ from that of non-condensation state because of distinguished heat and mass transfer process.

5) Although experimental research has been conducted to various IEC and IEC system, only the sensible cooling performance was investigated. No experimental work has been reported on the IEC performance with condensation from high humidity primary air. Both the sensible and latent heat recovery performance of IEC under various operating conditions needs in-depth study to understand its overall thermal performance.

Chapter 3

Proposition

3.1 Project title

This thesis focuses on the work related to the modeling and experimental study of IEC with an emphasis on its condensation state when IEC applied in hot and humid regions for energy recovery in A/C system. The proposed research work to be reported in this thesis is therefore entitled ‘Modeling and experimental study of indirect evaporative cooler (IEC) for energy recovery in hot and humid regions’.

3.2 Aims and objectives

The objectives of the research work are as follows:

To establish a simplified IEC model and integrate the model into building simulation software for annual hourly simulation of IEC energy recovery system considering both non-condensation and condensation conditions. A detail case study will be conducted.

To establish a numerical model of IEC considering condensation from high humidity primary air. Intensive parameter analysis under three operating states (non-condensation,

partial condensation and total condensation) will be comparatively studied.

To conduct parameter sensitivity analysis of IEC with condensation using established numerical model and optimize the most influential parameters.

To experimentally investigate the IEC performance under various operating conditions (wet/dry condition, dry/humid condition) and validate the established models.

3.3 Research methodologies

Experimental, numerical and analytical methods will be employed throughout the research work. The research flow chart is shown in Fig. 3.1.

Firstly, a simplified analytical model for IEC will be established, specially taking account the condensation from high humidity primary air. The model will be developed based on modified ε-NTU method. A method for judging three operating conditions (non-condensation, partial condensation and total condensation) of IEC will be proposed.

A simulation method will then be proposed by integrating the simplified model into TRNSYS software for annual dynamic simulation of IEC energy recovery system considering three operating states of IEC. A case study in Hong Kong will be conducted

based on the simulation method.

A novel numerical IEC model will be established by especially taking into consideration of condensation and wettability. The influence of nine parameters (temperature, humidity and velocity of two air flows, channel gap, wettability and cooler height) will be comparatively analyzed under three operating states (non-condensation, partial condensation and total condensation) using four proposed evaluation indexes.

Based on the numerical model, the parameter sensitivity analysis by orthogonal test will be presented. The parameter sensitivity was analyzed among seven parameters to find the most influential ones before the IEC optimization conducted.

An experimental IEC test rig will be set up to investigate the IEC performance under various operating conditions (wet/dry, dry/humid). The comparison study in term of sensible and latent cooling capacity, energy consumption, system efficiencies and COP can be made among four operating modes. In addition, the experimental data can be used for validation the established theoretical models.

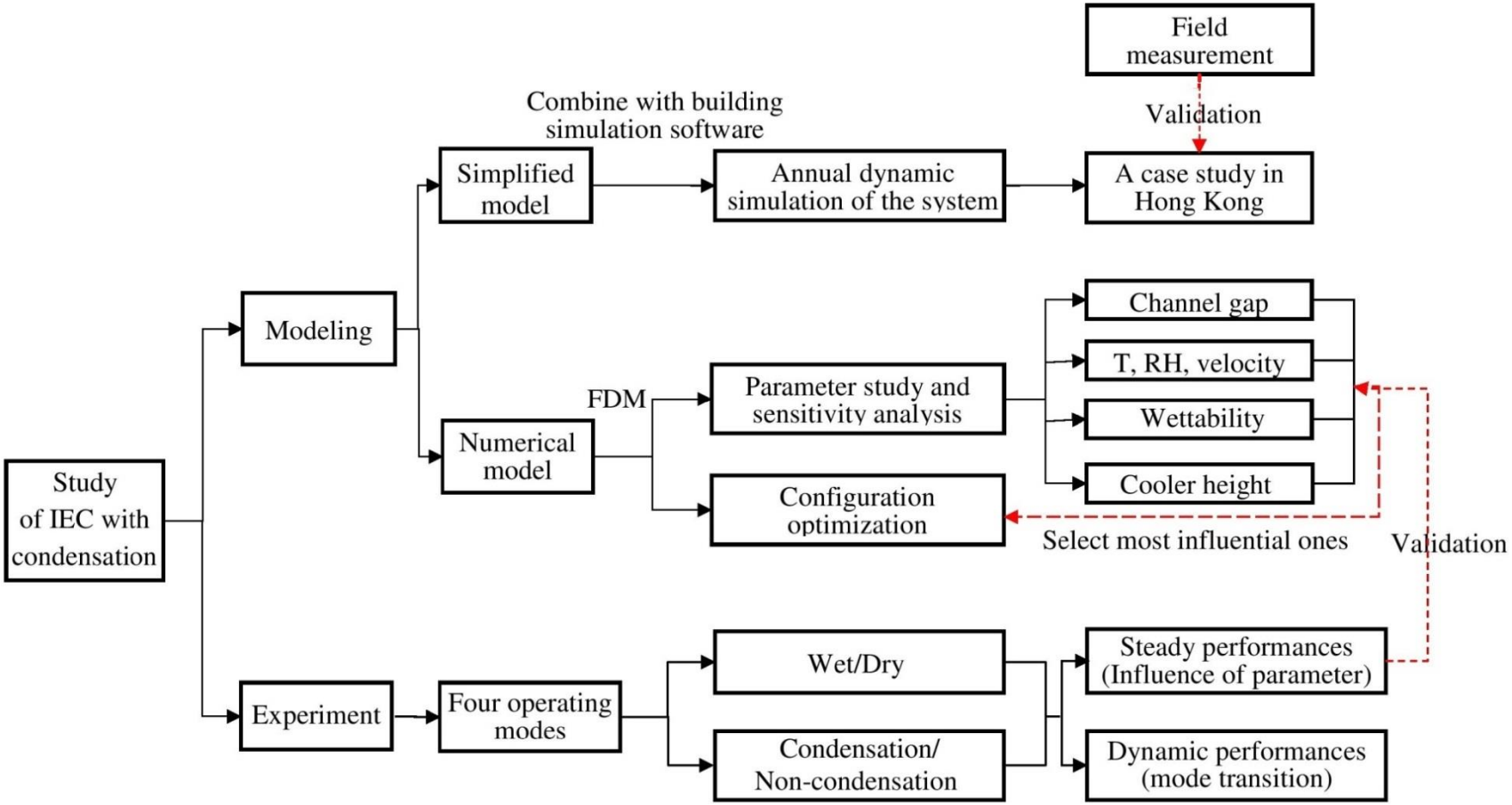

Fig. 3.1 Research flow chart of the thesis

Chapter 4

Simplified analytical model of IEC considering condensation

4.1 Introduction

Nowadays, IEC application is not limited to arid regions where it is initially used. In hot and humid regions, an IEC, installed before an AHU, is used to pre-cool the incoming fresh air for energy conservation of A/C system by recovering cooling capacity from exhausted air. Many studies have been conducted to investigate IEC performance for independent cooling and some studies focus on IEC hybrid system in aspect of energy saving potential and economic benefit.

However, it was found condensation in IEC was not considered in previous simulation work for system performance evaluation. It is understandable for neglecting condensation for two reasons: 1) most studied cases are in dry and moderate regions, where the fresh air humidity is not as high as in Hong Kong; 2) fresh air is usually used as both primary air and secondary air so that the plate surface temperature is always higher than the air dew point temperature. However, in a hot and humid region like Hong Kong, condensation would occur in dry channels. The heat and mass transfer process is much more complicated in this case and will greatly affect IEC performance.

The lacking of IEC model with condensation becomes obstacle in accurately predicting the performance of IEC heat recovery system in hot and humid regions. Besides, in engineering field, the annual performance of a system is usually evaluated by software simulation, in which the component model should satisfy three characteristics: 1) short computing time; 2) reasonable accuracy; 3) less input parameters and can be easily incorporated with software modules. However, the lacking of such IEC model considering condensation makes the existing simulation software incapable for direct simulation.

In this Chapter, therefore, a simplified analytical model for IEC is developed under different operating state especially under condensation state, aims to provide an easy-to-use component model for existing building simulation software. Correspondingly, a method for judging three IEC operating states (non-condensation, total condensation and partial condensation) is proposed. Finally, the model is validated by the published data from literatures.

4.2 Three condensation states

In IEC heat recovery system, the exhaust air from the indoor with lower humidity and temperature is used as secondary air for enhancing the evaporative cooling. The primary

air in the dry channels is cooled down by the low temperature adjacent wall. The schematic diagram of a typical plate type counter flow IEC is shown in Fig. 4.1 with geometrical dimensions and modeling coordinates. The inlet primary air with different humidity and temperature would result in three possible operating states of IEC, namely non-condensation, partial condensation and total condensation, as shown in Fig. 4.2.

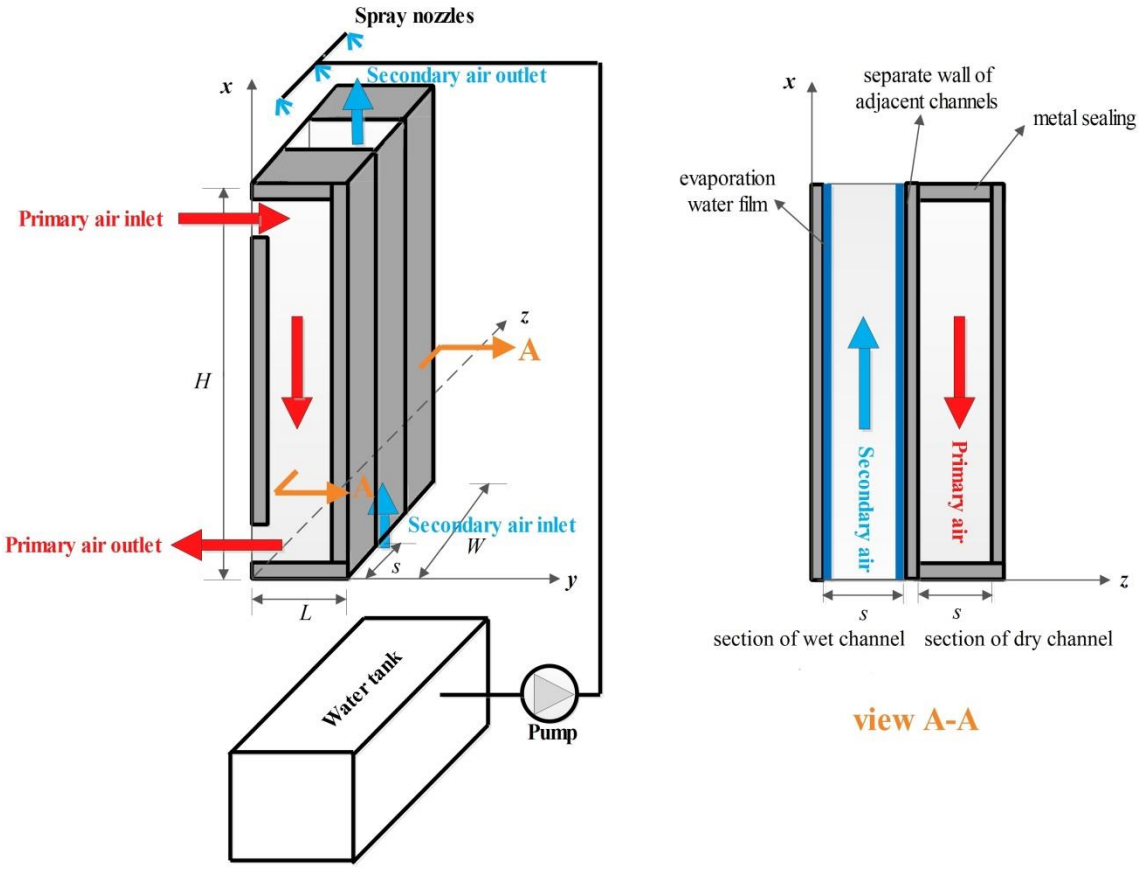

Fig. 4.1 Schematic diagram of plate type counter flow IEC

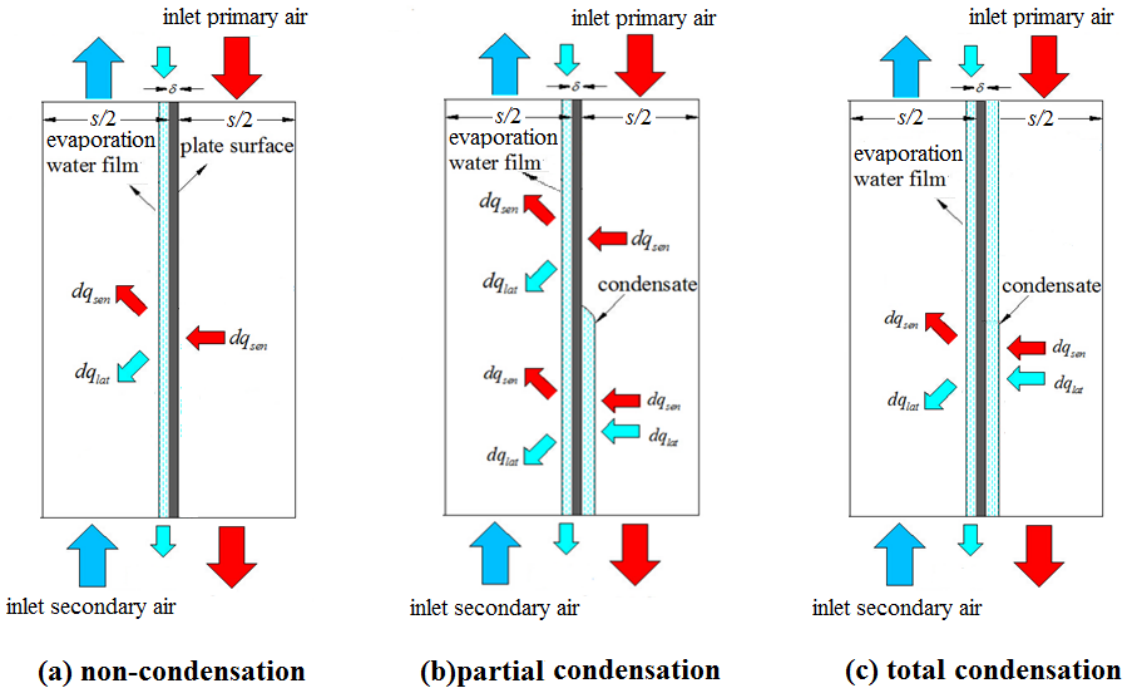

Fig. 4.2 Sketch diagrams of IEC under three condensation states

Non-condensation state occurs when the inlet primary air is dry and $t_{dew,p}$ is always lower than the plate surface temperature. The primary air is sensibly cooled and the outlet temperature is limited to the $t_{dew,p}$. Total condensation state occurs when the inlet primary air is very humid so that $t_{dew,p}$ is higher than the plate surface temperature at the inlet air entrance. Under partial condensation state, the condensation would not taking place until at one point the plate surface temperature is equal to the $t_{dew,p}$. Under both condensation states, the primary air is not only sensibly cooled but also dehumidified. Both the sensible and latent heat transfer is involved in the two channels simultaneously.

4.3 Simplified analytical model development

The models of IEC under three condensation states are developed on the basis of ε-NTU method as it is a user-friendly model with short computing time and appropriate for annual simulation. Firstly, proper deduction is made to redefine the heat transfer coefficient and the specific heat capacity for the wet surface, which can be applied to the evaporation and condensation surfaces. The models of IEC under three condensation states are then established by using the modified parameters and analogizing to the dry surface heat exchanger. A method for judging the three condensation states is also proposed. Lastly, the additional power consumption by the fans and pump is modeled for comprehensively evaluating the IEC performance.

The IEC models are built on the premise of the following assumptions: 1) heat and mass transfer processes are in steady state and performed in the direction perpendicular to the wall; 2) wet surface is fully covered by the stationary water film; 3) IEC is adiabatic; 4) heat and mass transfer coefficients are constant; 5) Le=1 for the evaporation and condensation surfaces; 6) flow pattern is counter current.

4.3.1 Derivation of modified parameters for wet surface

The following is the derivation process of solving the modified heat transfer coefficient

on the wet surface. In the water-air system, the saturated interface layer temperature t_{inter} is reasonably assumed to be equal to the water film temperature t_w. Total heat transfer between the water film and mainstream air is given by:

$$Q_{tot} = h(t - t_{\text{inter}}) + h_m h_{fg}(\omega - \omega_{\text{inter}}) \tag{4.1}$$

where, t and ω are the temperature and moisture content of the mainstream air flow, respectively; ω_{inter} is the saturated moisture content of the air at the interface temperature t_{inter}; the latent heat of the water vapor can be calculated as h_{fg}=1.84t_{wb}+2500 (kJ/kg).

If the total heat transfer rate is expressed by the wet-bulb temperature difference, it gives:

$$Q_{tot} = h_w(t_{wb} - t_{\text{inter}}) \tag{4.2}$$

For the moisture air, the isotherm of wet-bulb temperature can be approximated as isenthalpic. So the air enthalpy can be expressed in two ways:

$$i = c_{pa}t + h_{fg}\omega \tag{4.3}$$

$$i = c_{pa}t_{wb} + h_{fg}\omega_{sat} \tag{4.4}$$

where, ω_{sat} is the saturated moisture content at the t_{wb}, kg/kg.

By solving Eq. (4.3) and (4.4), the air temperature can be given by:

$$t = t_{wb} + \frac{h_{fg}}{c_{pa}}(\omega_{sat} - \omega) \tag{4.5}$$

By substituting Eq. (4.5) into Eq. (4.1) and assuming Lewis relationship is satisfied on both evaporation and condensation surfaces [Desrayaud & Lauriat 2001], i.e, $h_m = \frac{h}{c_{pa}}$, the total heat transfer rate yields to:

$$Q_{tot} = (t_{wb} - t_{inter})\left[h(1 + \frac{h_{fg}}{c_{pa} e}) \right] \tag{4.6}$$

where, $e = \frac{\partial t_{wb}}{\partial \omega_{sat}} \approx \frac{t_{wb} - t_{inter}}{\omega_{sat} - \omega_{inter}}$, which can be regarded as the slope of the line connecting two points of the saturated moisture air. The moisture content of the saturated air ω_{sat} under certain t_{wb} can be calculated by empirical equation recommended by ASHRAE.

$$In\left(P_{qb}\right) = \frac{c_1}{T} + c_2 + c_3 T + c_4 T^2 + c_5 T^3 + c_6 In\left(T\right) \tag{4.7}$$

$$\omega_{sat} = 0.622 \frac{P_{qb}}{B - P_{qb}} \tag{4.8}$$

where,

$c_1 = -5800.2206, c_2 = 1.3914993, c_3 = -0.048640239, c_4 = 0.41764768 \times 10^{-4},$
$c_5 = -0.14452093 \times 10^{-7}, c_6 = 6.5459673$

By comparing Eq. (4.2) and (4.6), the modified heat transfer coefficient based on wet-bulb temperature can be expressed as:

$$h_w = h(1 + \frac{h_{fg}}{c_{pa} e}) \tag{4.9}$$

The following is the deduction process of solving the modified specific heat capacity. The total heat transfer rate of the air flow can be calculated as:

$$Q_{tot} = m \cdot [c_{pa}(t_{out} - t_{in}) + h_{fg}(\omega_{out} - \omega_{in})] = m(i_{out} - i_{in}) \tag{4.10}$$

If the total heat transfer rate of the air flow is expressed by the wet-bulb temperature difference, given as:

$$Q_{tot} = m c_{paw}(t_{wb,out} - t_{wb,in}) \tag{4.11}$$

By comparing Eq. (4.10) and (4.11), the air enthalpy can be expressed as $i = c_{paw} \cdot t_{wb}$, Thus,

$$c_{paw} = \frac{\partial i}{\partial t_{wb}} \tag{4.12}$$

On the other hand, the enthalpy $i = c_{pa} t_{wb} + h_{fg} \omega_{sat}$ can also be written as:

$$\frac{\partial i}{\partial t_{wb}} = c_{pa} + h_{fg} \cdot \frac{\partial \omega_{sat}}{\partial t_{wb}} \tag{4.13}$$

By comparing Eq. (4.12) and (4.13), the modified specific heat capacity is given as:

$$c_{paw} = c_{pa} + \frac{h_{fg}}{e} \tag{4.14}$$

4.3.2 Simplified modeling of IEC under three condensation states

The models of IEC are established by applying the above h_w and c_{paw} to the evaporation and condensation surface. In this way, ε-NTU method can be applied to the wet surface heat exchanger by analogy to the dry surface heat exchanger. The mathematic equations of modeling IEC under non-condensation and total condensation are given in Table 4 .1. The model for partial condensation is given thereafter.

Table 4.1 Modified ε-NTU method for non-condensation and total condensation states

Parameter	Non-condensation	Total condensation
Heat transfer coefficient	$h_{w,e} = h(1+\frac{h_{fg}}{c_{pa}e})$	$h_{w,e} = h(1+\frac{h_{fg}}{c_{pa}e_e})$, $h_{w,c} = h(1+\frac{h_{fg}}{c_{pa}e_c})$
Specific heat capacity	$c_{paw} = c_{pa} + \frac{h_{fg}}{e_e}$	$c_{paw,e} = c_{pa} + \frac{h_{fg}}{e_e}$, $c_{paw,c} = c_{pa} + \frac{h_{fg}}{e_c}$
Slope of saturated air	$e_e = \frac{t_{wb,\mathrm{s,out}} - t_{wb,\mathrm{s,in}}}{\omega_{\mathrm{sat,s,out}} - \omega_{\mathrm{sat,s,in}}}$	$e_c = \frac{t_{wb,\mathrm{p,out}} - t_{wb,\mathrm{p,in}}}{\omega_{\mathrm{sat,p,out}} - \omega_{\mathrm{sat,p,in}}}$ $e_e = \frac{t_{wb,\mathrm{s,out}} - t_{wb,\mathrm{s,in}}}{\omega_{\mathrm{sat,s,out}} - \omega_{\mathrm{sat,s,in}}}$
Heat transfer rate	$Q_{tot} = m_p c_{pa}\left(t_{p.in} - t_{p,out}\right)$ $Q_{tot} = m_s c_{paw}(t_{wb,\mathrm{s,out}} - t_{wb,\mathrm{s,in}})$	$Q_{tot} = m_p c_{paw,p}(t_{wb,p,\mathrm{in}} - t_{wb,p,\mathrm{out}})$ $Q_{tot} = m_s c_{paw,s}(t_{wb,\mathrm{s,out}} - t_{wb,\mathrm{s,in}})$
Total heat transfer coefficient	$K = (\frac{1}{h} + \frac{\delta}{\lambda} + \frac{\delta_w}{\lambda_w} + \frac{1}{h_{w,e}})^{-1}$	$K = (\frac{1}{h_{w,\mathrm{e}}} + \frac{\delta}{\lambda} + \frac{\delta_w}{\lambda_w} + \frac{1}{h_{w,\mathrm{c}}})^{-1}$
Wet-bulb efficiency	$\varepsilon = \frac{1-\exp\left[-NTU\cdot(1-Cr)\right]}{1-Cr\cdot\exp\left[-NTU\cdot(1-Cr)\right]}$ $(Cr = \frac{m_p c_{pa}}{m_s c_{paw}}, NTU = \frac{KA}{m_p c_{Pa}})$ $\varepsilon = \frac{t_{p,in} - t_{p,out}}{t_{p,in} - t_{wb,\mathrm{s,in}}}$	$\varepsilon = \begin{cases} \frac{1-\exp\left[-NTU_w\cdot(1-Cr_w)\right]}{1-Cr_w\cdot\exp\left[-NTU_w\cdot(1-Cr_w)\right]} (Cr_w<1) \\ \frac{NTU_w}{1+NTU_w} (Cr_w=1) \end{cases}$ $(Cr_w = \frac{(mc_{paw})_{\min}}{(mc_{paw})_{\max}}, NTU_w = \frac{KA}{(mc_{paw})_{\min}})$ $\varepsilon = \frac{(t_{wb,in} - t_{wb,out})_{\max}}{t_{wb,p,in} - t_{wb,s,in}}$
Surface temperature	$t_{surf,out} = t_{p,out} - \frac{R_{p,out,d}\times(t_{p,out} - t_{s,in})}{R_{p,out,d} + R_w + R_{s,in,d}}$	$t_{p,out} = t_{wb,p,out} + (t_{p,in} - t_{wb,p,in})\exp(-\frac{hA}{m_p c_{pa}})$ $t_{surf,in} = t_{p,in} - K\cdot\frac{(t_{p,in} - t_{s,out})}{h_{w,\mathrm{c}}}$

The water film thickness in wet channel is estimated by Nusselt empirical formula [Nusselt 1916]:

$$\delta_w = \left(\frac{3\mu\Gamma}{\rho^2 g} \right)^{\frac{1}{3}} \tag{4.15}$$

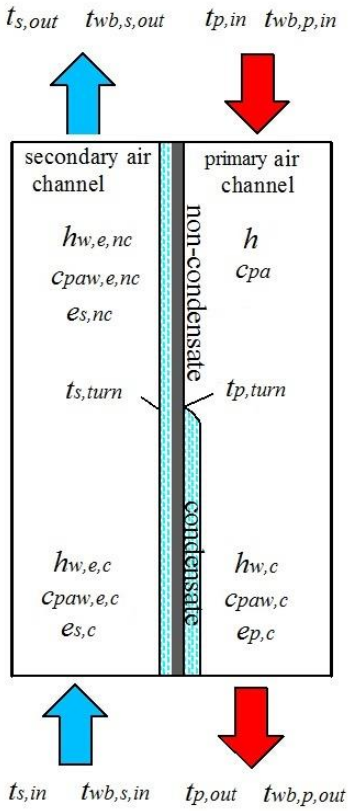

Fig. 4.3 Modified parameters under partial condensation state

As the channel gap of IEC is very small and the air velocity is usually less than 5 m/s for ensuring the efficient heat transfer, the air flow can be regarded as laminar flow in the IEC. So the heat transfer coefficient for the fully developed laminar flow in the parallel air channel can be calculated as [Shames 1988]:

$$h = \frac{0.023\left(\frac{u}{\upsilon} \right)^{0.8} \cdot Pr^{0.3} \cdot \lambda}{d_e^{\,0.2}} \tag{4.16}$$

For the plate type heat exchanger, the hydraulic diameter of the air channel can be calculated as: d_e =2s.

The diagram of partial condensation in IEC and corresponding modified specific heat capacity and heat transfer coefficient in different regions are shown in Fig.4.3. The detailed calculation procedures in the non-condensation and condensation regions are the same with those of Table 4.1. At the turning point (the point separates condensation and non-condensation region), the plate surface temperature should be equal to the $t_{p,dew,in}$. The heat balance equation at the turning point is given by:

$$h \cdot \left(t_{p,turn} - t_{p,dew,in} \right) = h_{w,e,nc} \cdot \left(t_{p,dew,in} - t_{wb,s,turn} \right) \tag{4.17}$$

The heat balance equations in the non-condensation and condensation regions are:

$$m_p c_{pa} \left(t_{p,in} - t_{p,turn} \right) = m_s c_{paw,e,nc} \cdot \left(t_{wb,s,out} - t_{wb,s,turn} \right) \tag{4.18}$$

$$m_p c_{paw,c} \left(t_{wb,p,turn} - t_{wb,p,out} \right) = m_s c_{paw,e,c} \left(t_{wb,s,turn} - t_{wb,s,in} \right) \tag{4.19}$$

$$t_{wb,p,turn} = f(t_{p,turn}, \omega_{p,in}) \tag{4.20}$$

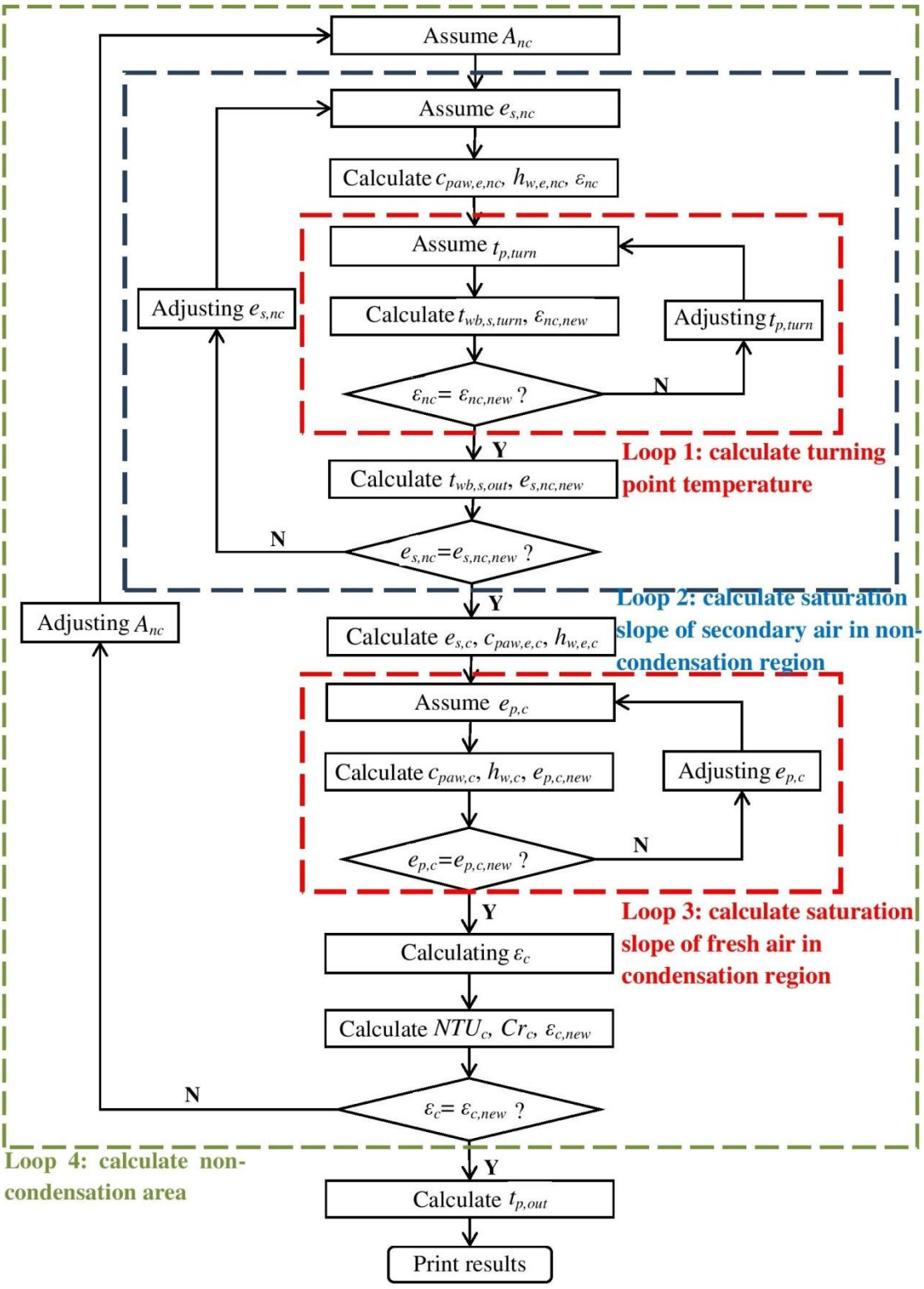

Fig. 4.4 Calculation flow chart of IEC on partial condensation state

The designed calculation flow chart of IEC on partial condensation state is shown in Fig.4.4. The moving boundary method is used.

4.3.3 Method for judging condensation state of IEC

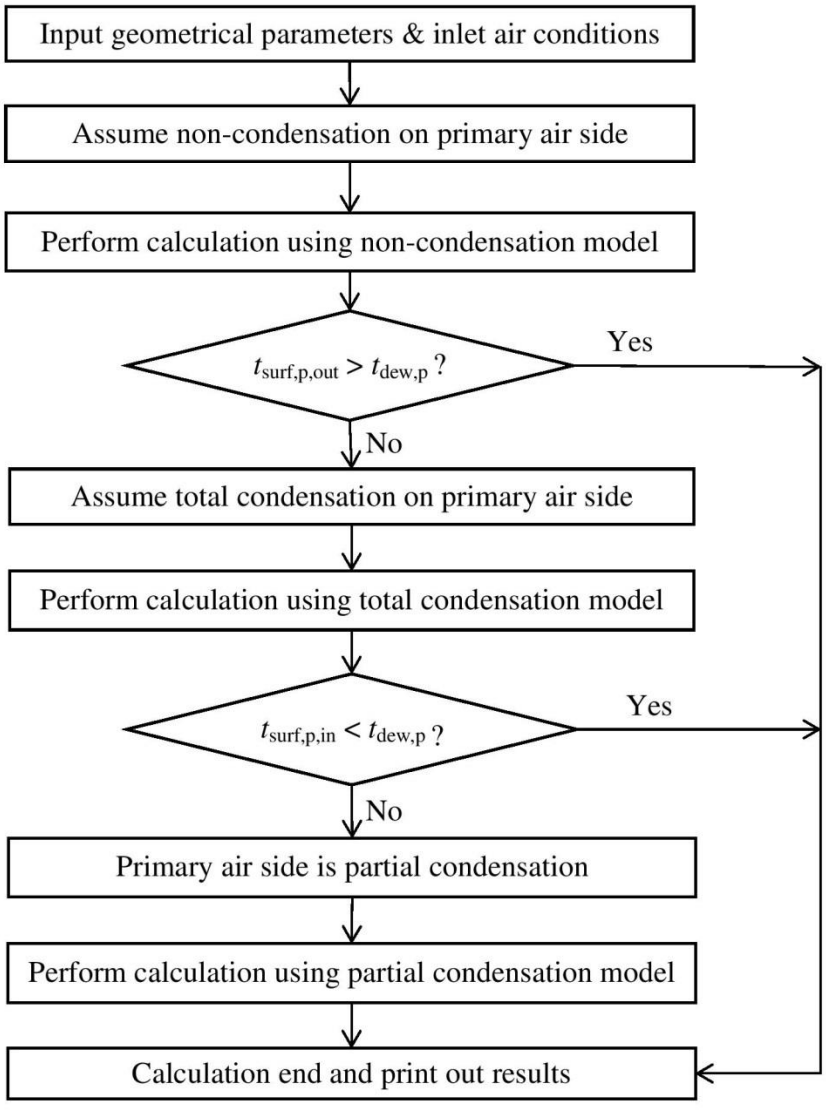

Fig. 4.5 Flow chart of judging IEC condensation state

The procedure of judging the three condensation states is proposed as Fig. 4.5. It is realized by three steps: making assumption of condensation state, comparing $t_{dew,p}$ with $t_{surf,out}$ and verifying the hypothesis. The assumption of IEC operating state is initially made to be non-condensation state. If it is invalid for $t_{surf,p,out} > t_{dew,p}$, the hypothesis is proved to be incorrect. The total condensation is then assumed. Similarly, if it is invalid for $t_{surf,p,in} < t_{dew,p}$, the hypothesis is proved to be incorrect and the operating state is confirmed to be partial condensation. The above thermal performance models of IEC were programmed by the self-defined MATLAB code. The judgment of operating states was conducted before performing the corresponding model.

4.4 Model of IEC energy consumption

The energy consumption is another important aspect for evaluating the performance of IEC heat recovery system. The energy-consumed components of IEC include supply air fan, exhaust air fan and circulation pump, which were calculated separately as follows. The power of air fans can be estimated by calculating the pressure drop using hydraulic calculation formulas:

$$\Delta P = \frac{f_{\mathrm{Re}}}{\mathrm{Re}} \cdot \frac{L}{d_e} \cdot \frac{\rho u^2}{2} \tag{4.21}$$

where f_{Re} is the friction coefficient; L is the length along the flow direction, m; Re is the Reynolds number, defined as $\mathrm{Re}=u\,d_e/\upsilon$.

The hydraulic diameter of the air channel is given by:

$$d_e = \frac{2ab}{a+b} \tag{4.22}$$

where a and b are the long side length and short side length of the channel cross section, m.

The friction coefficient can be calculated by empirical formula:

$$f_{\mathrm{Re}} = 96(1-1.3553\alpha+1.9467\alpha^2-1.7012\alpha^3+0.9564\alpha^4-0.2537\alpha^5) \tag{4.23}$$

where α is the dimensionless shape factor, given by α=b/a.

According to the experimental study, the resistance in the secondary air channel is 2.5~3 times larger than the primary air channel owing to the interaction with the spraying water drops [Zhao et al. 2010]. So the actual pressure drop in the primary air channel and secondary air channel can be calculated separately as:

$$\Delta P_p = \Delta P \tag{4.24}$$

$$\Delta P_s = 3\Delta P \tag{4.25}$$

The power of primary air fan is calculated as:

$$P_{p,\,fan} = \frac{V \times \Delta P_p}{3600 \times 1000 \times \eta_0 \times \eta_1} \times K \tag{4.26}$$

where $P_{p,\mathrm{fan}}$ is the power of the fan, kW; V is the air flow rate, m^3/h; η_0 is the internal efficiency of the fan, ranging from 0.7 to 0.8; η_1 is the mechanical efficiency, ranging from 0.85 to 0.95; K is motor capacity coefficient, ranging from 1.05 to 1.1. In the thesis, $\eta_{0,}\,\eta_1$ and K are supposed to be 0.75, 0.9 and 1.1, respectively.

The power consumption by the circulation pump is estimated as:

$$W = m_w \cdot g \cdot H_{tot} \cdot K \tag{4.27}$$

where m_w is the water flow rate, kg/s; H_{tot} is the total heat loss (m) of the water circulation system, which mainly consists of three parts: head loss of spray nozzle, head loss of gravity and head loss of valve.

$$H_{tot} = H_{nozzle} + H_{gravity} + H_{valve} \tag{4.28}$$

The recirculation water flow rate for fully covering the wet surface of IEC can be calculated by:

$$m_w = \Gamma \cdot (n_p + n_s) \cdot L \tag{4.29}$$

where the optimized water drenching density (Γ) of plate type IEC is 15~20 kg/m·h according to the experimental research [Zhang et al. 2006].

4.5 Model validation

The established models are validated under two different cases: non-condensation state and condensation state. Firstly, the experimental facility data derived by Alonso et al. [1998] were employed to validate the outlet air temperature of IEC under non-condensation state. The simulations were conducted by setting the same geometry and inlet air conditions as given in the experiments. There were three series of experimental cases presented with different range of inlet air temperature and RH. The comparison between the simulation results and experimental facility data are presented in Fig. 4.6. It is found that the developed model can predict the IEC performance with the largest discrepancy of 5.5% and average discrepancy of 2.7% for supply air temperature.

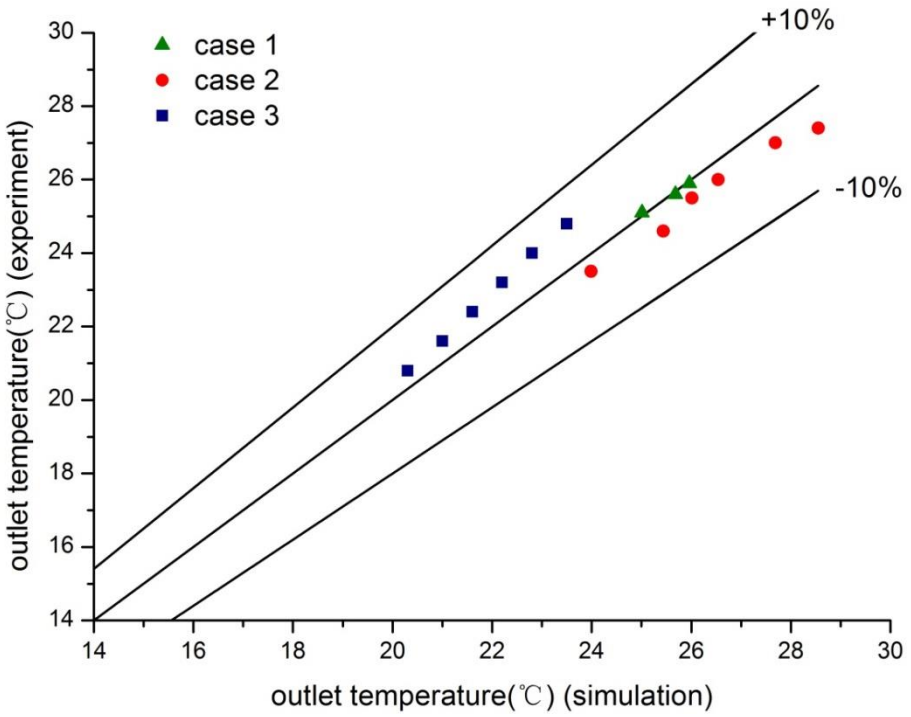

Fig. 4.6 Comparison between simulation and experiment results (non-condensation)

Next, the simulation results by present model under condensation states were validated by the numerical simulation results from latest published paper [Cui et al. 2015]. In this paper, the exhausted air (25℃, 50% RH) from an A/C room was used as the secondary air to pre-cool the humid fresh air. The temperature of the inlet fresh air ranged from 30℃ to 37.5℃ while RH ranged from 70% to 90%. The comparison between the present model and reference model are listed in Table 4.2. The present model can predict the outlet air temperature with the average discrepancy of 3.8% and largest discrepancy of 6.6%. The average discrepancy in predicting the outlet moisture content is 3.0% and largest discrepancy is 6.9%. The different results in predicting the outlet air parameters

may attribute to different mass transfer theories used. The numerical model in the reference is based on the Fick permeation law (film theory) while the present model based on the analogy law of the heat and mass transfer.

Table 4.2 Comparisons between the present model and reference model (condensation)

$t_{p,in}$	RH=0.7			RH=0.8			RH=0.9		
(℃)	Present	Ref.	Error	Present	Ref.	Error	Present	Ref.	Error
outlet air temperature(℃)									
30	22.5	21.9	2.9%	24.2	22.7	6.6%	24.9	23.6	5.9%
32.5	23.5	23.1	1.6%	26.0	24.3	6.6%	26.7	25.6	4.1%
35	25.6	24.9	2.6%	27.6	26.4	4.5%	28.4	27.9	2.0%
37.5	28.5	27.0	5.5%	29.4	28.7	2.4%	30.4	30.3	0.3%
outlet air humidity (g/kg)									
30	16.9	16.6	1.8%	18.2	17.4	4.4%	19.7	18.3	6.9%
32.5	18.6	17.9	3.5%	20.3	19.3	4.9%	21.9	20.9	4.6%
35	20.5	19.9	2.9%	22.5	21.8	3.1%	24.5	23.9	2.4%
37.5	22.8	22.6	0.9%	25.0	25.1	0.4%	27.5	27.6	0.4%

Through the validation above, the simplified model is reliable for accurately predicting the IEC performance in hot and humid regions.

4.6 Summary

In this Chapter, a simplified analytical model for IEC is developed under different operating state especially under condensation state. It aims to provide an easy-to-use component model to be integrated with building simulation software for annual

simulation of IEC heat recovery system when condensation would take place. Three possible operating states of IEC were identified in hot and humid regions, including non-condensation, partial condensation and total condensation. The model was developed on the basis of ε-NTU method by proper deduction and redefining two parameters (heat transfer coefficient and specific heat capacity) for the wet surface, so that they can be applied to the evaporation and condensation surfaces. The model is solved by the moving boundary method. Correspondingly, a method for judging the three operating states was proposed. Besides, the energy consumption model of IEC was established including the models for the fans and circulation pump. Finally, the model is validated by the published data in the literatures. The developed model can predict the IEC performances with average discrepancy of 2.7% for outlet temperature under non-condensation state, 3.8% for outlet temperature and 3.0% for outlet humidity under condensation state.

The availability of the model with reasonable accuracy and short compute time is expected to assist the development of system simulation method proposed in Chapter 5.

Chapter 5

Annual performance of IEC energy recovery system – method and case study

5.1 Introduction

In engineering fields, the annual performance prediction is important for the economic and technical evaluation of a technology. As indicated in Chapter 2, the annual performance predication and energy saving estimation are important aspects in IEC research and received wide research attentions. The most existing studies related to the IEC energy saving estimation are based on the single-stage IEC, DEC/IEC and desiccant/IEC. Although studies on IEC heat recovery system (schematic diagram shown in Fig. 5.1) have also been investigated, they were mainly certain typical weather conditions based, which is neither dynamic weather condition based, nor considers the hourly cooling load. In addition, in previous IEC heat recovery system reported, only sensible cooling capacity was detailed, without much attention paid to the latent cooling capacity of IEC owing to the condensation.

This chapter reports a novel method for annual simulation of IEC heat recovery system based on IEC component model described in Chapter 4. The simulation method is

expected to be greatly helpful for better predicting the IEC performances by considering possible condensation state in humid regions and taking account the dynamic weather conditions at hourly step. In this chapter, firstly, the simulation method by incorporating the IEC model into TRNSYS software is presented in detail. Secondly, a detail case study of a wet market in Hong Kong is presented. The hourly performance of IEC, chiller, fans and circulation pump in IEC heat recovery system are discussed. Besides, the simulation results are validated by the data collected from a field measurement.

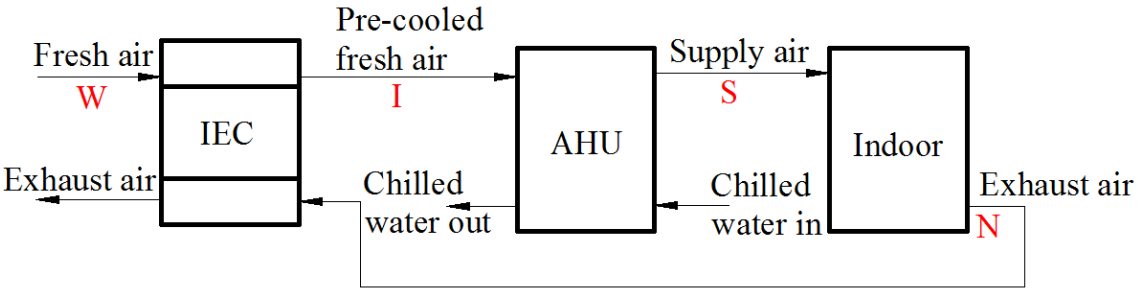

Fig. 5.1 Schematic diagram of IEC heat recovery system

5.2 Method for annual performance simulation

It is noted that the existing simulation software, such as Energyplus or TRNSYS, fails to take fully account of IEC condensation in humid regions. Besides, self-defined wet-bulb efficiency model are adopted without considering the IEC configuration and inlet air condition variation. So a novel dynamic simulation method is proposed by incorporating the validated IEC model considering condensation (developed in Chapter 4) with

TRNSYS software. The proposed method provides two advantages over the previous methods. Firstly, it considers the possible condensation according to different inlet air conditions. Secondly, the application of TRNSYS enables the simulation of the dynamic cooling load, indoor air parameter and free-cooling mode by adding control methods into the software.

The flow chart of simulation method is shown in Fig. 5.2. MATLAB is responsible for programming the code for IEC model, and energy balance model for AHU and indoor environment. TRNSYS is responsible for the simulation of the on/off state of the chiller, year-round dynamic cooling load and indoor temperature and humidity. All the above data could be exported from TRNSYS and read by the MATLAB code to perform dynamic simulation of IEC system.

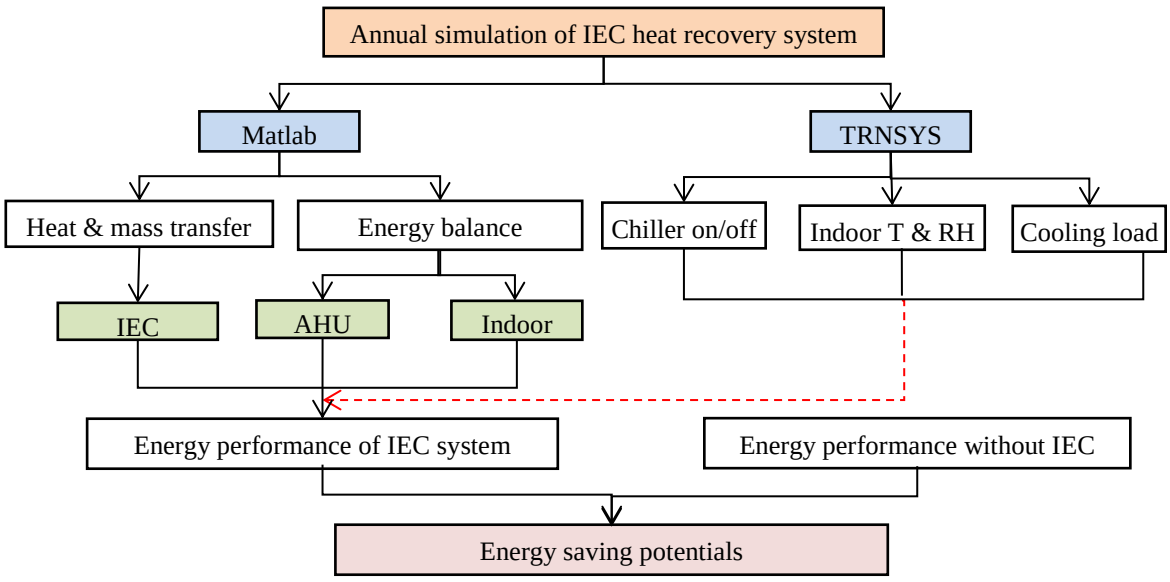

Fig. 5.2 Flow chart of simulation method for IEC heat recovery system

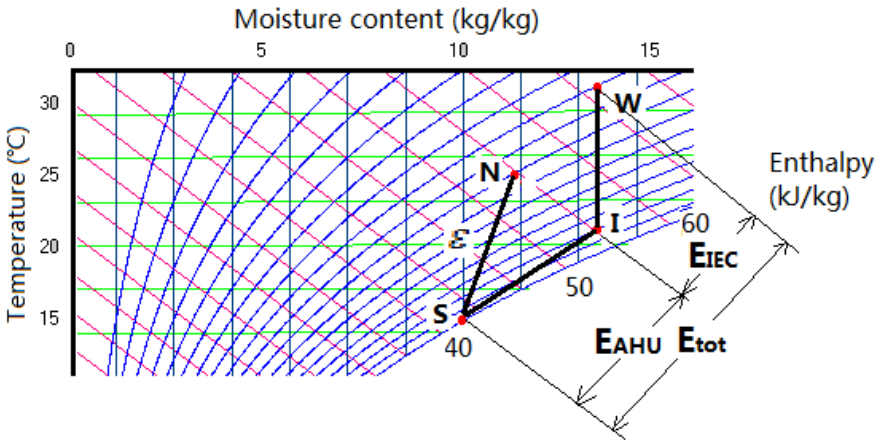

(a) IEC under non-condensation state

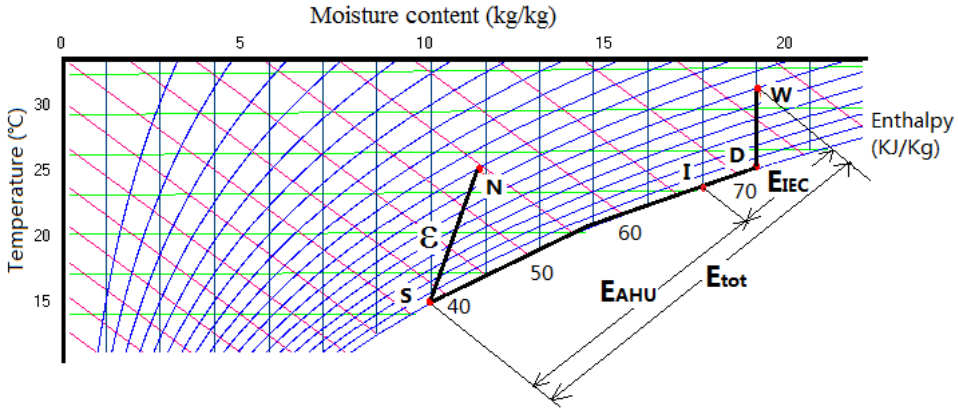

(b) IEC under condensation state

Fig. 5.3 Primary air handling process of IEC heat recovery system

Two kinds of primary air handling processes can be identified are shown in the psychometric chart in Fig. 5.3. Under non-condensation state (Fig. 5.3(a)), only sensible heat can be recovered by the IEC. The primary air is cooled with the temperature drop from 'W' to 'I' and then is further cooled in the AHU by removing the excess sensible heat and all the latent heat from 'I' to 'S'. In the end, the primary air is supplied to

indoor to eliminate the cooling load from ‘S’ to ‘N’. Under condensation state (Fig. 5.3(b)), both the sensible and latent heat can be recovered by the IEC. The primary air is firstly cooled by IEC from ‘W’ to ‘D’, and then dehumidified from ‘D’ to ‘I’ if the plate surface temperature is lower than the dew-point temperature of inlet air. The primary air is further cooled in AHU by removing the rest sensible and latent load.

According to the psychrometric chart, the energy saving by IEC and energy consumption by AHU are given by:

$$E_{IEC} = m_p \cdot \left(i_W - i_I \right) \tag{5.1}$$

$$E_{AHU} = m_p \cdot \left(i_I - i_s \right) \tag{5.2}$$

The flow rate of supply air varies according to the cooling load in VAV A/C system and can be determined by the indoor heat balance:

$$Q_{sen} = m_p \cdot c_{pa} \cdot (\mathrm{t}_N - \mathrm{t}_S) \tag{5.3}$$

where, Q_{sen} is the sensible cooling load, W; t_{N} and t_{S} are the indoor design temperature and supply air temperature, ℃.

A case study in Hong Kong using the proposed simulation method is conducted as follows.

5.3 Case introduction

The studied object is a wet market located in Hong Kong and 100% fresh air A/C system is adopted. The set point of the temperature and humidity in the conditioned room are 24℃ and 60%, and no heating is required in winter. There are two AHUs installed for the wet trade area and each one is responsible for half of the area. The layout of the wet market is shown in Fig. 5.4. The one-floor wet trade region with a total area of 260 m^2 and average height of 6.7 m lies in the inner zone with non-air-conditioned rooms scattered around. Another air-conditioned area is on the east side which regarded as adiabatic boundary. The detail of heat gain from building envelope, lighting, equipment, people and wet source are listed in Table 5.1. The schedule for lighting, equipment and people is from 6:00 to 24:00. The Hong Kong weather data is shown in Fig. 5.5.

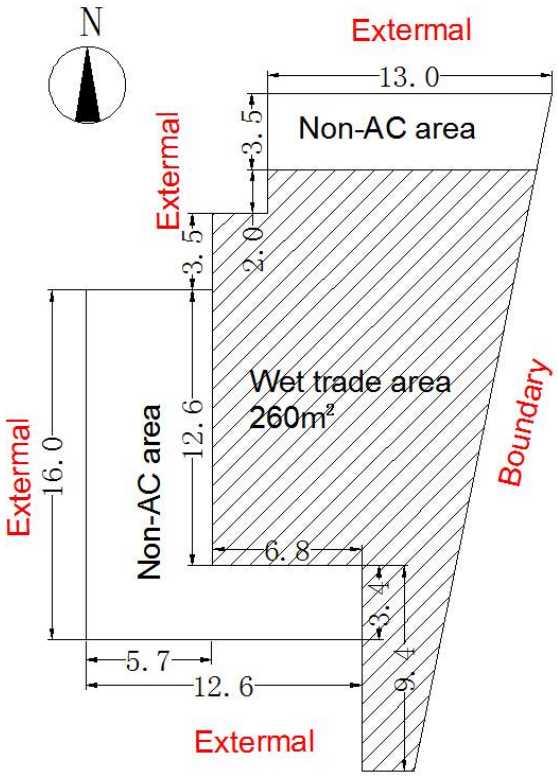

Fig. 5.4 Layout of the wet market

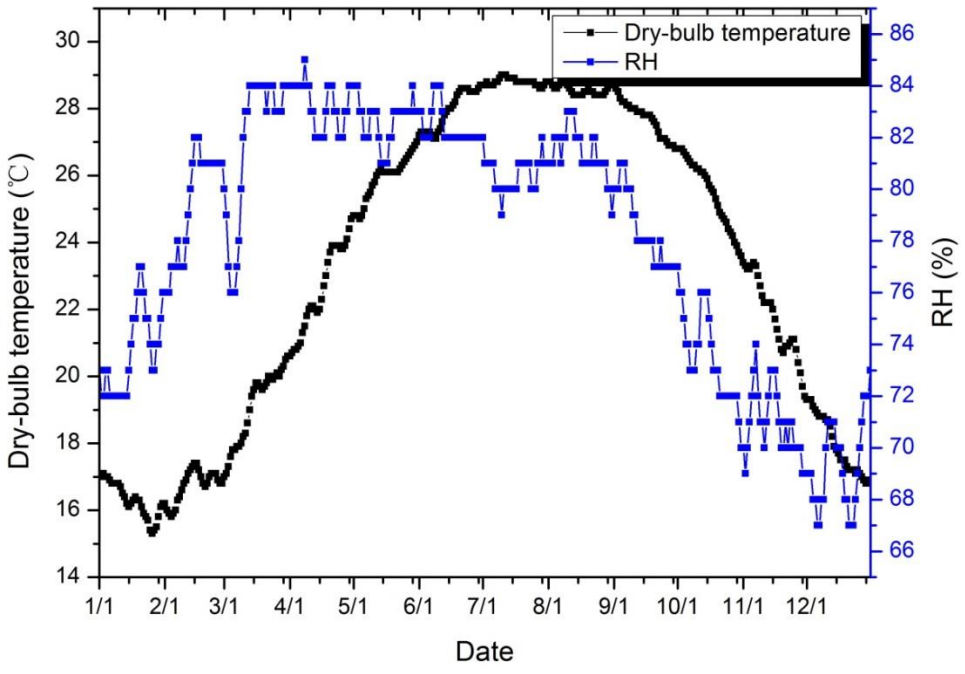

Fig. 5.5 Temperature and humidity in Hong Kong

Table 5.1 Detail of heat sources in wet market

Building envelope	Item	U-value ($W/m^2 \cdot ℃$)	Absorption coefficient
	external Walls	2.89	0.8
	Partition	2.64	_
	Roof	0.495	0.8
	Floor	2.341	_
Lighting	Item	Wattage(W/m^2)	Ballast
	overhead lighting	20	1
	task lighting	2.2	1
Equipment	Item	Wattage(W/m^2)	_
	electrical equipment	40	_
People	Item	Occupancy	Activity level
	People	142	light work
Wet source	Item	Area(m^2)	Evaporation rate (kg/h)
	water surface	36	78.5

The wet market adopts VAV A/C system with constant machine dew point temperature. The fresh air entering to the AHU is cooled to the designed machine dew point temperature of 12.8℃/12.8℃ (DB/WB) and the supply air temperature is 14 ℃ (1.2℃ temperature increase due to heat loss in the ducts). There are three A/C operation modes for the wet market listed in Table 5.2. The IEC only works on AC mode when the chiller is on. Under free cooling mode and ventilation mode, the fresh air should be bypassed and supplied directly into AHU in order to avoid the additional energy consumption by pump and fans of the IEC. The dimensions and configuration parameters of the IEC used in the case study are shown in Table 5.3. According to the unit size listed in Table

5.3, the head losses of H_{nozzle}, $H_{gravity}$ and H_{valve} are estimated to be 4.0m, 1.5m and 1.5m. Thus, the circulation water flow rate in this studied case can be calculated to be 2400 kg/h by Eq. (4.28) and Eq. (4.29).

Table 5.2 Three air-conditioning modes for the wet market

No.	Mode	Schedule/condition	Parameter
1	AC mode, VAV, chiller on	6:00~24:00, free cooling off	8.0 1/h (peak load); ≧4.0 1/h (part load)
2	Free cooling mode, chiller off	free cooling satisfy load	8.0 1/h
3	Ventilation mode, chiller off	24:00 ~ 6:00	8.0 1/h

Table 5.3 Dimensions and configuration parameters of the IEC

Parameters	Value
Channel length	0.7m
Channel width	0.7m
Primary air channel gap	5mm
Secondary air channel gap	5mm
Channel pairs	100
Secondary air to fresh air ratio	0.8

5.4 Results and discussion

5.4.1 IEC performance

The hourly sensible and latent cooling loads simulated by TRNSYS are shown in Fig.

5.6.

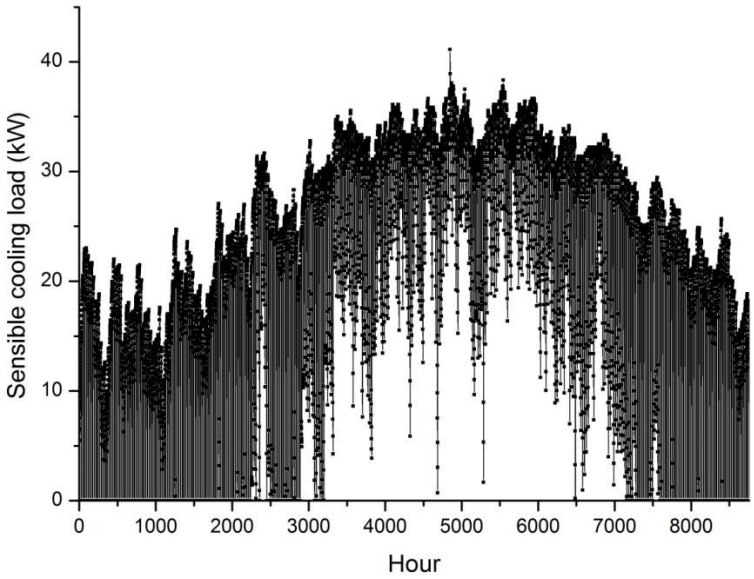

(a) sensible cooling load

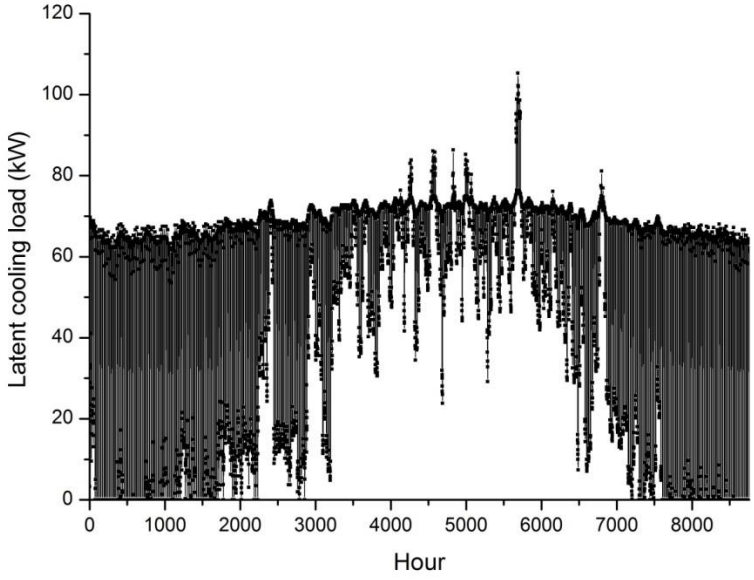

(b) latent cooling load

Fig. 5.6 Hourly cooling load in wet market

As the wet trade area locates in the inner zone of the building, the cooling load exists all

year round even in January and February. If the cooling load can be satisfied by the free cooling capacity, A/C system would be set as the free cooling mode with the chiller off in winter or transition season. The simulation results show that the chiller operation time is 4,938 hours and non-operation time (including free cooling mode and ventilation mode) is 3,822 hours. The annual cooling load for the wet trade area is 686,904 kWh, of which the sensible cooling load is 188,114 kWh and latent cooling load 498,790 kWh. Based on the heat balance Eq. (5.3), the maximum supply air volume for each AHU is calculated to be 6,228m^3/h.

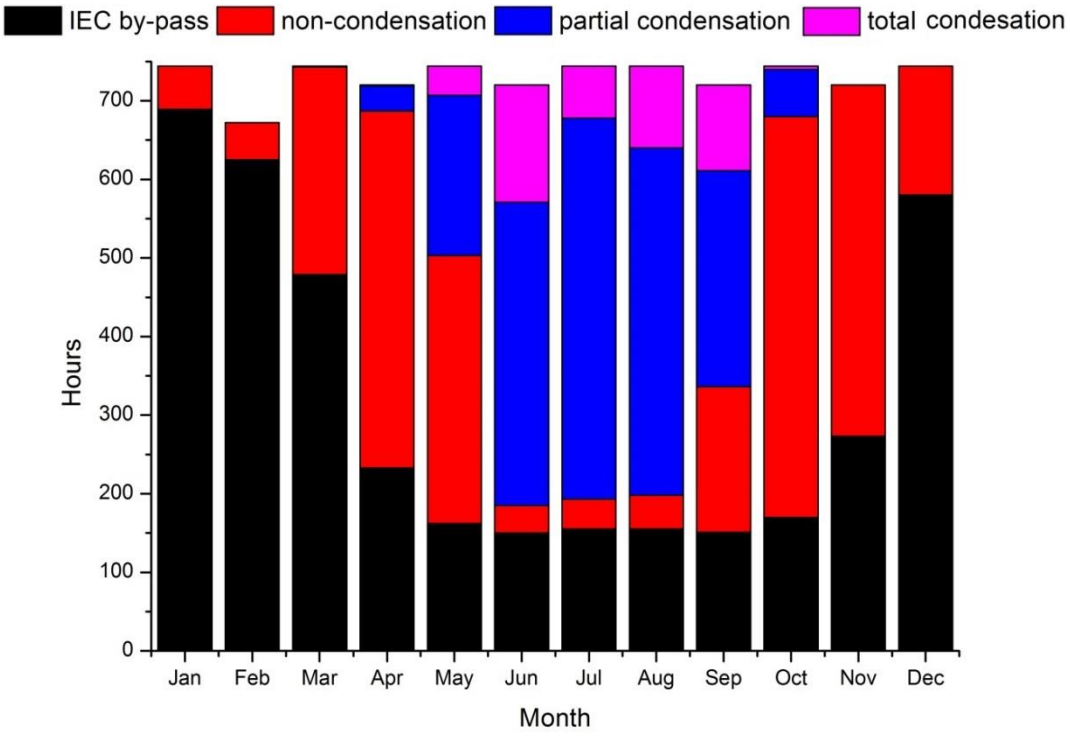

Fig. 5.7 Wettability frequency distribution in difference month

By adopting the method for judging IEC operating states with the weather data of the

typical meteorological year (TMY) in Hong Kong, the frequency distribution of the operating states in different months is shown in Fig. 5.7. In cooler months, such as December, January and February, free cooling mode can meet the cooling demand of the wet market in majority of the time. The IEC only operates at some peak load hours. In the transition seasons with mild temperature, such as March and November, the IEC almost works at non-condensation state because the moisture content of the fresh air is not as high as in the summer. From April to October, the chiller operates for a long time from 6:00 to 24:00 every day especially in June, July and August. Moreover, partial or even total condensation would occur from May to September. In the most hot and humid summer days, from June to August, the IEC nearly always operates under condensation state. The hour ratios of IEC operates in partial and total condensation states accounts for 74.3%, 74.1% and 73.4% in June, July and August, respectively. In a year, the non-condensation, partial condensation and total condensation state of IEC account for 52.3%, 38.2% and 9.5% of the total operation hours.

Through the results, we can see that the condensation from fresh air in IEC accounts for a large proportion of its annual operation time under Hong Kong weather, especially in hot and humid summer months when A/C is greatly needed. Therefore, the dehumidification effect has great influence on the performance of IEC and can not be ignored when modeling IEC in humid regions.

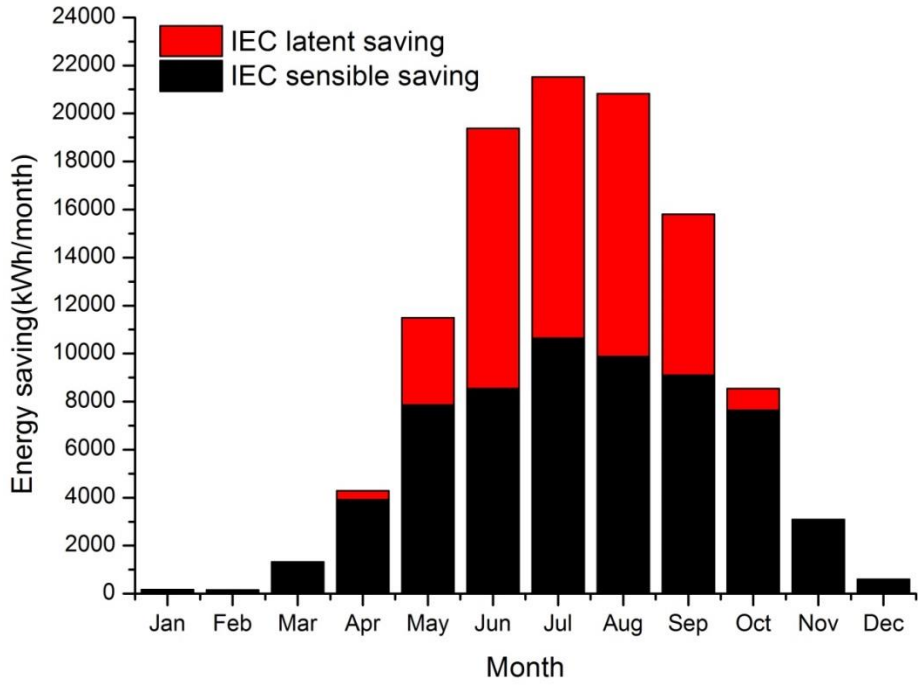

Fig.5.8 Sensible and latent cooling saving of IEC in different months

The sensible and latent cooling savings by IEC in different months are plotted in Fig. 5.8. The latent heat recovery performance is much better in summer than in winter owing to the condensation. In January, February, November and December, the sensible saving accounts for 100% of total saving. In June, July and August, the sensible saving accounts for 44.1%, 49.5% and 47.5% of the total monthly saving, respectively. The total annual energy saving by the IEC is 107,184 kWh, of which the sensible saving accounts for 58.7% and latent saving accounts for 41.3%. As the energy consumption of the A/C system without IEC heat recovery is 511,405 kWh, the hybrid IEC cooling system can save 21% of the energy.

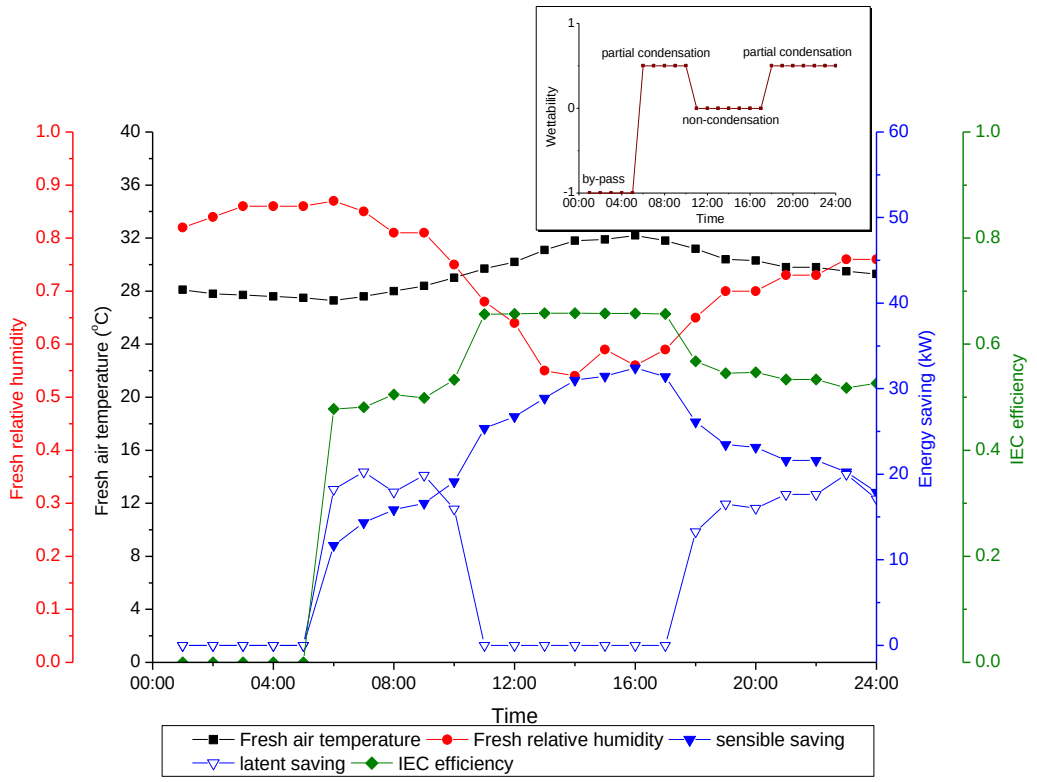

(a) typical hot and humid summer days (24th July)

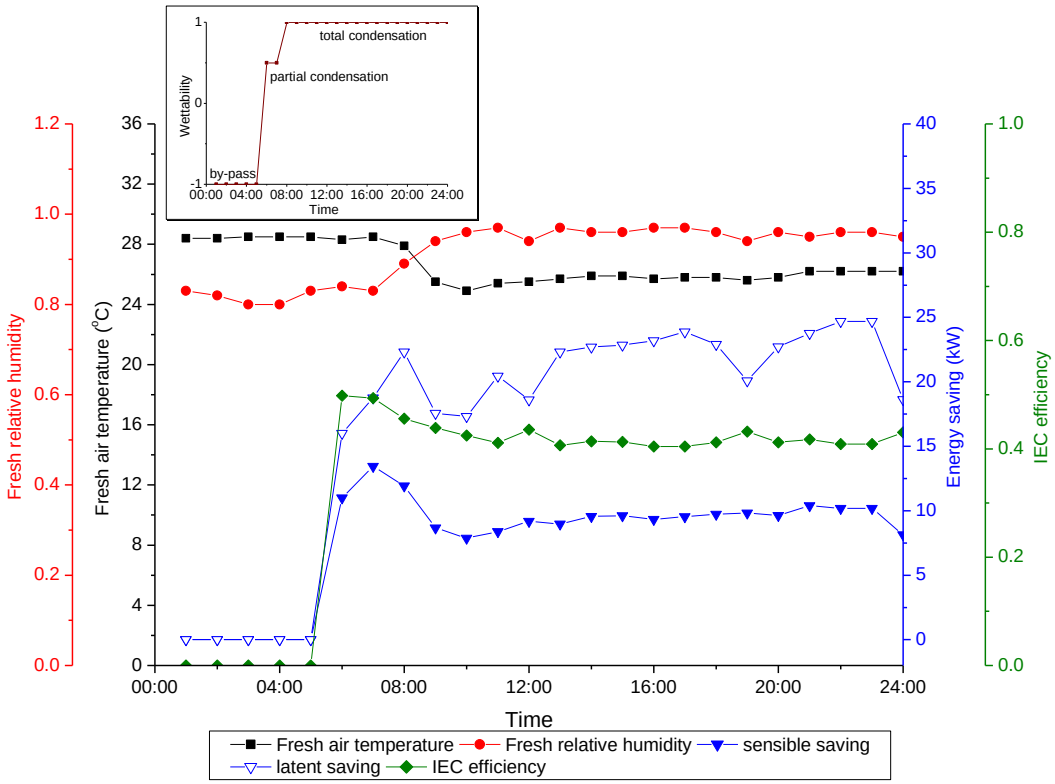

(b) extremely humid summer days (9th August)

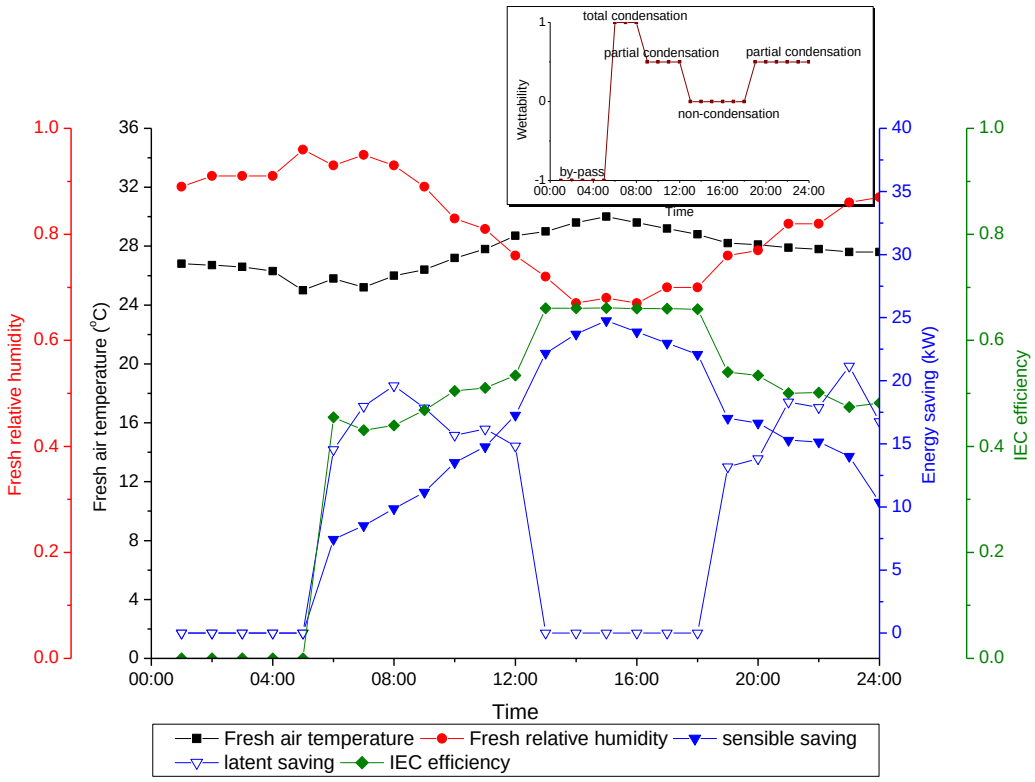

(c) summer day with large humidity variation (8th September)

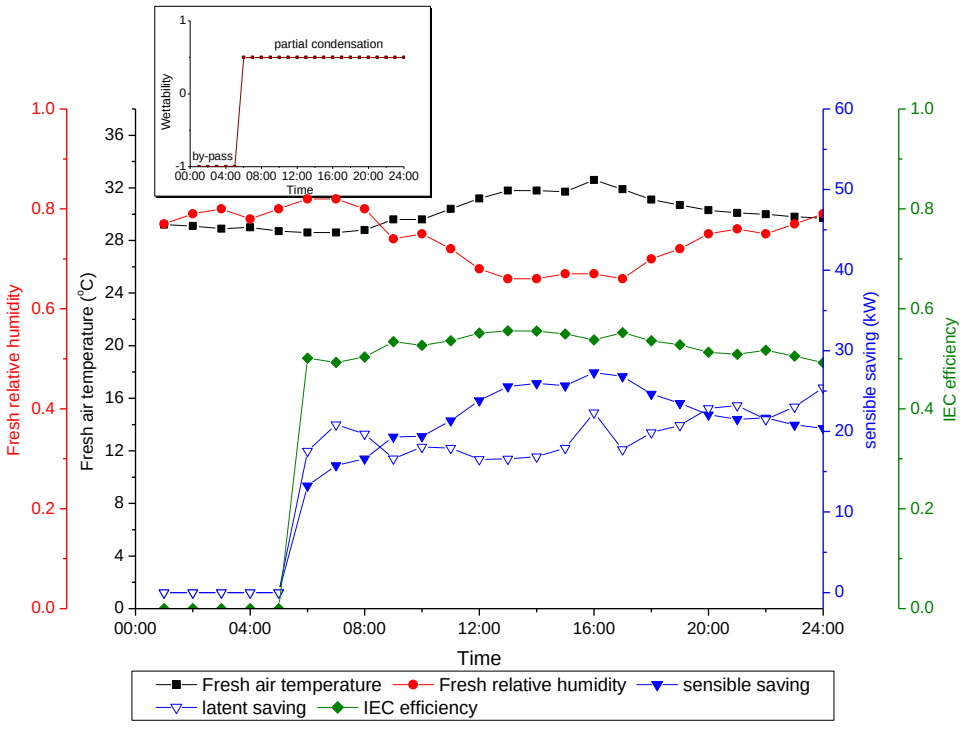

(d) relative dry and cool transition season (10th November)

Fig. 5.9 IEC performances on four typical days

The energy performances (including condensation state, sensible and latent saving and wet-bulb temperature efficiency) of the IEC in some typical days are shown in Fig. 5.9. It can be seen that the IEC efficiency remains almost steady if no condensation occurs, which varies only from 65.7% to 67.4% in four typical days. So the IEC efficiency can be regarded as constant under non-condensation state if the unit structure, secondary air condition and fresh air to secondary air ratio are determined. But when the fresh air humidity is high and results in condensation, the IEC efficiency decrease and the latent energy saving increases with the increase of the fresh air humidity. As presented in Fig. 5.9 (c), the IEC varies from total condensation to partial condensation and to non-condensation state in a day because of large variation of fresh humidity from 67% to 96%. Accordingly, IEC efficiency ranges from 43.1% to 66.0%. The lowest efficiency occurs at 7:00 when RH is 95.0% (highest of the day), and the latent energy recovery reaches the maximum of 18.0 kW, accounting for 67.8% of the total saving. In extremely humid days as Fig.14(b), the IEC operates almost under total condensation all day long and the average efficiency drops to 42.7% and latent energy saving accounts for 68.0% of the total energy saving.

5.4.2 Chiller performance

Fig. 5.10 shows the hourly chiller load of A/C system with and without IEC. It can be seen that the IEC shows a great potential in energy saving, and in particular reduces the peak load in summer months. The peak load of the chiller with IEC heat recovery is 137kW. Compared with the peak chiller load of 188kW without IEC heat recovery, the chiller capacity can be dramatically reduced by 27% so that the initial investment of the original A/C system can be cut down to a large extent. Therefore, in terms of economic benefit, the savings come from two aspects: the electricity saving during the operation and the deduction of the initial investment.

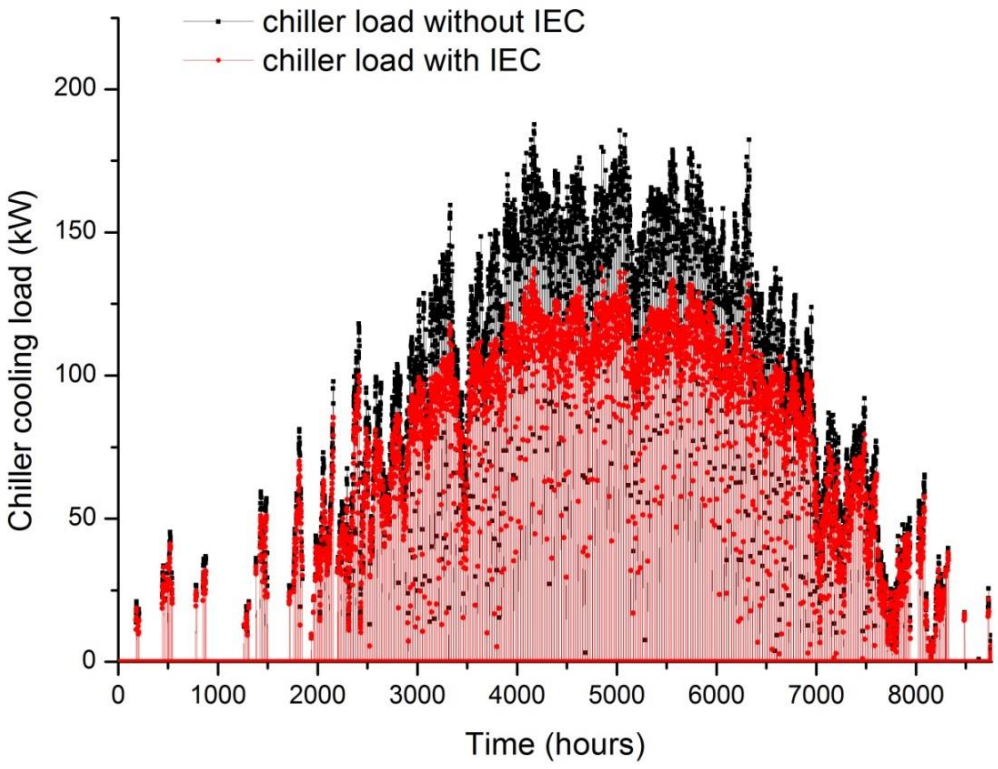

Fig. 5.10 Hourly chiller load of IEC heat recovery system

5.4.3 Annual power consumption

The models of fans and pump developed in Chapter 4.4 were used to simulate the annual energy consumption of IEC. The energy consumption of the fans varies with the dynamic cooling load and supply air rate. The energy consumption of the pump remains steady as long as IEC operates. The detailed simulation results were summarized in Table 5.4. The annual additional power consumption for one IEC is calculated to be 873 kWh/a. As there are two IECs installed in the wet market, the total power consumption is 1746 kWh/a.

Referring to the previous simulation results, the total annual energy saving by IEC is 107,184 kWh. The power saving is 23,819 kWh if the COP of chiller is 4.5. So the additional power consumption of IEC only takes up 7.3% of the total power saving.

Table 5.4 Simulation results of fans and pump

Items	Fresh air fan	Secondary air fan	Pump
Minimum air velocity (m/s)	2.7	2.2	_
Maximum air velocity (m/s)	4.9	3.9	_
Minimum power consumption(W)	26.1	49.0	50.3
Maximum power consumption(W)	83.9	157.8	50.3
Annual operation hours (h)	4938	4938	4938
Annual power consumption(kWh)	217	408	248

5.4.4 Comparison with field measurement

The data collected from a field measurement was used for validation of simulation results of IEC annual performance. The A/C system is located at Kowloon Park of Hong Kong. A testing IEC was installed in the A/C plant room to pre-cool the inlet fresh air, as shown in Fig. 5.11. The exhausted air from conditioned space was used as the secondary air with the same temperature and RH (24℃, 60%) as in the above simulation case. The inlet and outlet temperature, humidity, flow rate were collected by sensors and data loggers for one year with the operation schedule of 6:00 to 24:00 every day.

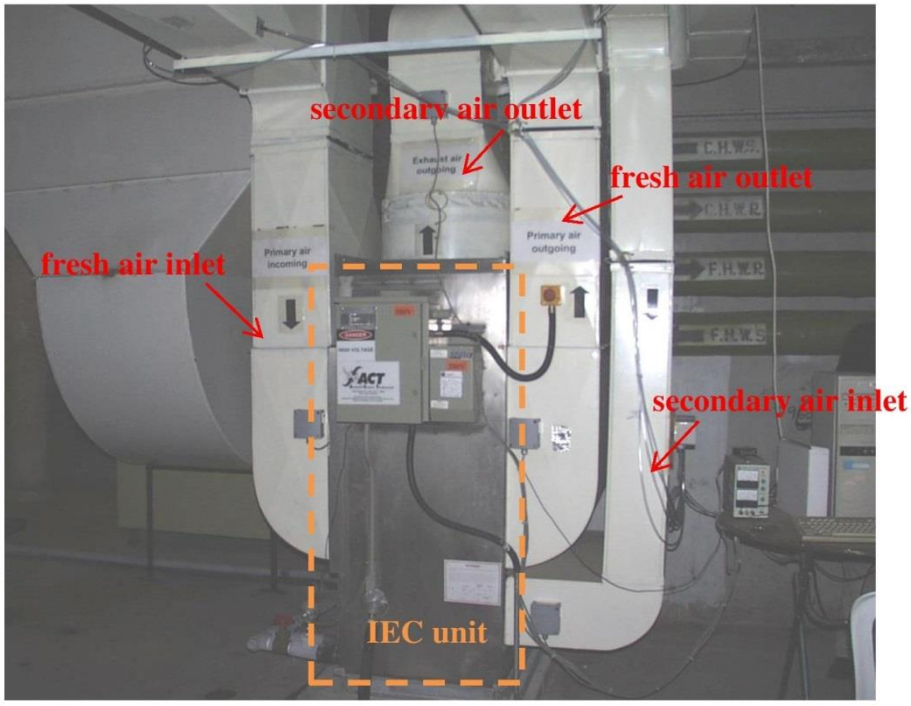

Fig. 5.11 Field measurement of IEC system in Hong Kong Kowloon Park

Unluckily, the detailed structure of IEC manufactured by Advanced Climate Technologies, Inc (Model: L-5) was lacking. The average air flow rate and air flow rate ratio were calculated to be around 2000 m^3/h and 0.8. The sensible and latent energy saving of the test rig were processed according to the collected temperature difference and humidity difference between the fresh air inlet and outlet. The total annual saving of the test rig was 12,246 kWh, of which sensible saving accounts for 59.1% and latent saving accounts for 40.9%. As mentioned above, the sensible and latent saving ratio accounts for 58.7% and 41.3% for the simulation results. Thus, the results calculated by the simulation models show good agreement with experimental study.

Because the cooling capacity of the IEC in the simulated case and field measurement case are different, the dimensionless sensible and latent savings were proposed for validation. The definition of the dimensionless sensible and latent savings is the monthly sensible and latent savings divided by the annual total saving. The comparison of energy savings between simulation and field measurement are shown in Fig. 5.12. A good agreement can be found between the simulation results and field measurement results, with the largest discrepancy of 1.3% in predicting the sensible saving and 2.7% in predicting the latent saving. So the proposed simplified analytical model and annual dynamic simulation method can well predict the IEC performance in hot and humid regions.

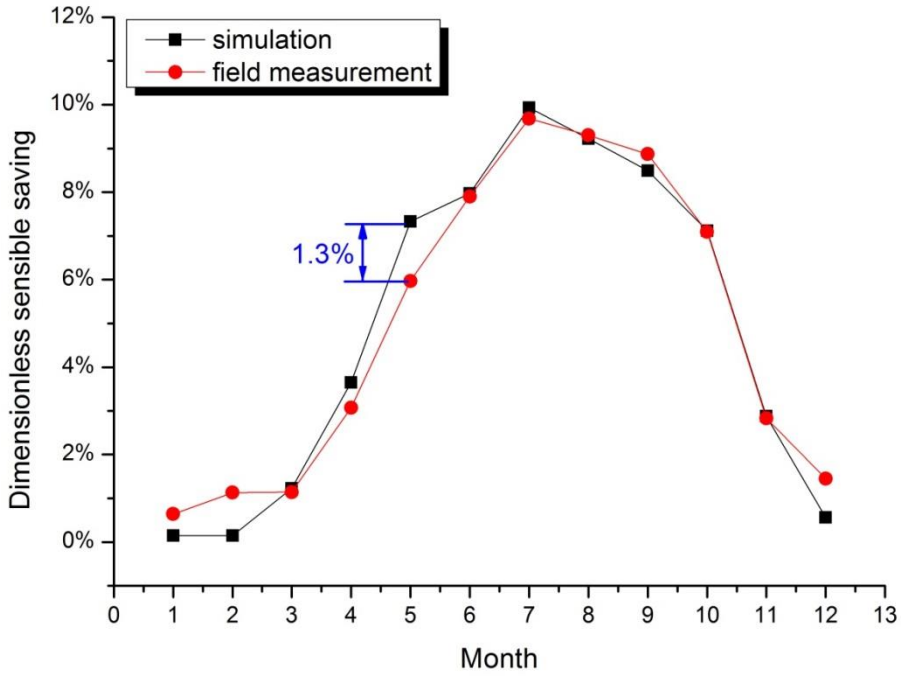

(a) sensible saving

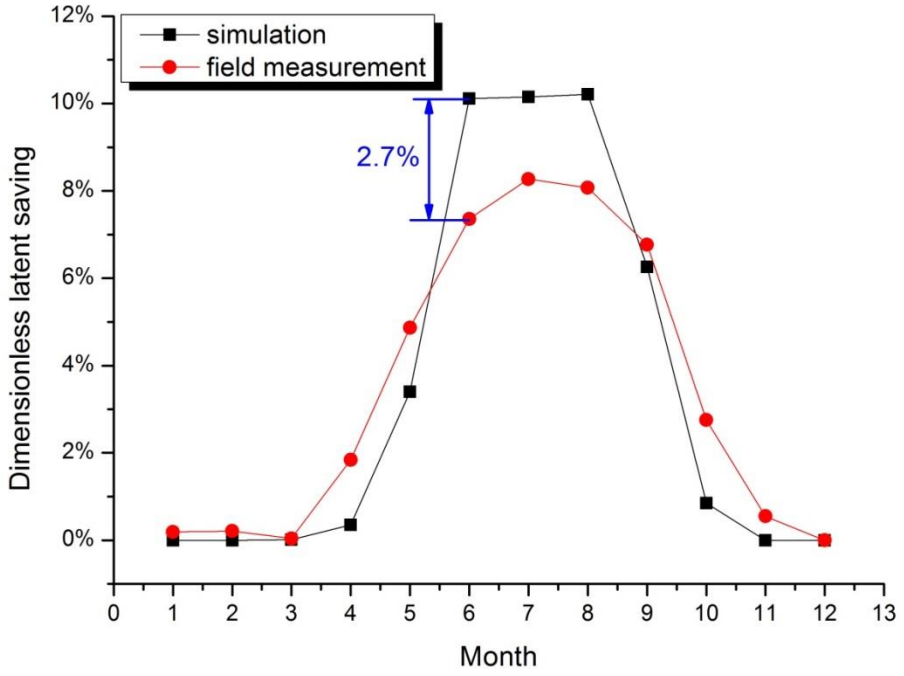

(b) latent saving

Fig. 5.12 Comparison of annual saving between simulation and field measurement

5.5 Summary

This chapter reports a novel method for annual performance simulation of IEC heat recovery system based on IEC component model developed in Chapter 4. The method is realized by incorporating the IEC model considering condensation with TRNSYS software. Thus, it takes the possible IEC condensation state into consideration and enables the hourly dynamic simulation of the cooling load, indoor air parameter and A/C mode. The highlighted results can be concluded as follows.

1) The condensation in IEC takes up a large proportion of operation hours in hot and humid regions, especially in summer. The non-condensation, partial condensation and total condensation state account for 52.3%, 38.2% and 9.5% in annual operation hours, respectively. The wet-bulb efficiency of IEC decreases as the inlet fresh air humidity increases, but the latent energy saving improves.

2) The IEC can handle both sensible and latent cooling saving in hot and humid regions. The sensible saving accounts for 58.7% and latent saving accounts for 41.3% of the total savings.

3) The IEC shows a great potential in energy saving and peak load reduction. The annual energy saving is 21% and peak load is reduced by 27% in the studied case.

Considering the additional power consumption by the fans and pump, the annual power consumption of IEC only takes up 7.3% of the total energy saving.

4) The simplified analytical model incorporated with TRNSYS can accurately predict the dynamic performance of IEC heat recovery system in hot and humid regions. The biggest discrepancy in predicting the monthly sensible saving is 1.3% and the latent saving is 2.7%.

Chapter 6

Numerical model of IEC considering condensation and parameter analysis

6.1 Introduction

As pointed out in Chapter 2, due to the wide application of IEC in dry regions, in most reported studies, modeling of IEC without condensation was adopted. Although very limited modeling work related to the IEC performance with condensation may also be identified [Yang et al. 2006, Cui et al. 2015], they focused on modeling using analytical correlations and film theory of mass transfer. Besides, both the reported simulation studies for IEC with condensation do not consider the variation of wet surface wettability. In fact, the fully wetted surface in secondary air channels can only be achieved under experimental conditions, in which enough circulation water flow rate can be guaranteed and no nozzle clogging is expected. In real application, however, insufficient wetting is suspected after long time operation. Furthermore, a comprehensive parameter study was neither presented, nor a series of indexes were proposed to evaluate not only sensible cooling performance but also latent one under IEC condensation state in reported literatures.

Therefore, a novel IEC numerical model considering condensation is developed in this Chapter. Four evaluation indexes are proposed to evaluate both the sensible and latent cooling performances of IEC comprehensively. Later, the effect of nine parameters (including temperature and humidity of primary air and secondary air, channel gap, wettability and cooler height) were analyzed under three operating states (non-condensation, partial condensation and total condensation). The comparison between some previous representative parameter studies and present study is listed in Table 6.1.

Table 6.1 Comparison with other parameter studies

Ref.	IEC type	Method	Studied parameters and ranges	Particular points
[Guo & Zhao 1998]	cross flow plate type IEC	FDM numerical simulation	air temperature (25~45℃), secondary air humidity (10~90%), primary air velocity (0.5~4.5m/s), mass flow ratio (0.5~2), wettability (0~1), channel gap (2~10mm)	two-dimensional numerical model was used to firstly investigated 6 parameters
[Riangvilaikul & Kumar 2010]	counter flow plate type RIEC	FDM numerical simulation	air temperature (25~45℃), air humidity (7~26g/kg), air velocity (1.5~6.0m/s), channel gap (1~10mm), channel length (0.1~3m), working to intake air ratio (0.05~0.95)	6 major operating parameters were studied for RIEC system. Wet-bulb and dew-point efficiencies were discussed
[Zhan et al. 2011]	M-cycle cross flow IEC	finite-element method	air temperature (20~40℃), air humidity (10~90%), primary air speed (0.5~4.0m/s), secondary air speed (0.17~1.62m/s),	analyses into relation between the wet-bulb effectiveness,

			supply-to-total air flow rate (0.1~0.9), channel gap (2~20mm), dimensionless channel length (50~600)	system COP and operational parameters were undertaken to M-cycle IEC
[Lee & Lee 2013]	counter flow RIEC with finned channels	experiment & numerical simulation	evaporation water flow rate (0.15 ~ 1.0 lpm), extraction ratio (0.2~0.5), air temperature (27.5~32℃), air humidity (9.19~18.11 g/kg)	counter flow fin-inserted RIEC were experimental tested and numerical simulated; influence of water flow rate were investigated
Present study	counter flow plate type IEC	FDM numerical simulation	primary air temperature (24~40℃), humidity (30~90%), velocity (0.5~5.0m/s); secondary air temperature (20~28℃), humidity (40~70%), velocity (0.5~5.0m/s); wettability (0~1), channel gap (2~10mm), IEC height (0.1~2.0m)	focus on IEC performance with condensation from high humidity primary air using four evaluation indexes

Compared with the simplified model developed in Chapter 4, the numerical model presented in this Chapter considers the surface wettability, evaporation water loss and condensate water loss but involves more complex numerical algorithm. Besides, the two models can be linked a systematic way: the sensible and latent heat transfer equations are established separately in the numerical model, while the total heat transfer equation is established directly by using two modified parameters suitable for the wet surface.

The two modified parameters are actually derived from numerical model.

6.2 Numerical model development

As stated in Chapter 4, according to different inlet air conditions, three possible operating states of IEC can be identified, which are total condensation, partial condensation and non-condensation, as shown in Fig. 4.1. The model is based on the following assumptions: 1) air flows are fully developed and thermal properties of the air and water are constant; 2) the unit is adiabatic; 3) both the water film and wall are very thin so the thermal resistances are negligible; 4) heat and mass are only transferred vertically across the separated plate; 5) condensate water temperature is equal to the dew point temperature of primary air; 6) Lewis number is unity in both evaporation and condensation surface.

The heat balance of secondary air is calculated as:

$$h_s(t_w - t_s)dA = c_{pa} m_s dt_s \tag{6.1}$$

The mass balance of secondary air is calculated as:

$$h_{ms}(\omega_{t_w} - \omega_s)d(\sigma A) = m_s d\omega_s \tag{6.2}$$

If the local plate surface temperature is higher than $t_{\mathrm{dew,p}}$, i.e., $t_w > t_{dew,p}$, only sensible heat exchange will take place in the primary air channels. The heat balance equation of the primary air, mass balance of evaporation water film and energy balance equation of the control volume are calculated as Eq. (6.3) to (6.5), respectively.

$$h_p(t_p - t_w)dA = c_{pa}m_p dt_p \tag{6.3}$$

$$dm_e = m_s d\omega_s \tag{6.4}$$

$$m_s di_s - c_{pa}m_p dt_p = d(c_{pw}t_{ew}m_e) \tag{6.5}$$

If the local plate surface temperature is lower than $t_{\mathrm{dew,p}}$, i.e., $t_w < t_{dew,p}$, the condensation will take place and the moisture is released from the primary air to the plate surface. The heat and mass balance equation of the primary air, mass balance of evaporation water film and condensate water film, as well as the energy balance equation of the control volume are calculated as Eq. (6.6) to (6.10), respectively.

$$h_p(t_p - t_w)dA = c_{pa}m_p dt_p \tag{6.6}$$

$$h_{mp}(\omega_p - \omega_{t_w})dA = m_p d\omega_p \tag{6.7}$$

$$dm_e = m_s d\omega_s \tag{6.8}$$

$$dm_c = -m_p d\omega_p \tag{6.9}$$

$$m_s di_s - m_p di_p = d(c_{pw} t_{ew} m_e) + d(c_{pw} t_{cw} m_c) \tag{6.10}$$

In sum, Eq. (6.1) ~ (6.5) form the enclosed governing equations of IEC without considering condensation; while the Eq. (6.1) ~ (6.2) and Eq. (6.6) ~ (6.10) form the enclosed governing equations of IEC with condensation. In the model, the moisture content of saturated air at plate surface temperature was simplified as a linear function of plate surface temperature, i.e., $\omega_{t_w} = at_w + b$ (kg/ kg). By fitting the exact solutions of moisture content of saturated air as Eq. (6.11) and (6.12), the constants *a* and *b* in the above simplified linear function were set as 0.0012 and -0.0107, respectively, for the temperature range of 20℃ to 30℃.

$$In\left(P_{qb}\right) = \frac{a_1}{T_w} + a_2 + a_3 T_w + a_4 T_w^{\ 2} + a_5 T_w^{\ 3} + a_6 In\left(T_w\right) \tag{6.11}$$

$$\omega_{t_w} = 0.622 \frac{P_{qb}}{B - P_{qb}} \tag{6.12}$$

where,

$$a_1 = -5800.2206, a_2 = 1.3914993, a_3 = -0.048640239, a_4 = 0.41764768\times10^{-4},$$
$$a_5 = -0.14452093\times10^{-7}, a_6 = 6.5459673$$

In the governing equations of IEC without condensation, we substitute Eq. (6.1) ~ (6.4) into Eq. (6.5) by adopting the enthalpy calculation equation for moisture air $i = c_p t + h_{fg}\omega$, and then re-arrange the equation, the plate surface temperature under non-condensation state can be obtained:

$$t_w = c_1 t_p + c_2 \omega_s + c_3 t_s + c_4 \tag{6.13}$$

where,

$$c_1 = \frac{h_p}{h_s + h_p + \sigma a h_{ms}(h_{fg} - c_{pw}t_{ew})}, c_2 = \frac{(h_{fg} - c_{pw}t_{ew})h_{ms}\sigma}{h_s + h_p + \sigma a h_{ms}(h_{fg} - c_{pw}t_{ew})}$$

$$c_3 = \frac{h_s}{h_s + h_p + \sigma a h_{ms}(h_{fg} - c_{pw}t_{ew})}, \; c_4 = \frac{(c_{pw}t_{ew} - h_{fg})h_{ms}b\sigma}{h_s + h_p + \sigma a h_{ms}(h_{fg} - c_{pw}t_{ew})}$$

In the governing equations of IEC with condensation, we substitute Eq. (6.1) ~ (6.2) and (6.6) ~ (6.9) into Eq. (6.10) and re-arrange the equation, the plate surface temperature under condensation state can be obtained:

$$t_w = c_5 t_p + c_6 \omega_p + c_7 t_s + c_8 \omega_s + c_9 \tag{6.14}$$

where,

$$c = h_s + h_p + ah_{fg}(\sigma h_{ms} + h_{mp}) - ac_{pw}(t_{ew}\sigma h_{ms} + t_{cw}h_{mp}) \text{ , } c_5 = \frac{h_p}{c} \text{ , } c_6 = \frac{h_{fg}h_{mp} - c_{pw}t_{cw}h_{mp}}{c} \text{ ,}$$

$$c_7 = \frac{h_s}{c}, \; c_8 = \frac{\sigma h_{fg}h_{ms} - \sigma c_{pw}t_{ew}h_{ms}}{c}, \; c_9 = \frac{bc_{pw}(t_{ew}h_{ms}\sigma + t_{cw}h_{mp}) - bh_{fg}(h_{ms}\sigma + h_{mp})}{c}.$$

The heat and mass transfer coefficients were estimated as follows. As the channel gap of the IEC is very small and the air velocity is usually less than 5m/s, the air flow can be regarded as laminar flow. The equation for calculating the heat transfer coefficient for the fully developed laminar flow in the parallel primary air channel and secondary air channel are:

$$h_p = \frac{0.023\left(\frac{u_p}{\upsilon_p}\right)^{0.8} \cdot Pr_p^{0.3} \cdot \lambda_p}{d_e^{0.2}} \tag{6.15}$$

$$h_s = \frac{0.023\left(\frac{u_s}{\upsilon_s}\right)^{0.8} \cdot Pr_s^{0.3} \cdot \lambda_s}{d_e^{0.2}} \tag{6.16}$$

The mass transfer coefficient (h_{mp}, h_{ms}) can be obtained accordingly by adopting the analogy law between heat and mass transfer, i.e., the Lewis relationship is satisfied and regarded as unity in air-water interaction surfaces [ASHRAE 1997, ASHRAE Handbook 2005, Huang et al. 2005]. So the mass transfer coefficients are:

$$h_{mp} = \frac{h_p}{c_p Le_p^{2/3}} \approx \frac{h_p}{c_p} \tag{6.17}$$

$$h_{ms} = \frac{h_s}{c_p Le_s^{2/3}} \approx \frac{h_s}{c_p} \tag{6.18}$$

Different number of transfer units (NTU) and dimensionless height (x^*) of IEC can be defined as follows:

$$NTU_p = \frac{h_p A}{m_p c_{pa}},\ NTU_{mp} = \frac{h_{mp} A}{m_p},\ NTU_s = \frac{h_s A}{m_s c_{pa}},\ NTU_{ms} = \frac{h_{ms} A}{m_s},\ NTU_e = A h_{ms},$$

$$NTU_c = A h_{mp},\ x^* = \frac{x}{H}$$

The above governing equations can be re-written in standard ordinary differential equations as Eq. (6.19) to (6.24). Then, the differential term is discretized into algebraic form by finite difference method (FDM) and numerical simulation results at each discrete node can be obtained by solving a set of algebraic equations simultaneously. The corresponding wall temperature under non-condensation state and condensation state at each discrete node can be calculated by Eq. (6.13) and Eq. (6.14), respectively.

$$\frac{dt_s}{dx^*} = NTU_s (t_w - t_s) \tag{6.19}$$

$$\frac{d\omega_s}{dx^*} = \sigma NTU_{ms}(\omega_{t_w} - \omega_s) \tag{6.20}$$

$$\frac{dt_p}{dx^*} = NTU_p(t_p - t_w) \tag{6.21}$$

$$\frac{d\omega_p}{dx^*} = NTU_{mp}(\omega_p - \omega_{t_w}) \text{ (if } \omega_p > \omega_{t_w}) \tag{6.22}$$

$$\frac{dm_e}{dx^*} = \sigma NTU_e(\omega_{t_w} - \omega_s) \tag{6.23}$$

$$\frac{dm_c}{dx^*} = -NTU_c(\omega_p - \omega_{t_w}) \text{ (if } \omega_p > \omega_{t_w}) \tag{6.24}$$

The boundary conditions for the above governing equations are:

$$\begin{cases} x^* = 1, t_p = t_{p,in} \\ x^* = 1, \omega_p = \omega_{p,in} \\ x^* = 0, t_s = t_{s,in} \\ x^* = 0, \omega_s = \omega_{s,in} \\ x^* = 1, m_c = 0 \\ x^* = 1, m_e = m_{e,in} \end{cases}$$

The simulation flow chart for solving the governing equations is shown as Fig. 6.1.

To solve the one-dimensional governing equations numerically, the height of the IEC was divided into a series of continuous elements. The grid independency of the

developed model has been checked with different mesh sizes from 10 to 250. The optimal number of domain elements was determined by increasing elements until the outlet primary air temperature and moisture content remains steady. As shown in Fig. 6.2, 100 elements were selected as a compromise between the calculation accuracy and time expense.

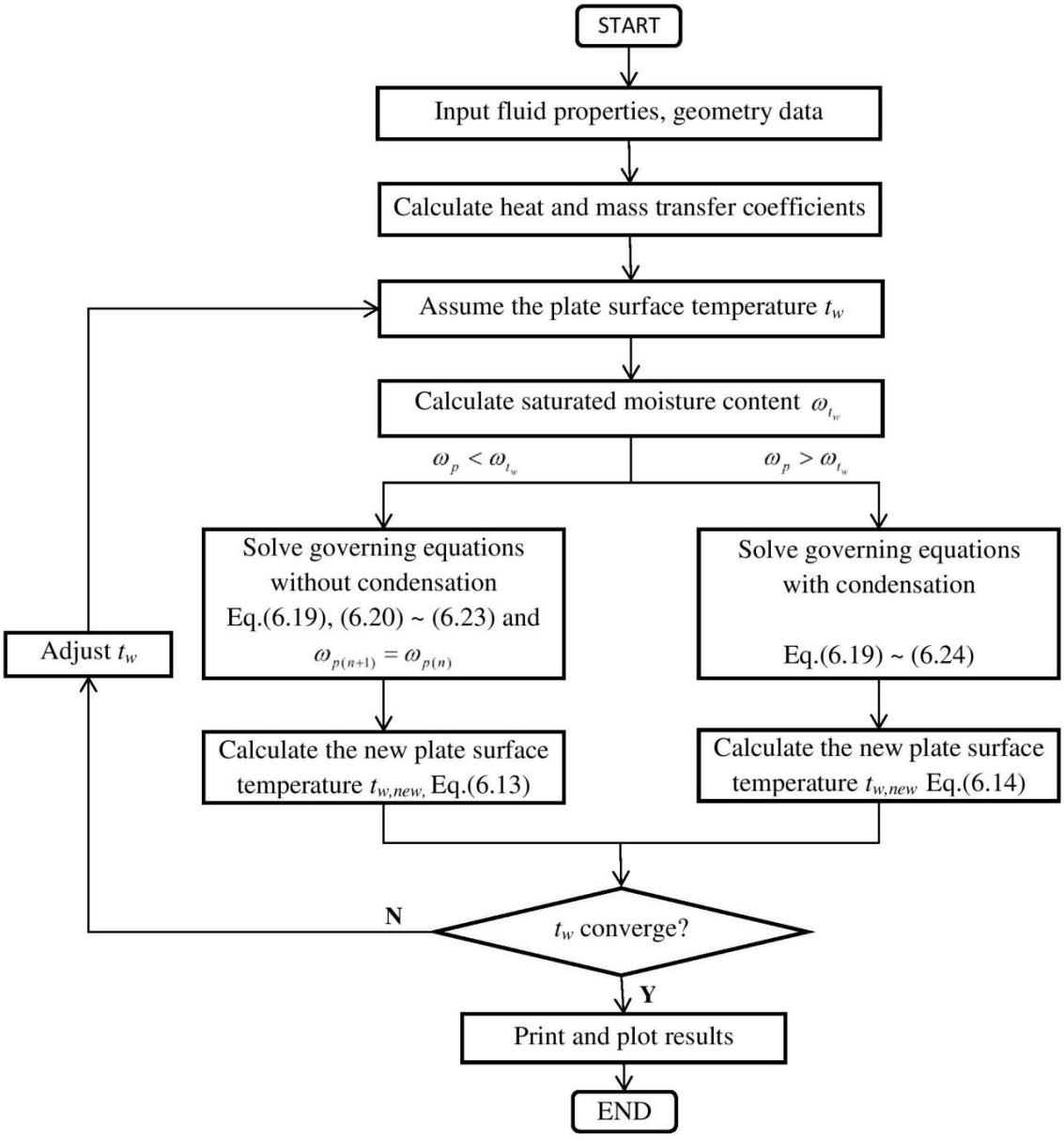

Fig. 6.1 Simulation flow chart for solving the IEC model

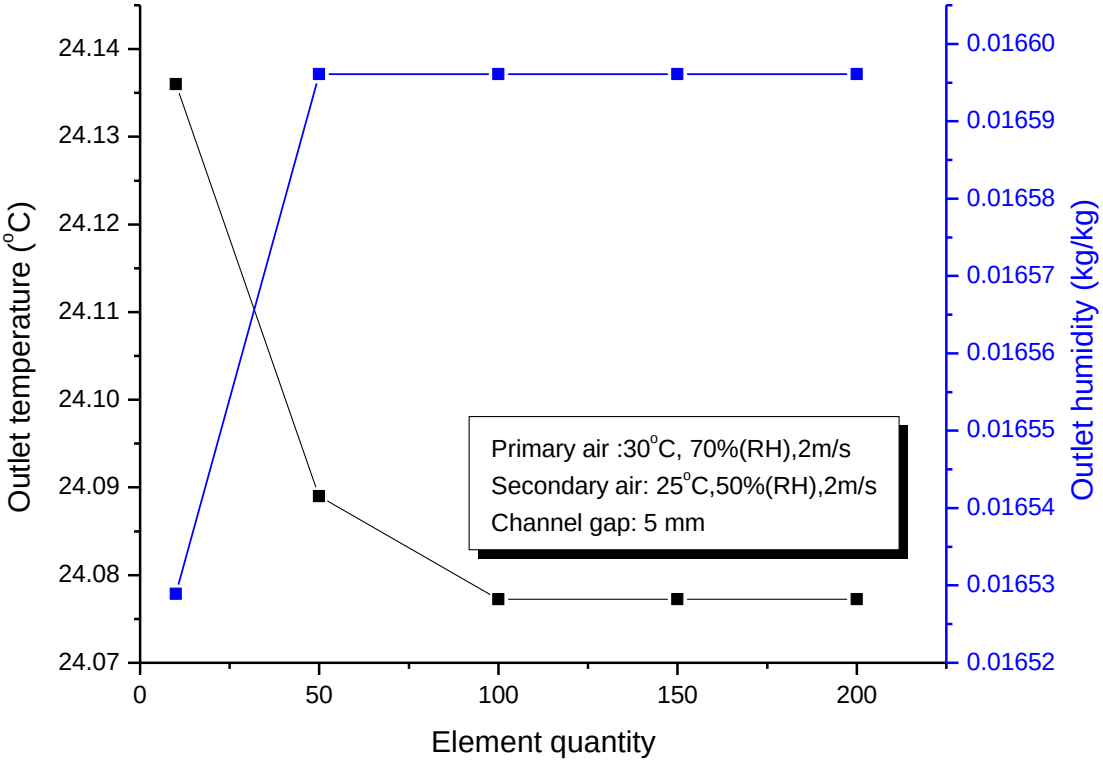

Fig. 6.2 Outlet parameters under different element quantity

Four evaluation indexes are proposed to evaluate IEC cooling performance under condensation state. The wet-bulb efficiency is used as an evaluation metric for rating the IEC in handling sensible heat [Duan et al. 2012]:

$$\eta_{wb} = \frac{t_{p,in} - t_{p,out}}{t_{p,in} - t_{wb,s}} \tag{6.25}$$

Three other indexes are proposed for evaluating IEC performance comprehensively,

including condensation ratio R_{con}, enlargement coefficient β and total heat transfer rate per unit mass q_{tot}. The R_{con} is defined as the proportion of condensation area to the total heat exchanger area as Eq. (6.26). The condensation ratio is 0 when there is no condensation and it is 1 when condensation takes place at the entire separating wall. The condensation ratio varies from 0 to 1 under partial condensation.

$$R_c = \frac{A_c}{A} \tag{6.26}$$

The ε is introduced for evaluating the enlarged heat transfer rate associated with condensation. As shown in Eq. (6.27), it is calculated as the total heat transfer rate divided by the sensible heat transfer rate. Under the non-condensation state, the enlargement coefficient equals 1.

$$\varepsilon = \frac{Q_{tot}}{Q_{sen}} = \frac{c_{pa} \cdot m_p \cdot (t_{p,in} - t_{p,out}) + h_{fg} \cdot m_p \cdot (\omega_{p,in} - \omega_{p,out})}{c_{pa} \cdot m_p \cdot (t_{p,in} - t_{p,out})} \tag{6.27}$$

The total heat transfer rate per unit mass q (kW/kg) is an index for evaluating the total heat removed from primary air per unit mass, expressed as:

$$q = \frac{Q_{tot}}{M_p} = \frac{c_{pa} \cdot m_p \cdot (t_{p,in} - t_{p,out}) + h_{fg} \cdot m_p \cdot (\omega_{p,in} - \omega_{p,out})}{m_p \cdot (\frac{H}{u_p})} \tag{6.28}$$

6.3 Model validation

The newly developed IEC model was validated by the data derived from published papers for two operation states: IEC non-condensation and IEC with condensation. Firstly, the numerical simulation results of a dew point IEC derived by Riangvilaikul & Kumar [2010] are employed to validate the temperature distribution of primary air and humidity distribution of secondary air under non-condensation state. In this kind of IEC, a certain fraction of the outlet primary air is diverted into the wet channel to act as the secondary air. The simulations were conducted by setting the same flow pattern, unit geometry and inlet air conditions as given in the literature. Two representative cases with high humidity (35℃, 21.1g/kg) and low humidity (35℃, 8.5g/kg) of inlet air were selected. The comparisons between the two models are presented in Fig. 6.3. It was found that the newly developed numerical model predicts the IEC performance with the discrepancy of 2.8% to 6.3% for outlet primary air and 1.7% to 5.0% for outlet secondary air humidity.

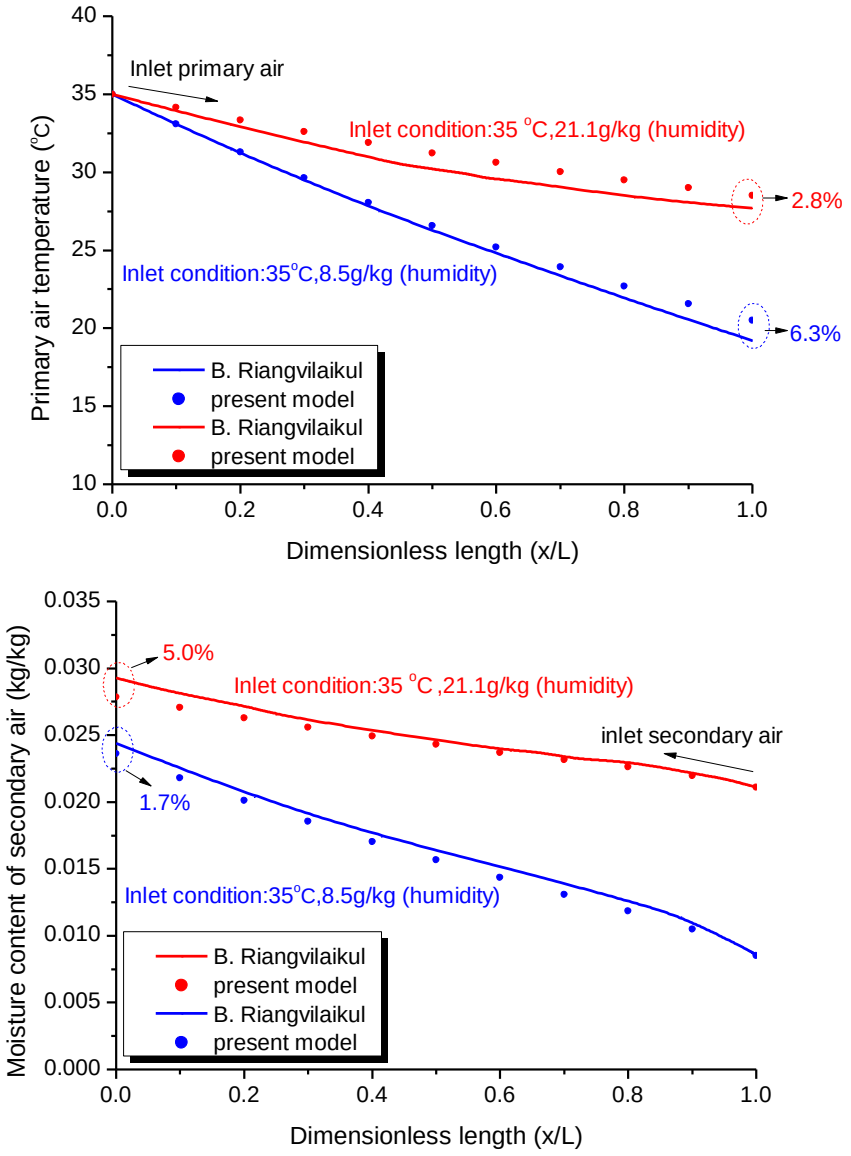

Fig. 6.3 Comparison of simulation results with published data (IEC non-condensation)

Next, the simulation results of present model under condensation state were validated by the simulation results in a recent published paper [Cui et al. 2015]. In this paper, the exhausted air (25℃, 50% RH) from an A/C room was used as the secondary air to pre-cool the humid fresh air. The temperature of the inlet fresh air ranges from 30℃ to 37.5℃

while RH ranges from 70% to 90%. The condensation takes place in all the simulation cases, so the primary air moisture content is reduced. The comparisons between the simulation results are shown in Fig. 6.4. It was found that the present numerical model can predict the outlet primary air temperature and humidity with the discrepancy of 5.9% and 2.4%, respectively. Act as a cooling device, the percentage difference of the sensible, latent and total heat transfer rate on primary air side was used as another discrepancy index between the two models, defined as $\left|\frac{q_{sen,pre}-q_{sen,lit}}{q_{sen,lit}}\right|=\left|\frac{t_{out,lit}-t_{out,pre}}{t_{in,lit}-t_{out,lit}}\right|$, $\left|\frac{q_{lat,pre}-q_{lat,lit}}{q_{lat,lit}}\right|=\left|\frac{\omega_{out,lit}-\omega_{out,pre}}{\omega_{in,lit}-\omega_{out,lit}}\right|$ and $\left|\frac{c_{pa}\cdot(t_{out,lit}-t_{out,pre})+h_{fg}\cdot(\omega_{out,lit}-\omega_{out,pre})}{c_{pa}\cdot(t_{in,lit}-t_{out,lit})+h_{fg}\cdot(\omega_{in,lit}-\omega_{out,lit})}\right|$. A discrepancy of 17.0% can be found in predicting the sensible heat transfer rate between the present model and reference's model; while the discrepancy for latent heat transfer rate was calculated to be 7.9% and total heat transfer rate was 10.9%. The discrepancy can be attributed to the different heat and mass transfer theory adopted in the two models, in which convection mass transfer model and heat and mass analogy theory was used for present model, while film theory of mass transfer was used in literature's model.

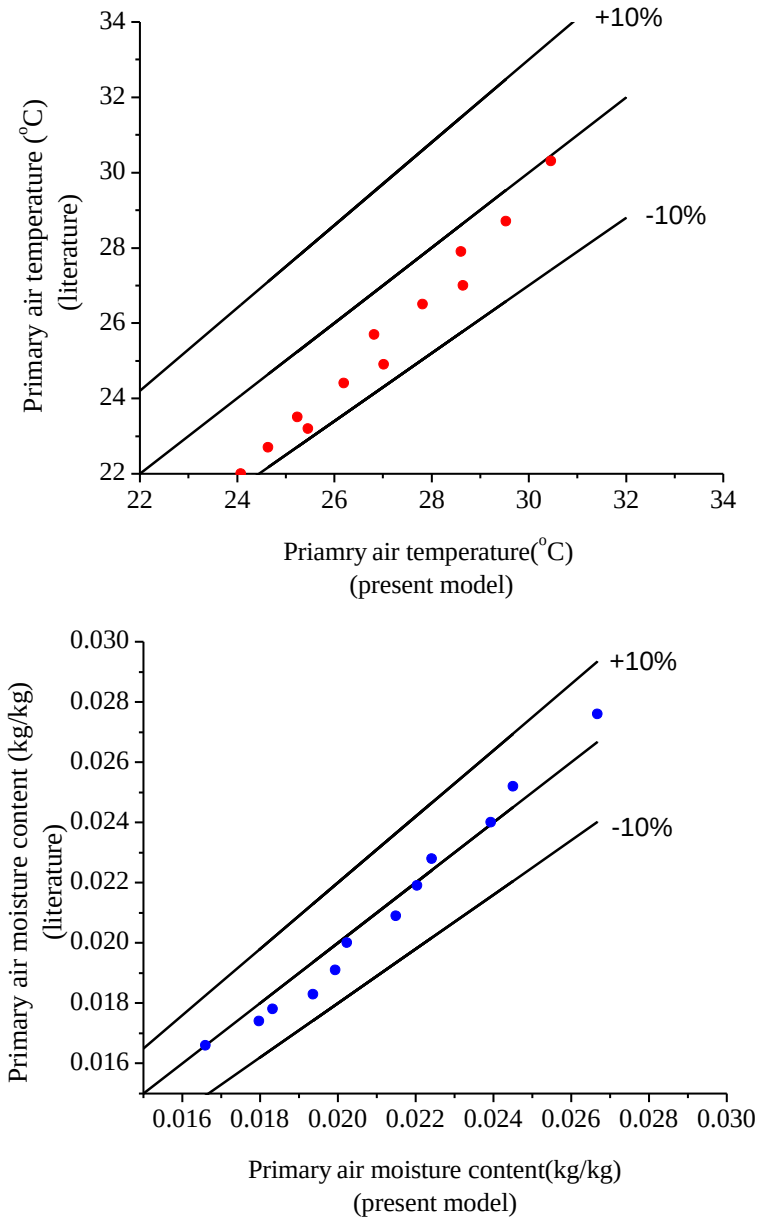

Fig. 6.4 Comparison of simulation results with published data (IEC condensation)

Based upon the validation, the newly developed IEC model can be used for the following parameter analysis.

6.4 Results and discussion

6.4.1 Temperature and humidity distribution

The air temperature and humidity distribution of the IEC are shown in Fig. 6.5 and 6.6. Fig. 6.5 presents the IEC performance under partial condensation for the case of RH_p =50% and Fig. 6.6 presents the performance under total condensation for the case of RH_p =70%.

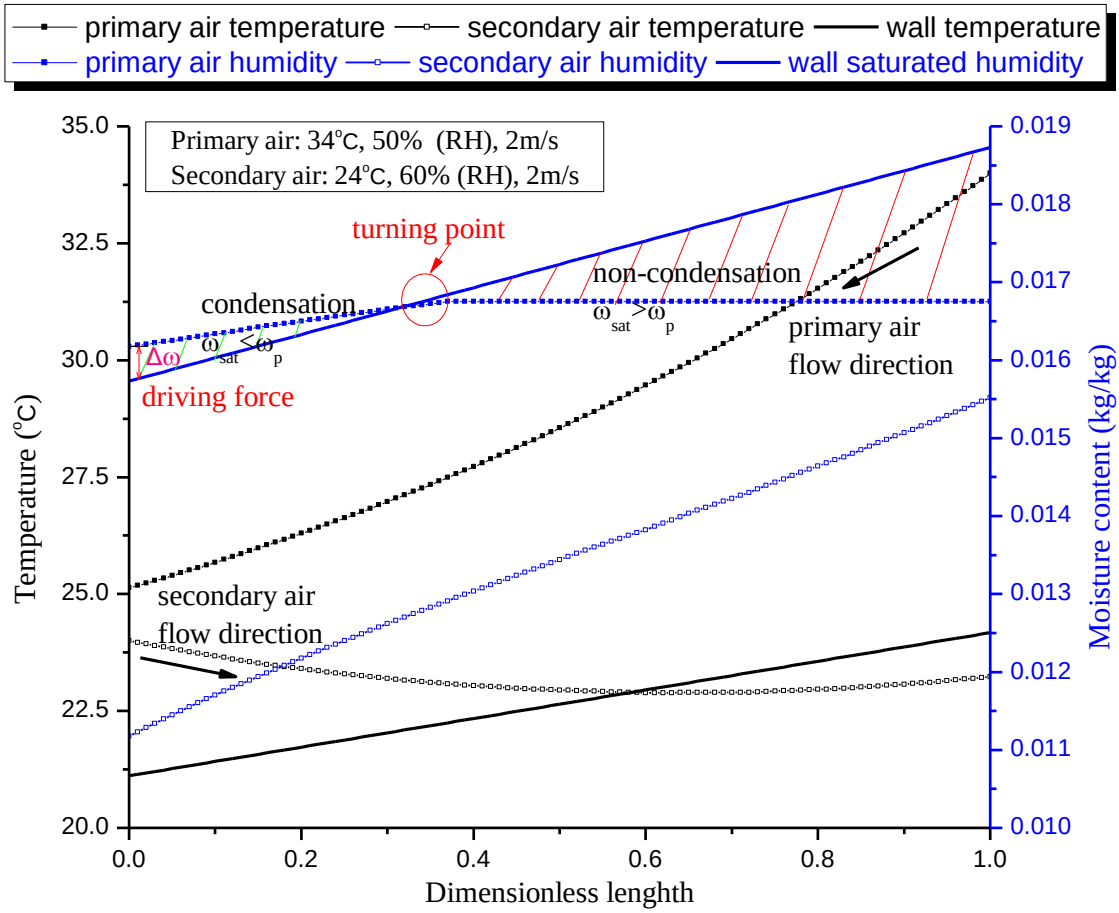

Fig. 6.5 Temperature and humidity distribution of partial condensation

As shown in Fig. 6.5, the primary air temperature keeps decreasing along the flow direction. The humidity remains unchanged at the beginning until it reaches the turning point where it begins to decline constantly. The turning point separates the condensation and non-condensation regions. In the non-condensation region, $\omega_{sat} > \omega_p$ while in the condensation region, $\omega_{sat} < \omega_{p.}$ At the turning point, the saturated humidity at the wall temperature is equal to the humidity of inlet primary air, in other words, the wall temperature is equal to the dew-point temperature of inlet primary air.

The condensation takes place for the reason that the primary air humidity is higher than the saturated humidity at the local wall temperature. So the excessive moisture of the primary air is condensed, releasing heat to the surroundings at the same time. The higher the primary air humidity and the lower the wall temperature, the larger the driving force of mass transfer and the more latent heat is released. In Fig. 6.5, the diving force increases along the primary air flow direction in the condensation region because the wall temperature decreases.

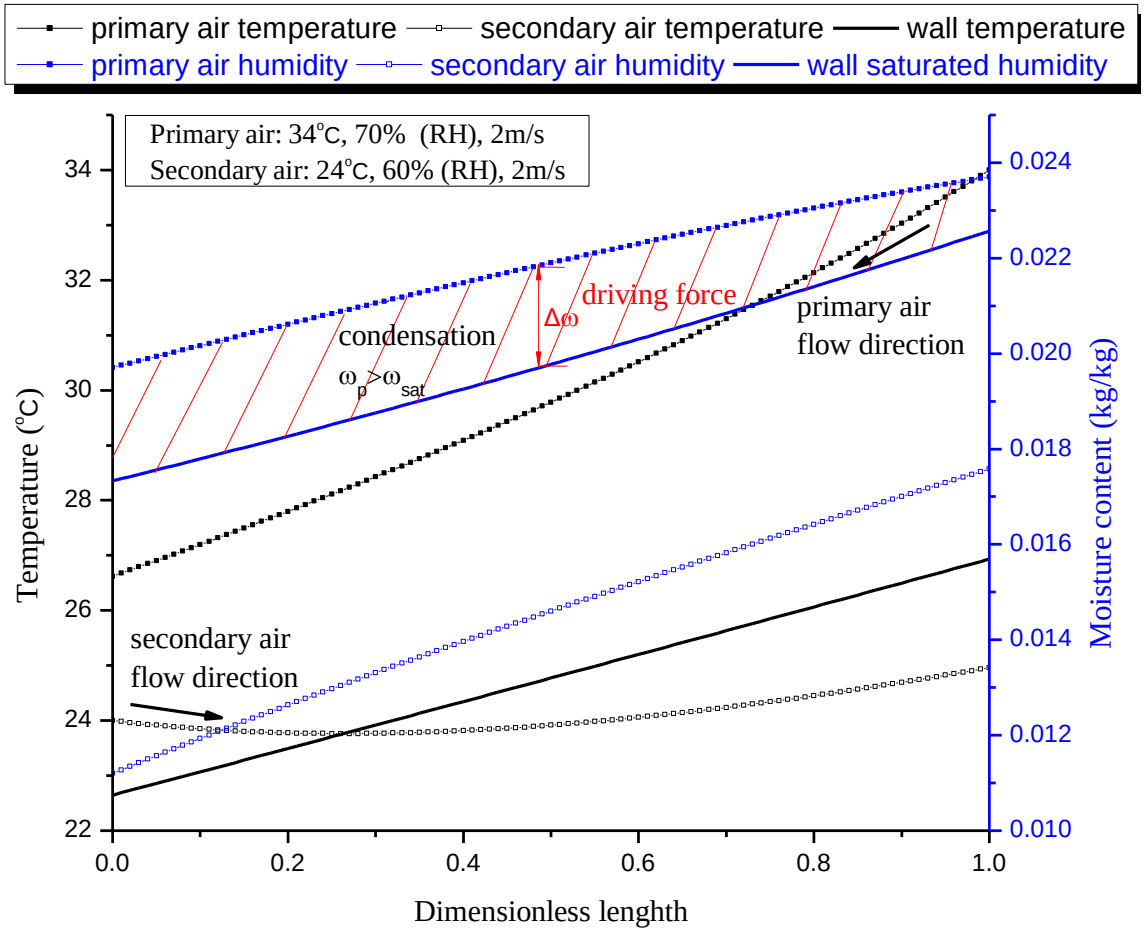

Fig. 6.6 Temperature and humidity distribution of total condensation

In Fig. 6.6, the primary air humidity keeps decreasing along the flow direction and no turning point exists. Because the inlet primary air humidity is higher than the saturated humidity at the entrance, the condensation takes place in the whole channel. It can be seen that the humidity difference increases along the primary air flow direction at the beginning and remains relatively constant thereafter. The higher inlet air humidity results in larger condensation area, greater mass transfer rate and higher wall temperature. The average wall temperature in Fig. 6.6 is 24.8℃, 2.2℃ higher than that

of Fig. 5.5 because of more heat released by the condensation.

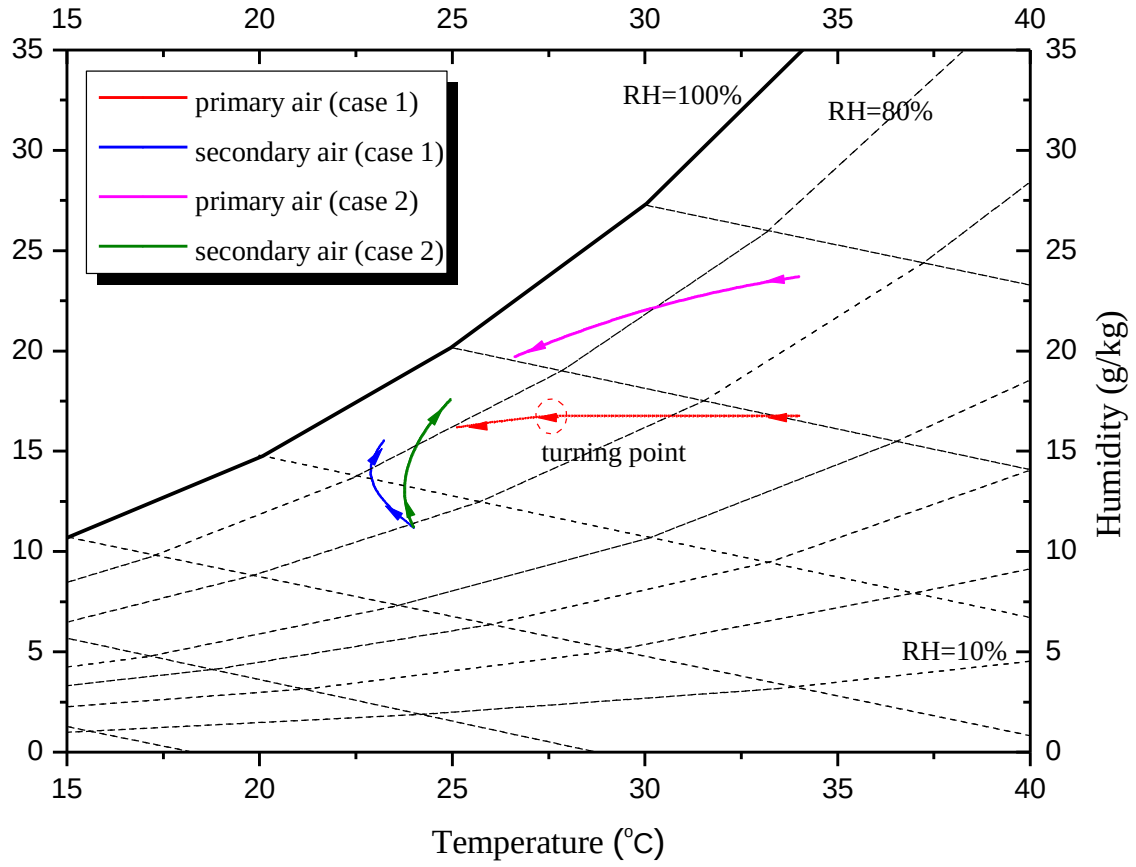

Fig. 6.7 Primary air and secondary air handling process under condensation state

Fig.6.7 shows the air handling processes of the above two cases in the psychrometric chart. It can be seen that the primary air with lower inlet humidity achieves lower outlet temperature, so the sensible heat transfer rate is larger. On the other hand, owing to the higher inlet air humidity, the latent heat transfer rate is enlarged and the outlet air humidity is reduced significantly owing to the stronger condensation. It provides a practical application field for IEC dehumidification in A/C system. Comparing the air

handling processes of the secondary air in the two cases, the outlet temperature, humidity and enthalpy under total condensation is significantly larger than that of partial condensation. Considering the enthalpy change of the primary air, it can be seen that under partial condensation state, the enthalpy drop was calculated to be 10.35 kJ/kg of which the sensible part accounts for 86.1%. While for total condensation, the enthalpy drop is 17.40 kJ/kg, 70% larger than that of partial condensation, but the sensible part only occupies 42.6%. It shows that the condensation can greatly increase the total heat transfer rate by enhancing the latent heat transfer, but decreasing the sensible heat transfer.

6.4.2 Intensive parameter analysis

Nine influential parameters (t_p, RH_p, u_p, t_s, RH_s, u_s, s, σ and H) were investigated by the newly developed model. In IEC heat recovery system, t_s and RH_s vary within a relatively small range as it is the exhausted air from A/C space. In order to compare the IEC performance under different humidity, three levels of RH_p (30%, 50% and 70%) were selected for each parameter simulation scheme. The detailed arrangement of parameter study is listed out in Table 6.2. For each studied parameter, the value varied in a range (marked in bold) and the rest remained unchanged. Then, the effects of various parameters on IEC under three operation states (non-condensation, partial condensation and total condensation) were presented and discussed with four

evaluations indexes.

Table 6.2 Ranges of various parameters

Studied object	Parameter values								
	t_p (℃)	RH_p (%)	u_p (m/s)	t_s (℃)	RH_s (%)	u_s (m/s)	s (mm)	σ -	H (m)
t_p	**24~40**	30,50,70	2.0	24	60	2.0	5	1	0.5
RH_p	35	**30~90**	2.0	24	60	2.0	5	1	0.5
u_p	35	30,50,70	**0.5~5**	24	60	2.0	5	1	0.5
t_s	35	30,50,70	2.0	**20~28**	60	2.0	5	1	0.5
RH_s	35	30,50,70	2.0	24	**40~70**	2.0	5	1	0.5
u_s	35	30,50,70	2.0	24	60	**0.5~5**	5	1	0.5
s	35	30,50,70	2.0	24	60	2.0	**2~10**	1	0.5
σ	35	30,50,70	2.0	24	60	2.0	5	**0~1**	0.5
H	35	30,50,70	2.0	24	60	2.0	5	1	**0.1~2**

6.4.2.1 Influence of primary air temperature

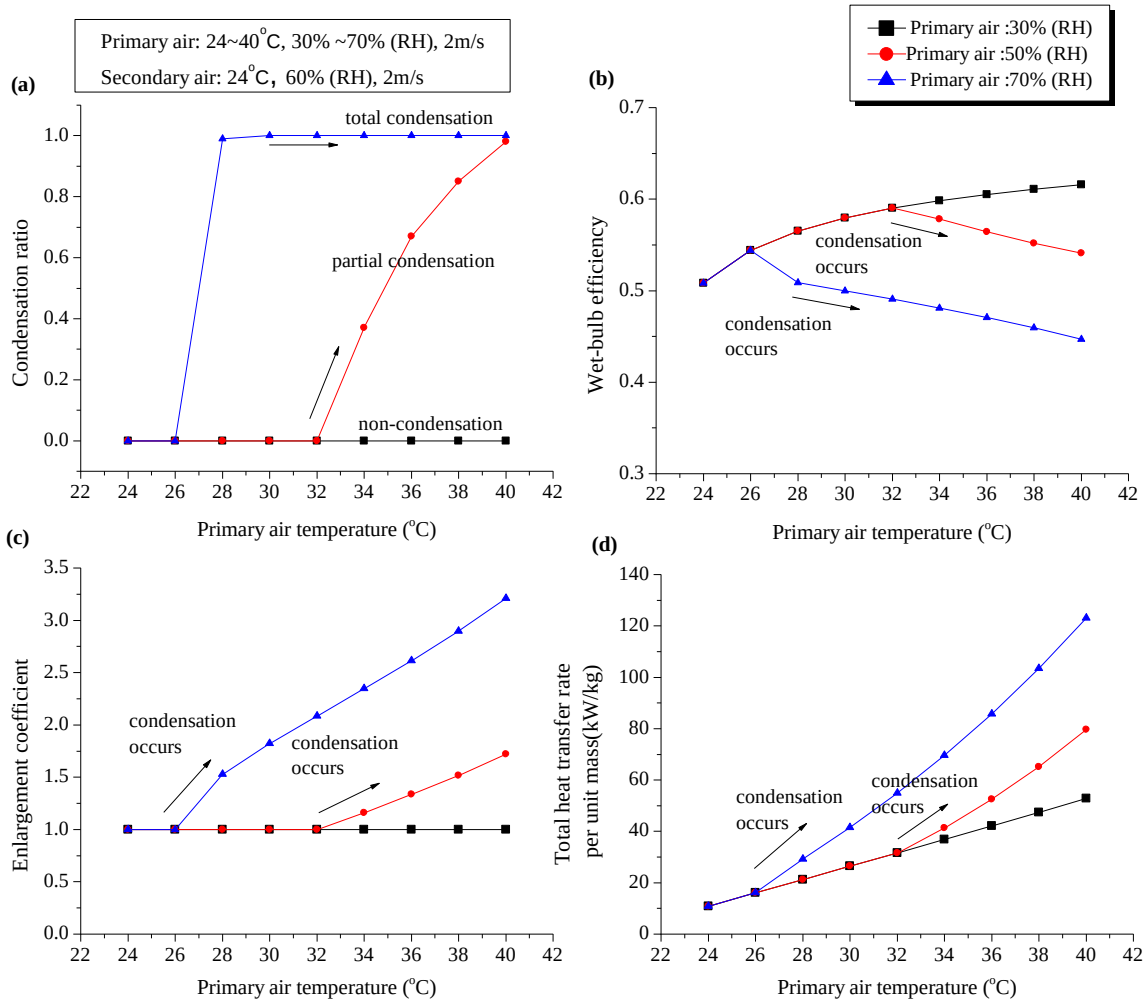

Fig.6.8 Influence of primary air temperature on: (a) R_c; (b) η_{wb}; (c) ε; (d) q

Fig.6.8 presents the influence of primary air temperature on the thermal performance of IEC. As the air temperature increases with constant RH, the moisture content increases accordingly. The condensation ratio improves significantly from 0 (non-condensation) to 1 (total condensation) when t_p increases from 32℃ to 40℃ with constant RH_p. Regarding η_{wb}, it improves with t_p under the non-condensation state because of the

larger temperature difference between the two channels. However, it decreases greatly with the increase of t_p once condensation occurs. The reason is that the heat released through the condensation process raises the wall temperature and outlet air temperature significantly. The higher the moisture contents, the stronger the condensation, and the more significantly η_{wb} declines. On the other hand, ε increases linearly with the increase of t_p under condensation state, which indicates a remarkable boost of latent heat removal of primary air. The latent heat transfer rate accounts for 69% of the total heat transfer rate and the corresponding enlargement coefficient is 3.2 under the condition of t_p=40℃ and RH_p=70%.

Considering the total heat transfer, it can be seen that under non-condensation state, the total heat transfer rate increased linearly from 10.9 kW/kg to 52.8 kW/kg when t_p increases from 24℃ to 40℃. However, the growth rate starts to speed up at t_p=32℃ when the partial condensation occurs. The rapid growth can be observed from 31.6 kW/kg to 79.6 kW/kg as t_p increases from 32℃ to 40℃. The growth rate was found to be 100% larger than that of non-condensation state. Moreover, when the condensation effect becomes stronger, such as 70% RH at total condensation state, the total heat transfer rate further improves. It is 55% to 68% larger than that of partial condensation state under the same primary air temperature.

6.4.2.2 Influence of primary air humidity

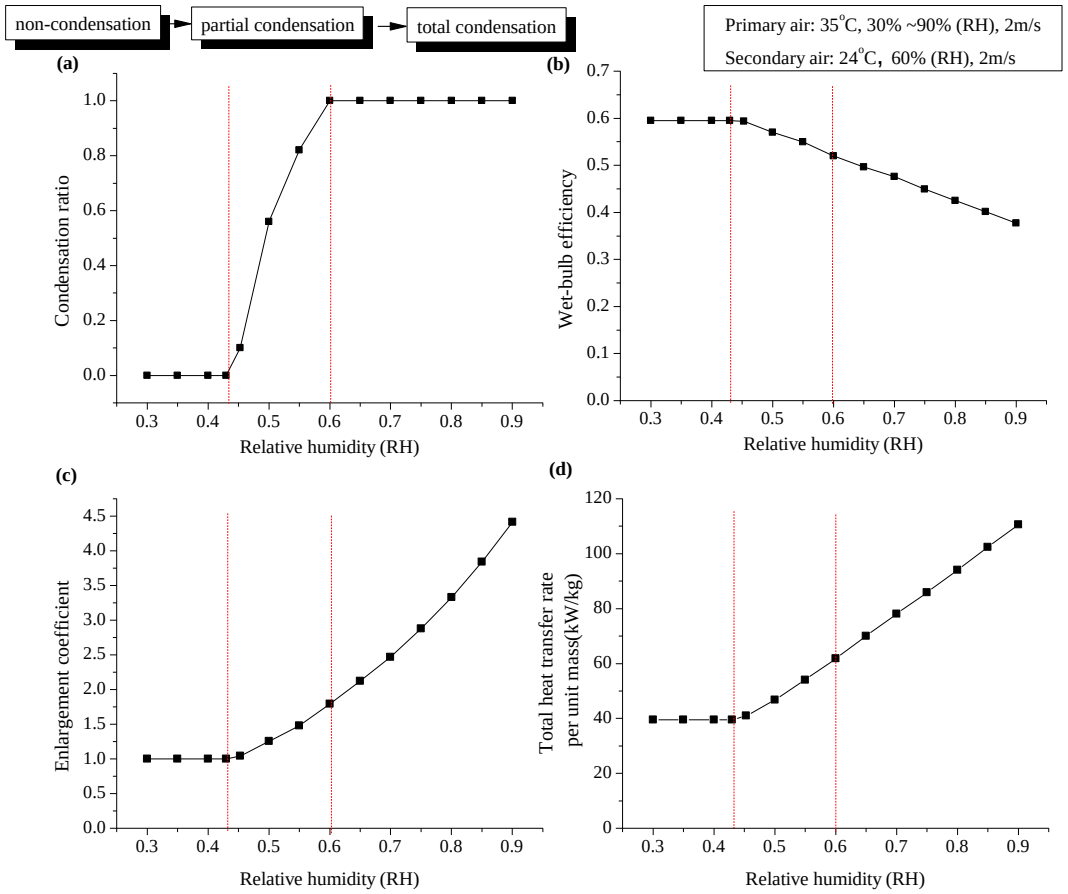

Fig. 6.9 Influence of primary air humidity on: (a) R_c; (b) η_{wb}; (c) ε; (d) q

Fig. 6.9 presents the influence of primary air RH on the thermal performance of IEC. With the increase of RH, the condensation ratio shows a growth tendency from 0 to 1, i.e., from non-condensation to partial condensation to total condensation. It improves linearly in the partial condensation region within a relative narrow RH range. Under the non-condensation state, η_{wb}, ε and q do not change with RH. However, η_{wb} decreases linearly with the increase of $RH_{p,in}$ under the condensation state. It drops by 22% as the

RH increases from 30% to 90%. The total heat transfer rate keeps unchanged under non-condensation state. Once the condensation occurs, it increases linearly with the rising of RH no matter under partial or total condensation states. The total heat transfer rate is 1.8 times larger than that of non-condensation state when the RH reaches 90%. The corresponding enlargement coefficient can reach up to 4.5, implying the latent heat transfer accounts for 78% of the total heat transfer.

6.4.2.3 Influence of primary air velocity

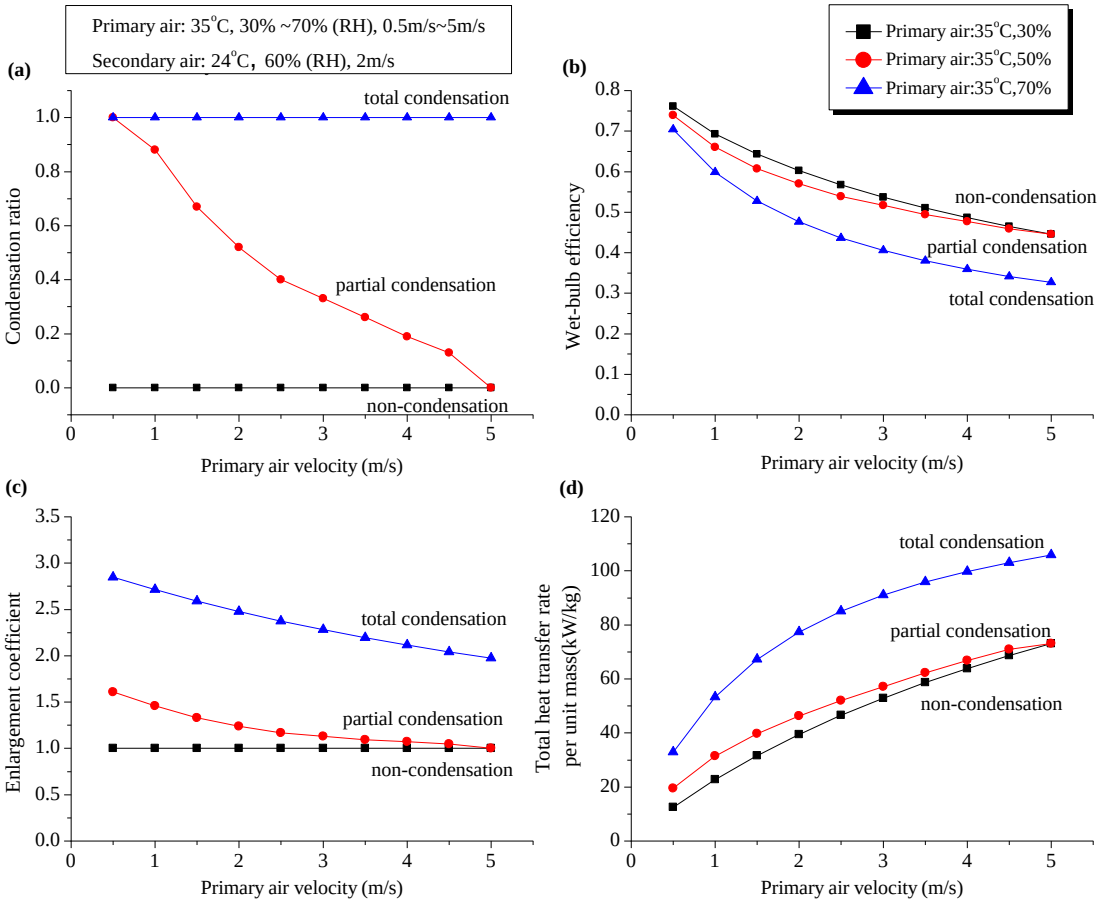

Fig. 6.10 Influence of primary air velocity on: (a) R_c; (b) η_{wb}; (c) ε; (d) q

Fig. 6.10 presents the influence of primary air velocity on the thermal performance of IEC. The increase of primary air velocity results in a larger mass flow rate, so the cooling effect of unit mass primary air is weakened. The condensation ratio declines from 1 (total condensation) to 0 (non-condensation) with the increase of primary air velocity for the case of t_p=35℃, RH_p=50%. Accordingly, the enlargement coefficient also decreases. In term of the wet-bulb efficiency, the curves of three operating states show similar trend, which decrease with the increase of primary air velocity. However, the decline trend for total condensation is more significant than that of the non-condensation state because it involves latent heat transfer process, which has a negative effect on the sensible heat transfer. For the total heat transfer rate, it improves with the increase of primary air velocity mainly because of more cooling carrier provided.

6.4.2.4 Influence of secondary air temperature

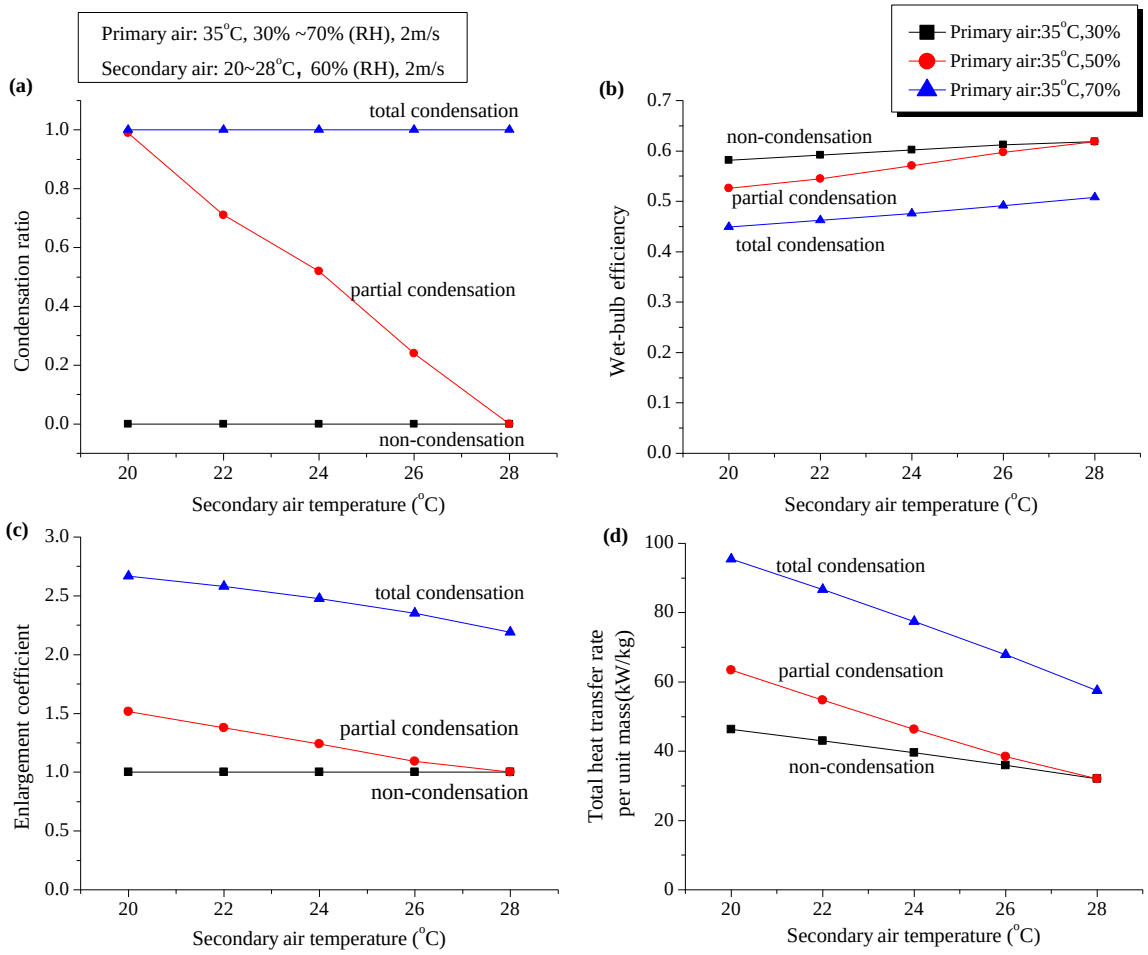

Fig. 6.11 Influence of secondary air temperature on: (a) R_c; (b) η_{wb}; (c) ε; (d) q

Fig. 6.11 presents the influence of secondary air temperature on the thermal performance of IEC. The wet-bulb temperature of secondary air, which also indicates the limit outlet temperature of primary air, will increase with the rising of dry-bulb temperature at constant RH. The higher the $t_{s,in}$, the smaller the temperature difference between the channels, and the less the heat is transferred. So the condensation ratio (at

the condition of t_p=35℃, RH=50%), keeps decreasing from total condensation to partial condensation to non-condensation with $t_{s,in}$ increases from 20℃ to 28℃. Because of the weakened cooling capacity of the secondary air, the enlargement coefficient also decreases a little for the condensation cases. Besides, the decline trend for the total heat transfer rate can be observed, but the trend is more significant for the condensation state compared with that of non-condensation state. For example, it declines from 46.3 kW/kg to 32.0 kW/kg under non-condensation state (30.9% decrease); from 63.4 kW/kg to 32.0 kW/kg under partial condensation state (49.5% decrease) and from 95.4 kW/kg to 57.5 kW/kg under total condensation state (65.9% decrease). It is owing to the simultaneous decline of the sensible and latent heat transfer.

6.4.2.5 Influence of secondary air humidity

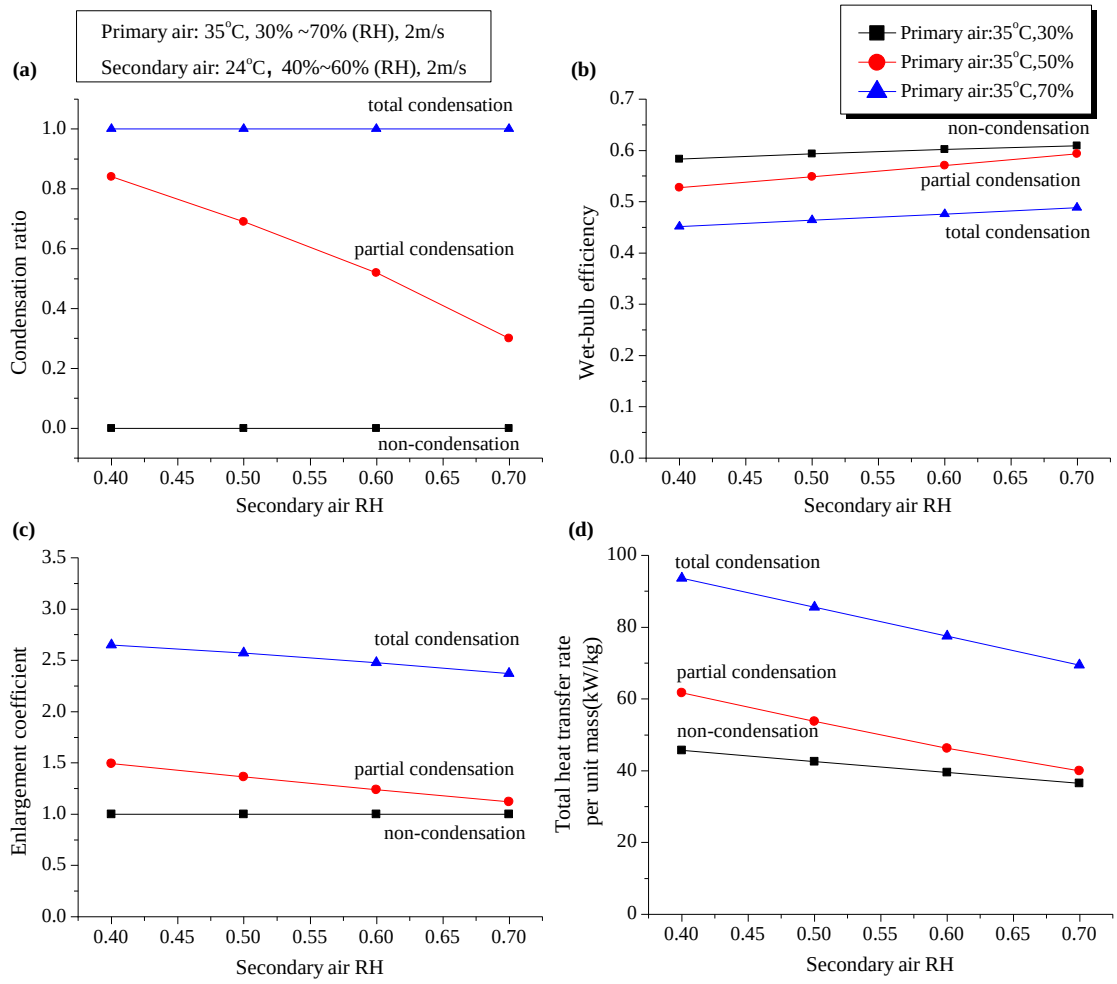

Fig. 6.12 Influence of secondary air humidity on: (a) R_c; (b) η_{wb}; (c) ε; (d) q

Fig. 6.12 presents the influence of secondary air humidity on the thermal performance of IEC. The wet-bulb temperature of secondary air increases with the increase of RH. As a result, the higher the RH, the less the cooling capacity could be provided. It will result in the decline of condensation ratio for partial condensation state, decrease of enlargement coefficient for two condensation states and reduction of total heat transfer for all the

three operation states. From the point of mass transfer mechanism, the secondary air with lower humidity owns a greater ability to evaporate because of the larger driven force brought by the water vapor concentration difference between the wall surface and mainstream air flow.

6.4.2.6 Influence of secondary air velocity

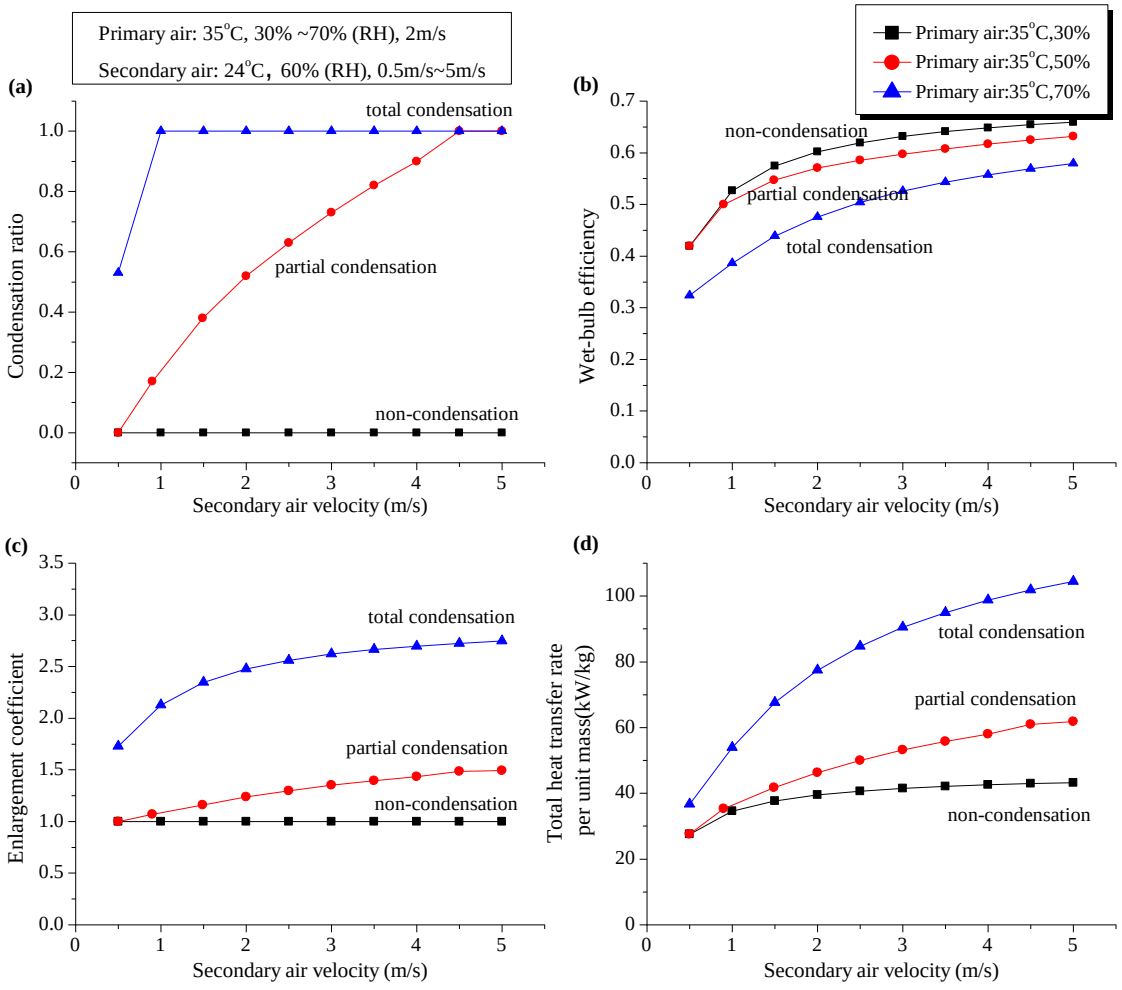

Fig. 6.13 Influence of secondary air velocity on: (a) R_c; (b) η_{wb}; (c) ε; (d) q

Fig. 6.13 presents the influence of secondary air velocity on the thermal performance of IEC. In contrast with the negative effect brought by the rise of primary air velocity, the increase of secondary air velocity can enhance the cooling effect because of the larger mass flow rate of the cooling media. As shown in Fig. 6.13, the condensation ratio improves from 0 to 1 dramatically as u_s increases from 0.5 m/s to 5.0 m/s. It can be deduced that the wall temperature is greatly reduced with the increase of m_s. The higher u_s can result in higher η_{wb}, larger ε and q.

However, the growth rates of η_{wb} and q are different between non-condensation state and condensation state. For non-condensation state, the growth rate is very significant at the beginning when u_s increases from 0.5m/s to 1.5m/s (m_s/m_p is about 0.25 to 0.75), and slows down thereafter. When u_s is larger than 3.0m/s (the flow rate ratio of secondary air to primary air exceeds 1.5), the improvement is limited. While for condensation state, the growing rate for η_{wb} and q are more obvious even though the flow rate ratio reaches 1.5. It can be explained as: the enhancement effect of adding secondary air flow rate not only improves the sensible heat transfer but also strengthen the latent heat transfer. Thus, the increase of u_s can be a more effective measure for enhancing the cooling effect of IEC under condensation state. But it also needs to pay attention that u_s should not be too large because it might result in insufficient mass transfer with water film.

6.4.2.7 Influence of channel gap

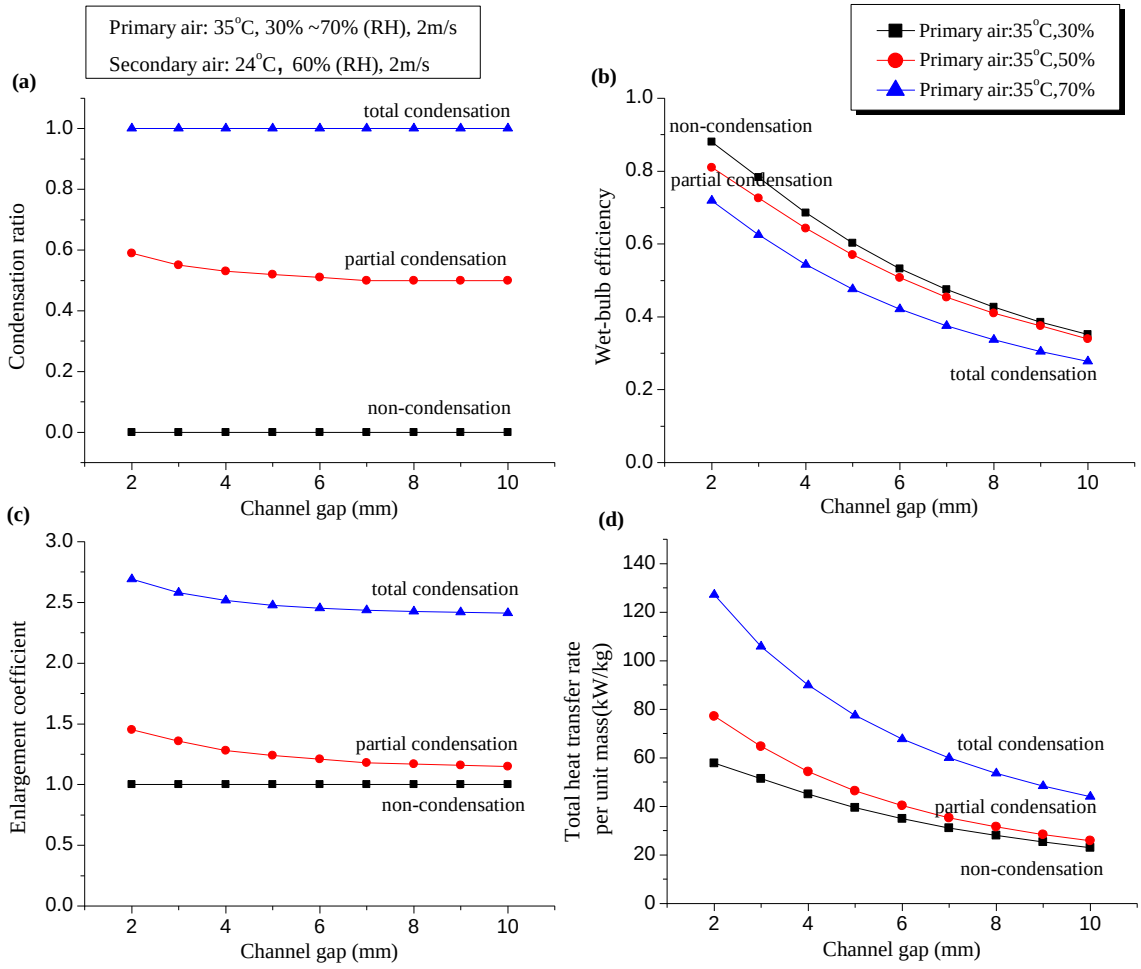

Fig. 6.14 Influence of channel gap on: (a) R_c; (b) η_{wb}; (c) ε; (d) q

Fig. 6.14 presents the influence of channel gap on the thermal performance of IEC. Channel gap was found to be one of the most influential factors under IEC non-condensation state in previous studies. In this study, the same conclusion is drawn for the condensation condition. It can be observed that the increase of channel gap results in dramatic decrease of η_{wb} and q. Meanwhile, the ε also drops a little with the increase of

channel gap. It is ascribed to the larger the channel gap, the more obviously the air bypasses, results in insufficient heat exchange with the cold walls. As the channel gap increases from 2mm to 10mm, the η_{wb} from 88% to 35% under non-condensation state and from 72% to 28% under total condensation state.

It is noticed that the channel gap has more significant impact on the condensation state as the downswing trend of q is more rapid compared with non-condensation state. It decreases dramatically from 57.8 kW/kg to 23.1 kW/kg under non-condensation state (60.0% decrease); from 77.1 kW/kg to 25.8 kW/kg under partial condensation state (66.5% decrease) and from 127 kW/kg to 44 kW/kg under total condensation state (65.4% decrease). It is owing to the increase of channel gap not only weakens the sensible heat transfer but also impairs the condensation process. The ratio declines especially when the channel gap is less than 5mm. So the q and ε changes most greatly in this range. Considering this finding, the optimal channel gap should be no more than 5mm when there is condensation takes place.

6.4.2.8 Influence of wettability

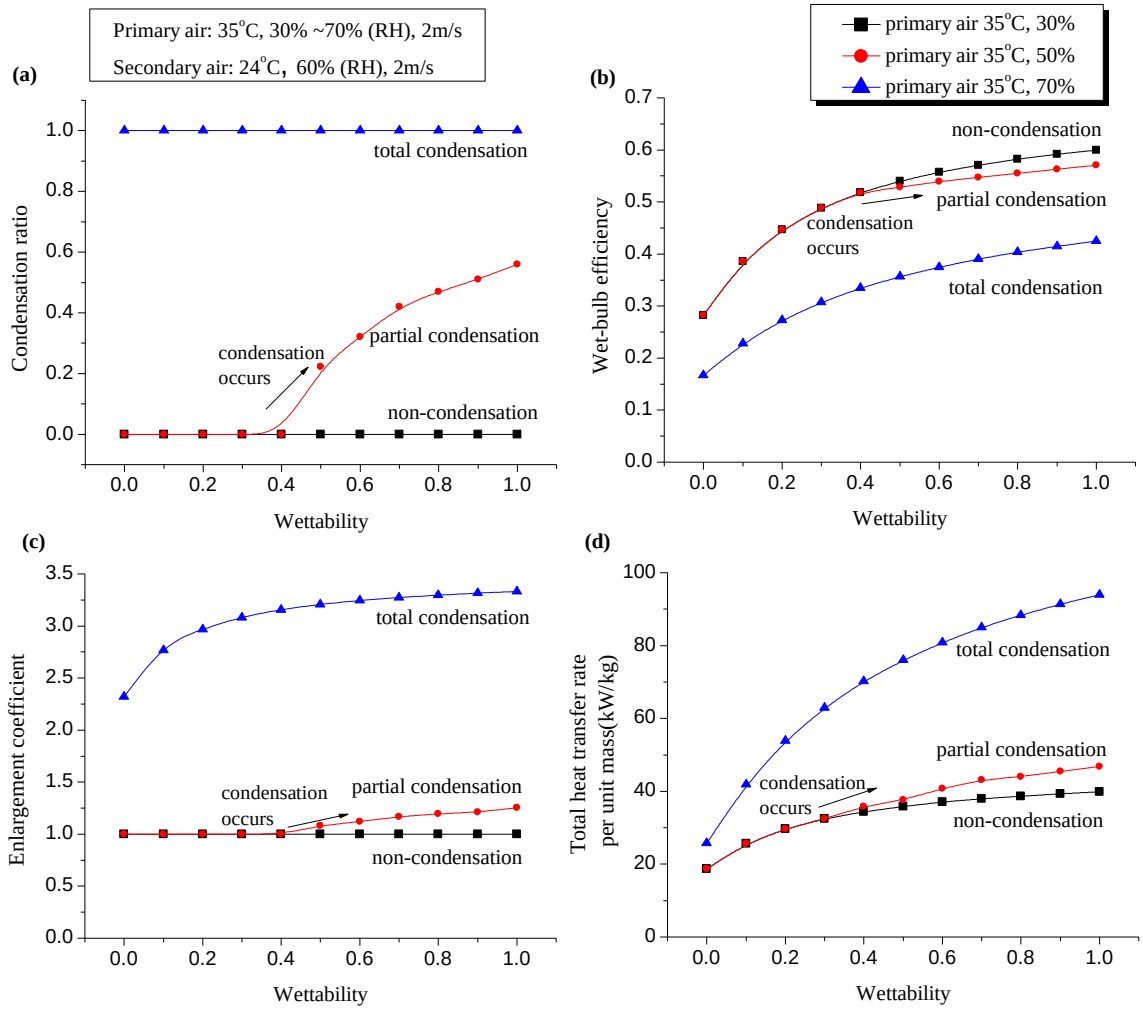

Fig. 6.15 Influence of wettability on: (a) R_c; (b) η_{wb}; (c) ε; (d) q

Fig. 6.15 presents the influence of wettability on the thermal performance of IEC. It has been shown in previous studies that improving the wettability of secondary air channel are effective measure to enhance the IEC efficiency. The reason is that the higher wettability increases the wet surface area for evaporation and reduced the wall

temperature. In present study, improving the wettability is also found to have positive effect on increasing η_{wb} and q for both non-condensation and condensation states. In addition, the improvement of wettability can also change the IEC operation condition. It is found that the condensation ratio increases from 0 to 0.58 when the wettability improves from 0 to 1.0 for the case of t_p=35℃, RH_p=50%.

However, the trends for η_{wb} and q improvement between non-condensation and condensation states are slightly different. For non-condensation state, both of the indexes improve most significantly at the beginning when the wettability increases from 0 to 0.4 and slows down when the wettability exceeds 0.4. While for condensation sate, the overall increase trend of η_{wb} is relatively smoother and the improvement of q is still significant when the wettability keeps increasing (although slower than trend at the beginning). It is attributed to the increase of wettability improve both the heat transfer rate and mass transfer rate, but the heat transfer rate is counteracted a little because of the wall temperature rise brought by the condensation. The enhancement of mass transfer is embodied in the increase of enlargement coefficient. Considering this finding, the increase of wettability may bring even better benefit for IEC performance under condensation state.

6.4.2.9 Influence of cooler height

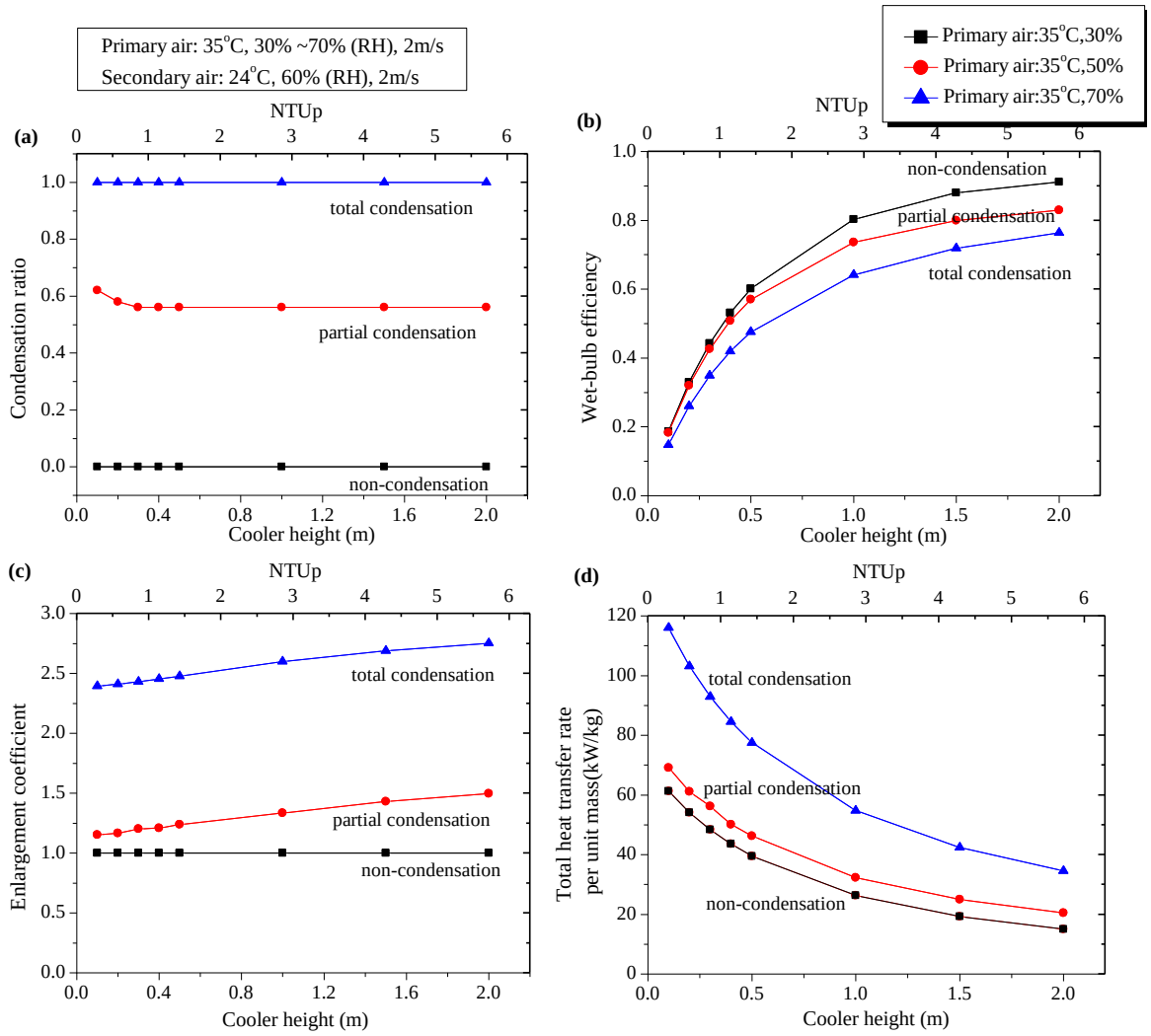

Fig. 6.16 Influence of cooler height on: (a) R_c; (b) η_{wb}; (c) ε; (d) q

Fig. 6.16 presents the influence of cooler height on the thermal performance of IEC. The increase of cooler height results in larger heat transfer area and NTU. It improves the η_{wb} and ε for condensation state. The trends of η_{wb} improvement with the increase of NTU under three operating states are similar. It improves very significantly when the

NTU is less than 1.5 and slows down greatly once the NTU exceeds 3.0. So the IEC manufacturing should compromise the cost and benefit. The q is found to decrease with the increase of NTU because this evaluation index takes the air mass into consideration. The improvement of heat transfer amount can not make up the adding of air mass inside the device so that the total heat gained by per unit mass is lowered.

6.5 Summary

This Chapter reports a novel numerical model of IEC considering condensation from primary air. The influences of nine parameters were comprehensively analyzed under three IEC operating states (non-condensation, partial condensation and total condensation) by using four evaluation indexes: condensation ratio, wet-bulb efficiency, enlargement coefficient and total heat transfer rate. The main results are as follows:

1) Compared with the other simulation results, the developed IEC model can predict $t_{p,out}$ and $\omega_{p,out}$ with the discrepancy of 5.9% and 2.4%, respectively. The discrepancies for predicting the sensible, latent and total heat transfer rate on primary air side are 17.0%, 7.9% and 10.9%, respectively. The discrepancy can be attributed to different heat and mass transfer theory adopted.

2) The condensation from primary air can raise the wall temperature and lower the wet-

bulb efficiency of IEC, but the total heat transfer rate is improved because of the combined sensible heat transfer and dehumidification. The wet-bulb efficiency drops by 22% as $RH_{p,in}$ increases from 30% to 90% (t_p=35℃, t_s=24℃, RHs=60%), but the total heat transfer rate is 1.8 times larger than that of non-condensation state when the RH reaches 90%.

3) The condensation from primary air tends to take place with higher primary humidity, smaller primary air velocity, lower secondary air temperature and humidity, higher secondary velocity, smaller channel gap and higher wettability. The stronger the condensation effect, the lower the wet-bulb efficiency, but the higher the enlargement coefficient and total heat transfer rate. The enlargement coefficient can reach up to 4.5, implying the latent heat transfer accounts for 77.8% of the total heat transfer.

4) For IEC condensation state, the increase of secondary air velocity, decrease of channel gap and improvement of wettability can achieve more obvious positive effect on enhancing IEC cooling capacity than in non-condensation state. In condensation sate, the wet-bulb efficiency and total heat transfer rate still increase significantly when u_s/u_p exceeds 1.5; the total heat transfer rate increases most rapidly when the channel gap < 5mm, so the optimal gap should be no more than 5mm; the total heat transfer rate still increases obviously when the wettability > 0.4.

Chapter 7

Parameter sensitivity analysis and configuration optimization

7.1 Introduction

For high efficient cooling system, the parameter study, sensitivity analysis and configuration optimization are crucial because they could provide valuable guidance for favorable operating conditions and system design. A lot of such studies have been conducted to IEC under its non-condensation state. The models of IEC including traditional IEC, RIEC and M-cycle IEC were established and solved numerically or analytically to investigate the influence of inlet air conditions (temperature, humidity and velocity) and unit geometry on its performances [Jradi & Riffat 2014, Hasan 2010 & 2012, Zhan et al. 2011]. A sensitivity analysis was performed by Bolotin et al. [2015] based on ε-NTU method to determine the preferable operating conditions for the cross-type IEC and RIEC. Kim et al. [2015] conducted a comprehensive sensitivity study by 2^k-factorical experiment design approach. The influence ranking of seven parameters was obtained and a practical thermal performance correlation was derived by linear regression.

The optimization of IEC mainly includes the optimization of NTU_p, geometry size and

air flow ratio. A global optimization method based on the entransy theory was proposed to be applied on EC by Yuan and Chen [2012]. The optimal NTU_p to achieve maximum efficiency of IEC was discussed among three commercial prototypes [Hsu et al. 1989] as well as a cross-flow dew-point IEC [Anisimov et al. 2015]. Pandelidis and Anisimov [2015] conducted an optimization study on the hole arrangement and size of the secondary and primary part in the dry channels of M-cycle IEC. Anisimov et al. [2015] proposed a novel combined parallel and counter flow RIEC and optimized NTU_p and air flow ratio accordingly. Goldsworthy and White [2011] optimized the regeneration temperature and supply/regeneration flow ratio of a desiccant IEC cooling system. In sum, the parameter study, sensitivity analysis and configuration optimization of IEC operates under non-condensation state had been well investigated.

However, the relevant research on IEC with condensation is very limited. Although model work can be found in open literatures [Cui et al. 2015, Yang et al. 2006], the intensive parameter study, sensitivity analysis and optimization were not presented. So the intensive parameter study was conducted using a novel IEC model considering condensation in Chapter 6. This Chapter is a follow-up research focusing on IEC parameter sensitivity analysis and configuration optimization under condensation state. It can be deduced that the optimized IEC configuration under condensation state may differ from that of non-condensation state because of distinguished heat and mass

transfer process.

The detail research flow chart is shown in Fig.7.1. Firstly, seven parameters (t_p, RH_p, t_s, RH_s, u_p/u_s, s, H) were selected for parameter sensitivity analysis. The orthogonal test was designed and simulations results were analyzed. At last, the most influential and engineering controllable parameters were optimized.

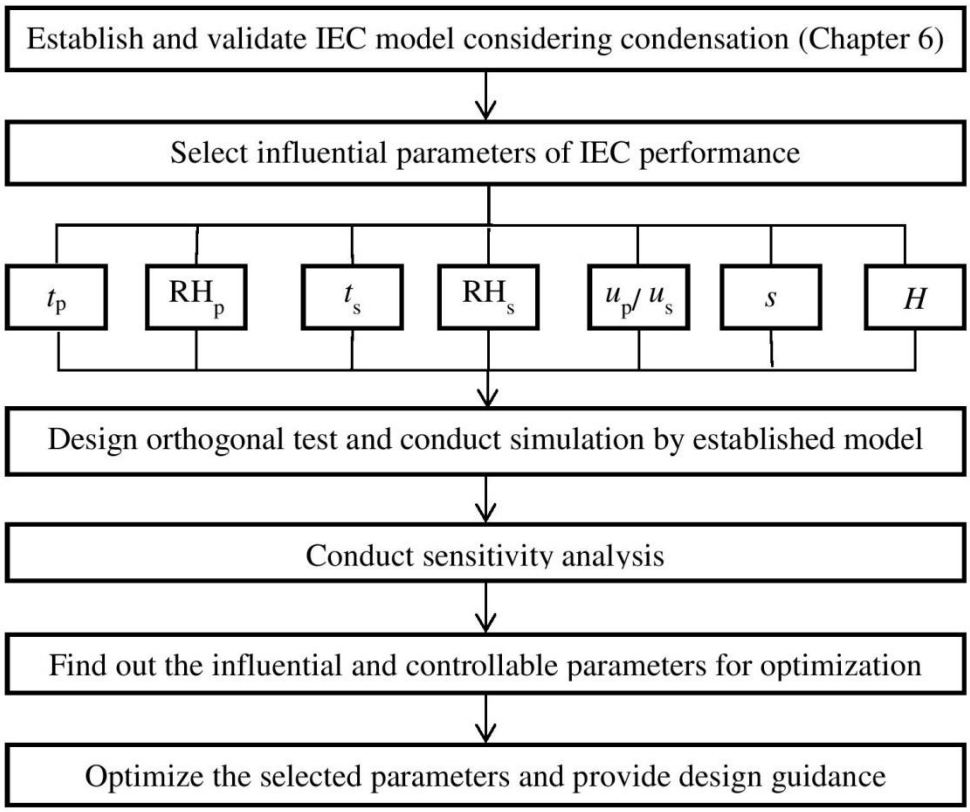

Fig. 7.1 Research flow chart for parameter sensitivity analysis and optimization

7.2 Modeling

The parameter sensitivity analysis and optimization are based on the validated models. The IEC thermal performance is based on the numerical model developed in Chapter 6 and the power consumption is based on the analytical model developed in Chapter 4, Section 4.4. The IEC schematic diagram with geometrical identifications (such as channel gap *s* and cooler height *H*) is shown in Fig. 4.1.

Three evaluation indexes are proposed as the objectives for sensitivity analysis from the aspect of sensible, latent and total cooling capacities. The wet-bulb efficiency is used as an evaluation index for rating the sensible cooling ability of IEC:

$$\eta_{wb} = \frac{t_{p,in} - t_{p,out}}{t_{p,in} - t_{wb,s}} \tag{7.1}$$

The enlargement coefficient ε is used for evaluating the enlarged heat transfer rate associated with condensation. The larger the ε, the more latent heat accounts for.

$$\varepsilon = \frac{Q_{tot}}{Q_{sen}} = \frac{c_{pa} \cdot m_p \cdot (t_{p,in} - t_{p,out}) + h_{fg} \cdot m_p \cdot (\omega_{p,in} - \omega_{p,out})}{c_{pa} \cdot m_p \cdot (t_{p,in} - t_{p,out})} \tag{7.2}$$

The total heat transfer rate Q_{tot} is used for evaluating the overall heat transfer rate of IEC,

which can be calculated and rewritten as:

$$Q_{tot} = \varepsilon \cdot Q_{sen} = \varepsilon \cdot m_p \cdot c_{pa} \cdot (t_{p,in} - t_{p,out}) = \eta_{wb} \cdot \varepsilon \cdot m_p \cdot c_{pa} \cdot (t_{p,in} - t_{wb,s,in}) \qquad (7.3)$$

The values of m_p, $t_{p,in}$ and $t_{wb,s,in}$ are decided by the air flow rate demand, outdoor weather condition and indoor design parameter. They are engineering uncontrollable once the application field selected. Thus, for a certain project, the value of $\eta_{wb} \cdot \varepsilon$ plays an important role in determining the total heat transfer rate and needs to be optimized. The synthetic index calculated by $\eta_{wb} \cdot \varepsilon$ is therefore proposed as the objective for optimization.

7.3 Sensitivity analysis method

7.3.1 Orthogonal test

The orthogonal test is a high efficient, fast and economical design method for the multiple factors with multiple levels. By arranging the representative experiment reasonably using the orthogonal test table, the importance of each factor and optimized level combination can be obtained with minimal number of experiments.

Seven parameters (t_p, RH_p, t_s, RH_s, u_p/ u_s, s and H) are selected for the sensitivity analysis to determine the most influential parameters for IEC performance under

condensation state. The rank of parameter influence on three indexes (η_{wb},, ε and $\eta_{wb} \cdot \varepsilon$) are analysed. The rank of influence on η_{wb}, ε and $\eta_{wb} \cdot \varepsilon$ represent the rank of influence on sensible heat transfer, latent heat transfer and total heat transfer, respectively.

The ranges of t_p and RH_p are selected according to the weather condition in hot and humid regions; t_s and RH_s are based on the usual range in an A/C room. In majority application cases, supply air to exhausted air rate ratio (u_p/u_s) equals to 1. However, in some special application fields, such as clean room and rooms contain contaminants, positive and negative pressure should be provided respectively to prevent contaminants entering or spreading outside the room. Therefore, u_p/u_s can be smaller or larger than 1. Besides, the commonly recommended air velocity of IEC is 2~4 m/s considering the pressure drop and adequate heat transfer, thus u_p/u_s ranges from 0.5 to 2. Based on the two points, the range of u_p/u_s is determined to be 0.5 ~2 in the sensitivity analysis. The u_s and L are set to be 2.0 m/s and 0.5 m, respectively. The number for channel pairs is 50 in the simulation. Three levels are selected for each parameter before the orthogonal test table can be determined. The ranges and levels of the parameters are listed in Table 7.1. The standard seven-parameter and three-level orthogonal test table $L_{18}(3^7)$ is selected and the simulation is conducted according to the arrangement of $L_{18}(3^7)$. The total number of simulation is 18 times, which is much less than the comprehensive simulation scheme (3^7=2187).

Table 7.1 Parameter ranges and levels in orthogonal test

No.	Parameter	Range	Level 1	Level 2	Level 3
1	t_p (℃)	30~38	30	34	38
2	RH_p (%)	60~90	60	75	90
3	t_s (℃)	22~28	22	25	28
4	RH_s (%)	40~70	40	55	70
5	u_p/ u_s	0.5~2	0.5	1.25	2
6	s (mm)	2~10	2	6	10
7	H (m)	0.5~2	0.5	1.25	2

7.3.2 Data analysis methods

Two methods were adopted in analysing the results of orthogonal test: range method and analysis of variance method.

7.3.2.1 Range method

The range method is one of the most commonly used analysis methods. It can rank the influence of parameters and select the optimal combination of levels with simple calculation. However, it can not estimate the error and the accuracy is also limited. The influence of parameter can be evaluated by R_j in the range method, which is calculated as Eq.(20). The larger the R_j, the more influential the parameter.

$$R_j = \max[\bar{y}_{j1}, \bar{y}_{j2}, ...] - \min[\bar{y}_{j1}, \bar{y}_{j2}, ...] \quad (7.4)$$

where, R_j is the range of factor *j*; $\bar{y}_{jk}$ is the average of y_{jk}; y_{jk} is the sum of experimental index on level *k* of factor *j*.

Based on the range method, the parameter - index trend is usually used as a visualized way for displaying the influence of each parameter on the index. The level of the parameter is used as x-axis and the average index under different level is used as y-axis.

7.3.2.2 Analysis of variance method

Analysis of variance method is a rigorous statistical method for analyzing the data. It can provide accurate results on the ranking of parameter influence and significance test, but needs more complex calculation. The influence of parameter can be evaluated by total sum of squared deviations (*S*), calculated by Eq.(7.5). The larger the *S*, the more influential the parameter. The significant of a certain parameter can be investigated by F-test method.

The total sum of squared deviations is calculated as:

$$S = \sum_{i=1}^{a} (y_i - \bar{y})^2 = \sum_{i=1}^{a} y_i^2 - \frac{1}{a} (\sum_{i=1}^{a} y_i)^2 \tag{7.5}$$

where, y_i is the experiment data at the time *i*; *a* is the number of experiment; $\bar{y}$ is the

average value of the experiment data;

The sum of squared deviations in column *j* can be calculated as:

$$S_j = \frac{a}{b}\sum_{k=1}^{b}(\bar{y}_{jk} - \bar{\bar{y}})^2 = \frac{b}{a}\sum_{k=1}^{b} y_{jk}^2 - \frac{1}{a}(\sum_{i=1}^{a} y_i)^2 \tag{7.6}$$

where, *b* is the number of factor levels; $\bar{y}_{jk}$ is the average value for level *k* in column *j*;

The freedom of the total sum of squared deviations is:

$$f = a - 1 \tag{7.7}$$

The freedom of the sum of squared deviations in column *j* is:

$$f_j = b - 1 \tag{7.8}$$

The statistics index F_A is calculated as:

$$F_A = \frac{S_A / f_A}{S_e / f_e} \tag{7.9}$$

where, F_A is the *F* ratio of factor A; S_A is the sum of squared deviations of factor A; S_e is

the sum of squared deviations of experimental error; f_A is the freedom of factor A and f_e is the freedom of error.

The threshold $F_{0.01}(f_A, f_e)(\alpha=0.01)$ for the freedom of f_A and freedom of f_e can be checked in the statistics toolbox. If $F_A > F_{0.01}(f_A, f_e)$, the influence of factor in column j is significate. If not, the influence is not significant.

The contribution ratio of factor j can be calculated as:

$$\rho_j = \frac{S_j - f_j \cdot V_e^{'}}{S}(\%) \tag{7.10}$$

where, $V_e^{'}$ is the average sum of squared deviations of errors.

7.4 Sensitivity analysis results

The results of parameter sensitivity analysis using range method and analysis of variance method are presented in this section. The rank of parameter influence on η_{wb}, ε and $\eta_{wb} \cdot \varepsilon$ are presented as well as their contribution ratio and significance of influence.

The orthogonal table $L_{18}(3^7)$ and corresponding simulation results are presented in Table 7.2. It can be seen from Table 7.2 that both η_{wb} and ε varies in a large range between

0.171 to 0.905 and 1.0 to 5.19, respectively, results in a variation of $\eta_{wb}\varepsilon$ from 0.49 to 3.39. Besides, a larger η_{wb} corresponds with a smaller ε. It means that under condensation condition, the latent heat transfer increases with the sensible heat transfer decreases.

Table 7.2 Simulation results of orthogonal test

Case	t_p (℃)	RH_p (%)	t_s (℃)	RH_s (%)	u_p/u_s	s (mm)	H (m)	η_{wb}	ε	$\eta_{wb}\cdot\varepsilon$
1	30	0.6	22	0.4	0.5	2	0.5	0.792	2.17	1.72
2	30	0.75	25	0.55	1.25	6	1.25	0.588	2.19	1.29
3	30	0.9	28	0.7	2	10	2	0.382	3.07	1.17
4	34	0.6	22	0.55	1.25	10	2	0.592	1.86	1.10
5	34	0.75	25	0.7	2	2	0.5	0.533	2.37	1.26
6	34	0.9	28	0.4	0.5	6	1.25	0.393	4.27	1.68
7	38	0.6	25	0.4	2	6	2	0.560	2.07	1.16
8	38	0.75	28	0.55	0.5	10	0.5	0.349	3.37	1.18
9	38	0.9	22	0.7	1.25	2	1.25	0.692	4.71	3.26
10	30	0.6	28	0.7	1.25	6	0.5	0.491	1.00	0.49
11	30	0.75	22	0.4	2	10	1.25	0.331	2.22	0.74
12	30	0.9	25	0.55	0.5	2	2	0.905	3.74	3.39
13	34	0.6	25	0.7	0.5	10	1.25	0.682	1.68	1.14
14	34	0.75	28	0.4	1.25	2	2	0.773	3.02	2.34
15	34	0.9	22	0.55	2	6	0.5	0.209	4.28	0.89
16	38	0.6	28	0.55	2	2	1.25	0.663	1.85	1.23
17	38	0.75	22	0.7	0.5	6	2	0.860	3.58	3.08
18	38	0.9	25	0.4	1.25	10	0.5	0.171	5.19	0.89

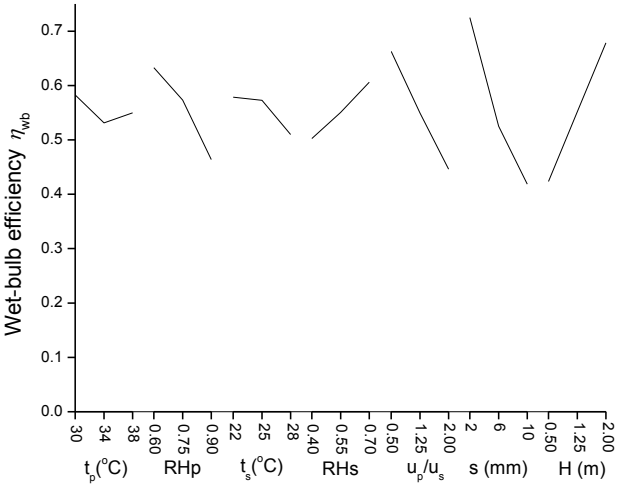

(a) Factors - η_{wb} trend

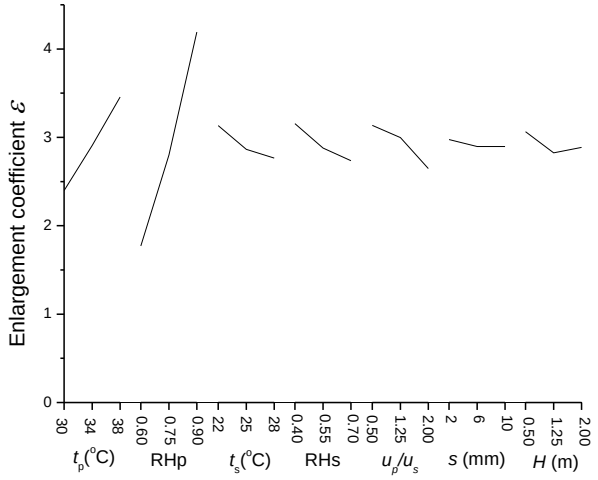

(b) Factor - ε trend

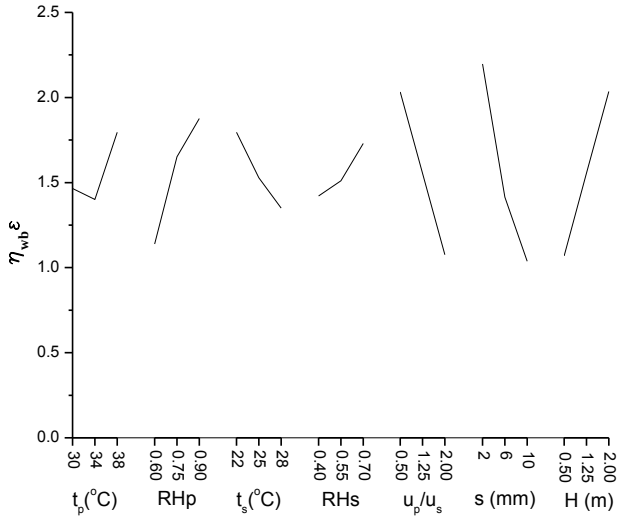

(c) Factor - $\varepsilon \cdot \eta_{wb}$ trend

Fig.7.2 Factors - index trend calculated by range method

The index range of each parameter is calculated by the range method introduced in Section 7.3.2.1. In order to display the influence of each parameter in a visualized way, the factors - index trends are presented in Fig. 7.2. In term of wet-bulb efficiency, the rank of influence for the seven parameters is $s > H > u_p/ u_s > RH_p > RH_s > t_s > t_p$; for the enlargement coefficient is: $RH_p > t_p > u_p/ u_s > RH_s > t_s > H > s$; for the synthetic index is: $s > H > u_p/ u_s > RH_p > t_s > t_p > RH_s$. As the wet-bulb efficiency, enlargement coefficient and synthetic index reflect the sensible, latent and total heat transfer, receptively, the rank of parameter influence on the three kinds of heat transfer can be obtained.

The analysis of variance method can provide more accurate results and more information (Table 7.3) compared with the range method. In addition, the F-test can be used for judging the significance of a parameter. The parameter which has a significant impact on the index is marked with '√' in Table 7.3. It can be seen from Table 7.3, the rank of parameter influence is the same with what obtained from the range method. For the wet-bulb efficiency, the rank is: $s > H > u_p/u_s > RH_p > RH_s > t_s > t_p$; for the enlargement coefficient is: $RH_p > t_p > u_p/u_s > RH_s > t_s > H > s$; for the synthetic index is: $s > H > u_p/u_s > RH_p > t_s > t_p > RH_s$.

Table 7.3 Results by analysis of variance method

Parameter / Index	t_p (℃)	RH_p (%)	t_s (℃)	RH_s (%)	u_p/u_s	s (mm)	H (m)
Variance analysis results for η_{wb}							
Variance	0.008	0.091	0.019	0.032	0.142	0.298	0.195
Contribution	7.1%	10.6%	1.4%	3.1%	17.0%	37.0%	23.8%
Significance*						√	√
Variance analysis results for ε							
Variance	3.398	17.974	0.443	0.553	0.766	0.026	0.190
Contribution	14.4%	76.9%	1.8%	2.3%	3.2%	0.8%	0.7%
Significance*	√	√		√	√		
Variance analysis results for $\eta_{wb} \cdot \varepsilon$							
Variance	0.544	1.711	0.625	0.314	2.731	4.203	2.801
Contribution	1.8%	10.8%	2.4%	17.0%	18.7%	30.1%	19.2%
Significance**						√	√

* α=0.05 was used for F-test.

** α=0.1 was used for F-test.

From Table 7.3, we can see that the wet-bulb efficiency is greatly influenced by the channel gap and cooler height, while the enlargement coefficient is mainly decided by the primary air humidity, which contributes 76.9% to the influence. Channel gap and cooler height have significant influence on the synthetic index, which contribute 30.1% and 19.2%, receptively. Because the synthetic index reflects the total heat transfer process in the IEC operation, which is the most important concern in its design and operation, the channel gap and cooler height are selected as the most influential and engineering controllable parameters to be optimized.

7.5 Configuration optimization

The channel gap and cooler height are two controllable parameters in the design process and they have great influence on the IEC performance according to the sensitivity analysis, therefore their values needs to be optimized based on reasonable ranges of other parameters that are outside of engineering control. As the cooler height varies with the shape of the IEC, it is hard to be used as an index for the optimization. So the optimized results can be given in NTU values for universal reference for the two reasons: 1) cooler height is the only factor affects the heat transfer area ($A=H \cdot L \cdot 2n_p$) as the cooler length and channel pairs are fixed in the study; 2) heat transfer area is the only factor influences the NTU if the channel gap and inlet air conditions are fixed.

7.5.1 Parameter setting

The parameter values in IEC optimization are listed in Table 7.4. The channel gap varied from 2 mm to 10 mm when optimized while the other parameters kept unchanged at certain levels. As the optimized channel gap obtained from this paper is within the range of 2~5 mm, and 2~5 mm gap is also the normal dimension for the market products, the cooler height is therefore optimized under the two limits of channel gap. The cooler height varies from 0.2~1.2 m under s=2 mm and 0.5~3.0 m under s=5 mm when optimized in order to restrict NTU within a normal range. Two representative levels of

primary air temperature (30℃, 35℃) and three RH (40%, 60% and 80%) are selected to represent the weather condition in hot and dry regions, hot and mid-humid regions as well as hot and humid regions. In IEC heat recovery system, t_s and RH_s generally vary within a relatively small range as the exhausted air from A/C space is used. So a constant t_s and RH_s (24℃, 60%) are used in the optimization. The u_p/u_s is set to be 1 because the fresh air supply rate is usually equal to the air exhaust rate in order to keep a normal indoor pressure.

Table 7.4 Parameter values in IEC optimization

Parameter	Optimization parameter	
	s (mm)	*H* (m)
t_p	30℃, 35℃	30℃, 35℃
RH_p	40%, 60%, 80%	40%, 60%, 80%
t_s	24℃	24℃
RH_s	60%	60%
u_p/ u_s	1	1
s	2~10mm	2mm, 5mm
H	0.5m, 1.0m	0.2~1.2m (*s*=2mm, NTU_p: 1.7~10.3) 0.5~3.0m (*s*=5mm, NTU_p: 1.4~8.5)

7.5.2 Optimization of channel gap

According to previous research, the smaller the channel gap, the higher the IEC efficiency. However, the smaller channel gap can lead to larger pressure loss so that the energy consumption by the fan would increase. So there should be a trade-off between

the efficiency improvement and energy consumption. In this study, a net energy saving is proposed as an optimization objective, which is given by:

$$E_{net} = E_{saving} - E_{fan} \tag{7.11}$$

$$E_{saving} = \frac{Q_{saving}}{COP} = \frac{m_p \cdot (i_{p,in} - i_{p,out})}{COP} \tag{7.12}$$

where, E_{net} is the net energy saving by IEC, W; E_{saving} is the total energy saving by IEC, W; E_{fan} is the energy consumption by the primary and secondary air fans, W; Q_{saving} is the total heat recovery by IEC, W; COP is the coefficient of performance of a central A/C , which is set to be 4.5.

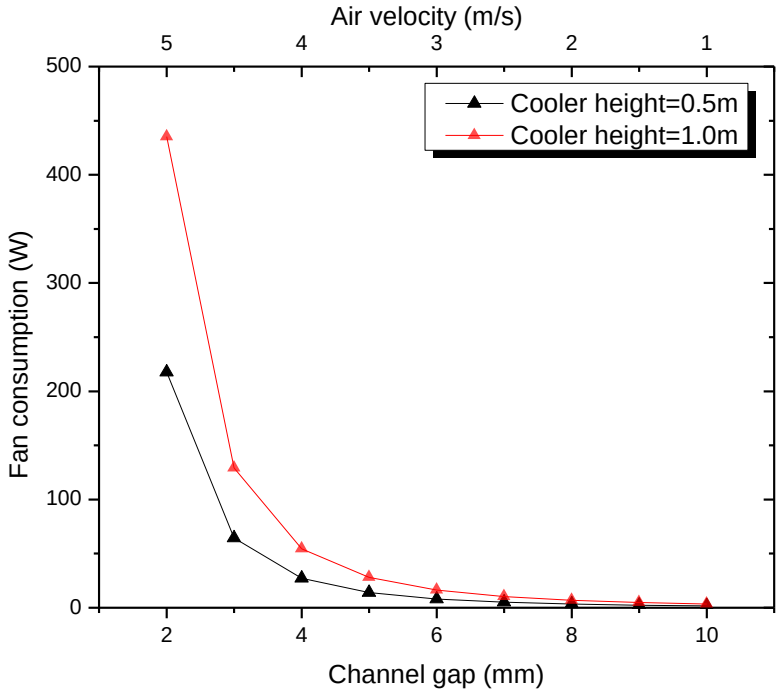

Fig. 7.3 Fan consumption under different channel gap

The model introduced in Section 4.4 in Chapter 4 was adopted to calculate the fan consumption. Fig. 7.3 presents the fan consumption under different channel gap. It can be seen that the fan consumption decreases as the channel gap increases and it drops dramatically when the channel gap increases from 2mm to 4mm.

Fig. 7.4 shows the total energy saving by IEC under different channel gap, which is calculated as: $E_{saving}=m_p\ (i_{p,in}-i_{p,out})/COP$. It can be seen that the saving decreases with the increase of channel gap, especially within the channel gap between 2 mm and 4 mm. It is because the larger the channel gap, the more air is by-passed directly without heat transfer with the cold surface. Besides, it can be noticed that the energy saving of IEC under condensation state is larger than that of non-condensation state. It can be attributed to the condensation enlarges the total heat transfer rate by bringing in latent heat transfer. In addition, the decrease trend of the total energy saving under condensation is more significant than that of non-condensation state, especially when the channel gap ranges from 2 mm to 4 mm.

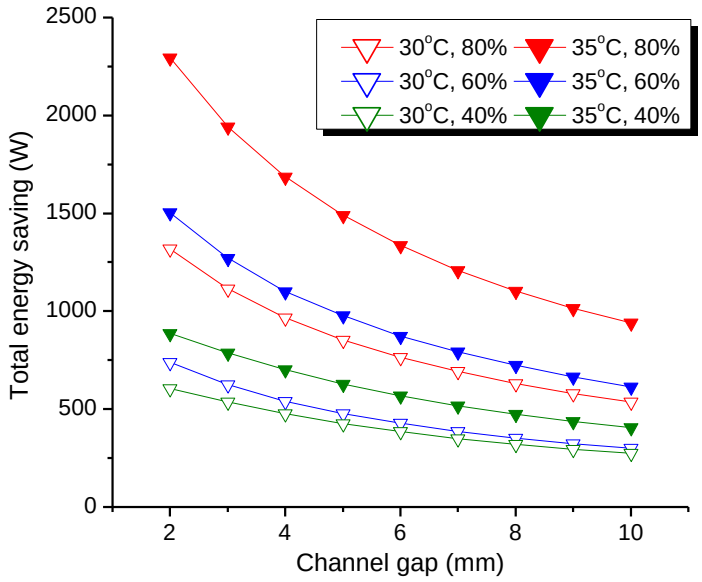

(a) Cooler height=0.5m

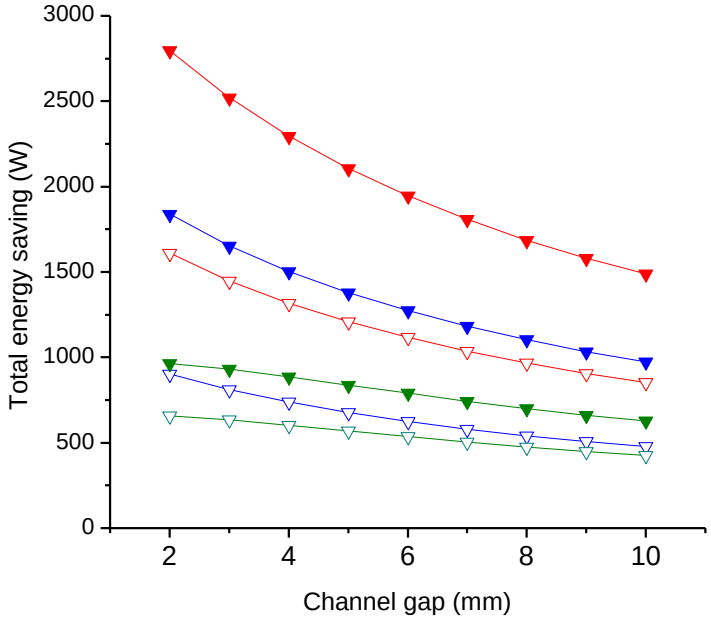

(b) Cooler height=1.0m

Fig. 7.4 Total energy saving under different channel gap

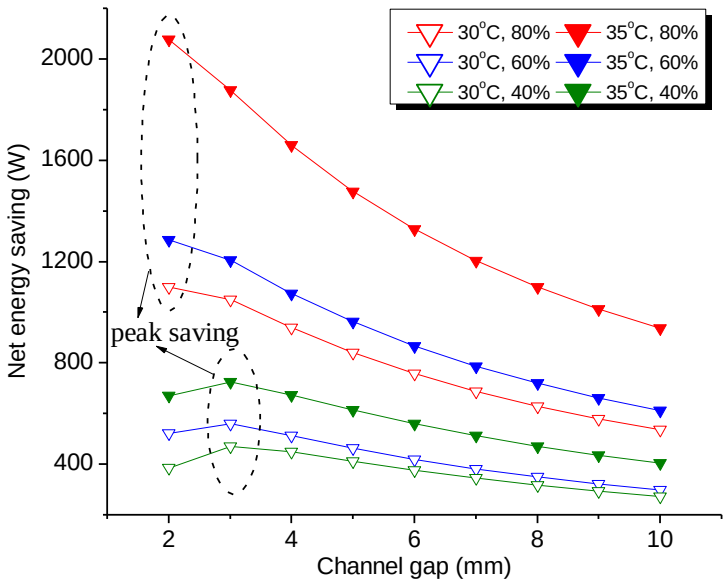

(a) Cooler height=0.5m

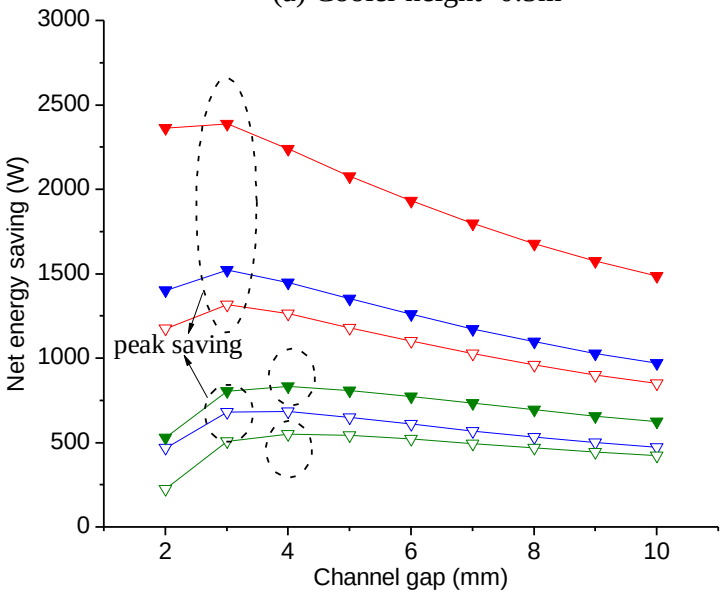

(b) Cooler height=1.0m

Fig. 7.5 Net energy saving under different channel gap

Fig. 7.5 presents the net energy saving under different channel gap. The optimal channel gap is achieved when the net energy saving is the largest. The net energy saving reaches the peak point when the channel gap ranges from 3 mm to 4 mm under the dry primary

air condition (RH=40%); while it ranges from 2mm to 3mm under the humid primary air condition (RH=60% and 80%). So the optimal channel gap of IEC under condensation state is a little smaller than that of traditional non-condensation state. It can be explained as follows. The total energy saving under condensation state increases more rapidly with the decrease of channel gap because of simultaneous enhancement of sensible and latent heat transfer processes. The consumption of the fans, however, remains almost unchanged.

7.5.3 Optimization of cooler height

The increase of cooler height, on one hand, improves the efficiency by adding the heat transfer area, but on the other hand, increases the pressure drop of IEC and its manufacturing cost. So there is a trade-off between the improvement of efficiency and increase of fan consumption and equipment manufacturing cost. Similarly, net money saving is proposed as an optimization objective which is calculated as:

$$M_{net} = E_{pri} \cdot (E_{saving} - E_{fan}) - \frac{I}{365 \times 24 \times T} \tag{7.13}$$

where, M_{net} is the net money saving of IEC, HKD/h; E_{pri} is the electricity price, HKD/kWh; I is the initial investment of IEC, HKD; T is the lifetime of IEC, which is set as 10 years.

The manufacturing cost of IEC is assumed to be in direct proportion to its heat transfer area.

$$I = A \cdot C_{IEC} = 2 \cdot H \cdot L \cdot n_p \cdot C_{IEC} \tag{7.14}$$

where, C_{IEC} is the manufacturing cost per unit area, HKD/m^2, which is set to be 150 HKD/m^2 based on the average quotation on the market.

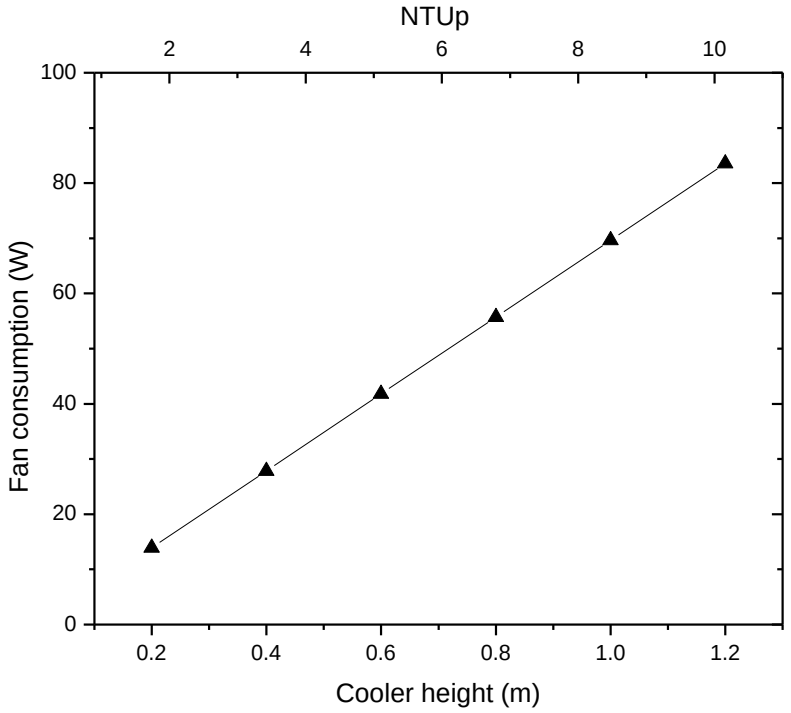

Fig. 7.6 Fan consumption under different cooler height

Fig. 7.6 shows the fan consumption under different cooler height. Because the cooler height can not be easily used as an index for IEC with different shape, $NTU_p=(h_p \cdot A)/(m_p c_{pa})$ is used as the optimization index in this research as stated

previously. We can see that the fan consumption increases linearly with the increase of cooler height and NTU_p.

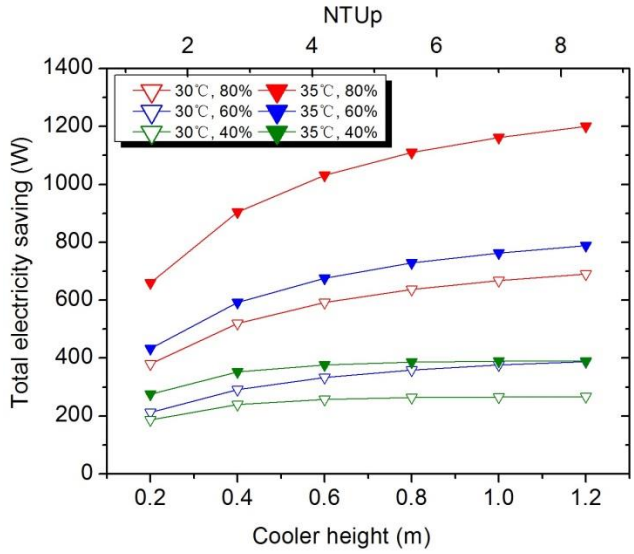

(a) Channel gap s=2mm

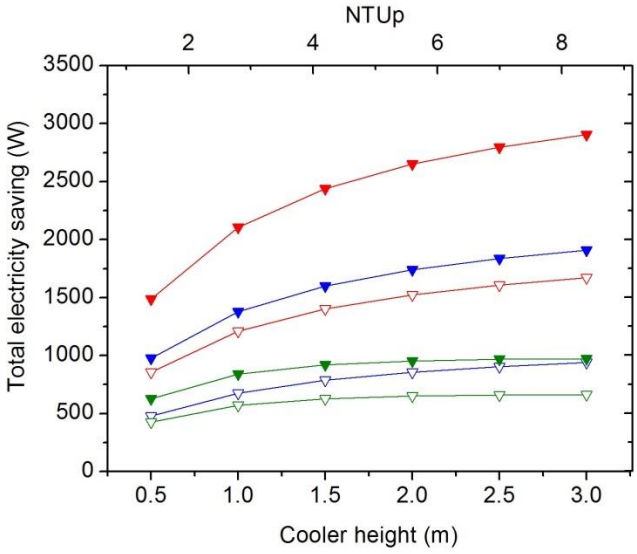

(b) Channel gap s=5mm

Fig. 7.7 Total energy saving under different cooler height

The total energy saving under different cooler height and NTU_p is presented in Fig. 7.7. The total energy saving increases with the increase of NTU_p, but the increase rate slows

down when NTU_p reaches a certain value. It was found the slow-down trend under condensation state is less obvious than that of non-condensation state. It can be seen from Fig.12 that the total energy saving under the low primary air humidity (RH=40%) remains almost steady when NTU_p exceeds 4.0. However, it keeps increasing until NTU_p exceeds 8.0 under high humidity air condition.

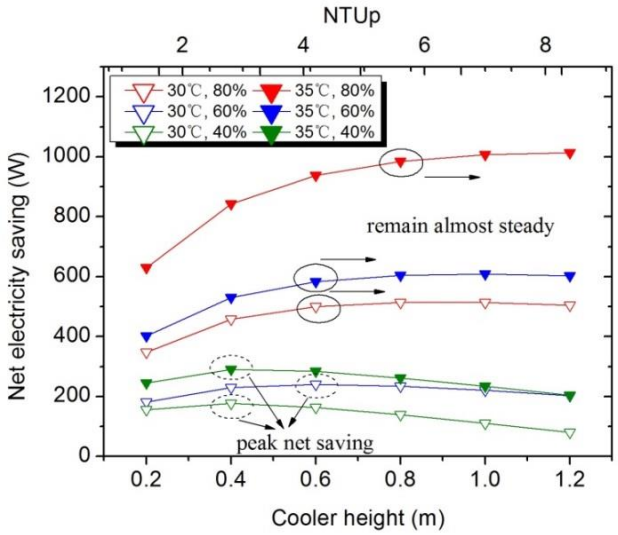

(a) Channel gap s=2mm

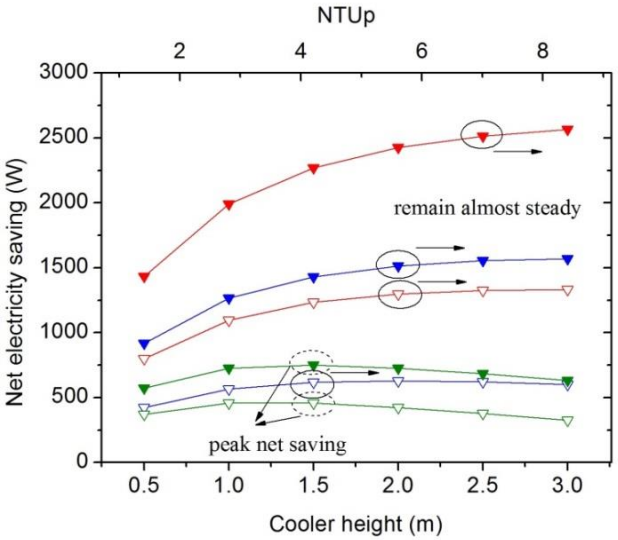

(b) Channel gap s=5mm

Fig. 7.8 Net money saving under different cooler height

Fig. 7.8 presents the net money saving under different cooler height and NTU_p. The peak net saving is achieved when NTU_p is about 3~4 under low RH_p, while it remains almost steady when NTU_p reaches 5~7 under high RH_p. It means that the heat transfer area of IEC should be manufactured larger when applied in humid regions. It can be explained as follows. Under the condensation operation of IEC, the larger heat transfer area not only improves the sensible heat transfer rate but also increases the latent heat transfer rate. The benefit brought by the total energy saving increase is more than the additional consumption by the fan when adding the heat transfer area.

As the manufacturing cost of IEC is a big unknown and varies greatly in different manufactory, three levels of manufacturing cost from 100 to 200 HKD/m^2 were selected to investigate the influence of manufacturing cost on the optimal NTU_p. The results are shown in Fig. 7.9. It can be seen that the influence of manufacturing cost has a limited influence on the IEC optimal NTU_p, especially when the channel gap is very small. Under the channel gap of 2mm, the optimal NTU_p under IEC condensation state is about 5~7 when the manufacturing cost ranges from 100 HKD/m^2 to 200 HKD/m^2, which is larger than that of non-condensation state. Under the channel gap of 5mm, the situation can be slightly different. The optimal NTU_p increases a little as the manufacturing cost decreases from 200 HKD/m^2 to 100 HKD/m^2 on both non-condensation and condensation state. It means that the heat transfer area of IEC should be manufactured to

be larger when the manufacturing cost is lower. Overall, the optimal NTU_p is about 3~4 (non-condensation) and 4~7 (condensation) under 200 HKD/m^2 manufacturing cost, while it increases to about 4~5 (non-condensation) and 5~7 (condensation) under 100 HKD/m^2 manufacturing cost.

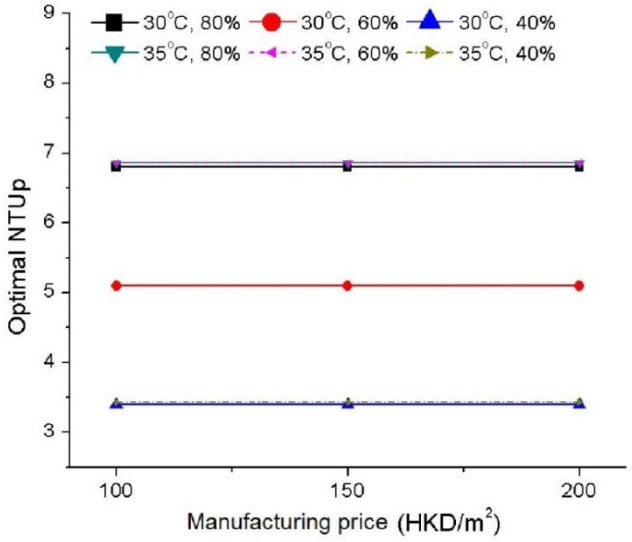

(a) channel gap s=2mm

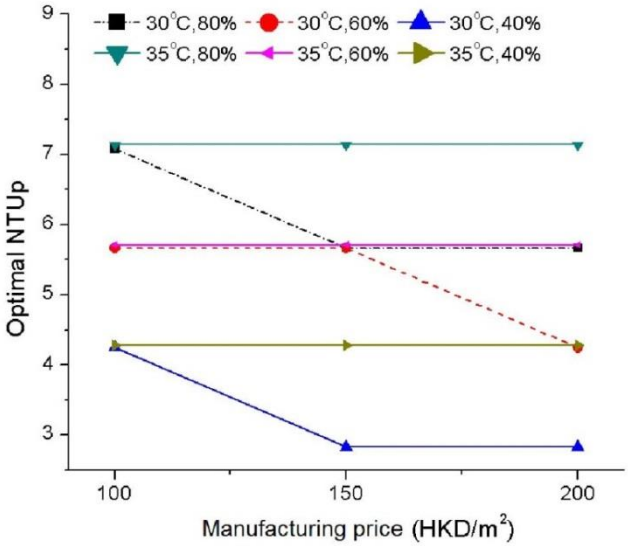

(b) channel gap s=5mm

Fig. 7.9 Optimal NTU_p under different manufacturing price of IEC

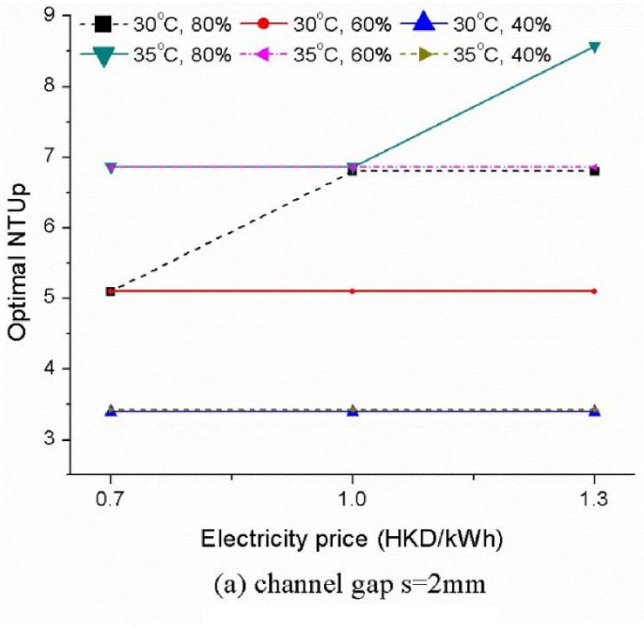

(a) channel gap s=2mm

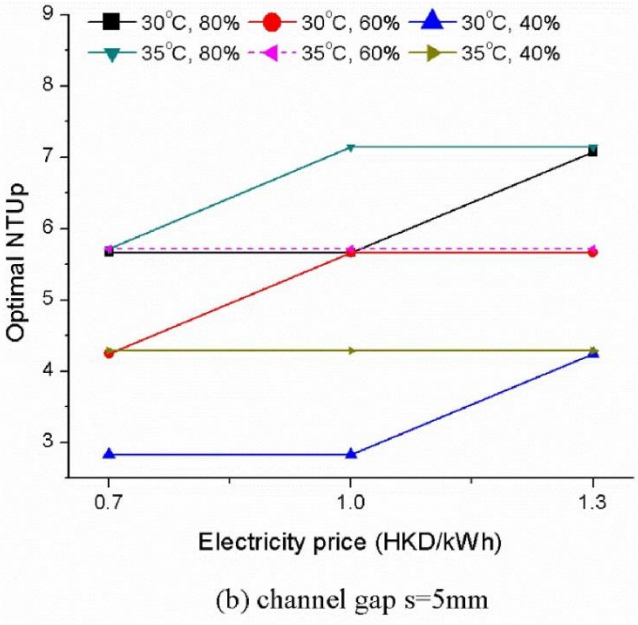

(b) channel gap s=5mm

Fig. 7.10 Optimal NTU_p under different electricity price

The main benefit of IEC application in an A/C system is energy saving, which can be converted into electricity bill saving in industry. Fig. 7.10 presents the influence of electricity price on the optimal NTU_p of IEC. It can be seen that the optimal NTU_p

decreases with the decrease of electricity price under both condensation and non-condensation states. It means that the IEC should be manufactured to be larger if the electricity price is high, so that more bill fee can be saved. Under the channel gap of 5mm, the optimal NTU_p is about 4~5 when the electricity price is 1.3 HKD/kWh and it drops to 3~4 when electricity price decreases to 0.7 HKD/kWh under non-condensation state. Under condensation state, the optimal NTU_p is about 6~7 under the electricity price of 1.3 HKD/kWh and it drops to 4~6 when the electricity price is 0.7 HKD/kWh.

Table 7.5 Results comparison with other literatures

Ref.	IEC type and flow pattern	Optimized value	Application
[Anisimov et al. 2015]	Combined parallel and counter flow	NTU_p:1.5~2.8	Cooling alone
[Bolotin et al. 2015]	Traditional and regenerative, cross flow	$NTU_p \approx 5.0$	Cooling alone
[Anisimov et al. 2015]	Traditional IEC, cross flow	$NTU_p \approx 6.0$	summer: IEC winter: HE
[Hsu et al. 1989]	Unidirectional flow Counter flow Two closed loop with extraction	$NTU_p=4$; $NTU_p=7$; $NTU_p=10$	Cooling alone
[Fakhrabadi & Kowsary 2016]	regenerative IEC	*s*: 4~6 mm	Cooling alone
[Zhan et al. 2011]	M-cycle cross-flow IEC	*s*: ≤4 mm	Cooling alone
Present	Traditional, counter flow	NTU_p: 3~5; *s*: 3~4 mm (non-condensation)	Heat recovery

	NTU_p: 4~7; *s*: 2~3 mm (condensation)

In sum, the optimal NTU_p of IEC in pre-cooling system is 3~5 under non-condensation state and 4~7 under condensation state by considering the thermal performance, fan consumption, manufacturing price and electricity price. The results compared with other relevant literatures are listed in Table 7.5.

7.6 Summary

This chapter reports the parameter sensitivity analysis and optimization of IEC under condensation state. The main conclusions are summarized as:

1) Unlike the previous reported studies for IEC with no condensation, in current study, the sensitivity analysis of IEC under condensation condition was conducted and influence ranking of each parameter was reported. The enlargement coefficient and synthetic index were proposed to evaluate the latent and total heat transfer performance. The channel gap and cooler height were found to have significant impact on the wet-bulb efficiency η_{wb}. The primary air humidity had the dominate influence on the enlargement coefficient ε. The channel gap and cooler height had the most important effect on the synthetic index $\eta_{wb}\varepsilon$. The influence rank of parameters for the synthetic index is: $s > H > u_p/u_s > RH_p > t_s > t_p > RH_s$.

2) The optimized channel gap and NTU_p under IEC condensation condition in this study were found to be different from previous reported studies, in which condensation was not considered. The optimized channel gap is 2–3 mm and 3–4 mm under condensation and non-condensation state, respectively. The optimized NTUp is 4–7 and 3–5, respectively. Thus, in practical engineering, the channel gap of IEC should be manufactured to be a little smaller and heat transfer area should be manufactured to be larger than that of dry regions when IEC used in humid area where condensation may likely take place. Besides, the heat transfer area of IEC should be made larger when the manufacturing cost is lower and the electricity price is higher.

Chapter 8

Experimental study of IEC thermal performance

8.1 Introduction

To reduce the energy consumption in an A/C system, energy recovery can be adopted by installing a heat exchanger before an AHU to pre-cool the incoming fresh air using the exhaust air from A/C space. The heat exchanger can be a traditional sensible air-to-air heat exchanger (plate, fin-plate and fin-tube), heat recovery wheel (sensible and enthalpy), indirect evaporative cooler (dry-coil and wet-coil) or any novel heat exchangers.

The traditional sensible air-to-air heat exchanger, acting as an air cooler, is regarded as a reliable and durable heat recovery device in a ventilated A/C system, which is also introduced in ASHRAE Handbook [2008]. The modeling of this device has been fundamentally studied [Hewitt 2008, Barrow et al. 1986, Huang & Shah 1992, An & Choi 2012], however, limited experimental works had been presented in literatures. Fernández-Seara et al. [2011] experimentally analyzed an air-to-air heat recovery unit equipped with a sensible polymer plate heat exchanger (PHE) in residential buildings, but no condensation case was reported. Gendebien et al. [2013] developed a model for

an air-to-air heat exchanger dedicated to heat recovery ventilation considering dry and partially wet regimes. The experimental tests were conducted but focused on validation of the proposed semi-empirical model.

The IEC is another heat exchanger which can be used for energy recovery in an A/C system. The experimental study and filed measurement have been conducted to various kinds of IEC and IEC system. However, all the experimental work focuses on evaluating the sensible cooling ability of IEC from the aspects of either operational performance (EER, wet-bulb efficiency, cooling capacity) or impact factors. No experimental study can be found on evaluating both the sensible and latent cooling performance of IEC with condensation from primary air. It can be a research gap for IEC energy recovery technology applied in humid regions. In sum, the intensive experimental study on evaluating the performances of both traditional air cooler and IEC with condensation is lacking.

Therefore, in this Chapter, an experimental study was conducted to evaluate the plate type air cooler performance under four operating modes (dry/wet and low/high humidity). Under dry operating mode, the air cooler serves as a traditional air cooler; while under wet operating mode, it works as an IEC. So comparisons can be made between traditional air cooler and IEC under same configuration. The cooler dynamic

performances during different operating mode transition and steady performances under different parameter influence were investigated as well. The experiment study aims at, on one hand, comparatively testing the operational characteristics of traditional air cooler and IEC under both non-condensation and condensation states, on the other hand, verifying the model in Chapter 6.

8.2 Description of test rig

The schematic diagram and photograph of the test rig are shown in Fig. 8.1 and Fig. 8.2, respectively. A cross-flow plate type heat exchanger was designed and fabricated as the core component of the test rig. The heat exchanger is stacked with alternative primary air and secondary air channels which is separated by the thin aluminum plates. Both the channels are supported by the plastic corrugated sheets and the aluminum plates are hydrophilic-coated to improve its wettability. The geometric parameters of the experimental heat exchanger module are listed in Table 8.1. This heat exchanger can be used as a traditional air cooler, which uses the cool exhausted air from air-conditioned room to pre-cool the hot fresh air in an A/C system for energy conversation.

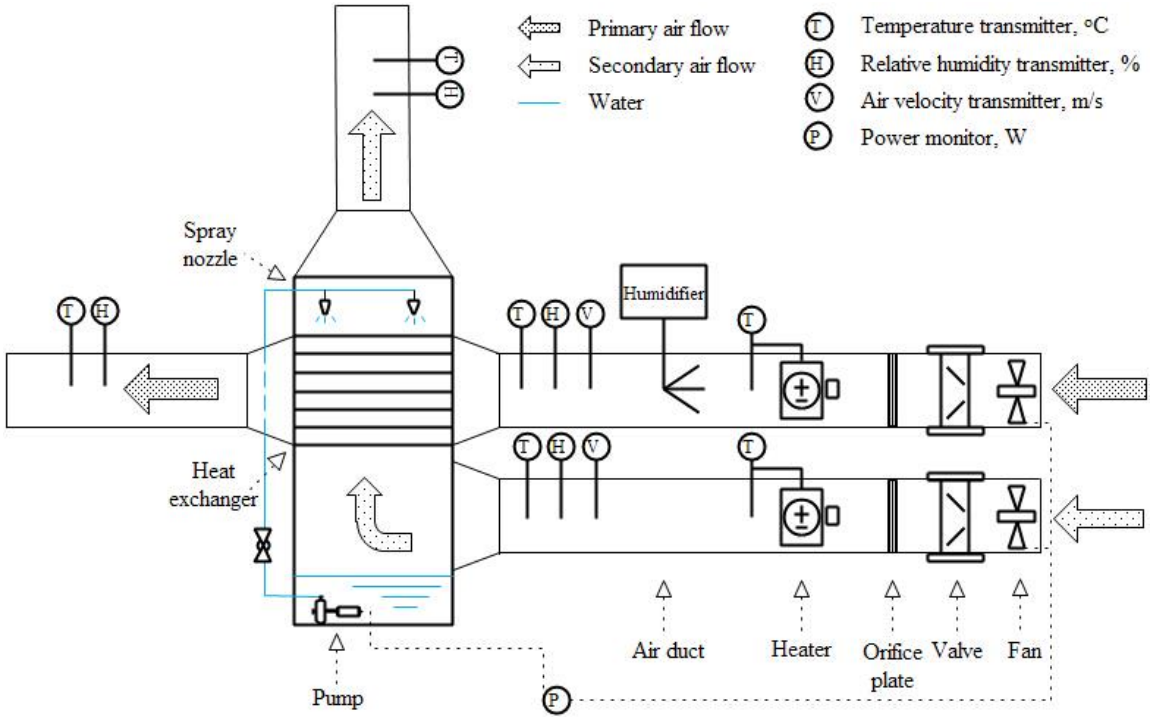

Fig. 8.1 Schematic diagram of the test rig

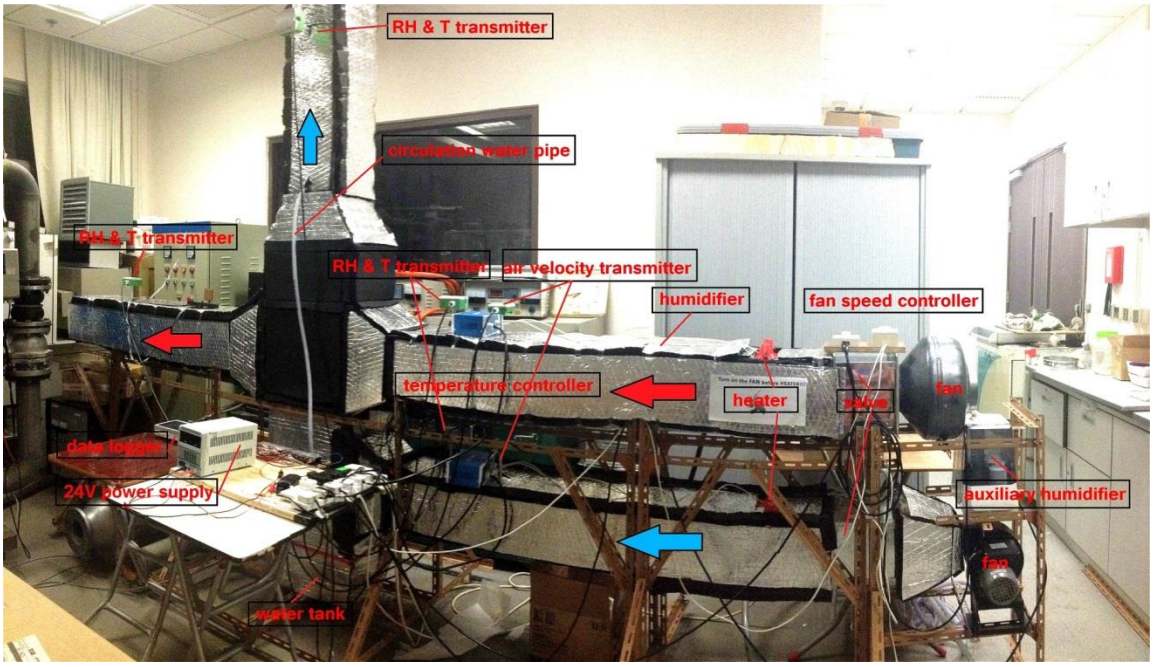

Fig. 8.2 Real picture of the test rig

Table 8.1 Geometric parameters of experimental heat exchanger module

Parameters	Value
Cooler length (L)	0.4m
Cooler width (W)	0.2m
Cooler height (H)	0.4m
Primary air channel gap (s)	4mm
Secondary air channel gap (s)	4mm
Channel pairs (n)	25
Plate thickness (δ)	0.15mm

An IEC consisted of the above heat exchanger, a water circulation and distribution system has been assembled. Two water spray nozzles connected with the PVC pipes are hang vertically on the top of the heat exchanger to wet the secondary air channels. The pipes are supported by the steel angles inside the air duct. An submerged pump is fixed at the bottom of the water tank to enable the water spraying and circulation.

In sum, the plate type air cooler in the test rig can operate as two different air coolers. It works as an IEC when water spraying system is turned on and operates as a traditional air cooler without water spraying. To investigate and compare the cooling performance of the two kinds of air coolers under various operating conditions, an experimental setup was established. The test rig is composed of IEC, four air ducts (primary air inlet, primary air outlet, secondary air inlet and secondary air outlet), fans, valves, orifice plate, electrical heater, eletrode humidifier, control devices and data collection system. The test rig is set up in a closed A/C room, where the room temperature is controlable.

The indoor air is used as both inlet primary air and secondary air, and then further treated by the heater and humidifier installed inside the ducts to reach a desired inlet air condition. The heat exchanger as well as all the air duct surfaces are insulated with neoprene foam to prevent heat loss to surroundings. During the experiment, the air temperature can be adjusted to the pre-setting values by Proportion Integration Differentiation (PID) controllers. The varible speed controller is used to adjust the inlet air velocity entering the heat exchanger. The ranges of the controllable parameters in the experiment are summaried in Table 8.2.

Table 8.2 Ranges of various parameters in experiment

Parameter	Symbol	Unit	Range
Inlet primary air temperature	$t_{p,in}$	℃	27.1~34.4
Inlet primary air humidity	$\omega_{p,in}$	g/kg	12.1~20.5
Inlet primary air velocity	$u_{p,in}$	m/s	1.34~5.21
Inlet secondary air temperature	$t_{s,in}$	℃	22.3~28.4
Inlet secondary air humidity	$\omega_{s,in}$	g/kg	10.2~14.8
Inlet secondary air velocity	$u_{s,in}$	m/s	1.77~4.87

The primary air temperature is based on the temperature range in hot seasons, when A/C is needed. The secondary air conditions are based on the temperature and humidity ranges in an A/C room. The humidification rate provided by the humidifer remains at a relative constant value when it operated. The data measuring devices included four temperature and humidity transmitters (Pt 1000 sensor, E+E Co., Model: EE160), two

air velocity transmitters (hot-film anemometer, E+E Co., Model: EE65) and one power meter. A 24V DC battery was used to provide the power supply to all the transmitters. The measurement instruments and specification are shown in Table 8.3. The photographs of measuring and control devices are shown in Fig. 8.3.

Table 8.3 Specification of different measuring instruments

Parameters	Device	Range	Accuracy
Air dry bulb temperature	Pt1000 Model: EE160	-15~60℃	±0.3℃
Air relative humidity	Pt1000 Model: EE160	10~95% RH	±2.5% RH
Air velocity	Hot film anemometer Model: EE65	0~10 m/s	±0.2m/s
Power consumption	Power meter	0~10A 0~2200W	0.01W

Under each test case, the inlet and outlet air parameters are measured by the transmitters and recorded by the data logger (GRAPHTEC GL820). The collected data include the inlet and outlet temperatures and relative humidity of primary air and secondary air, and inlet air velocities of the two air streams. All the air parameters data were recorded at 2 seconds step. The steady state is defined as the outlet temperature and relative humidity variations are within 0.1℃ and 1% for 5 minutes. The average values of the measured data in the 5 minutes span are used for steady operation analysis. The power consumptions of the two air fans and circulation pump are measured by the power meter.

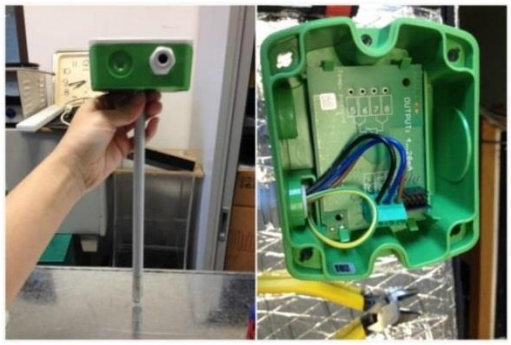

(a) RH & T transmitter

(b) Velocity transmitter

(c) Temperature PID controller

(d) Fan speed controller

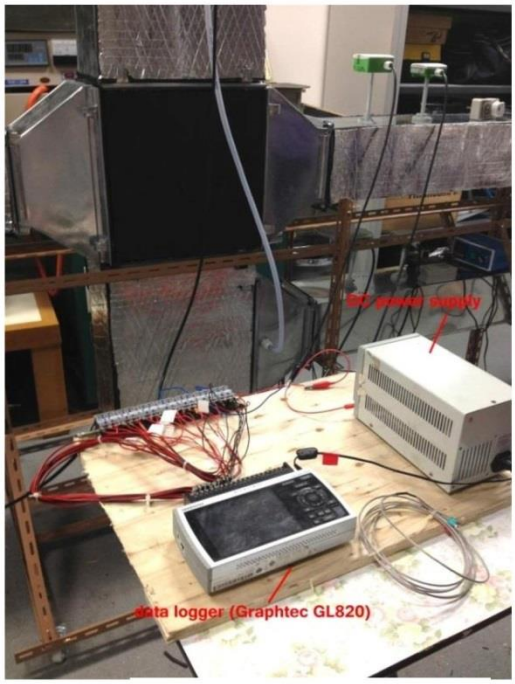

(e) Data logger

(f) Power meter

Fig. 8.3 Measuring and control device in the test rig

8.3 Four operating modes

Four operating modes of the air cooler are explored for comparison study, including: dry operation state with low humidity air, dry operation state with high humidity air, wet operation with low humidity air and wet operation with high humidity air. The on/off state of circulation pump distinguishes the wet and dry operating mode; and on/off state of humidifier creates the high and low humidity primary air. Under wet operating mode, the air cooler acts as an indirect evaporative cooler, while under dry operating mode, it is a traditional plate type air cooler. So the performances of the two kinds of air cooler can be compared under the same configuration. Meanwhile, the air cooler performance under high and low air humidity can also be experimentally investigated in order to compare the energy recovery performance in different climate regions. Under the low humidity primary air condition, there would be only sensible heat transfer on the primary air side. Under the high humidity primary air condition, however, the condensation is likely to take place in the primary air channels because the plate surface temperature could be lower than the primary air dew point temperature. The schematic diagram of the heat and mass transfer process under the four operating modes is shown as Fig. 8.4.

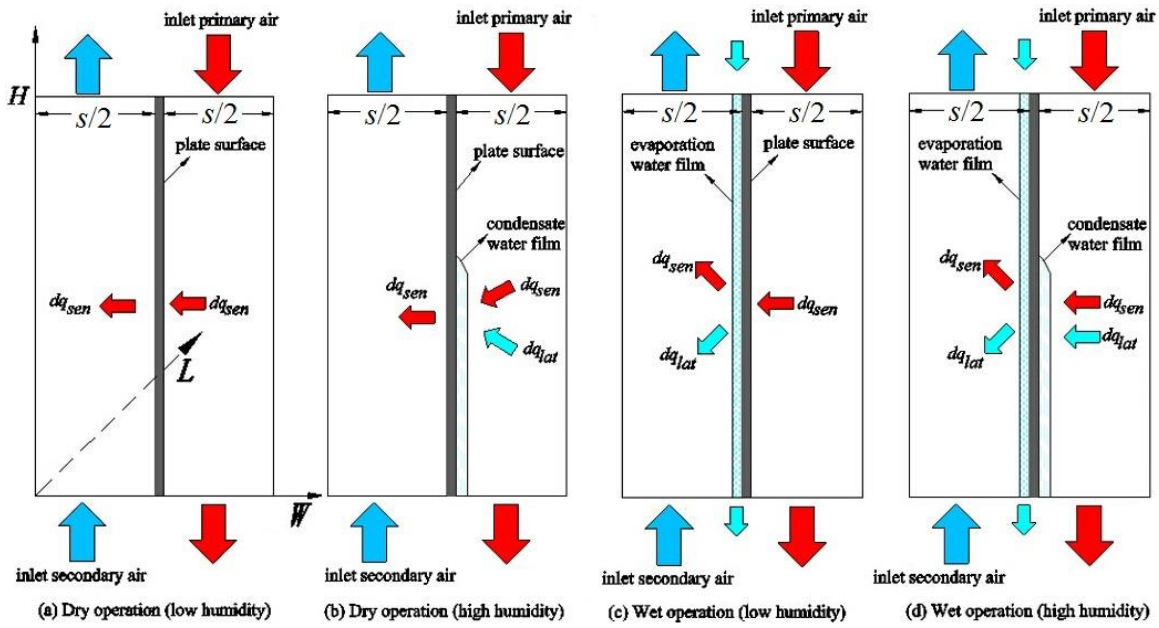

Fig. 8.4 Heat and mass transfer process of air cooler under four operating modes

The settings of pump and humidifier, controllable parameters and performance indicators under four operating modes are listed in Table 8.4.

Table 8.4 Four operating modes in the experiment

Operation mode	HE Type	Circulation pump	Humidifier	Controllable parameters	Performance indicator
Dry operation (low humidity)	Traditional	Off	Off		$Q_{sen,,}$ η, COP
Dry operation (high humidity)	Traditional	Off	On	$t_{p,in,,}$ $t_{s,in}$	$Q_{sen,,}$ $Q_{lat,}$ $Q_{tot,}$ η, η_{lat}, COP
Wet operation (low humidity)	IEC	On	Off	$u_{p,in,,}$ $u_{s,in}$	$Q_{sen,,}$ η_{wb}, COP
Wet operation (high humidity)	IEC	On	On		$Q_{sen,,}$ $Q_{lat,}$ $Q_{tot,}$ η_{wb}, $\eta_{lat,,}$ COP

8.4 Performance indicator and uncertainty analysis

Sensible efficiency η is used to evaluate the sensible heat transfer of traditional heat exchanger, expressed as:

$$\eta = \frac{t_{p,in} - t_{p,out}}{t_{p,in} - t_{s,in}} \tag{8.1}$$

The wet-bulb efficiency η_{wb} is used for rating an IEC, expressed as:

$$\eta_{wb} = \frac{t_{p,in} - t_{p,out}}{t_{p,in} - t_{wb,s,in}} \tag{8.2}$$

The above two performance indicators are commonly used for rating the traditional heat exchanger and IEC under non-condensation state, respectively. Under condensation state, latent efficiency η_{lat} is introduced for rating the latent heat transfer for both kinds of heat exchangers, given as:

$$\eta_{lat} = \frac{\omega_{p,in} - \omega_{p,out}}{\omega_{p,in} - \omega_{s,in}} \tag{8.3}$$

In this study, the traditional heat exchanger and IEC is used as energy recovery device or fresh air pre-cooling device in an A/C system, thus their cooling capacity can be

evaluated by the primary air cooling rate. The sensible cooling capacity, latent cooling capacity and total cooling capacity can be calculated as following equations, respectively.

$$Q_{sen} = m_p \cdot c_{pa} \cdot (t_{p,in} - t_{p,out}) \tag{8.4}$$

$$Q_{lat} = m_p \cdot h_{fg} \cdot (\omega_{p,in} - \omega_{p,out}) \tag{8.5}$$

$$Q_{tot} = Q_{sen} + Q_{lat} = m_p \cdot (i_{p,in} - i_{p,out}) \tag{8.6}$$

The COP of an air cooler is defined as the ratio of total cooling capacity to total power consumption, expressed as:

$$COP = \frac{Q_{tot}}{P} = \frac{m_p \cdot (i_{p,in} - i_{p,out})}{P} \tag{8.7}$$

For the traditional heat exchanger, the total power consumption is contributed by the fans, while for IEC, the total consumption includes fans and pump.

The uncertainties of experimental results are caused by errors in the measuring process. The uncertainty analysis is conducted to examine the validity of collected data by measuring devices. The uncertainty analysis of all the measuring data in the experiment

as well as the calculated performance indicators have been conducted using the method given in the reference [Coleman & Steele 2009]. The uncertainty analysis results are listed in Table 8.5.

Table 8.5 Uncertainty analysis results

Indicator	Nominal value		Relative uncertainty	
Symbol	Low humidity*	High humidity**	Low humidity*	High humidity**
V_p	288 m^3/h	288 m^3/h	± 4.5%	± 4.5%
V_s	360 m^3/h	360 m^3/h	± 3.6%	± 3.6%
η	45%	45%	± 8.7%	± 8.7%
η_{wb}	61%	51%	± 4.2%	± 4.8%
η_{lat}	0% (wet)	36% (wet)	NA	± 12.1%
	0% (dry)	0% (dry)	NA	NA
Q_{sen}	657 W (wet)	548 W (wet)	± 6.1 % (wet)	± 6.6% (wet)
	314 W (dry)	314 W (dry)	± 9.4 % (dry)	± 9.4% (dry)
Q_{lat}	0 W (wet)	718 W (wet)	NA (wet)	± 12.7% (wet)
	0 W (dry)	0 W (dry)	NA (dry)	NA (dry)
Q_{tot}	657 W (wet)	1266 W (wet)	± 6.1% (wet)	± 7.7% (wet)
	314 W (dry)	314 W (dry)	± 9.4% (dry)	± 9.4% (dry)
COP	5.2 (wet)	10.0 (wet)	± 6.1% (wet)	± 7.8% (wet)
	3.0 (dry)	3.0 (dry)	± 9.4% (dry)	± 9.4% (dry)

* Low humidity: u_p=2.0 m/s, u_s=2.5 m/s, t_p=30 ℃, RH_p=45%, t_p=22.5 ℃, RH_s=68%.

**High humidity: u_p=2.0 m/s, u_s=2.5 m/s, t_p=30 ℃, RH_p=75%, t_p=22.5 ℃, RH_s=68%.

8.5 Results and discussion

8.5.1 Energy conservation analysis and result validation

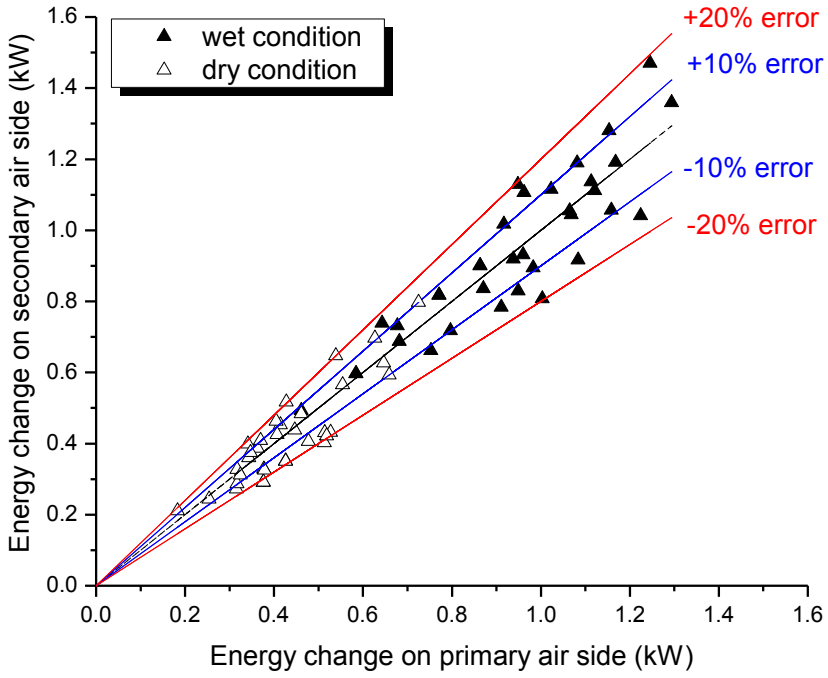

Fig. 8.5 Energy balance of two air streams

The enthalpy reduction of primary air should be equal to the enthalpy increase of secondary air based on energy balance theory. The energy conversation equations on primary air side and secondary air side are given as:

$$Q_p = m_p \cdot (i_{p,in} - i_{p,out}) \tag{8.8}$$

$$Q_s = m_s \cdot (i_{s,out} - i_{s,in}) \tag{8.9}$$

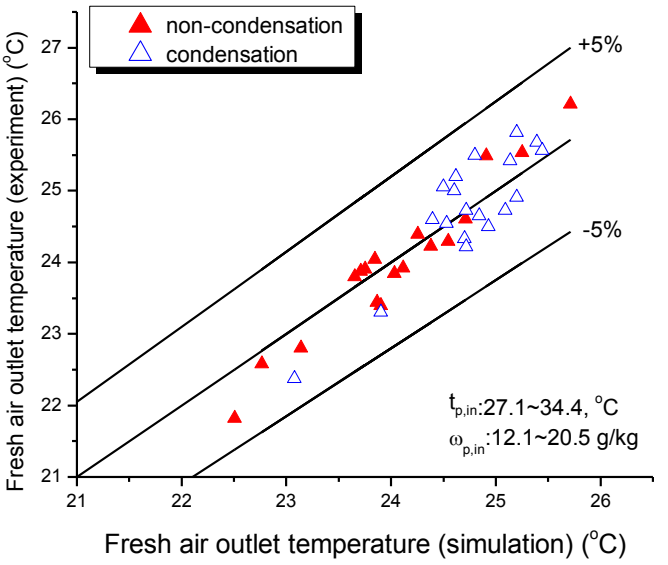

(a) comparison of outlet temperature

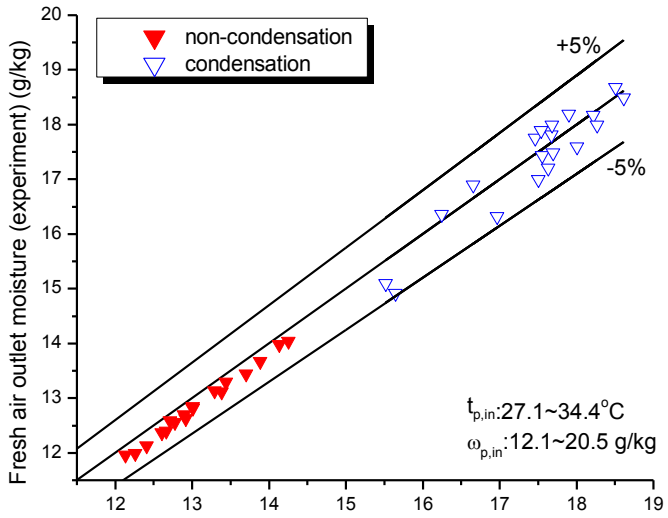

(b) comparison of outlet moisture content

Fig. 8.6 Comparison of primary air outlet conditions between experiment and simulation

Fig. 8.5 presents the comparison of enthalpy changes between the two air streams under both wet and dry operating conditions. The discrepancies of all the experiment results are found to be within ±20%. Besides, all the experiment results under wet operating

mode (IEC mode) are compared with the simulation results based on the model in Chapter 6 by setting the same operating conditions and unit configuration, as shown in Fig. 8.6. It is found that discrepancies in predicting IEC outlet temperature and humidity are within ±5% under both condensation and non-condensation states.

8.5.2 Dynamic performance when switching operating mode

Dynamic performance of the air cooler when switching from one operating mode to another is experimentally studied. The air parameters were monitored from the initial steady operating state to the variation process when one operation condition changed (turn on the pump or humidifier), and finally to another steady operating state. The influence of certain operating condition could be observed clearly through the dynamic test. Four representative cases were tested. The simulation results of the outlet parameters by model in Chapter 6 under the final steady conditions are plotted (marked by a straight line) in all the figures in order to be compared with experiment results.

8.5.2.1 Switch from dry to wet operating mode (low humidity primary air)

Fig. 8.7 shows the temperature variation of outlet primary air when the air cooler is switched from dry to wet operating mode under low humidity inlet air condition. It can be seen that the outlet primary air temperature decreases as soon as the circulation pump

is turned on and the air cooler is changed from a traditional air cooler to an IEC. The temperature decreases dramatically from the initial steady state of 29.5℃ to another steady state of 26.6℃.

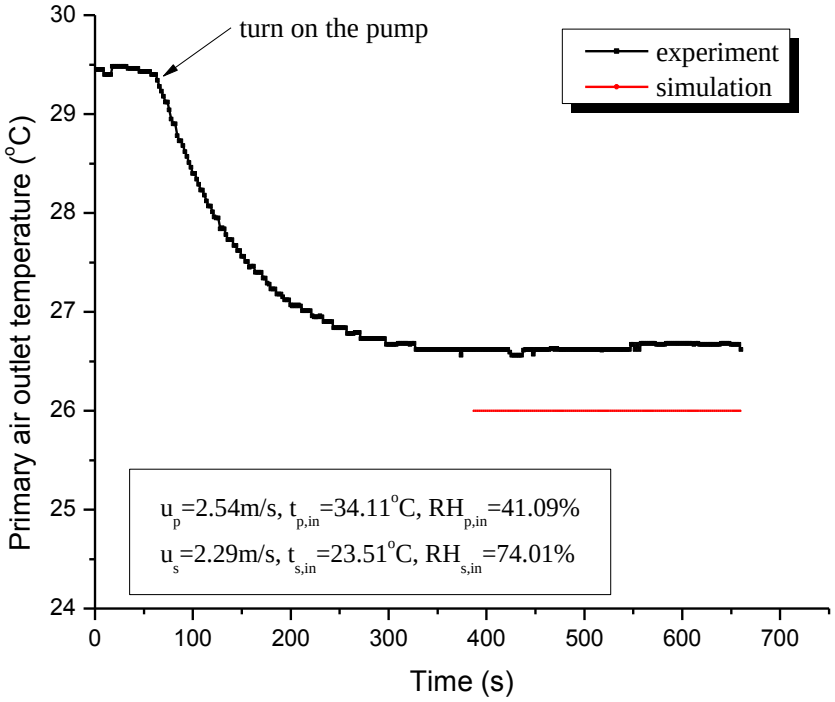

Fig. 8.7 Outlet air temperature variation when switching from dry to wet operating mode (low humidity primary air)

The decrease of outlet air temperature indicates the increase of cooling capacity and enhancement of heat transfer process. The improvement of cooling capacity under wet operating mode is because the water film in the secondary air channels lowers the plate surface temperature and improves the heat transfer rate by evaporation. It can be calculated that the total heat transfer rate under dry operating mode in Fig. 8.7 is 541

kW, while it is 882 kW under wet operating mode, 63% larger than that of dry operating mode. So the cooling capacity of IEC is greatly improved compared with that of traditional air cooler.

8.5.2.2 Switch from dry to wet operating mode (high humidity primary air)

Fig. 8.8 shows the temperature and humidity variation of outlet primary air when the air cooler is switched from dry to wet operating mode under high humidity inlet air condition. Unlike the case in section 8.5.2.1, condensation occurs in this case as the inlet air humidity is high (RH=76%), results in reduction of outlet air moisture content. The outlet primary air temperature decreases from 26.3℃ to 24.4℃ as soon as the pump is turned on. Meanwhile, the moisture content of the outlet primary air decreases from 19.4 g/kg to 17.2 g/kg, indicating the latent heat is removed by condensation. The principle can be explained as follows. The plate surface temperature is lowered by the water evaporation under wet operating mode, so that the dew point temperature of high humidity air can be higher than the plate surface temperature, results in condensation and dehumidification. In sum, the transition from dry to wet operating mode under high humidity air condition can bring two benefits: increasing the sensible heat transfer rate and enhancing the latent heat transfer rate.

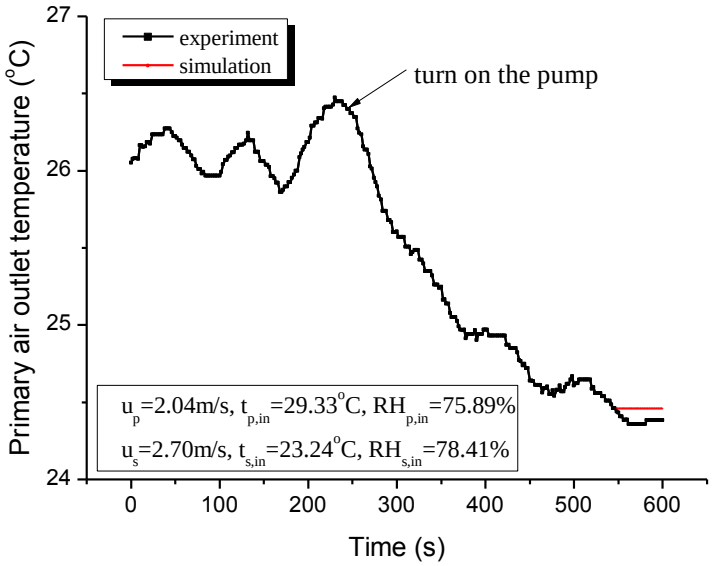

(a) outlet primary air temperaure

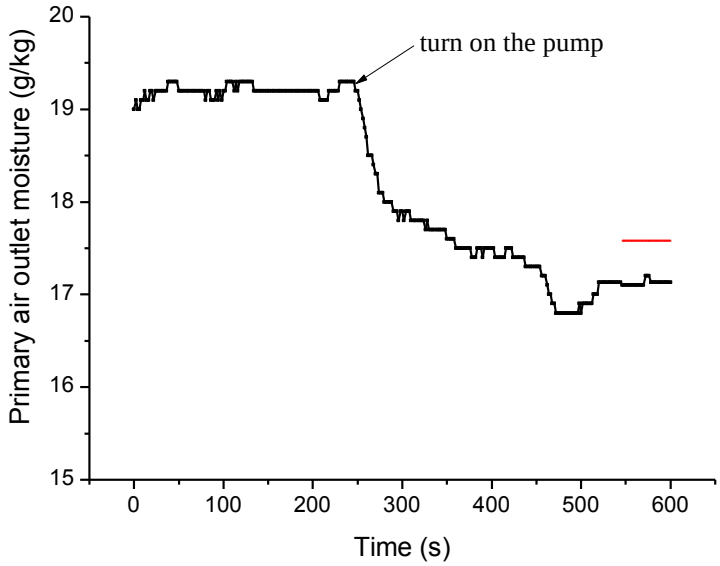

(b) outlet primary air moisture content

Fig. 8.8 Outlet air parameters variation when switching from dry to wet operating mode (high humidity primary air)

It can be calculated that the sensible heat transfer rate under dry operating mode in Fig. 8.8 is 290 kW; while it is 472 kW under wet operating mode. In addition, the latent heat

transfer rate under wet operating mode is 524 kW. So the total heat transfer rate is greatly improved by 2.4 times when switching the operating mode from dry to wet. The enlargement of total heat transfer rate under high humidity condition is more significant than that of low humidity condition.

8.5.2.3 Switch from low to high humidity inlet primary air (wet operating mode)

Fig. 8.9 shows the temperature and humidity variation of outlet primary air when the inlet primary air is switched from low humidity to high humidity under wet operating mode. It can be seen that the outlet primary air temperature increases from 23.0℃ to 24.7℃ as soon as the humidifier is turned on. During the transition process, $RH_{p,in}$ increases from 48.8% to 84.7%. The rise of outlet air temperature shows a decline of sensible heat transfer rate. Meanwhile, there is a significate moisture content difference (3.1 g/kg in average) between the inlet and outlet primary air, which indicates the condensation from primary air. So the latent heat transfer of the air cooler is enhanced by condensation.

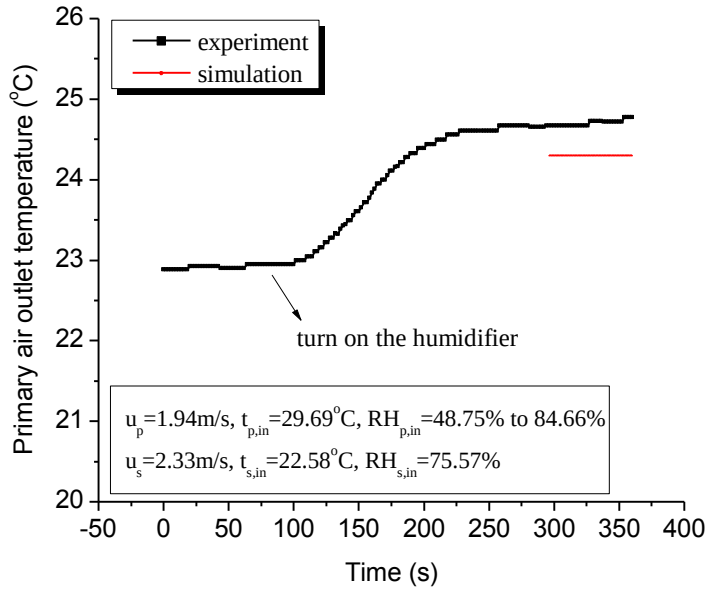

(a) outlet primary air temperaure

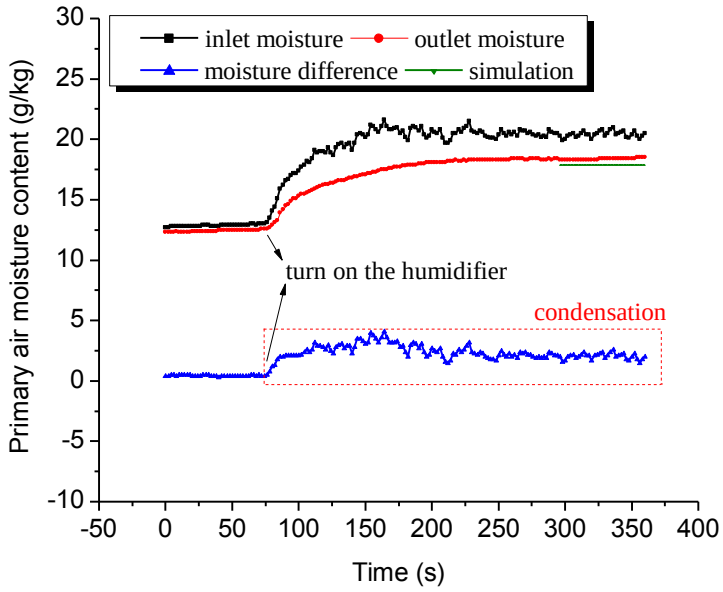

(b) outlet primary air moisture content

Fig. 8.9 Outlet air parameters variation when switching from low to high humidity inlet primary air (wet operating mode)

In sum, the transition of IEC operating mode from non-condensation to condensation

will reduce the sensible heat transfer rate but improves latent heat transfer rate. It can be explained as follows. The heat released during the condensation process will increase the plate surface temperature, thus the driving force of sensible heat transfer between the plate surface and primary air will be lowered. In Fig. 8.9, the sensible cooling capacity of IEC under non-condensation state is calculated to be 608W; while it is 454W under condensation state. The sensible heat transfer rate is reduced by 25% owing to the condensation. The latent heat transfer rate, however, increases from 0 to 701W, making the total heat transfer rate 1155 kW under condensation state. Thus, the total cooling capacity is enlarged by 90%. It can be deduced that the IEC has a very promising potential for energy recovery in an air-conditioning system in hot and humid regions, because of its advantages in reducing both sensible and latent load.

8.5.2.4 Switch from low to high humidity inlet primary air (dry operating mode)

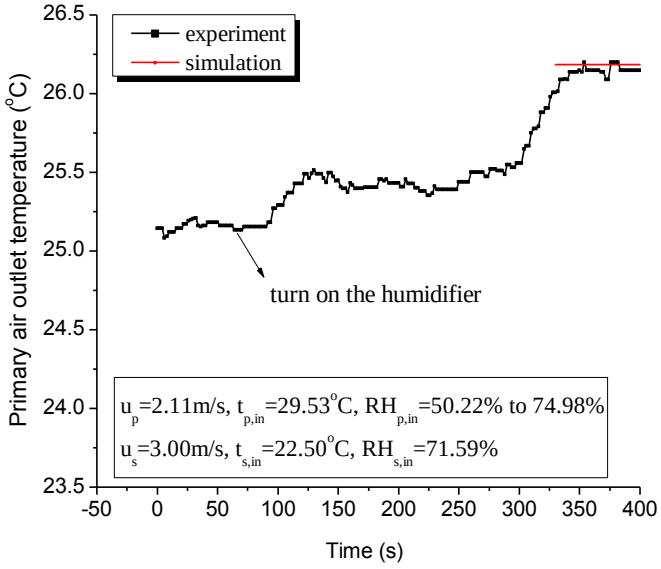

(a) outlet primary air temperaure

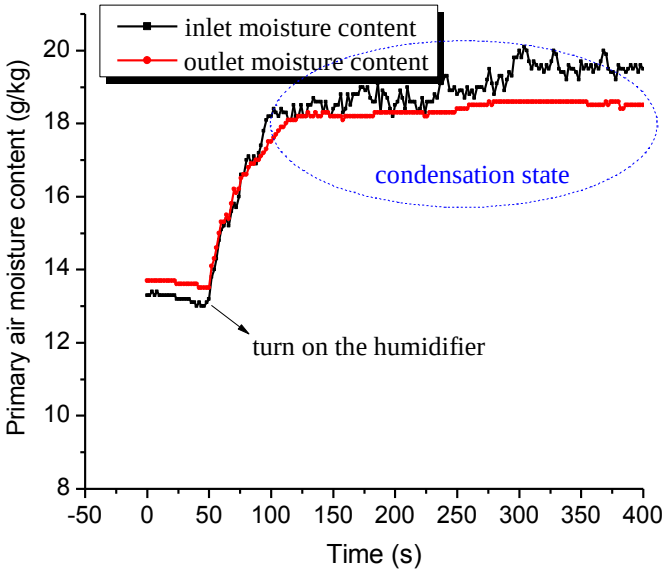

(b) outlet primary air moisture content

Fig. 8.10 Outlet air parameters variation when switching from low to high humidity inlet primary air (dry operating mode)

Fig. 8.10 shows the temperature and humidity variation of outlet primary air when the inlet primary air is switched from low humidity to high humidity under dry operating mode. Similar with the pervious case in section 8.5.2.3, the outlet primary air temperature increases and moisture content decreases because of condensation. The outlet primary air temperature increases by 1.0 ℃, results in a reduction of sensible heat transfer rate by 99 kW. The outlet primary air moisture content decreases by 0.7 g/kg, results in an increase of latent heat transfer rate by 247 kW. The total heat transfer rate is improved by 34%. The increase of latent and total heat transfer rate in this case is less significate than the case in section 8.5.2.3. The reason can be explained as: the plate surface temperature of the air cooler under wet operating mode is lower than that of dry operating mode, so the driving force of latent heat transfer (difference between the saturated moisture content at plate surface temperature and mainstream primary air moisture content) is larger than that of dry operating mode.

8.5.3 Influence of parameters

The influences of $t_{p,in}$, $u_{p,in}$, $t_{s,in}$ and $u_{s,in}$ variation under four operating modes are discussed. Under low humidity condition, the sensible efficiency η and wet-bulb efficiency η_{wb} are used for rating the traditional air cooler and IEC, respectively. Under high humidity condition, the latent efficiency η_{lat} is also used except for η and η_{wb}. Besides, the simulation results by numerical model in Chapter 6 under each case are

given in order to be compared with experiment results.

8.5.3.1 Influence of primary air temperature

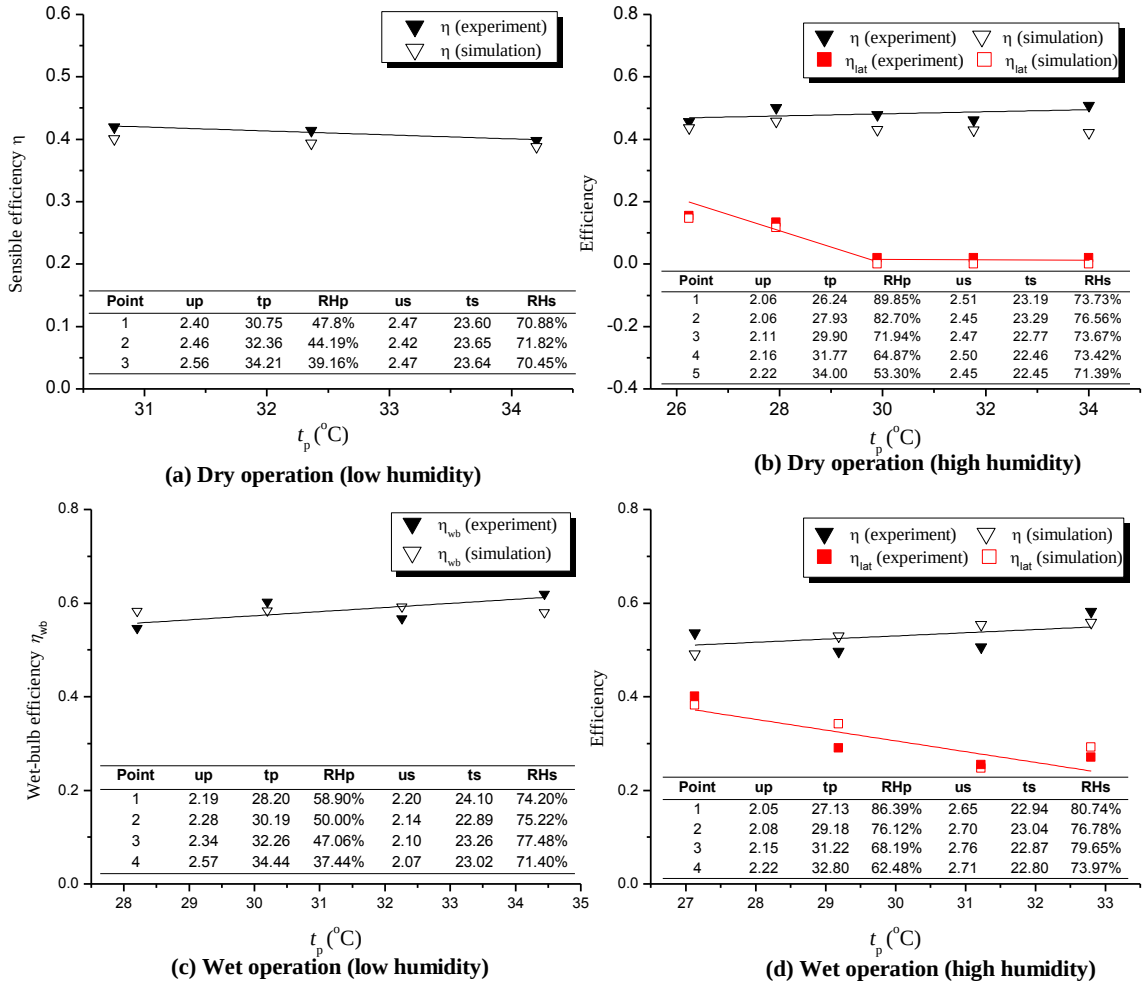

Fig. 8.11 Influence of t_p under four operating modes

Fig. 8.11 presents the influence of primary air temperature under four operating modes. It can be seen that sensible efficiency is not sensitive to t_p increase under dry operation mode. The sensible efficiency varies in a very small range between 40% ~42% under

low humidity condition and 46%~51% under high humidity condition, as shown in Fig. 8.11(a) and Fig. 8.11(b). The latent efficiency, however, decreases from 16% to 0 with $t_{p,in}$ increases from 26℃ to 34℃ under high humidity condition. The decrease of latent efficiency is because the condensation is weakened as the plate surface temperature increases.

The influence of t_p has larger impact on the air cooler under wet operating mode (IEC). The η_{wb} increases from 55% to 62% under low air humidity condition and increases from 54% to 58% under high air humidity condition, as shown in Fig.11(c) and Fig.11(d). The η_{wb} increase rate under high air humidity condition is less significant than that of low air humidity condition. It is because the condensation increases the plate surface temperature by releasing latent heat and brings negative effect on sensible heat transfer. Besides, the increase of $t_{p,in}$ has significant negative effect on the latent heat transfer by rising the plate surface temperature. As shown in Fig. 8.11(d), the η_{llat} decreases from 40% to 27% when $t_{p,in}$ increases from 27℃ to 33℃.

8.5.3.2 Influence of primary air velocity

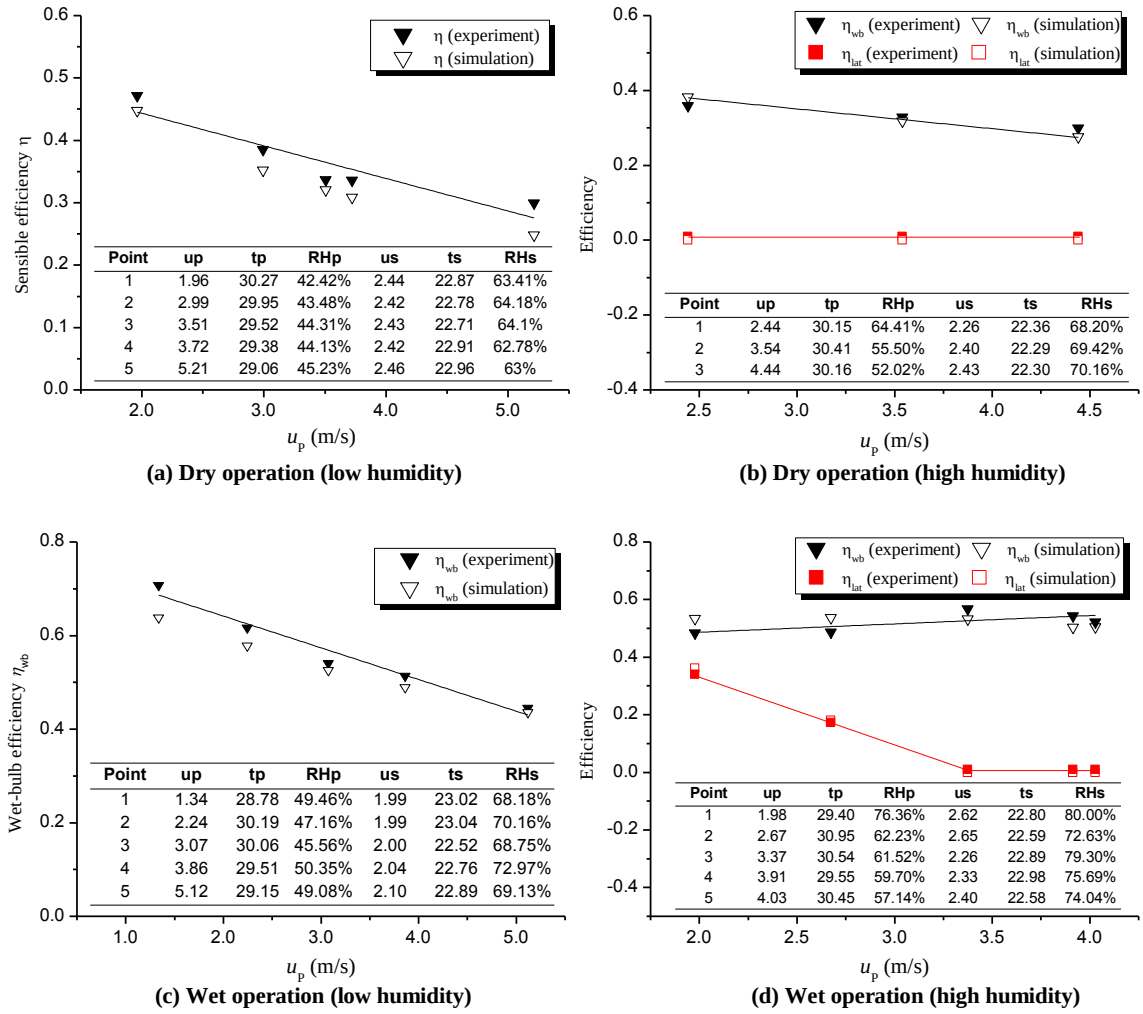

Point	up	tp	RHp	us	ts	RHs
1	1.96	30.27	42.42%	2.44	22.87	63.41%
2	2.99	29.95	43.48%	2.42	22.78	64.18%
3	3.51	29.52	44.31%	2.43	22.71	64.1%
4	3.72	29.38	44.13%	2.42	22.91	62.78%
5	5.21	29.06	45.23%	2.46	22.96	63%

(a) Dry operation (low humidity)

Point	up	tp	RHp	us	ts	RHs
1	2.44	30.15	64.41%	2.26	22.36	68.20%
2	3.54	30.41	55.50%	2.40	22.29	69.42%
3	4.44	30.16	52.02%	2.43	22.30	70.16%

(b) Dry operation (high humidity)

Point	up	tp	RHp	us	ts	RHs
1	1.34	28.78	49.46%	1.99	23.02	68.18%
2	2.24	30.19	47.16%	1.99	23.04	70.16%
3	3.07	30.06	45.56%	2.00	22.52	68.75%
4	3.86	29.51	50.35%	2.04	22.76	72.97%
5	5.12	29.15	49.08%	2.10	22.89	69.13%

(c) Wet operation (low humidity)

Point	up	tp	RHp	us	ts	RHs
1	1.98	29.40	76.36%	2.62	22.80	80.00%
2	2.67	30.95	62.23%	2.65	22.59	72.63%
3	3.37	30.54	61.52%	2.26	22.89	79.30%
4	3.91	29.55	59.70%	2.33	22.98	75.69%
5	4.03	30.45	57.14%	2.40	22.58	74.04%

(d) Wet operation (high humidity)

Fig. 8.12 Influence of u_p under four operating modes

Fig. 8.12 presents the influence of primary air velocity under four operating modes. It can be seen from Fig. 8.12(a) that the sensible efficiency η decreases from 47% to 30% when u_p increases from 2.0 m/s to 5.2 m/s under dry operating mode with low humidity inlet air. The same conclusion can be drawn to the wet operating mode (IEC). The η_{wb}

decreases from 64% to 44% when u_p increases from 1.3 m/s to 5.1 m/s as shown in Fig. 8.12(c).

The air cooler operates under high humidity condition can be different from that of low humidity condition because the condensation is involved. The condensation from primary air results in latent heat transfer, and influences the sensible heat transfer as well. In Fig. 8.12(d), it can be seen that the latent efficiency η_{lat} decreases from 34% to 0 when u_p increases from 2.0 m/s to 4.0 m/s, indicating the IEC operation state switches from condensation to non-condensation. Meanwhile, η_{wb} increase a little from 49% to 52%. The increase of u_p affects η and η_{wb} from two aspects. On one hand, η and η_{wb} decreases as the increase of cooled media, on the other hand, the η_{lat} could decline to zero, switching the operation state from condensation to non-condensation. This improves the sensible efficiency by eliminating condensation. The comprehensive effects decide the variation of η_{wb}.

8.5.3.3 Influence of secondary air temperature

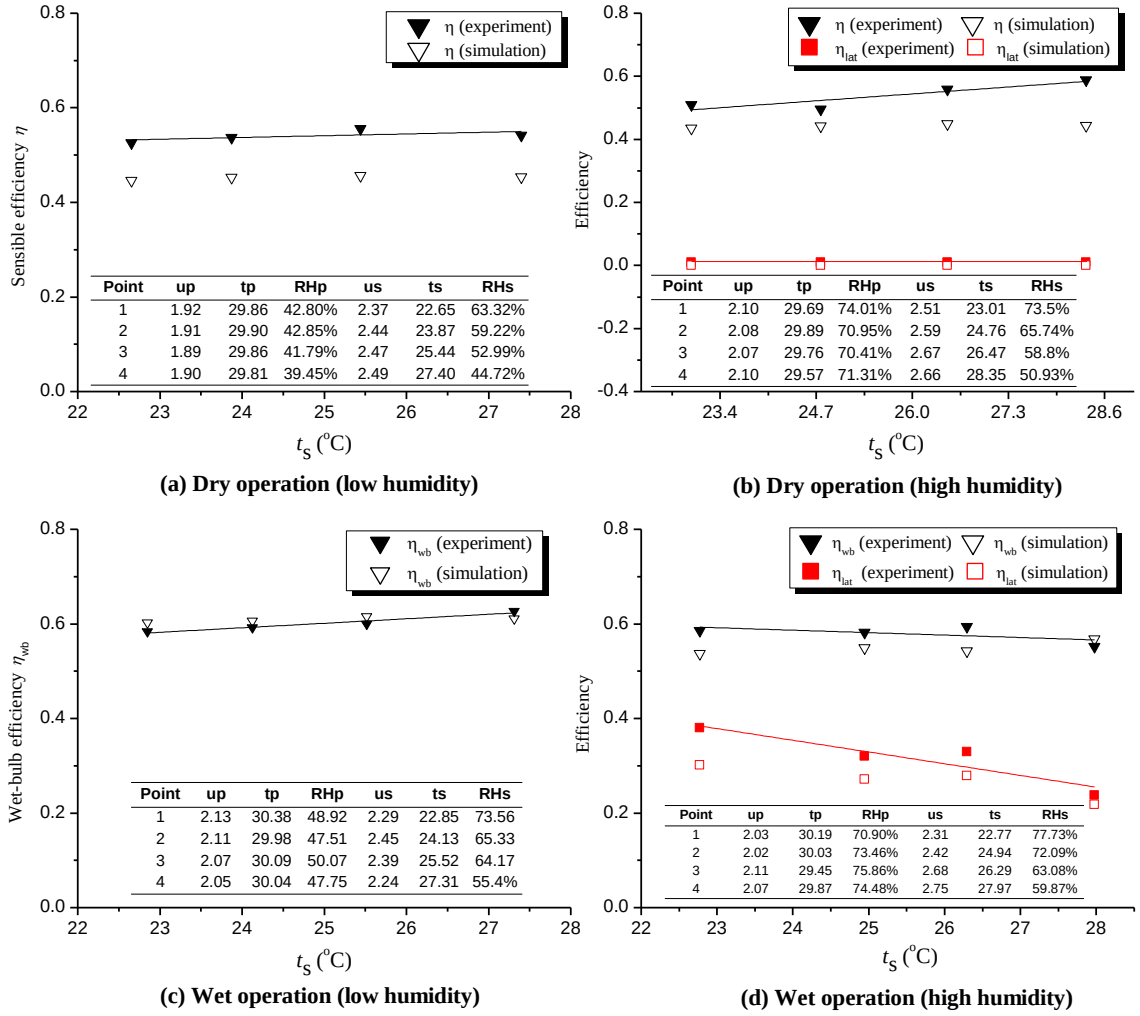

Fig. 8.13 Influence of t_s under four operating modes

Fig. 8.13 presents the influence of secondary air temperature under four operating modes. It can be seen from Fig. 8.13(a) that the sensible efficiency η increases a little from 52.7% to 54.2% with t_s increases from 22.6℃ to 27.4℃ under dry operation mode. The same conclusion can be drawn to the wet operating mode (IEC). The η_{wb} increases

from 58% to 63% when t_s increases from 22.8℃ to 27.3℃ as shown in Fig. 8.13(c). So the thermal efficiency of IEC is more sensitive to the change of t_s compared with that of traditional air cooler.

Under wet operating mode with high inlet air humidity (Fig. 8.13(d)), it can be seen that η_{lat} decreases significantly from 38% to 24% with t_s increases from 22.8℃ to 28℃, while η_{sen} fluctuates a little. The decline of η_{lat} can be attributed to the rise of plate surface temperature as t_s increases. In addition, it is much easier to condense in IEC compared with traditional air cooler by comparing Fig. 8.13(c) and Fig. 8.13(d). In Fig. 8.13(c), no condensation occurs even when RH_p exceeds 70%. In Fig. 8.13(d), however, condensation exists under all air conditions.

8.5.3.4 Influence of secondary air velocity

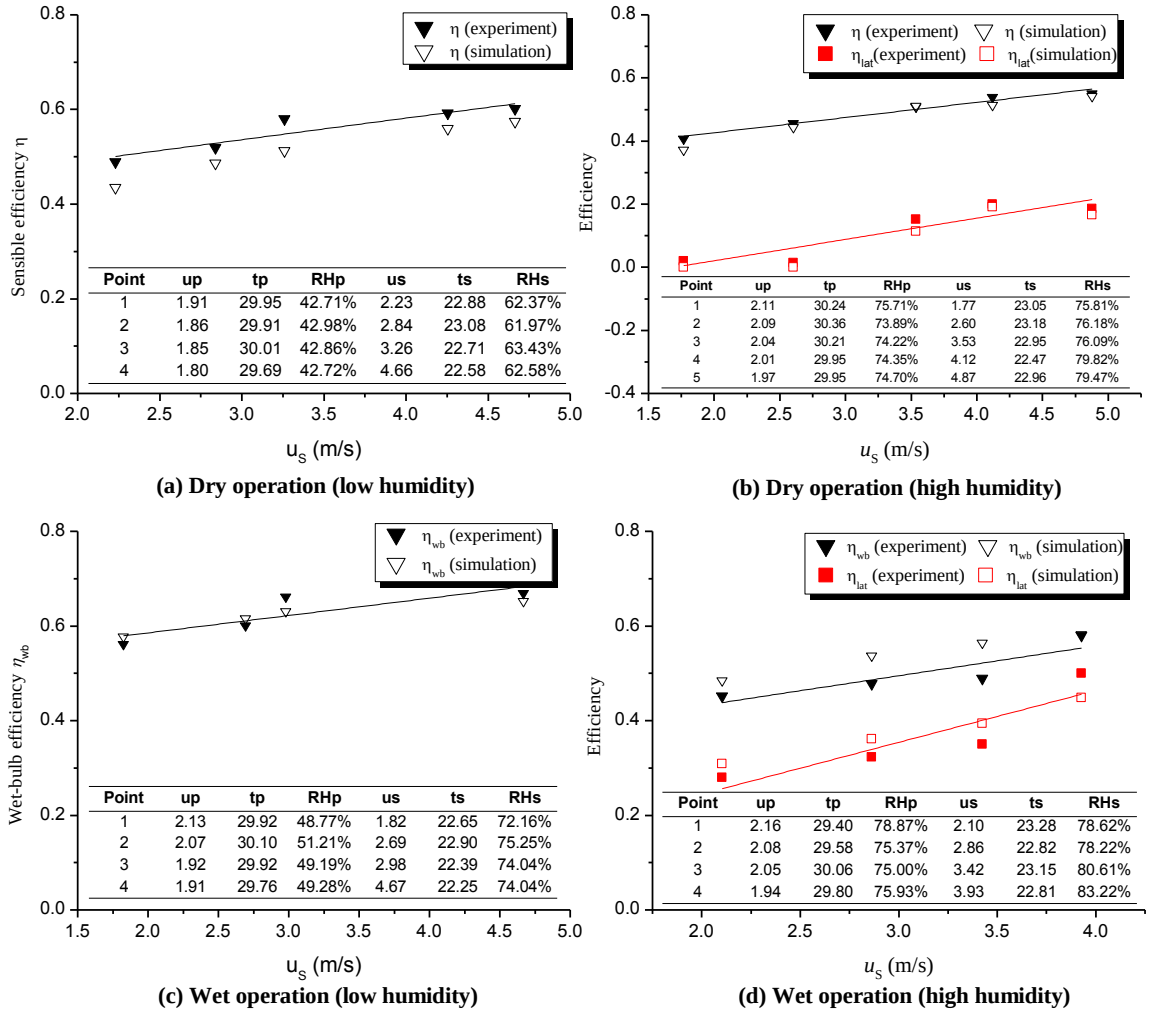

Fig. 8.14 Influence of u_s under four operating modes

Fig. 8.14 presents the influence of secondary air velocity under four operating modes. It can be seen from Fig. 8.14(a) that the sensible efficiency η increases significantly from 49% to 60% with u_s increases from 2.2 m/s to 4.7 m/s under dry operating mode with low humidity inlet air. The same conclusion can be drawn to the wet operating mode

(IEC) with low humidity inlet air. The η_{wb} increases from 56% to 67% when u_s increases from 1.8 m/s to 4.7 m/s as shown in Fig. 8.14(c).

Under high humidity conditions, both sensible efficiency η and latent efficiency η_{lat} of traditional air cooler increase with the increase of u_s. The η improves from 41% to 55% and η_{lat} increase from 0 to 19% as shown in Fig, 8.14(b). So u_s has a great impact on the air cooler thermal performance and can even change its operation state from non-condensation to condensation. Similarly, both η_{wb} and η_{lat} for IEC improve dramatically from 45% to 58% and 28% to 50%, respectively, with u_s increases from 2.1 m/s to 3.9 m/s (Fig, 8.14(d)). The increase of η_{lat} is more significant than that of η_{wb}。 In sum, increasing u_s is an effective way to improve the sensible and latent cooling capacities for both IEC and traditional air cooler.

8.5.4 Cooling capacity analysis

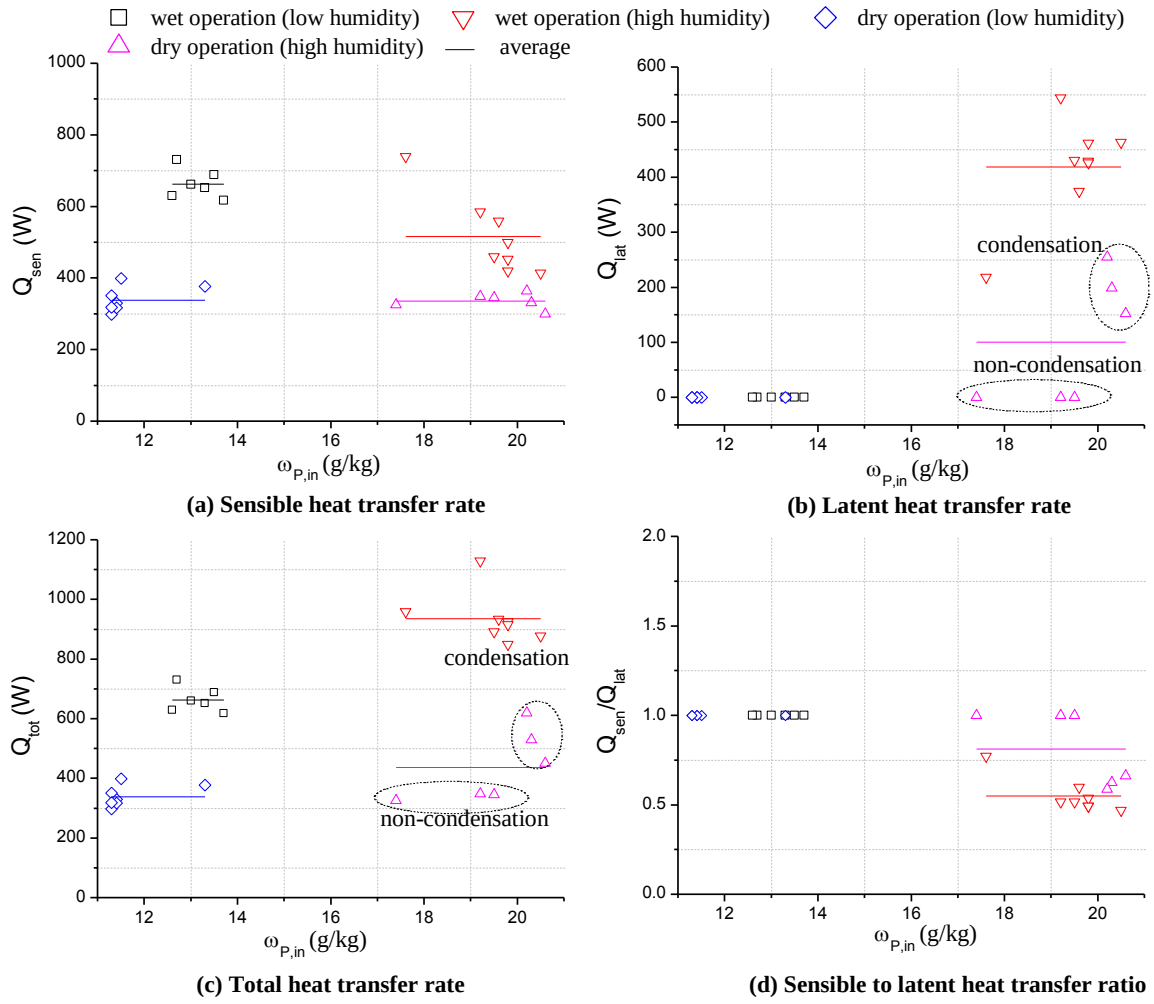

Fig. 8.15 Comparison of cooling capacities under four operating modes

Different cooling capacities, including Q_{sen}, Q_{lat} and Q_{tot}, are compared among four operating modes under the same conditions as shown in Fig. 8.15 (t_p≈30 ℃, u_p≈2 m/s, t_s≈23 ℃, RH_s≈70%, u_s≈2.5 m/s). It can be seen that the ranking for Q_{sen} is: wet operation (low humidity) > wet operation (high humidity) > dry operation (low humidity) > dry operation (high humidity); the ranking for Q_{lat} is: wet operation (high humidity) > dry

operation (high humidity) > wet operation (low humidity) = dry operation (low humidity) and the ranking for Q_{tot} is: wet operation (high humidity) > wet operation (low humidity) > dry operation (high humidity) > dry operation (low humidity). So the IEC performs much better than the traditional air cooler no matter under low humidity or high humidity regions. The Q_{sen} of IEC under low humidity condition is 96% larger than that of the traditional air cooler. The Q_{lat} of IEC is 3.1 times larger than that of traditional air cooler. The Q_{tot} of IEC under high humidity condition is 176% larger than that of traditional air cooler under low humidity condition. Besides, as shown in Fig. 8.15(d), Q_{sen}/Q_{lat} of IEC under high humidity condition is 0.62, so Q_{lat} accounts for a large proportion of Q_{tot} under condensation state.

8.5.5 Energy consumption and COP

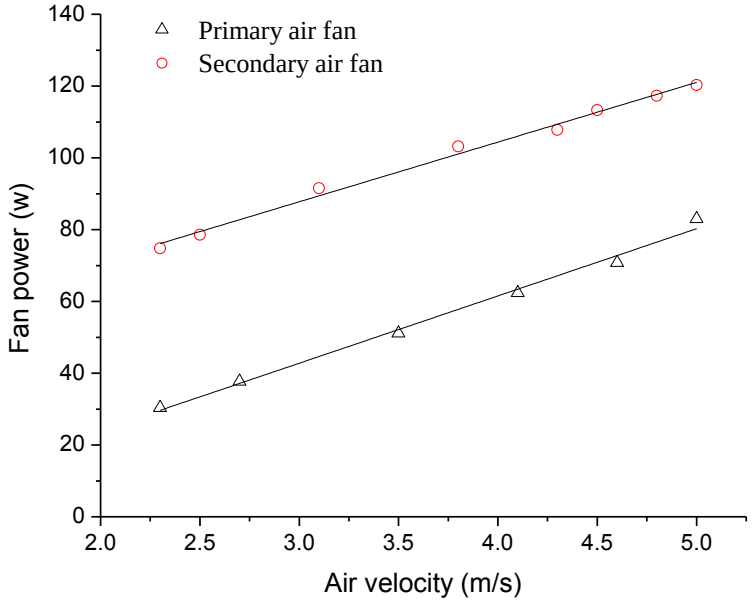

Fig. 8.16 Fan power consumption under different air velocity

Fig. 8.16 shows the fan power consumption measured by the power meter under different air velocity. The nominal power of the primary air fan and secondary air fan are 95W and 120W, respectively. The supply air flow rate is adjusted by the fan speed controller. It can be seen that fan power increases linearly with air velocity increases. The measured fan power consumptions are used for COP calculation thereafter.

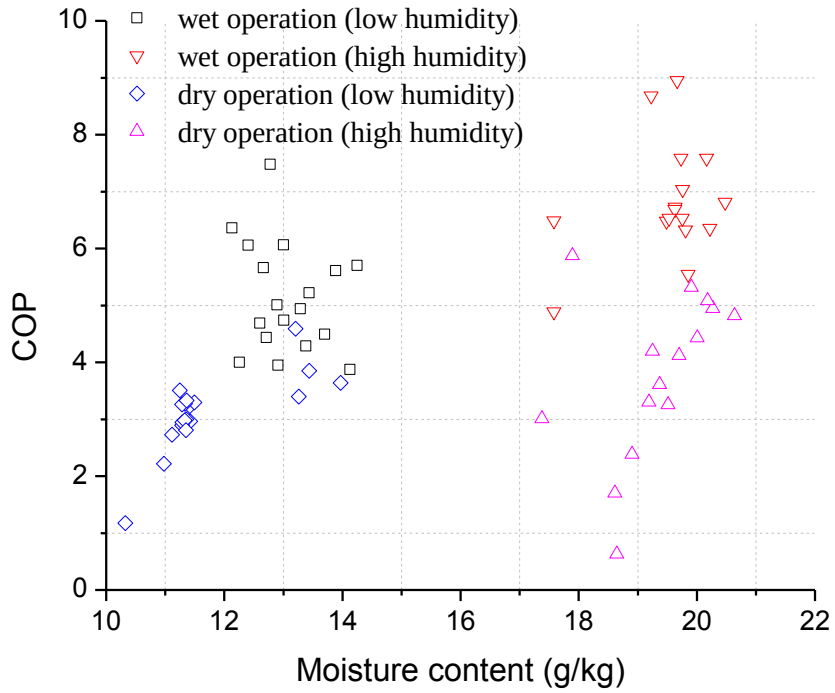

Fig. 8.17 COP of air cooler under four operating modes

Fig. 8.17 shows the COP of air cooler under four operating modes. It can be seen that COP varies in a wide range because the cooling capacity of the air cooler largely depends on the ambient air conditions. The average COP ranking among the four operating modes is: wet operation (high humidity) > wet operation (low humidity) > dry operation (high humidity) > dry operation (low humidity). The highest COP can reach

up to 9.0 under wet operating mode. However, the maximum COP of the air cooler under dry operating mode is only 6.0. Thus, it is highly efficient to apply IEC in hot and humid regions for energy recovery in an air-conditioning system.

8.6 Summary

This Chapter presents an experimental study of plate type air cooler performance under four operating modes. The air cooler works as a traditional cooler under dry operating mode and works as an IEC under wet operating mode. The cooler dynamic performances during different operating mode transition were investigated. The steady performances under different parameter influence were also comparatively studied. The results are summarized as follows:

1) By switching the air cooler from dry to wet operating mode, the outlet primary air temperature could be significantly reduced (2 ~ 3℃ in the studied case). Under high humidity inlet air condition, condensation or dehumidification (2.2 g/kg in the studied case) was observed when switching operating mode from dry to wet. Thus, not only sensible but also latent cooling load could be reduced by IEC when it is applied in hot and humid regions for energy recovery.

2) By switching the air cooler from low to high humidity operating mode, condensation could be observed and the outlet primary air temperature increases accordingly, which means that the sensible heat transfer decreases while latent heat transfer increases. The dehumidification by IEC (3.1 g/kg in the studied case) is much more obvious than that of traditional air cooler (0.7 g/kg in the studied case).

3) The η and η_{wb} are improved by increasing $t_{p,in,}$ and u_s, and decreasing u_p and $t_{s,in}$, of which decreasing u_p and increasing u_s are most effective. The η_{lat} can be improved by decreasing $t_{p,in,,}$ u_p and $t_{s,in}$, and increasing u_s. The thermal efficiency of IEC is more sensitive to the parameters variation compared with traditional air cooler.

4) The sensible, latent and total cooling capacities (Q_{sen}, Q_{lat} and Q_{tot}) were compared among four operating modes under the same air conditions and cooler configuration. The IEC performed much better than the traditional air cooler under both low and high humidity conditions. The Q_{tot} of IEC under high humidity condition is 176% larger than that of traditional air cooler under low humidity condition.

5) The COP of air cooler under four operating modes were compared. The COP varies in a wide range under different operating mode. The highest COP (9.0) was achieved by IEC under high air humidity. The COP of the air cooler with high humidity inlet air is higher than that of low humidity inlet air, so it is highly efficient for operating IEC in hot and humid regions for energy recovery in an A/C system.

Chapter 9

Conclusions and recommendations for future work

9.1 Conclusions

A detailed research work of an IEC with condensation in hot and humid region has been investigated and reported, including firstly establishing a simplified analytical IEC model, secondly proposing a simulation method for predicting IEC annual performance, thirdly developing a numerical IEC model for intensive parameter study, sensitivity analysis and configuration optimization and finally experimentally investigating the performance of air cooler under various operating states in the thesis. The conclusions are as follows.

A simplified analytical model for an IEC was developed in Chapter 4. Unlike all other reported IEC models, the IEC model specifically took into account three possible operating states of IEC in hot and humid regions, including non-condensation, partial condensation and total condensation. Besides, a method for judging the three operating states was firstly proposed. The model was validated by the published data from literature, with an acceptable predicting discrepancy of no greater than ±3.8%.

A novel method for annual performance simulation of an IEC heat recovery system based on the IEC component model developed in Chapter 4. A detailed case study in Hong Kong was presented. Results show that the condensation in the IEC takes up a large proportion of operation hours in hot and humid regions, especially in summer. The non-condensation, partial condensation and total condensation state account for 52.3%, 38.2% and 9.5% in annual operation hours, respectively. Because of condensation, the IEC can handle both sensible and latent cooling saving. The latent saving accounts for 41.3% of the total savings. Besides, the IEC shows a great potential in energy saving and peak load reduction. The annual energy saving is 21% and peak load is reduced by 27% in the studied case. The simulation results were validated by the field measurement.

A novel numerical model for IEC, with focusing on condensation state, was developed in Chapter 6 and validated by the published data from literatures. Unlike the limited modeling work of IEC with condensation, the proposed model considers the surface wettability ratio. Besides, for the first time, the influences of nine parameters (t_p, RH_p, u_p, t_s, RH_s, u_s, s, σ and H) were comparatively analyzed under three IEC operating states (non-condensation, partial condensation and total condensation). It is found that the stronger the condensation effect, the lower the wet-bulb efficiency, but the higher the enlargement coefficient and total heat transfer rate. The increase of secondary air velocity, decrease of channel gap and improvement of wettability can achieve more

obvious effect on enhancing IEC cooling capacity than in non-condensation state.

Unlike the previous reported sensitivity and optimization studies for IEC with no condensation, in Chapter 7, the sensitivity analysis of IEC under condensation condition was conducted based on the model in Chapter 6. The synthetic index $\eta_{wb}\varepsilon$, reflecting the total heat transfer, was proposed as an objective for sensitivity analysis and optimization. The influence rank of parameters for the synthetic index is: $s > H > u_p/u_s > RH_p > t_s > t_p > RH_s$. The optimized channel gap and NTU_p under IEC condensation condition are found to be different from previous reported studies, in which condensation was not considered. The optimized channel gap is 2–3 mm and 3–4 mm under condensation and non-condensation state, respectively. The optimized NTU_p is 4–7 and 3–5, respectively.

An experimental study is presented in Chapter 8 to investigate a plate type air cooler's performance under four operating modes (wet/dry and low/high humidity). The air cooler works as a traditional cooler under dry operating mode and works as an IEC under wet operating mode. The cooler dynamic performances during different operating mode transition were investigated. The steady performances (sensible and latent cooling efficiency) under different parameter influence (t_p, u_p, t_s, u_s) were also comparatively studied. The IEC performed much better than the traditional air cooler under both low

and high humidity conditions. The highest COP (9.0) was achieved by the IEC with high air humidity.

The outcomes of the research work reported in this thesis could make impacts to the advancement of IEC energy recovery technology in hot and humid regions, contributing to a new approach for energy saving in A/C systems. The simplified analytical model for the IEC reported in this thesis is the first one of its kind, because, firstly, it considers three possible operating states (non-condensation, partial condensation and total condensation), secondly, it assists dynamic simulation of IEC system by available simulation software. The annual dynamic simulation method reported in this thesis can be used as a useful way for much more accurately predicating the saving potential of IEC by taking hourly weather conditions, cooling load, chiller states and possible condensation. The intensive parameter study, sensitivity analysis and optimization results based on the newly developed numerical model considering condensation is expected to provide useful guidance for IEC favorable operating conditions and building more efficient IEC in hot and humid regions, which have not been reported by previous studies. The experimental study, specifically took into account both the sensible and latent cooling performance of IEC, is the first of its kind in open literature. It provides experimental-based operating data for traditional air cooler and IEC applied in both dry and humid regions. The outcomes of the work are expected to be globally applicable,

and they will be particularly useful in hot and humid regions like Hong Kong where energy-saving in A/C systems has always been a challenge.

9.2 Proposed further work

Following the successful completion of the research work reported in this thesis, a number of future related possible studies are proposed as follows.

The case study reported in Chapter 5 is a 100% fresh air A/C system, which, in theory, is the most suitable application field. In most engineering cases, however, semi-centralized A/C system, in which fresh air only takes up a part of total air supply, is more widely used. The energy saving potential of IEC heat recovery system applied in semi-centralized A/C system is suggested to be further investigated. Study results can provide references for wider application of this technology in many other fields, such as, sports center, hotels and shopping malls.

The IEC model presented in Chapter 6 is based on the 1-D numerical model, in which some assumptions are assumed (steady water film, neglect heat resistance of water film and wall, etc.) to enable the solution by FDM. With the rapid development of CFD technology, 3D model of IEC with less possible assumptions can be established and solved for more accurate numerical solution closer to reality.

As reported in the thesis, condensation would take place in IEC under high humidity environment. In particular, it almost operates in condensation state in summer months. It benefits energy recovery in A/C system by removing a part of latent load. However, if the condensate accumulated in the small IEC channels, it would clog the channel and increase the flow resistance. Thus, the condensate needs to be removed constantly and strategies should be made to accelerate the drainage of condensate water. Two possible methods are proposed: 1) surface treatment by using hydrophobic coating to improve drainage; 2) structure improvement by adding drain pipe system at the bottom of the unit.

References

Alonso, J. S. J., Martinez, F. R., Gomez, E. V., & Plasencia, M. A. G. (1998). Simulation model of an indirect evaporative cooler. Energy and buildings, 29(1), 23-27.

An, C. S., & Choi, D. H. (2012). Analysis of heat-transfer performance of cross-flow fin-tube heat exchangers under dry and wet conditions. International Journal of Heat and Mass Transfer, 55(5), 1496-1504.

Anisimov, S., & Pandelidis, D. (2015). Theoretical study of the basic cycles for indirect evaporative air cooling. International Journal of Heat and Mass Transfer, 84, 974-989.

Anisimov, S., Pandelidis, D., & Danielewicz, J. (2015). Numerical study and optimization of the combined indirect evaporative air cooler for air-conditioning systems. Energy, 80, 452-464.

Anisimov, S., Pandelidis, D., & Jedlikowski, A. (2015). Performance study of the indirect evaporative air cooler and heat recovery exchanger in air conditioning system during the summer and winter operation. Energy, 89, 205-225.

Anisimov, S., Pandelidis, D., Jedlikowski, A., & Polushkin, V. (2014). Performance investigation of a M (Maisotsenko)-cycle cross-flow heat exchanger used for indirect evaporative cooling. Energy, 76, 593-606.

ASHRAE handbook, (2008). Heating, Ventilating, and Air-Conditioning Systems and Equipment (I-P Edition), American Society of Heating, Refrigerating and Air-Conditioning Engineers, Inc., 2008.

ASHRAE Handbook: Fundamentals. Mass transfer, Atlanta, GA; 2005. p. 9 (Ch.5).

ASHRAE, F. (2009). Fundamentals Handbook. IP Edition.

ASHRAE. Fundamentals (1997), American Society of Heating, Refrigeration and Air Conditioning Engineers, USA.

Baca, I. M., Tur, S. M., Gonzalez, J. N., & Román, C. A. (2011). Evaporative cooling efficiency according to climate conditions. Procedia Engineering, 21, 283-290.

Bajwa, M., Aksugur, E., & Al-Otaibi, G. (1993). The potential of the evaporative cooling techniques in the gulf region of the Kingdom of Saudi Arabia. Renewable energy, 3(1), 15-29.

Banks, P. J. (1981). A General Theory of Wet Surface Heat Exchangers and its Application to Regenerate Efaporative Cooling. Journal of heat transfer, 103, 579.

Barrow, H., Mistry, J., & Clayton, D. (1986). Numerical and Exact Mathematical Analyses of Two Dimensional Rectangular Composite Fins. In Proc. 8th International Heat Transfer Conference, San Francisco (Vol. 2, pp. 367-372).

Bolotin, S., Vager, B., & Vasilijev, V. (2015). Comparative analysis of the cross-flow indirect evaporative air coolers. International Journal of Heat and Mass Transfer, 88, 224-235.

Bom G, Foster R, Dijkstra E, Tummers M (1999). Evaporative air-conditioning: applications for environmentally friendly cooling. Washington D.C: The World Bank.

Bosnjacovic, F., 1965, ‘‘Technische Thermodinmik,’’ Theodor Steinkopf, Dresden.

Chen PL, Qin H, Huang YJ, Wu H, Blumstein C (1993). The energy-saving potential of precooling incoming outdoor air by indirect evaporative cooling. ASHRAE Trans 1993;99(Pt 1).

Chen PL (1994). Feasibility studies on indirect evaporative cooling in China. HVAC, 5, 3–5 [in Chinese].

Chen PL (1988a). Discussion on the application prospect of indirect evaporative cooling in China. HVAC, 2, 24–9 [in Chinese].

Chen PL (1988b). The application of indirect evaporative cooling in air conditioning. Refrigeration Technology, 3:1–8 [in Chinese].

Chengqin, R., & Hongxing, Y. (2006). An analytical model for the heat and mass transfer processes in indirect evaporative cooling with parallel/counter flow configurations. International journal of heat and mass transfer, 49(3), 617-627.

Chu Wai Shing (2002), Energy performance of indirect evaporative heat recovery system in Hong Kong, Master Thesis, Hong Kong Polytechnic University.

Cianfrini, C., Corcione, M., Habib, E., & Quintino, A. (2014). Energy performance of air-conditioning systems using an indirect evaporative cooling combined with a

cooling/reheating treatment. Energy and Buildings, 69, 490-497.

Costelloe, B., & Finn, D. (2003). Indirect evaporative cooling potential in air–water systems in temperate climates. Energy and Buildings, 35(6), 573-591.

Costelloe, B., & Finn, D. (2007). Thermal effectiveness characteristics of low approach indirect evaporative cooling systems in buildings. Energy and Buildings, 39(12), 1235-1243.

Cruz, E. G., & Krüger, E. (2015). Evaluating the potential of an indirect evaporative passive cooling system for Brazilian dwellings. Building and Environment, 87, 265-273.

Cui, X., Chua, K. J., & Yang, W. M. (2014). Use of indirect evaporative cooling as pre-cooling unit in humid tropical climate: an energy saving technique. Energy Procedia, 61, 176-179.

Cui, X., Chua, K. J., Islam, M. R., & Ng, K. C. (2015). Performance evaluation of an indirect pre-cooling evaporative heat exchanger operating in hot and humid climate. Energy Conversion and Management, 102, 140-150.

Cui, X., Chua, K. J., Islam, M. R., & Ng, K. C. (2015). Performance evaluation of an indirect pre-cooling evaporative heat exchanger operating in hot and humid climate. Energy Conversion and Management, 102, 140~150.

Cui, X., Chua, K. J., Yang, W. M., Ng, K. C., Thu, K., & Nguyen, V. T. (2014). Studying the performance of an improved dew-point evaporative design for cooling

application. Applied Thermal Engineering, 63(2), 624-633.

D. Pescod (1974), An evaporative air cooler using to plate heat exchanger, Common wealth Scientific and Industrial Research Organization (C.S.I.R.O.), Division of Mech. Eng., Internal Report No. Tr 2, Highett, Victory, Australia.

De Antonellis, S., Joppolo, C. M., Liberati, P., Milani, S., & Molinaroli, L. (2016). Experimental analysis of a cross flow indirect evaporative cooling system. Energy and Buildings, 121, 130-138.

Delfani, S., Esmaeelian, J., Pasdarshahri, H., & Karami, M. (2010). Energy saving potential of an indirect evaporative cooler as a pre-cooling unit for mechanical cooling systems in Iran. Energy and Buildings, 42(11), 2169-2176.

Desrayaud, G., & Lauriat, G. (2001). Heat and mass transfer analogy for condensation of humid air in a vertical channel. Heat and mass transfer, 37(1), 67-76.

Di YH, Liu JP, Huang X (2010). Climate demarcating for application of evaporative cooling air conditioning. HVAC, 40(2), 108–11 [in Chinese].

Di YH. (2008). Fundamental study on the design of climate based evaporative cooling air conditioning technology. China: Xi'an University of Architecture and Technology. (in Chinese).

Ding. J, Ren. C. (2007). Study on heat and mass transfer coefficient of indirect evaporative cooling in plate heat exchanger. Building Energy & Environment, 26(5), 1-6. (in Chinese).

Ding. J, Ren. C. (2006). Study on the Laminar Properties of Indirect Evaporative Cooling in Plate Heat Exchanger. Industrial heating, 35(2), 24-28. (in Chinese)

Duan, Z. (2011) Investigation of a Novel Dew Point Indirect Evaporative Air Conditioning System for Buildings [Ph.D. Thesis]. Nottingham University of Nottingham.

Duan, Z., Zhan, C., Zhang, X., Mustafa, M., Zhao, X., Alimohammadisagvand, B., & Hasan, A. (2012). Indirect evaporative cooling: Past, present and future potentials. Renewable and Sustainable Energy Reviews, 16(9), 6823-6850.

El Hourani, M., Ghali, K., & Ghaddar, N. (2014). Effective desiccant dehumidification system with two-stage evaporative cooling for hot and humid climates. Energy and Buildings, 68, 329-338.

Elberling L (2006). Laboratory Evaluation of the Coolerado Cooler – Indirect Evaporative Cooling Unit. Pacific Gas and Electric Company.

El-Dessouky, H., Ettouney, H., & Al-Zeefari, A. (2004). Performance analysis of two-stage evaporative coolers. Chemical Engineering Journal, 102(3), 255-266.

Enteria, N., Yoshino, H., Takaki, R., Mochida, A., Satake, A., & Yoshie, R. (2013). Effect of regeneration temperatures in the exergetic performances of the developed desiccant-evaporative air-conditioning system. International Journal of Refrigeration.

Erens, P. J., & Dreyer, A. A. (1993). Modelling of indirect evaporative air coolers.

International journal of heat and mass transfer, 36(1), 17-26.

Facao, J., & Oliveira, A. C. (2000). Thermal behaviour of closed wet cooling towers for use with chilled ceilings. Applied Thermal Engineering, 20(13), 1225-1236.

Fakhrabadi, F., & Kowsary, F. (2016). Optimal design of a regenerative heat and mass exchanger for indirect evaporative cooling. Applied Thermal Engineering, 102, 1384-1394.

Fan L. (2009). Experimental research on hydrophilic property of tubular indirect evaporative cooler (TIEC), Master thesis, Xi'an Polytechnic University, China.(in Chinese)

Fan L., Huang X., Wu Z. (2007). The Preliminary Study of the Improvement of Hydrophilic and Antibacterial Performance of the Evaporative Cooling Air-conditioning Unit, Building Energy Conservation, 2007(12): 9~13.

Farmahini-Farahani, M., & Heidarinejad, G. (2012). Increasing effectiveness of evaporative cooling by pre-cooling using nocturnally stored water. Applied Thermal Engineering, 38, 117-123.

Fernández-Seara, J., Diz, R., Uhía, F. J., Dopazo, A., & Ferro, J. M. (2011). Experimental analysis of an air-to-air heat recovery unit for balanced ventilation systems in residential buildings. Energy conversion and management, 52(1), 635-640.

Finocchiaro, P., Beccali, M., & Nocke, B. (2012). Advanced solar assisted desiccant and

evaporative cooling system equipped with wet heat exchangers. Solar Energy, 86(1), 608-618.

Gendebien, S., Bertagnolio, S., & Lemort, V. (2013). Investigation on a ventilation heat recovery exchanger: Modeling and experimental validation in dry and partially wet conditions. Energy and buildings, 62, 176-189.

Global Energy Statistical Yearbook 2015. URL: https://yearbook.enerdata.net/#energy-consumption-data.html

Goldsworthy, M., & White, S. (2011). Optimisation of a desiccant cooling system design with indirect evaporative cooler. International Journal of refrigeration, 34(1), 148-158.

Gómez, E. V., Martínez, F. R., Diez, F. V., Leyva, M. M., & Martín, R. H. (2005). Description and experimental results of a semi-indirect ceramic evaporative cooler. International Journal of Refrigeration, 28(5), 654-662.

Guo, X. C., & Zhao, T. S. (1998). A parametric study of an indirect evaporative air cooler. International communications in heat and mass transfer, 25(2), 217-226.

H.W. Coleman, W.G. Steele, (2009). Experimentation, Validation, and Uncertainty Analysis for Engineers, third ed., A John Wiley & Sons, Inc.

Halasz, B. (1998). A general mathematical model of evaporative cooling devices. Revue générale de thermique, 37(4), 245-255.

Halliday, S. P., Beggs, C. B., & Sleigh, P. A. (2002). The use of solar desiccant cooling

in the UK: a feasibility study. Applied Thermal Engineering, 22(12), 1327-1338.

Hao, X., Zhu, C., Lin, Y., Wang, H., Zhang, G., & Chen, Y. (2013). Optimizing the pad thickness of evaporative air-cooled chiller for maximum energy saving. Energy and Buildings, 61, 146-152.

Hasan, A. (2010). Indirect evaporative cooling of air to a sub-wet bulb temperature. Applied Thermal Engineering, 30(16), 2460-2468.

Hasan, A. (2012). Going below the wet-bulb temperature by indirect evaporative cooling: analysis using a modified ε-NTU method. Applied Energy, 89(1), 237-245.

Heidarinejad, G., & Bozorgmehr, M. (2008). Heat and mass transfer modeling of two stage indirect/direct evaporative air coolers. ASHRAE journal Thailand.

Heidarinejad, G., & Moshari, S. (2015). Novel modeling of an indirect evaporative cooling system with cross-flow configuration. Energy and Buildings, 92, 351-362.

Heidarinejad, G., Bozorgmehr, M., Delfani, S., & Esmaeelian, J. (2009). Experimental investigation of two-stage indirect/direct evaporative cooling system in various climatic conditions. Building and Environment, 44(10), 2073-2079.

Heidarinejad, G., Heidarinejad, M., Delfani, S., & Esmaeelian, J. (2008). Feasibility of using various kinds of cooling systems in a multi-climates country. Energy and Buildings, 40(10), 1946-1953.

Hettiarachchi, H. D., Golubovic, M., & Worek, W. M. (2007). The effect of longitudinal heat conduction in cross flow indirect evaporative air coolers. Applied Thermal

Engineering, 27(11), 1841-1848.

Hewitt, G. F. (2008). Heat exchanger design handbook (Vol. 98). Begell House.

Higgins C, Reichmuth H. (2007). Desert CoolAireTM Package Unit Technical Assessment Field Performance of a Prototype Hybrid Indirect Evaporative Air-conditioner. New Buildings Institute.

Hsu, S. T., Lavan, Z., & Worek, W. M. (1989). Optimization of wet-surface heat exchangers. Energy, 14(11), 757-770.

Huang X, Liu M, Yu XY. (2002). Analysis of the application status-quo of evaporative cooling technology used in Xinjiang Textile Industry. Cotton Textile Technology, 30(4):14–8 [in Chinese].

Huang X, Qu Y, Di YH. (2004). Application of multi-stage evaporative cooling air conditioning system to northwest China. Heating, Ventilation, and Air Conditioning, 34(6):67–71 [In Chinese].

Huang X, Zhou B, Yu XY, Zhang XL, Xiao MY. (2005). Application of three-stage evaporative cooling air conditioning systems in Xinjiang region. Heating, Ventilation, and Air Conditioning, 35(7):104–7 [In Chinese].

Huang X., Zhou B., Yu X., Zhang X. & Xiao M (2006). Experimental study on water distribution uniformity of tubular indirect evaporative coolers. Heating Ventilating & Air Conditioning, 12, 015.

Huang, C. C., Yan, W. M., & Jang, J. H. (2005). Laminar mixed convection heat and

mass transfer in vertical rectangular ducts with film evaporation and condensation. International journal of heat and mass transfer, 48(9), 1772-1784.

Huang, L. J., & Shah, R. K. (1992). Assessment of calculation methods for efficiency of straight fins of rectangular profile. International journal of heat and fluid flow, 13(3), 282-293.

I.H. Shames, Mechanics of Fluids, 2nd ed., McGraw-Hill, New York, 1988.

Jaber, H., and Webb, R. L., 1989, 'Design of Cooling Towers by the Effectiveness-NTU Method,' ASME J. Heat Transfer, 111, pp. 837–843.

Jaber, S. (2016). An assessment of the economic and environmental feasibility of evaporative cooling unit. Applied Thermal Engineering, 103, 564-571.

Jaber, S., & Ajib, S. (2011). Evaporative cooling as an efficient system in Mediterranean region. Applied Thermal Engineering, 31(14), 2590-2596.

Jain, D. (2007). Development and testing of two-stage evaporative cooler. Building and Environment, 42(7), 2549-2554.

Jain, S., Dhar, P. L., & Kaushik, S. C. (1995). Evaluation of solid-desiccant-based evaporative cooling cycles for typical hot and humid climates. International journal of Refrigeration, 18(5), 287-296.

Jain, V., Mullick, S. C., & Kandpal, T. C. (2013). A financial feasibility evaluation of using evaporative cooling with air-conditioning (in hybrid mode) in commercial buildings in India. Energy for Sustainable Development, 17(1), 47-53.

Jiang Y, Zhang XS. (2006). The research of direct evaporation cooling and its application in air-cooled chiller unit. Building Energy and Environment, 25(2):7–12 [in Chinese].

Jiang, Y., & Xie, X. (2010). Theoretical and testing performance of an innovative indirect evaporative chiller. Solar Energy, 84(12), 2041-2055.

Jradi, M., & Riffat, S. (2014). Experimental and numerical investigation of a dew-point cooling system for thermal comfort in buildings. Applied Energy, 132, 524-535.

Kettleborough, C. F., & Hsieh, C. S. (1983). The thermal performance of the wet surface plastic plate heat exchanger used as an indirect evaporative cooler. Journal of Heat Transfer, 105(2), 366-373.

Khalajzadeh, V., Farmahini-Farahani, M., & Heidarinejad, G. (2012). A novel integrated system of ground heat exchanger and indirect evaporative cooler. Energy and Buildings, 49, 604-610.

Kim, M. H., Jeong, D. S., & Jeong, J. W. (2015). Practical thermal performance correlations for a wet-coil indirect evaporative cooler. Energy and Buildings, 96, 285-298.

Kim, M. H., Park, J. S., & Jeong, J. W. (2013). Energy saving potential of liquid desiccant in evaporative-cooling-assisted 100% outdoor air system. Energy, 59, 726-736.

Kloppers, J. C., & Kröger, D. G. (2005). Cooling tower performance evaluation:

Merkel, Poppe, and e-NTU methods of analysis. Journal of Engineering for Gas Turbines and Power, 127(1), 1-7.

Krüger, E., Cruz, E. G., & Givoni, B. (2010). Effectiveness of indirect evaporative cooling and thermal mass in a hot arid climate. Building and Environment, 45(6), 1422-1433.

Kulkarni, R. K., & Rajput, S. P. S. (2010). Performance evaluation of two stage indirect/direct evaporative cooler with alternative shapes and cooling media in direct stage. International Journal of Applied Engineering Research, 1(4), 800.

La, D., Dai, Y. J., Li, Y., Tang, Z. Y., Ge, T. S., & Wang, R. Z. (2013). An experimental investigation on the integration of two-stage dehumidification and regenerative evaporative cooling. Applied Energy, 102, 1218-1228.

Lee, J., & Lee, D. Y. (2013). Experimental study of a counter flow regenerative evaporative cooler with finned channels. International Journal of Heat and Mass Transfer, 65, 173-179.

Lee, J., Choi, B., & Lee, D. Y. (2013). Comparison of configurations for a compact regenerative evaporative cooler. International Journal of Heat and Mass Transfer, 65, 192-198.

Liu, Z., Allen, W., & Modera, M. (2013). Simplified thermal modeling of indirect evaporative heat exchangers. HVAC&R Research, 19(3), 257-267.

Luo Rong, Huang Xiang, Jin Guiming. (2013). Analysis on Energy Efficiency of a

Hybrid Liquid Desiccant and Evaporative Cooling System in Hong Kong. CC&AC, 1, 4-7.

M. Poppe, H. Rögener, Berechnung von Rückkühlwerken. VDI-Wärmeatlas, 1991, pp. Mi 1eMi 15.

Maclaine-Cross, I. L., & Banks, P. J. (1981). A general theory of wet surface heat exchangers and its application to regenerative evaporative cooling. Journal of heat transfer, 103(3), 579-585.

Maisotsenko, V., Gillan, L. E., Heaton, T. L., & Gillan, A. D. (2003). U.S. Patent No. 6,581,402. Washington, DC: U.S. Patent and Trademark Office.

Mavroudaki, P., Beggs, C. B., Sleigh, P. A., & Halliday, S. P. (2002). The potential for solar powered single-stage desiccant cooling in southern Europe. Applied Thermal Engineering, 22(10), 1129-1140.

Merkel, F., ''Verdunstungskühlung,'' 1925, VDI-Zeitchrift, Vol. 70, pp. 123–128.

Moshari, S., Heidarinejad, G., & Fathipour, A. (2016). Numerical investigation of wet-bulb effectiveness and water consumption in one-and two-stage indirect evaporative coolers. Energy Conversion and Management, 108, 309-321.

NAEEEC (National Appliance and Equipment Energy Efficiency Committee) -Status of Air Conditioners in Australia, updated with 2005 data. 2006.

Navon, R., & Arkin, H. (1994). Feasibility of direct-indirect evaporative cooling for residences, based on studies with a desert cooler. Building and Environment, 29(3),

393-399.

Pandelidis, D., & Anisimov, S. (2015). Numerical analysis of the heat and mass transfer processes in selected M-Cycle heat exchangers for the dew point evaporative cooling. Energy Conversion and Management, 90, 62-83.

Perez-Lombard, L., Ortiz, J., & Pout, C. (2008). A review on buildings energy consumption information. Energy and buildings, 40(3), 394-398.

Pescod, D. (1968). Unit air cooler using plastic heat exchanger with evaporatively cooled plates. Australian refrigeration, Air conditioning and heating, 22(9), 22-26.

Pescod, D. (1974). Effects of turbulence promoters on the performance of plate heat exchangers. Heat Exchangers: Design and Theory Sourcebook, 601-615.

Pescod, D. (1979). A heat exchanger for energy saving in an air-conditioning plant. ASHRAE Transactions, 85(2), 238-251.

Pomianowski, M., Andersen, C. H., & Heiselberg, P. (2015). Technical Potential of Evaporative Cooling in Danish and European Condition. Energy Procedia, 78, 2421-2426.

Porumb, B., Bălan, M., & Porumb, R. (2016). Potential of Indirect Evaporative Cooling to Reduce the Energy Consumption in Fresh Air Conditioning Applications. Energy Procedia, 85, 433-441.

Qiu, G, A novel evaporative/desiccant cooling system, PhD thesis, 2007, The University of Nottingham, UK.

Ren. C, Zhang. L. (2005). Three-dimensional Numerical Simulation indirect evaporative cooler by CFD. Energy Conservation. (6), 14-17. (In Chinese)

Riangvilaikul, B., & Kumar, S. (2010). An experimental study of a novel dew point evaporative cooling system. Energy and Buildings, 42(5), 637-644.

Riangvilaikul, B., & Kumar, S. (2010). Numerical study of a novel dew point evaporative cooling system. Energy and Buildings, 42(11), 2241-2250.

Rubio-Castro, E., Serna-González, M., Ponce-Ortega, J. M., & Morales-Cabrera, M. A. (2011). Optimization of mechanical draft counter flow wet-cooling towers using a rigorous model. Applied Thermal Engineering, 31(16), 3615-3628.

San Jose Alonso, J. F., Martínez, F. J., Gomez, E. V., & Plasencia, M. A. (1998). Simulation model of an indirect evaporative cooler. Energy and buildings, 29(1), 23-27.

Saudi Arabian Standards Organization, SASO36 Evaporative Air Coolers [S], 1997.

Song Y, Long W, Huang X. (2010). Evaporative cooling air conditioning technology based on low-carbon economy. Heating, Ventilation and Air conditioning 2010; 40(7):55–7.

Stabat, P., & Marchio, D. (2004). Simplified model for indirect-contact evaporative cooling-tower behaviour. Applied Energy, 78(4), 433-451.

Steeman, M., Janssens, A., & De Paepe, M. (2009). Performance evaluation of indirect evaporative cooling using whole-building hygrothermal simulations. Applied

Thermal Engineering, 29(14), 2870-2875.

Stoitchkov, N. J., & Dimitrov, G. I. (1998). Effectiveness of crossflow plate heat exchanger for indirect evaporative cooling. International journal of refrigeration, 21(6), 463-471.

Stoitchkov, N. J. (1989). Heat and mass transfer in plastic plate heat exchangers with indirect evaporative cooling. In Proceedings Clima 2000—The Second World Congress on Heating, Ventilating, Refrigerating and Air-Conditioning, Vol. V, Sarajevo.

Tulsidasani, T. R., Sawhney, R. L., Singh, S. P., & Sodha, M. S. (1997). Recent research on an indirect evaporative cooler (IEC) part 1: optimization of the COP. International journal of energy research, 21(12), 1099-1108.

Velasco Gómez, E., Tejero González, A., & Rey Martínez, F. J. (2012). Experimental characterization of an indirect evaporative cooling prototype in two operating modes. Applied Energy, 97, 340-346.

W. Nusselt, (1916). Die oberflachenkondensation des wasserdampfes. VDI Zeitschrift, 60, pp. 569–578.

W.E. Ranz, W.R. Marshall, Evaporation from drops. 1, Chem. Eng. Prog. 48(1952) 141e146.

W.E. Ranz, W.R. Marshall, Evaporation from drops. 2, Chem. Eng. Prog. 48(1952) 173e180.

Watt, J. R., & Brown, W. K. (1997). Evaporative air conditioning handbook-3rd edition. Fairmont Press.

Wilke, W.(1962). Wärmeübergang am Rieselfilm. VDI-Forschungsheft-490, Düsseldorf, p. 36.

Xuan, Y. M., Xiao, F., Niu, X. F., Huang, X., & Wang, S. W. (2012). Research and application of evaporative cooling in China: A review (I)–Research. Renewable and Sustainable Energy Reviews, 16(5), 3535-3546.

Y.A Cengel. (2006). Heat and Mass Transfer: A Practical Approach, McGraw-Hill Companies, Inc., Singapore.

Yang Shiming. Heat transfer [M]. 2nd ed. Beijing: Higher Education Press, 1992. (In Chinese).

Yang, H., Ren, C., & Cui, P. (2006). Study on performance correlations of an indirect evaporative cooler with condensation from primary airflow. HVAC&R Research, 12(3), 519-532.

Yang, H. X., Ren, C. Q, Lu, L.(2003). Energy Performance Test of the Indirect Evaporative Heat Exchanger at Kowloon Park. Report for Four Gay Engineering Co. Ltd., Department of Building Services Engineering, The Hong Kong Polytechnic University.

You SJ, Zhang H, Liu YH, Sun ZQ. (1999).Performance of the direct evaporative air humidifier/cooler with aluminum packing and its use in air-cooled chiller units.

HVAC, 25(5): 41–3 [in Chinese].

Yu, F. W., & Chan, K. T. (2005). Application of direct evaporative coolers for improving the energy efficiency of air-cooled chillers. Journal of Solar Energy Engineering, 127(3), 430-433.

Yuan, F., & Chen, Q. (2012). A global optimization method for evaporative cooling systems based on the entransy theory. Energy, 42(1), 181-191.

Zhan, C., Duan, Z., Zhao, X., Smith, S., Jin, H., & Riffat, S. (2011). Comparative study of the performance of the M-cycle counter-flow and cross-flow heat exchangers for indirect evaporative cooling–paving the path toward sustainable cooling of buildings. Energy, 36(12), 6790-6805.

Zhan, C., Zhao, X., Duan, Z., & Riffat, S. B. (2010). Numerical study on indirect evaporative cooling performance comparison between counterflow and crossflow heat exchangers. International Journal of Low-Carbon Technologies, ctq046.

Zhan, C., Zhao, X., Smith, S., & Riffat, S. B. (2011). Numerical study of a M-cycle cross-flow heat exchanger for indirect evaporative cooling. Building and Environment, 46(3), 657-668.

Zhang D, Huang X & Wu Z (2006). Experimental study on optimization of spraying water density of evaporative cooling, Xi'an Institute of Engineering Science and Technology, 20(2): 191-194. (In Chinese).

Zhao Z, Ren C, Tu M, et al (2010) , Experimental investigation on plate type heat

exchanger used as indirect evaporative cooler, Journal of refrigeration, 31(1), 45~49.

Zhao, X., Li, J. M., & Riffat, S. B. (2008). Numerical study of a novel counter-flow heat and mass exchanger for dew point evaporative cooling. Applied thermal engineering, 28(14), 1942-1951.

Zhao, X., Liu, S., & Riffat, S. B. (2008). Comparative study of heat and mass exchanging materials for indirect evaporative cooling systems. Building and Environment, 43(11), 1902-1911.

Zhou B, Huang X. (2005). Feasibility analyses on the application of the Indirect Evaporative cooling technology in textile air conditioning. Cotton Textile Technology, 33(1): 24–8 [in Chinese].

Zhu D. S. (2004). Evaporative cooling air conditioning in hospital in Xinjiang. Refrigeration and Air-Conditioning, 3: 50–3 [In Chinese].